The role of DNA sensor signalling pathway in lymphoma

LAM RUNYI ADELINE

BSc (Hons), National University of Singapore

A THESIS SUBMITTED FOR THE DEGREE OF DOCTOR OF PHILOSOPHY

NUS Graduate School of Integrative Science and Engineering

National University of Singapore

2014

Declaration Page

I hereby declare that this thesis is my original work and it has been written by me in its entirety. I have duly acknowledged all the sources of information which have been used in the thesis.

This thesis has also not been submitted for any degree in any university previously.

Lam Runyi Adeline

10th Jan 2014

Publications

Peer-reviewed articles

1. Lam AR, Koo CX, Tey CS, Shen YJ, Karim SAM, Akira S, Ishii KJ and Gasser S. The DNA sensor ZBP1 counters ATM-mediated tumour suppression of Eμ-*Myc*-induced B-cell lymphomagenesis. *Manuscript in preparation.*
2. Lam AR*, Le Bert N*, Ho SSW, Shen YJ, Tang LFM, Xiong, GM, Croxford JL, Koo CX, Ishii KJ, Akira S, Raulet DH and Gasser S. RAE-1 ligands for the NKG2D receptor are regulated by STING-dependent DNA sensor pathways in lymphoma**.** (March 3, 2014) Cancer Res, 10.1158/0008-5472.CAN-13-1703.* Both authors contributed equally
3. Lam AR*, Chwee JY*, Le Bert N*, Sauer M, Pogge von Strandmann E, and Gasser S. (2013). Regulation of self-ligands for activating natural killer cell receptors. Ann Med *45*, 384-394. * All authors contributed equally.

Book Chapters

1. Shen YJ, Lam AR, Ho SSW, Koo CX, Le Bert N and Gasser S. Cancer pathogenesis and DNA sensing, in Ishii KJ and Choon KT, *Biological DNA sensor: the impact of nucleic acid acids on diseases and vaccinology* (pp.205-229). Academic Press. ISBN: 9780124047327.

Acknowledgements

I would like to thank the generous financial support from NGS in my PhD education. I would like to thank my supervisor Dr. Stephan Gasser for his guidance and support throughout my PhD. I would also like to express my gratitude towards my TAC members, Prof Jean Pierre Abastado, A/Prof Lu Jinhua and Dr Manoj Krishnan for taking their time to provide me with excellent feedback on the project. Special thanks to Rashi for her help in troubleshooting and setting up the experimental protocol at the start of my PhD. I would also like to express my gratitude to Dr. Paul Hutchinson, Guo Hui and Fei Chuin for providing technical assistance with the flow cytometer and cell sorter. I would like to thank Dr Lee Sae Kyung, Dr Ludovic Croxford and Dr Nina Le Bert for providing invaluable advice in the project. I would like to express my heartfelt thanks to past and present lab members for the assistance they had provided, the friendships and encouragements throughout the period. Thank you for making the lab an enjoyable place to work. I would also like to express my gratitude to all who had provided assistance and advice to me. Finally, I would like to express my sincere thanks towards my family and friends who had supported me in one way or the other.

Table of Contents

Summary

The immunoreceptor NKG2D recognizes ligands that are upregulated on infected cells and tumor cells. The expression of NKG2D ligands is induced by the DNA damage response (DDR), which is often constitutively active in tumor cells. We found that DDR-induced NKG2D ligand expression depends on the DNA sensor pathway initiated by STING, TBK1 and IRF3. Cytoplasmic DNA accumulated in response to DNA damage and was also detected in tumor cell lines that constitutively express NKG2D ligands. Transfection of DNA into ligand-negative cells was sufficient to induce NKG2D ligand expression. Our results suggest that genomic damage in tumor cells results in the activation of Sting-dependent nucleic acid sensor pathways, leading to expression of NKG2D ligands, and enabling tumor immunosurveillance. To investigate the exact DNA sensor that might be involved, we cross mice deficient in *Zbp1* (Z-DNA-binding protein 1), which is a type I IFN-inducible candidate cytosolic DNA sensor, to the Eμ-*Myc* mice. Surprisingly, the survival of Eμ-*Myc* mice was increased in absence of ZBP1. The DDR response was enhanced in tumor cells of *Zbp1*-deficient Eμ-*Myc* mice, resulting to an increase in apoptosis. Our data suggest a novel function for ZBP1 in Eμ-*Myc* mouse model.

List of Abbreviations

7AAD	7-amino-actinomycin D
ADP	Adenosine diphosphate
AF488	Alexa Fluor 488
AF647	Alexa Fluor 647
AKT	Protein kinase B
APC	Allophycocyanin
ATCC	American type culture collection
BCL1L12	BCL2-like 12
BCR/ABL	Breakpoint cluster region-Abelson
BRCA	Breast cancer
BrdU	Bromodeoxyuridine
BSA	Bovine serum albumin
CD	Cluster of differentiation
CHK	Checkpoint kinase
Cy3	Cyanine3
DMSO	Dimethyl sulfoxide
DNA	Deoxyribonucleic acid
DNAM-1	DNAX accessory molecule-1
E2F1	E2F transcription factor 1
FCS	Fetal calf serum
FITC	Fluorescein-5-isothiocyanate
GAPDH	Glyceraldehyde-3-phosphate dehydrogenase

GFP	Green fluorescent protein
HER	Human epidermal growth factor receptor
HIN	Hemopoietic interferon-inducible nuclear protein
HPRT	Hypoxanthine-guanine phosphoribosyltransferase
IL	Interleukin
ICAM-1	Intercellular adhesion molecule 1
IFN	Interferon
IFN-γ	Interferon-gamma
Ig	Immunoglobulin
IRES	Internal ribosome entry site
i.p	Intraperitoneal
IP10	Interferon gamma-induced protein 10
MHC	Major Histocompatibility Complex
miRNA	MicroRNA
MRE	Meiotic recombination
MSCV	Murine stem cell virus
Mult1	Murine UL16-binding-protein-like transcript-1
NBS	Nijmegen breakage syndrome
NF-κB	Nuclear factor kappa-light-chain-enhancer of activated B cells
NK	Natural killer
NKG2D	Natural killer group 2, member D

PBS	Phosphate buffered saline
PE	Phycoerythrin
PerCP-Cy5.5	Peridinin-chlorophyll protein
PE-Cy7	Phycoerythrin-cyanine7
PCR	Polymerase Chain Reaction
Pkr	Protein kinase R
Poly A: U	Polyadenylic: polyuridylic acid
Poly I: C	Polyinosinic: polycytidylic acid
RAS	Rat sarcoma
RB/pRB	Retinoblastoma protein
RNA	Ribonucleic acid
RPMI	Roswell park memorial institute
SDS-PAGE	Sodium dodecyl sulfate polyacrylamide gel electrophoresis
SD	Standard deviation
SEM	Standard error of mean
TNF-α	Tumour necrosis factor alpha
UTR	Untranslated region
Wrn	Werner syndrome, RecQ helicase-like
WT	Wild type
XRCC	X-ray repair cross-complementing protein

List of Figures

Chapter 1: Introduction

1. Introduction

In addition to cell intrinsic barriers to tumor formation mediated by tumor suppressors such as p53, the immune system has also been implicated in tumor surveillance in several settings. The various modes of tumor cell recognition by the immune system are topics of intense interest. Optimal immune responses to autologous cells generally only occur when the cells are first exposed to pathogen-associated molecular patterns, or when the cells are subjected to disease related stress. In infections, such signals often emanate from various pattern recognition receptors (PRR) such as toll-like receptors (TLRs) and numerous intracellular sensors that detect viral or microbial DNA and RNA in the cytoplasm. The initial recognition of cancer cells, on the other hand, is thought to require the activation of pathways triggered by disease-associated stress. This study examines interactions between these modes of signaling.

1.1 DNA damage response (DDR)

1.1.1 Overview of the DNA damage response (DDR)

The DNA damage response (DDR) is a signal-transduction pathway that directs cell-cycle transitions, DNA replication, DNA repair and apoptosis. The major regulators of the DDR are the phosphoinositide 3-kinase (PI3K)-related protein kinases (PIKKs), including ataxia-telangiectasia mutated (ATM) and ATM and RAD3-related (ATR). ATM and ATR have similar biochemical and functional characteristics. Both are large kinases with significant sequence homology and tend to phosphorylate Ser or Thr residues that are followed by Gln. Both phosphorylate an overlapping set of substrates that results in cell-cycle arrest and DNA repair.

The ATM and ATR kinase are activated by different genomic insults. ATM kinase is preferentially activated by DNA double strand breaks (DSB) while ATR kinase, is generally activated by stalled replication forks that occur during DNA replication. In addition, it has been demonstrated that ATR kinase is activated by ultraviolet light, single strand DNA breaks, and chemical agents that interrupt DNA replication and give rise to stalled replication forks.

The DNA damage sensors, the MRE11–RAD50–NBS1 (MRN) complex that detects DNA double-strand breaks (DSBs) or replication protein A (RPA) and the RAD9–RAD1–HUS1 (9-1-1) complex that detects exposed regions of single-stranded DNA, enlist ATM (through the MRN complex) and ATR (through RPA and the 9-1-1 complex), which is bound by ATR-interacting protein (ATRIP) upon sensing damaged DNA (Figure 1.1).These would then phosphorylate (P) the histone variant H2AX on Ser139 (known as γH2AX) in the region proximal to the DNA lesion (Stiff et al., 2004; Ward and Chen, 2001). γ H2AX is crucial to recruit mediator of DNA damage checkpoint 1 (MDC1) that further maintains and amplifies DDR signalling by promoting further build up of the MRN complex and activation of ATM. BRCA1 is recruited at sites of DNA damage on phosphorylation by ATM and ATR. Many of the recruited proteins as well as the core histones at the position of the breaks, undergo extensive post-translational modifications (PTMs; including phosphorylation, ubiquitylation, sumoylation, acetylation, methylation and poly (ADP)-ribosylation) (Polo and Jackson, 2011). Finally, DDR signalling would move away from the damaged locus due to the activation of diffusible kinases CHK2 (which is mainly phosphorylated by

ATM) and CHK1 (which is mainly phosphorylated by ATR) with converging signalling on downstream effectors such as p53 and the cell division cycle 25 (CDC25) phosphatases. Depending on the extent of genomic damage, DDR-mediated cellular outcomes may be cell death by apoptosis; transient cell cycle arrest followed by repair of DNA damage and continuation of proliferation; or cellular senescence caused by the persistence of unrepaired DNA damage.

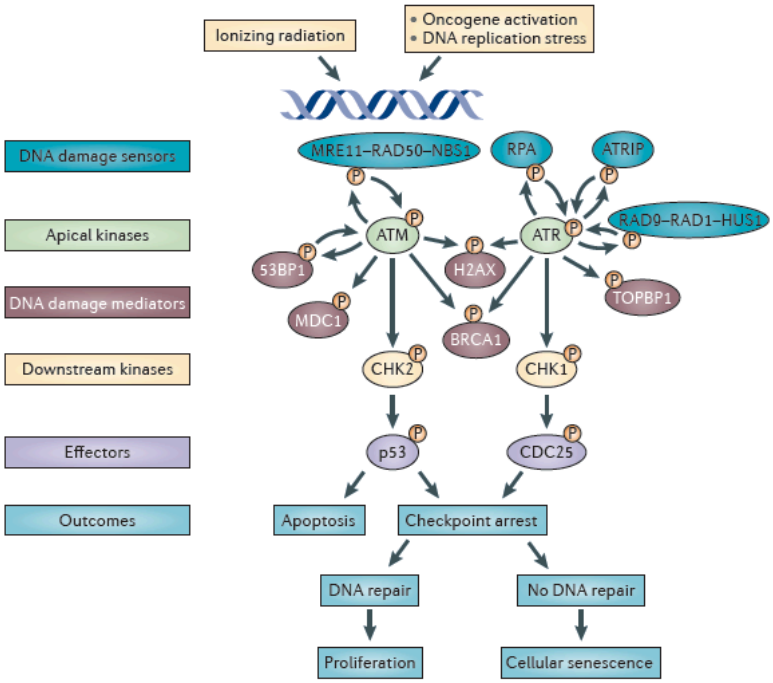

Figure 1.1 Overview of the DNA damage response (DDR).
The DDR pathway consists of two main DNA damage sensors that would recruit the apical kinases ataxia-telangiectasia mutated (ATM) and ataxia telangiectasia and RAD3-related (ATR), which is bound by ATR-interacting protein (ATRIP) in response to genomic insults. These in turn phosphorylate (P) the histone variant H2AX on the chromatin surrounding the DNA breaks. ATM and ATR would phosphorylate the downstream kinases such as CHK2 and CHK1, which would in turn activate downstream effectors such as p53 and the cell division cycle 25 (CDC25) phosphatases. DDR-mediated cellular outcomes may be cell death by apoptosis; cell cycle arrest followed by repair of DNA damage; or cellular senescence. Reprinted by permission from Macmillan Publishers Ltd: Nature Reviews Cancer publication(Sulli et al., 2012), copyright 2012.

1.1.2 Overview of ataxia-telangiectasia mutated (ATM)

ATM is a large protein with a molecular weight of 350 kDa and consists of 3,056 residues. The carboxy-terminal active site of ATM contains a PI3K domain, which constitutes about 10% of this large protein. The rest of it most probably contains regulatory and interaction domains that determine its modes of activation and broad substrate specificity. Other important sites are those that undergo posttranslational modifications during ATM activation (Figure 1.2). The lack of structural data due to technical challenges in ATM crystallization is currently obstructing the understanding of the functional significance of ATM domains.

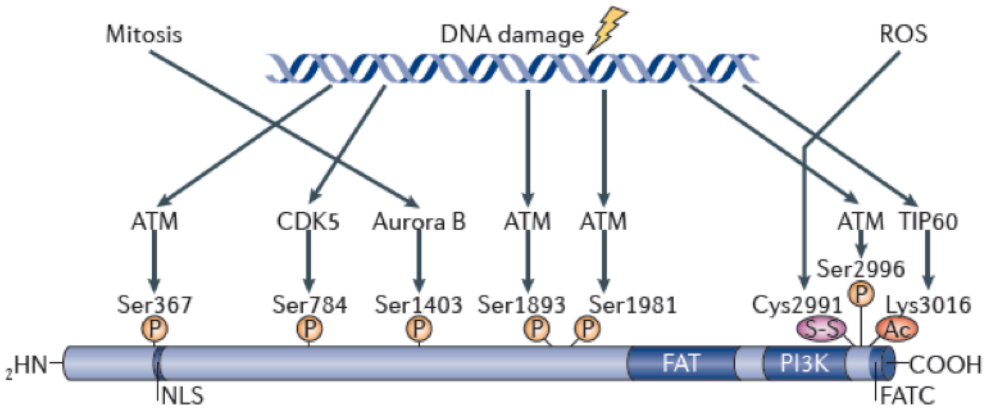

Figure 1.2 Schematic representation of ATM with its major domains. The sites of posttranslational modifications link to ATM activation in various situations and the proteins responsible for these modifications, including ATM itself (see text for details), are indicated. Ac, acetylation; FATC, FAT carboxy-terminal; NLS, nuclear localization sequence; P, phosphorylation; ROS, reactive oxygen species; S-S, disulphide bridge. Reprinted by permission from Macmillan Publishers Ltd: Nature Reviews Molecular Biology (Shiloh and Ziv, 2013), copyright 2013.

The physiological consequences of loss of ATM as opposed to having inactive ATM may not be the same from evidence using mice with different *Atm* mutations (Choi et al., 2010). *Atm*-knockout mice display characteristic traits of ataxia-telangiectasia with the exception of neurodegeneration and hence portray a relatively moderate phenotype (Barlow et al., 1996; Borghesani et al., 2000; Elson et al., 1996; Xu et al., 1996). Strikingly, mice

producing physiological levels of catalytically inactive (kinase-dead) ATM were embryonic lethal and conditional expression of the mutant protein in the immune system caused significant genomic instability in lymphoid cells (Daniel et al., 2012; Yamamoto et al., 2012). The mechanistic explanations are not available, but one hypothesis could be that as kinase-dead ATM was recruited to DSB sites, the presence of catalytically inactive ATM within the DDR network proximal to these sites harshly affects the damage response pathway. These studies clearly show that the presence of the inactive form of ATM severely affects the cellular response to genotoxic stress more than its loss.

ATM assembles and coordinates the huge array of DSB response proteins in response to induction of acute DNA damage. ATM phosphorylates and thus regulates the activity of several protein kinases, which in turn phosphorylate their own substrates. A map containing the functional links of ATM to effectors that have been documented in detail are shown in (Shiloh and Ziv, 2013). However, proteomic screens point to hundreds more potential ATM substrates (Bensimon et al., 2010; Matsuoka et al., 2007; Mu et al., 2007). This huge array of downstream effectors is not common when compared with the most diversified protein kinases and questions whether ATM is a promiscuous or specific protein kinase.

1.1.3 Overview of the DNA repair pathways

Damage to DNA could trigger specific repair pathways depending on the type of lesions and the stage of the cell cycle (Figure 1.3).

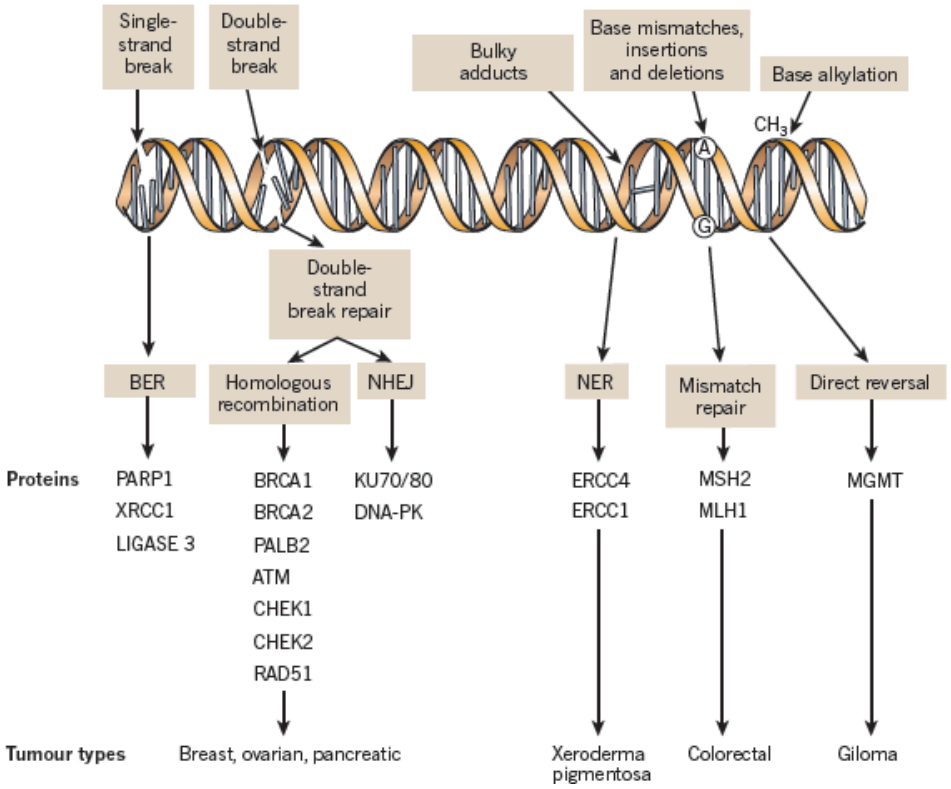

Figure 1.3 Overview of the DNA repair pathways.
DNA can undergo various lesions, from single-strand breaks (SSBs) to base alkylation events, which would be repair by specific repair factors. The important proteins involved in each DDR mechanism, the tumour types usually characterized by DDR defects and the drugs that target these defects are shown. BER, base excision repair; NER, nucleotide excision repair; NHEJ, non-homologous end-joining. Reprinted by permission from Macmillan Publishers Ltd: Nature(Lord and Ashworth, 2012) ,copyright 2012.

1.1.3.1 Base Excision Repair (BER)

Most of the slight changes to DNA, such as oxidative lesions, alkylation products and single-strand breaks (SSBs), are repaired through a series of processes that is known as base excision repair (BER). In BER, damaged bases are first cut out from the double helix, and the damaged region of the DNA backbone is then cleaved and substituted with newly synthesized DNA (Figure 1.4) (David et al., 2007; Sancar et al., 2004b). DNA glycosylase is responsible for recognizing oxidized/reduced bases, alkylated (usually methylated) bases, deaminated bases (e.g., uracil, xanthine), or base mismatches and plays an important role in initiating BER (Sancar et al., 2004b). Organisms usually contain enzymes recognizing uracil (uracil-DNA glycosylase), alkylated purines (methyl-purine glycosylase), oxidized/reduced pyrimidines (homologues of *E. coli*endonuclease III), or oxidized purines (homologs of *E. coli* Fapy glycosylase or 8-oxoguanine glycosylase) (Sancar et al., 2004b). The enzymes poly (ADP-ribose) polymerase 1 and 2 (PARP1 and PARP2), which act as sensors and signal transducers for lesions, such as SSBs, also play a role in BER(Lord and Ashworth, 2012).

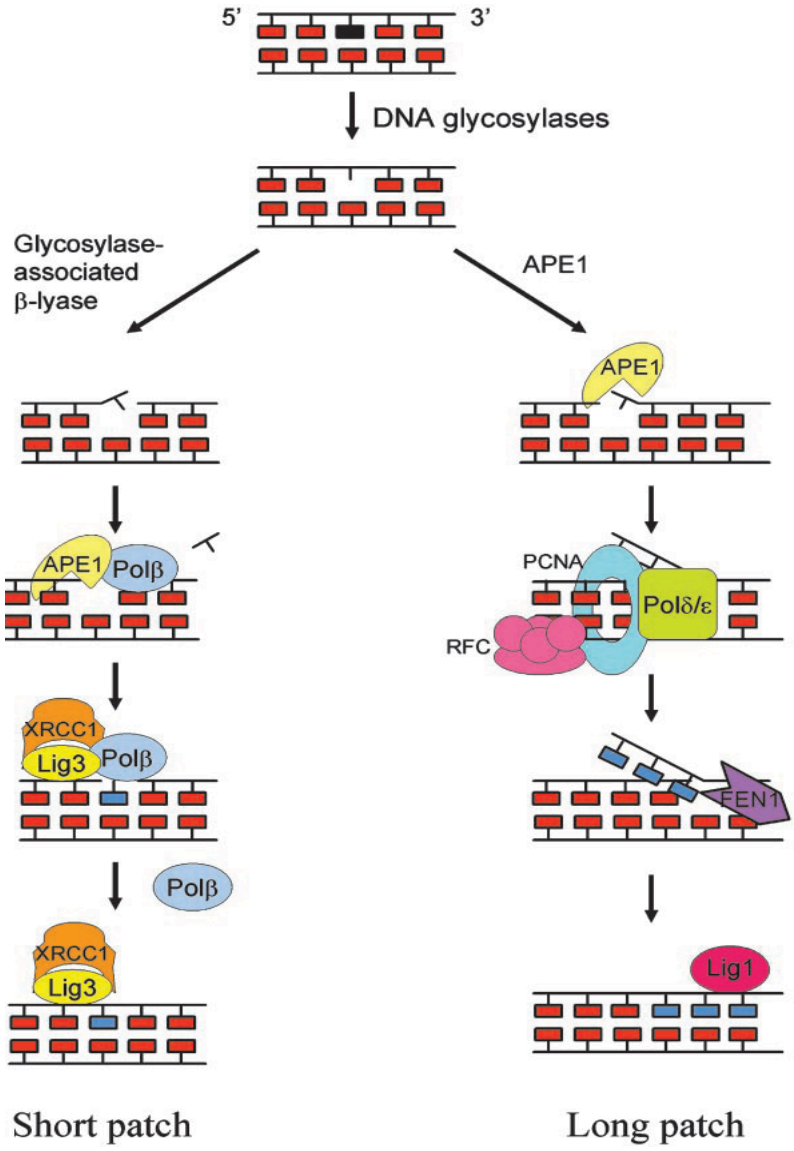

Figure 1.4 Base excision repair mechanisms in mammalian cells.
A damaged base is removed by a DNA glycosylase to generate an abasic (AP) site. The repair patch may be a single nucleotide (short patch) or 2–10 nucleotides (long patch). In the short patch pathway, the base damage is removed by a glycosylase/AP lyase that cleaves the phosphodiester bond 3' to the AP site. APE1 endonuclease then cleaves the 5' bond to the site and recruits Polβ to fill the 1-nt gap that is ligated by Lig3/XRCC1 complex. The long patch pathway usually occurs when the AP site is generated by hydrolytic glycosylases or by spontaneous hydrolysis, repair. APE1 cleaves the 5' phosphodiester bond, and the RFC/PCNA-Polδ/ε complex is responsbile for repair synthesis and nick translation, displacing several nucleotides. The overhang is cleaved off by FEN1 endonuclease and the long-repair patch is ligated by Ligase 1. Reprinted from (Sancar et al., 2004b) with permission from the Annual Review of Biochemistry, Volume 73 © 2004 by Annual Reviews, http://www.annualreviews.org.

1.1.3.2 Nucleotide Excision Repair (NER)

The bulkier single-strand lesions that changes the DNA helical structure, such as those caused by ultraviolet light, are repaired by nucleotide excision repair (NER) (Cleaver et al., 2009). NER is often further divided into transcription-coupled NER (TC-NER), which happens where the lesion blocks, and is detected by elongating RNA polymerase; and global-genome NER (GGR), in which the lesion affects base pairing and distorts the DNA helix. Although these processes identify lesions using distinct processes, the repair processes are quite similar. DNA surrounding the lesion is cut out and then replaced using the normal DNA replication machinery. Excision repair cross-complementing protein 1 (ERCC1) is crucial to this excision step. On GGR, XPC-RAD23B-Centrin2 complex detects the damage while in TC-NER damage is recognized through the stalling of RNA polymerase II on the actively transcribed strand of a gene. Xeroderma pigmentosum, complementation group A (XPA), RPA, xeroderma pigmentosum, complementation group B (XPB) and xeroderma pigmentosum, complementation group D (XPD) stabilize the damaged DNA and xeroderma pigmentosum, complementation group G (XPG) and ERCC1•XPF structure-specific endonucleases cleave the 3' and 5'side of the nucleotide fragment containing the damaged DNA (Figure 1.5). DNA polymerases will fill in the missing nucleotides and the newly synthesized DNA fragment is ligated by DNA ligaseIII-XRCC1 and DNA ligase I (Figure 1.5).

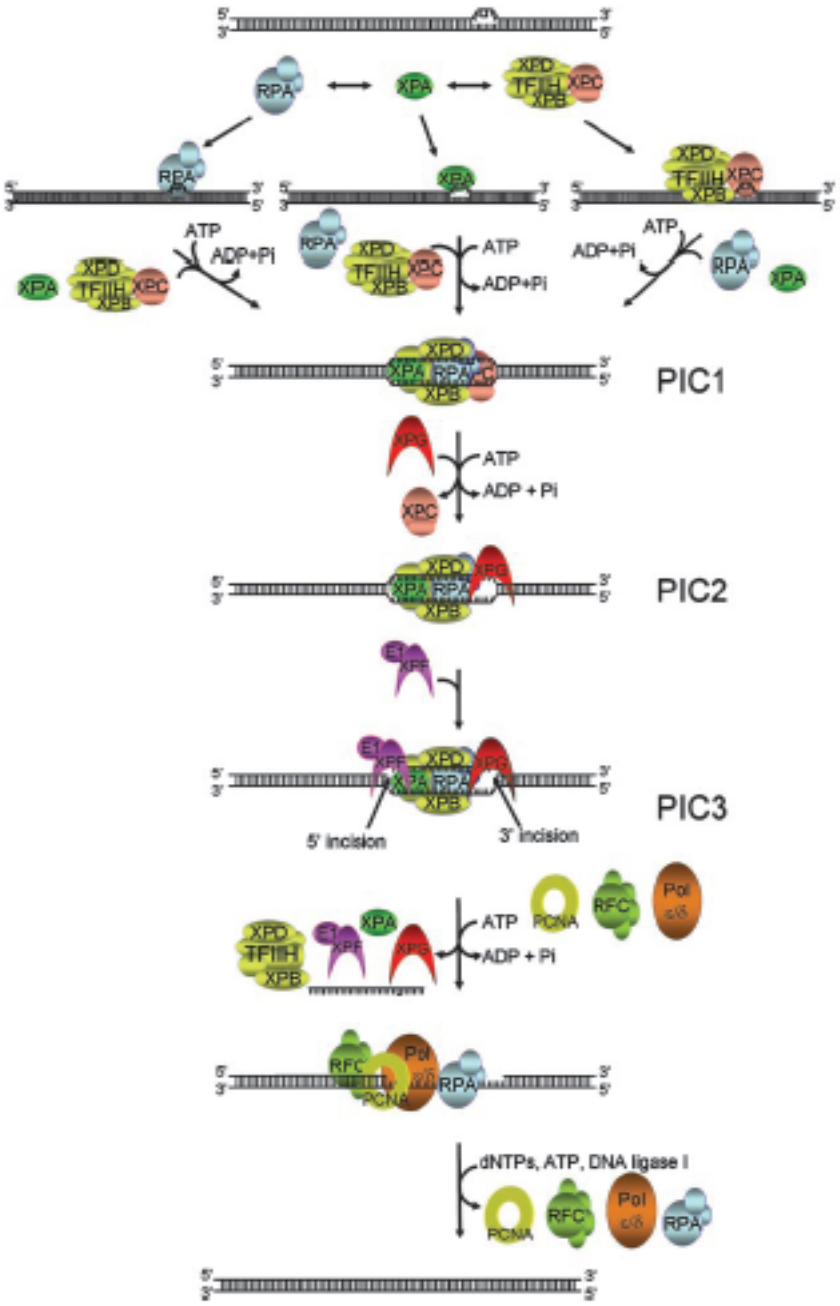

Figure 1.5 Overview of human nucleotide excision pathway.
The four repair factors, RPA, XPA, XPC-TFIIH, recognize the damage and form a complex at site. If the site contains a lesion, ATP hydrolysis by the XPB and XPD helicases unwinds the duplex around the lesion, making a stable preincision complex 1 (PIC1) at the damage site. XPG then replaces XPC in the complex to form a more stable preincision complex 2 (PIC2). Finally, XPF•ERCC1 is recruited to the damage site to form preincision complex 3 (PIC3). The damaged strand is incised by XPG and XPF•ERCC1, releasing the oligomer containing the damaged strand. Polδ/ε will fill up the gap with the help of replication accessory proteins PCNA and RFC. Reprinted from (Sancar et al., 2004b) with permission from the Annual Review of Biochemistry, Volume 73 © 2004 by Annual Reviews, http://www.annualreviews.org.

1.1.3.3 Repair of double-strand breaks (DSB)

The repair of double strand breaks (DSB) is mediated by non-homologous end joining (NHEJ) or homologous recombination repair (HRR; also known as homology-directed repair (HDR)). HRR is a high fidelity repair pathway that usually occurs in the S and G2 phases of the cell cycle and it would reinstate the original DNA sequence to the site of damage. A portion of the DNA sequence around the DSB is deleted (known as resection) and the DNA sequence on a homologous sister chromatid is used as a template for the synthesis of new DNA at the DSB site (Lord and Ashworth, 2012). HR repairs DNADSBs through the double-strand break repair (DSBR) or the synthesisdependent strand-annealing repair (SDSA) (Figure 1.6). In both scenarios, the MRN complex is needed to detect DSBs. After incision, the 3' end single-stranded DNA coated with RPA and RAD51 invades into a homologous recipient DNA duplex. During DSBR, two Holliday junctions are created, each between four strands of DNA that are then converted into recombination products while SDSA results in non-crossover products. DNA polymerases would fill in missing nucleotides at the end of the invading 3' DNA strand. BRCA1, BRCA2, RAD51 and partner and localizer of BRCA2 (PALB2) are important proteins involved in HRR.

In NHEJ, the two ends of a DNA DSB are connected and resealed without the need for sequence homology between the ends (Helleday et al., 2008). NHEJ acts throughout the cell cycle. Sometimes this process can result in deletion or mutation of DNA sequences at or around the DSB area. The heterodimer of the 70 and 80 kDa Ku autoantigens (KU70 and KU80) recognize the broken DNA ends and forms the DNA-binding component of

DNA-dependent protein kinase (DNA-PK) (Figure 1.6). Ku aligns the DNA ends followed by DNA polymerases or nucleases that fill in or removes the DNA single-stranded overhangs, respectively to produce the two DNA blunt ends (Figure 1.6). The XRCC4/DNA ligase IV ligation complex then joins the DNA ends together (Figure 1.6). Compared with HRR, NHEJ, although mechanistically simpler, have a higher mutation rate.

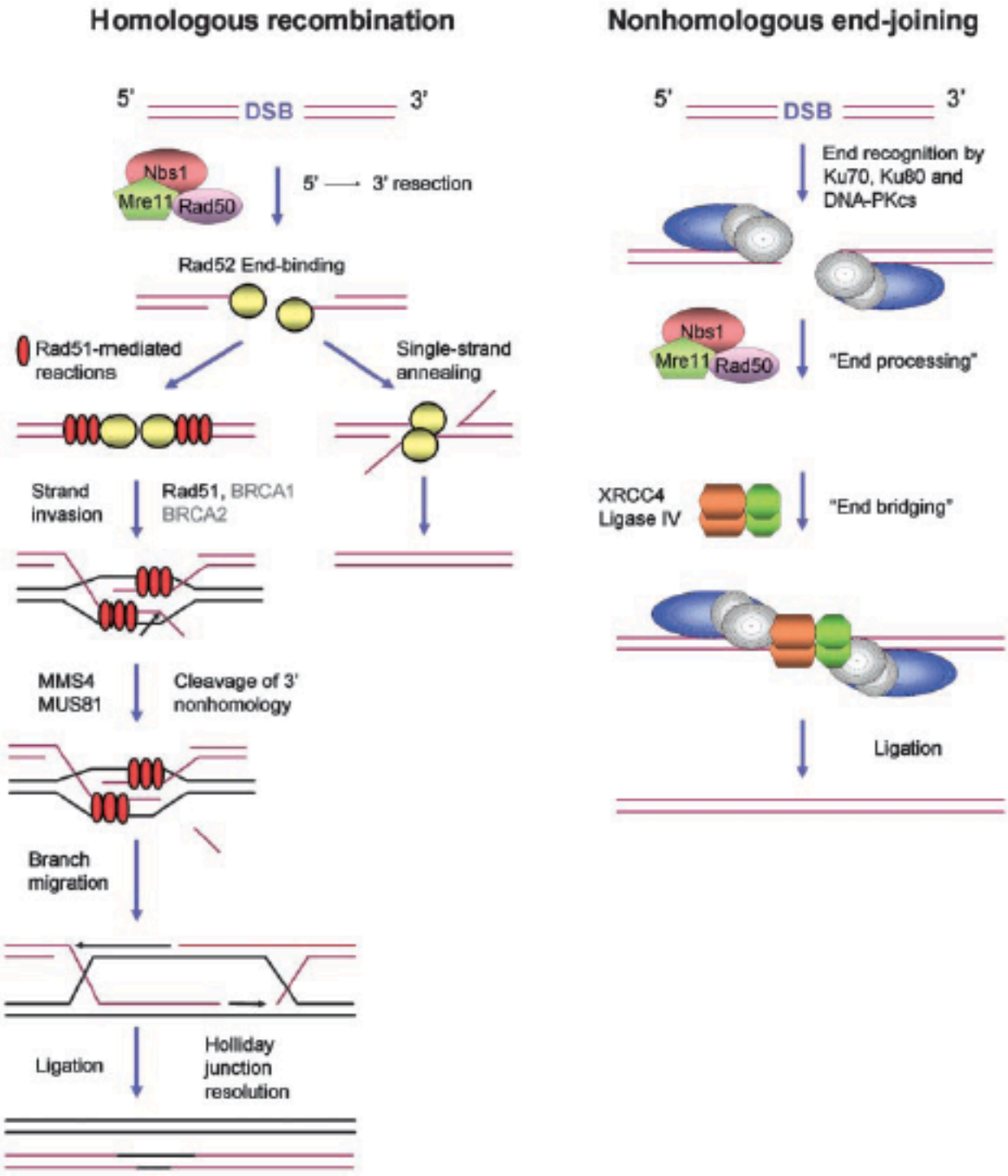

Figure 1.6 Mechanisms of homologous recombination and non-homologous end joining. Double-strand breaks are repaired by either homologous recombination or by nonhomologous end-joining. An important intermediate in homologous recombination is the Holliday intermediate, in which the two recombining duplexes are joined covalently by single-strand crossovers. Resolvases such as MUS81-MMS4 cleave the Holliday junctions to separate the two duplexes. In the single-strand annealing (SSA) mechanism, the duplex is digested by a 5' to 3' exonuclease to reveal microhomology regions that promote pairing, trimming, and ligation. Reprinted from (Sancar et al., 2004b) with permission from the Annual Review of Biochemistry, Volume 73 © 2004 by Annual Reviews, http://www.annualreviews.org.

1.1.3.4 Mismatch Repair

Mismatch repair is important to the DDR and it focuses mainly with dNTP misincorporation and formation of 'insertion and deletion' loops that form during DNA replication. These errors cause base 'mismatches' in the DNA sequence that change the helical structure of DNA. The heterodimers, MUTSα or MUTSβ recognize AG or TC mismatches between the old and the newly synthesized strand, and trigger a cascade of events to remove the mismatched nucleotide and allow the replication machinery to use the original DNA template to restore the damaged DNA strand back to its original form (Figure 1.7). The proteins encoded by the mutS and mutL homologue genes, such as *MSH2* and *MLH1* play an important role in mismatch repair.

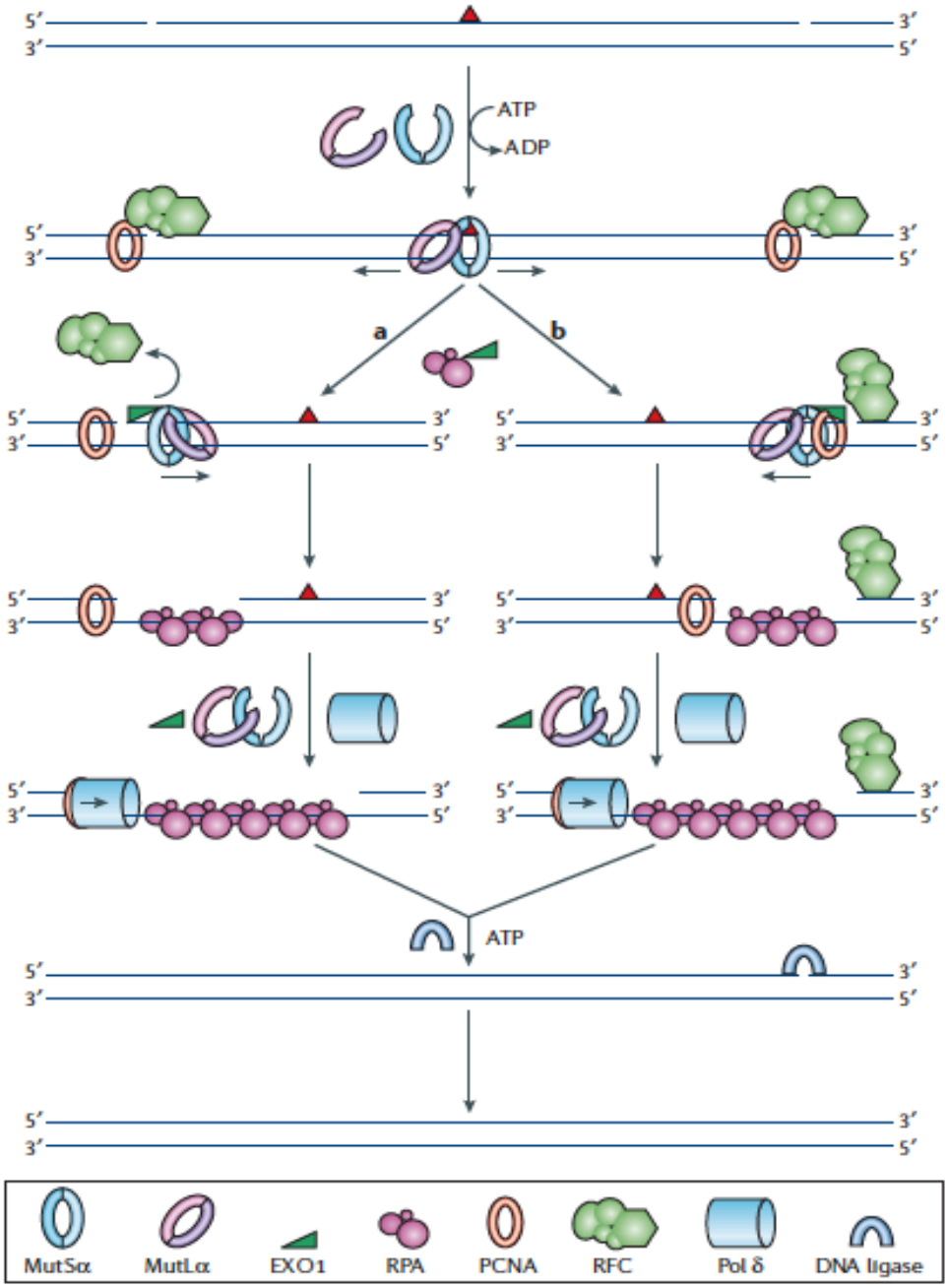

Figure 1.7 Human mismatch-repair system.
The mismatch (red triangle)-bound MutSα (orMutSβ) recruits MutLα, which undergoes an ATP-driven conformational switch, releasing the sliding clamp from the mismatch site. **a** | Clamps that diffuse upstream meet replication factor C (RFC) that is bound at the 5′ terminus of the strand break and replacing it with exonuclease-1 (EXO1) which would degrade the strand in a 5′→3′ direction. The single-stranded gap is stabilized by replication protein A (RPA). **b** | Clamps that move downstream meet a PCNA molecule that is bound at the 3′ terminus of the strand break. The recruitment and the activation of EXO1 lead to the degradation of the region between the original discontinuity and the mismatch. In both scenarious, after the mismatch is removed, MutLα inhibits EXO1 activity. A complex consisting of DNA polymerase δ (Pol δ) and proliferating cell nuclear antigen (PCNA) fills the gap and DNA ligase I seals the remaining nick to complete the repair process. Reprinted by permission from Macmillan Publishers Ltd: Nature Reviews Molecular Cell Biology (Jiricny, 2006), copyright 2006.

1.1.4 Role of DDR in tumorigenesis

Genomic instability is one of the hallmarks of cancer (Stratton et al., 2009). Although the specific DDR defects are unknown in most cancers, there is an indisputable connection between a particular DDR defect and the neoplastic phenotype in several cases. For example, 15% of sporadic colorectal tumours show abnormal shortening or lengthening of dinucleotide repeat sequences characteristic of microsatellite instability, which may be due to defective mismatch repair that results in an inability to repair DNA replication errors. Microsatellite instability is also found in the familial form of the disease known as hereditary non-polyposis colorectal cancer (HNPCC), which is linked with loss-of-function mutations in mismatch repair genes, such as *MSH2* and *MLH1*. Mutations in *ATM* increase the susceptibility of carriers to cancer and are found in approximately 0.5–1.0% of the population (Renwick et al., 2006; Swift et al., 1987). People with mutations in both alleles of *ATM* would be diagnosed with the neurodegenerative and cancer predisposition disorder ataxia-telangiectasia (Savitsky et al., 1995). Mutations in *ATR* are uncommon and probably only result in viability when they are heterozygous or hypomorphic.

DDR has been proposed to represent an important barrier to tumorigenesis (Bartek et al., 2001; Bartkova et al., 2005; Gorgoulis et al., 2005a). Uncontrolled cell proliferation, caused by oncogene activation or inactivation of certain tumour suppressors, results in DNA-replication stress and persistent DNA-damage, leading to activation of the ATR/ATM-mediated signaling. This would cause cell death or senescence in cell-culture models and during tumorigenesis *in vivo* (Bartkova et al., 2005; Campisi and D'adda

Di Fagagna, 2007; Gorgoulis et al., 2005b; Halazonetis et al., 2008b). The DDR is activated in early neo-plastic lesions and acts as a barrier against malignancy (Bartkova et al., 2006; Gorgoulis et al., 2005b). Inactivation of this barrier, arising through mutational or epigenetic inactivation of DDR components, is then selected for during tumour development, which would promote tumorigenesis. This model for the DDR as an anticancer barrier provides explanation for the high frequency of DDR defects in human cancers (Halazonetis et al., 2008b).

1.2 NKG2D ligands

The activating receptor NKG2D is a C-type lectin-like molecule that is expressed on NK cells, activated mouse $CD8^+$ T cells, a subset of mouse $TCR\gamma\delta^+$ T cells, and all human $CD8^+$ and $TCR\gamma\delta^+$ T cells (Mistry and O'Callaghan, 2007). NKG2D is a homodimeric type II transmembrane glycoprotein present on human chromosome 12, within the NK gene complex, and in a syntenic position on mouse chromosome 6 (Coudert and Held, 2006).

NKG2D recognizes ligands that are distant homologues of major histocompatibility complex (MHC) class I proteins (Raulet, 2003). One arm of innate immune recognition, important in the context of both cancer and infection, is the NKG2D-NKG2D-ligand system (Gasser and Raulet, 2006c; Raulet, 2003).This is a critical arm of innate immunity, in which transformed or infected cells increase their expression of various cell surface ligands for NKG2D. Engagement of the NKG2D receptor on natural killer cells or certain T cell subsets stimulates these effector cells to kill tumor cells and/or provoke an inflammatory response that aids in tumor control (Guerra et al., 2008; Raulet and Guerra, 2009).

Multiple NKG2D ligands have been identified in humans and mice (Figure 1.8). In humans, the NKG2D ligands include MICA and MICB (MHC class I chain–related proteins A and B), both encoded by genes in the MHC, and up to six different proteins called ULBPs (UL16- binding proteins), also known as RAET1 proteins (Raulet et al., 2013). In mice, the NKG2D ligands is divided into three subgroups, including five different isoforms of RAE-1 (retinoic acid early inducible-1) proteins, one MULT1 (murine UL16-binding protein-like transcript 1) protein, and three different isoforms of H60 proteins (though not all mouse strains express all the isoforms) (Raulet et al., 2013).

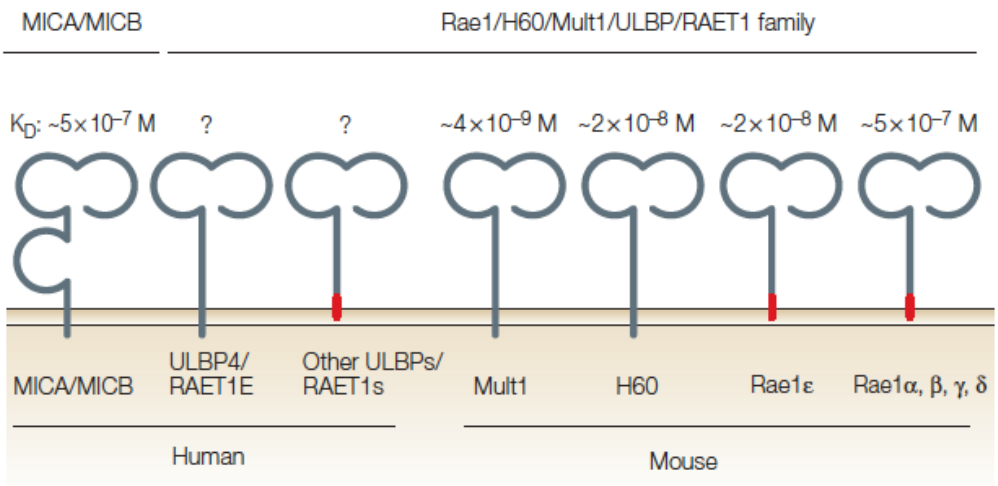

Figure 1.8 Domain structures and affinities of various NKG2D ligands. The affinities of the various ligands for NKG2D, represented as the equilibrium dissociation constant (KD), are shown above each ligands. Reprinted by permission from Macmillan Publishers Ltd: Nature Reviews Immunology (Raulet, 2003), copyright 2003.

NKG2D ligands are usually not expressed on healthy cells but are up regulated during cellular stress. NKG2D ligands can be regulated at several stages of biogenesis, including transcription, RNA stabilization, protein stabilization, and cleavage from the cell membrane by several distinct pathways (Figure 1.9).

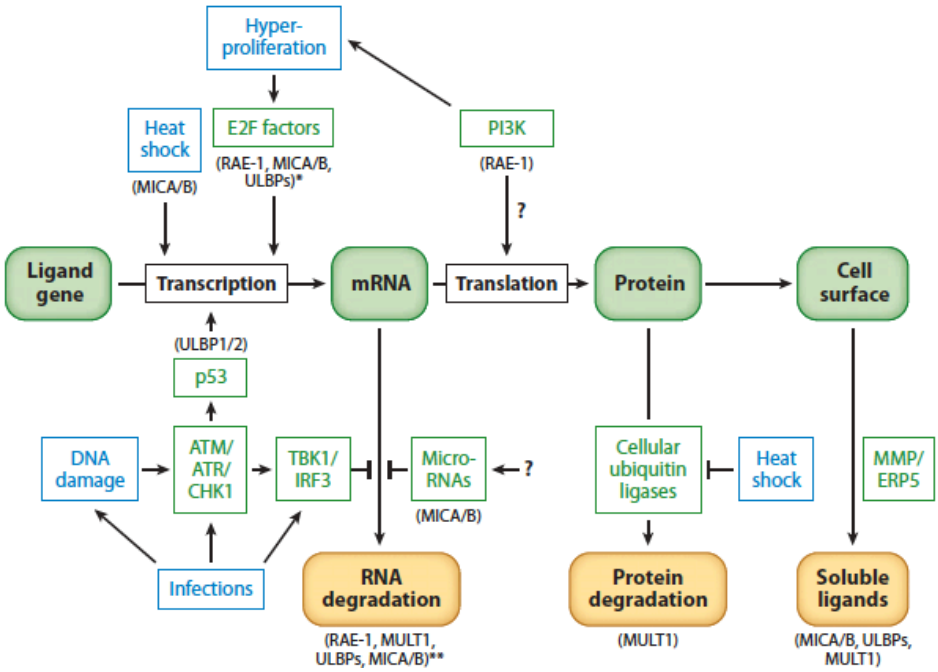

Figure 1.9 Regulation of NKG2D ligands at different stages of ligand biogenesis and degradation.
The regulatory signals and pathways that regulate NKG2D ligands are shown, together with information on whether they act transcriptionally, by stabilizing or targeting ligand mRNAs, by stabilizing ligand proteins, or by cleavage of the ligand from the cell surface. Reprinted from (Raulet et al., 2013) with permission from the Annual Review of Immunology, Volume 31 © 2013 by Annual Reviews, http://www.annualreviews.org.

1.2.1 Regulation of NKG2D ligands by the DDR

The link between NKG2D ligands and DDR was initially observed through *in vitro* cell culture. Drugs or irradiation that damaged DNA consistently induced several NKG2D ligands in mouse *in vitro* cell lines, including RAE-1, MULT1, and H60 (Gasser et al., 2005; Gasser and Raulet, 2006b). In the case of human cell lines, DNA-damaging agents induced the expression of ULBP1, 2, and 3 and, in some cases, MICA and MICB (Cerboni et al., 2007; Gasser et al., 2005; Soriani et al., 2009). Depending on the nature and severity of DNA damage, the DDR would induce cell cycle arrest, DNA

repair or apoptosis and is proposed to represent an important barrier to tumorigenesis (Bartek et al., 2001; Bartkova et al., 2005; Gorgoulis et al., 2005a). Previously we demonstrated that the DDR molecules ATR , ATM and CHK1 , but not p53, are required for inducing NKG2D ligand expression in response to DNA damage (Gasser et al., 2005). Inhibition of these molecules in tumor cell lines inhibited NKG2D ligand expression, indicating that a sustained DDR is essential for maintaining expression of NKG2D ligands. To add to the significance, tumor cells *in situ*, including precancerous lesions, exhibit constitutive activation of ATM and other components of the DDR (Bartkova et al., 2005; Popa et al., 2011). The DDR has also been implicated in the induction of p53, apoptosis and senescence, which constitute intrinsic modes of tumor suppression (Halazonetis et al., 2008a; Mallette and Ferbeyre, 2007).

In addition to transformed cells, the DDR can also be activated in rapidly proliferating cells because of DNA replication stress. Stimulation of cultured human T cells with mitogens, super-antigens, or antigens were shown to induce NKG2D ligands in vitro, and the expression of the ligands could be decrease by treating the cells using drugs or siRNAs that inhibit the DDR (Cerboni et al., 2007). However, mouse T cells that are stimulated to proliferate *in vitro* do not induce NKG2D ligands (Diefenbach et al., 2000; Gasser et al., 2005).

The DDR can be induced during infection to enable NK cells and T cells to eliminate infected cells. In one study, pre-B cells infected with Abelson murine leukemia virus increases the expression of activation- induced cytidine deaminase (AID), which deaminates bases in DNA, thereby inflicting

DNA damage and resulting in NKG2D upregulation in the infected pre-B cells (Gourzi et al., 2006). Studies showed that HIV infection of cells in culture results in induction of ULBP1 and 2 (Ward et al., 2009). This process is dependent on the Vpr protein encoded by HIV, which would activate the ATR kinase and thereby activates the DDR. A subsequent study showed that the HIV Vif protein also impacts NKG2D ligand expression by inhibiting it (Norman et al., 2011). Vif targets the degradation of the antiviral host protein APOBEC3G that would deaminate cytosine residues in the HIV genome, causing mutations that inactivate the viral genome. A study suggested that DNA damage created while repairing these mutations induces the DDR and hence the expression of NKG2D ligands on infected cells (Norman et al., 2011). HIV Vif partially offsets this effect by reducing the amounts of APOBEC3G in infected cells.

1.2.2 Regulation of NKG2D ligands by other pathways

MICA and MICB expression can be upregulated in response to heat shock (Groh et al., 1996). The heat shock transcription factor (HSF1) was found to bind to heat shock response elements (HSE) in the MICA promoter in response to heat shock (Fionda et al., 2009). Optimal induction of NKG2D ligands in response to heat shock was found to require binding sites for Sp-family transcription factors (Venkataraman et al., 2007b). No heat shock elements have been described for mouse NKG2D ligand genes.

Proliferative signals could activate the NKG2D ligands. Activating E2F family of transcription factors were shown to regulate the transcription of mouse *Raet1*, but not *H60* or *Mult1* family members (Jung H, 2012). In a human cell line, expression of MICA, MICB, ULBP2, ULBP3 and possibly

ULBP1 was associated with proliferation and increased activity of the *MICA* and *MICB* promoters (Jung H, 2012; Rabinovich et al., 2003; Venkataraman et al., 2007a).

NKG2D ligands can be regulated by oncogene activation. Overexpression of the adenovirus E1A oncogene upregulated NKG2D ligands on mouse and human cells (Routes et al., 2005) and inhibition of BCR/ABL activity downregulated MICA and MICB cell surface expression in the K562 chronic myelogenous leukaemia cell line (Boissel et al., 2006). However, the expression of MICA and MICB expression in breast cancer cell lines was regulated by HER2/HER3 mediated activation of the PI3K/AKT pathway, but not the DDR (Okita et al., 2012). Similarly, we found that oncogenic H-RAS induced the expression of RAET1 in a PI3K-dependent, but DNA damage independent manner (Liu et al., 2012).

NKG2D ligands can be regulated by miRNAs. The function of p53 was dispensable for induction of NKG2D ligand expression in response to DNA damage, but p53 was found to induce the expression of ULBP1 and ULPB2. Paradoxically, p53 was also shown to downregulate ULBP2 by inducing the expression of microRNAs that target ULBP2 transcripts suggesting a complex regulation of NKG2D ligands by p53 (Gasser et al., 2005; Gasser and Raulet, 2006a; Heinemann and Paschen, 2012). In addition to p53-induced microRNAs, a group of endogenous, ubiquitously expressed cellular miRNAs control MICA and MICB expression by binding to the 3' UTR sites of MICA and MICB in various human tissues and in cell lines (Heinemann et al., 2012; Stern-Ginossar et al., 2008; Tsukerman et al., 2012). MICA is also targeted by an IFN-γ-induced miRNA (Yadav et al., 2009).

1.2.3 Role of NKG2D ligands in tumourigenesis

The expression of NKG2D ligands by tumour cell lines has been shown to make the cells more prone to NK-cell killing. In addition, NKG2D was found to be important in tumour surveillance in spontaneous cancer models *in vivo*. Mice deficient in NKG2D were crossed with the TRAMP (transgenic adenocarcinoma of the mouse prostate) mice and they developed spontaneous prostate tumours at a higher frequency (Guerra et al., 2008). The authors also assessed the role of NKG2D in a model of lymphoid tumorigenesis using transgenic mice in which the oncogene *Myc* is constitutively expressed in B cells and they found that B-cell lymphomas arose significantly earlier in the NKG2D deficient transgenic mice. These observations provides genetic evidence of a role for NKG2D in early tumour surveillance of prostate and lymphoid malignancies *in vivo*, which would provide potential cancer immunotherapy by manipulation of NKG2D-dependent tumour surveillance.

Many independent pathways that are activated in cancer cells are likely to act together in the induction of NKG2D ligands (Figure 1.10). In the early stages of tumorigenesis, the cell undergoes a hyperproliferative in association with the activation of oncogenes or the loss of gatekeeper tumor suppressors. Cell cycle entry usually needs active E2F transcription factors, which also transcriptionally activate various NKG2D ligands. Proliferation is also linked to the induction of MICA, MICB, and several ULBPs in human cells (Jung et al., 2012; Venkataraman et al., 2007a). In addition, several oncogenes have been proposed to transcriptionally activate NKG2D ligand genes (Raulet et al., 2013).

The hyperproliferative state usually results in activation of p19ARF and/or the DDR, both of which activate the p53 tumor suppressor, which act as a key barrier to tumorigenesis. Activated p53 can promote transcription of certain NKG2D ligands, such as ULBP1 and 2 (Li et al., 2011; Textor et al., 2011) in human cells. Finally, the heat shock stress response, which is commonly activated in tumor cells (Garrido et al., 2006), has been linked to transcription of MICA and MICB ligands in human cells.

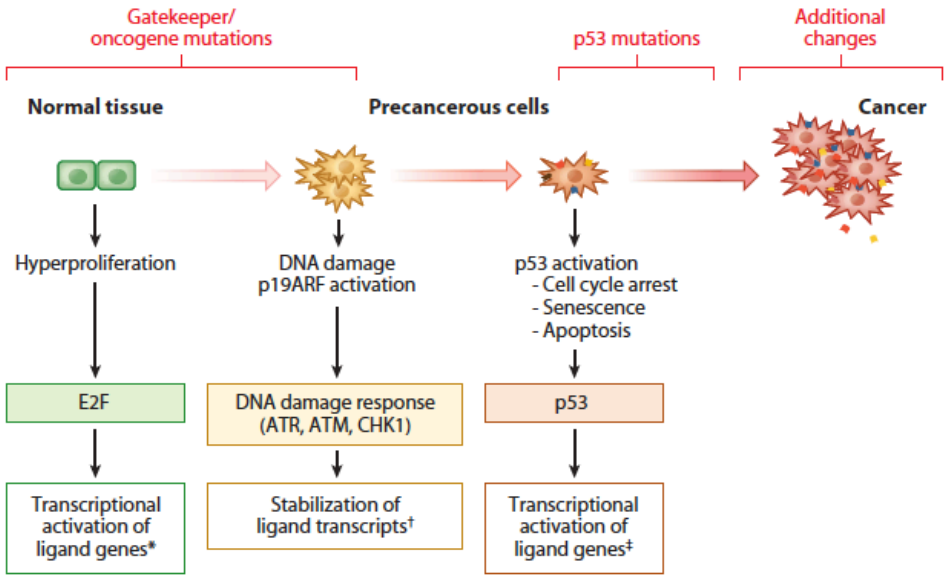

Figure 1.10 Regulation of NKG2D ligands in the multistep process of tumorigenesis.
The figure shows various regulators of NKG2D ligand expression in the multistep process of tumorigenesis. Tumorigenesis may initiate with loss of gatekeeper tumor suppressors and activation of oncogenes, resulting in hyperproliferation. Reprinted from (Raulet et al., 2013) with permission from the Annual Review of Immunology, Volume 31 © 2013 by Annual Reviews, http://www.annualreviews.org.

1.3 Nucleic acid sensing

The cellular innate immune system consists of different groups of cellular sensors, to sense and eliminate microbes rapidly in a non-specific manner. They include the Toll-like receptors (TLRs), retinoid acid-inducible gene I (RIG-I)-like receptors (RLRs) and other cytosolic nucleic acid sensors, and nucleotide-binding and oligomerization domain (NOD)-like receptors (NLRs) (Figure 1.11).

The importance of these sensors in protecting against pathogens is shown by their ubiquitous distribution, diversity, strategic positions as sentinels (both on cell surfaces and within intracellular compartments), and the increased risks infections in humans and mice carrying loss-of-function mutations that affect these receptors or their signaling partners. They function mainly to detect various pathogen-associated molecular patterns (PAMPs) such as lipopolysaccharide (LPS), lipopeptides, RNA and DNA or damage-associated molecular patterns (DAMPs) released from stressed or dying cells. Excessive activation might lead to autoimmune disease. An example is systemic lupus erythematosus (SLE), which has been linked to aberrant DNA recognition Although SLE is a multifactorial disease, several causes of SLE-like diseases have been identified such as mutations in deoxyribonuclease I, II and III (Hornung and Latz, 2010).

Many PRRs, including some of the TLRs and cytoplasmic RNA/DNA sensors, trigger a TANK-binding kinase 1 (TBK1) and interferon regulator factors 3 (IRF3)-dependent type I interferon and cytokine response (Figure 1.7). Recently identified candidate cytosolic DNA sensors include ZBP1 (Z-DNA-binding protein 1); AIM2 (absent in melanoma 2); IFI16 (interferon,

gamma inducible protein 16) and its mouse ortholog p204; HMGB1 (high mobility group box protein 1); LRRFIP1 (leucine rich repeat (in FLII) interacting protein 1); DDX41 (DEAD (Asp-Glu-Ala-Asp) box polypeptide 41) and cyclic guanosine monophosphate-adenosine monophosphate synthase (cGAS) (Hornung et al., 2009; Sun et al., 2013; Takaoka et al., 2007; Unterholzner et al., 2010a; Yanai et al., 2009a; Yang et al., 2010; Zhang et al., 2011b). With the exception of AIM2, upon recognizing DNA these sensors activate TBK1 and/or the related serine threonine kinase IKK-related kinase epsilon (IKK ε). Activated TBK1 or IKK ε directly phosphorylate IRF3, which is translocated to the nucleus and stimulates transcription of numerous genes that are critical in the immune response, including *Ifnb* (Fitzgerald et al., 2003; Pomerantz and Baltimore, 1999; Sharma et al., 2003; Shimada et al., 1999). Although TBK1 and IKK ε appear to be partially functionally redundant, IKK ε is preferentially expressed in lymphocytes, whereas TBK1 is constitutively expressed in embryonic and adult fibroblasts (Perry et al., 2004) and our own unpublished data) and is required in these cells for normal IRF3 activation and IFN-β production induced by dsRNA (Hemmi et al., 2004). In response to activation, cytoplasmic IRF3 is phosphorylated, undergoes dimerization and translocates into the nucleus (Hiscott et al., 2003; Honda and Taniguchi, 2006; Takeda and Akira, 2005; Taniguchi et al., 2001). Nuclear IRF3 binds to the IFN-stimulated response element (ISRE) in the promoter regions of IFN-β, chemokine (C-C motif) 5(*Ccl5*) and other target genes, thereby upregulating their transcriptional activities (Kim et al., 2000; Parekh and Maniatis, 1999).

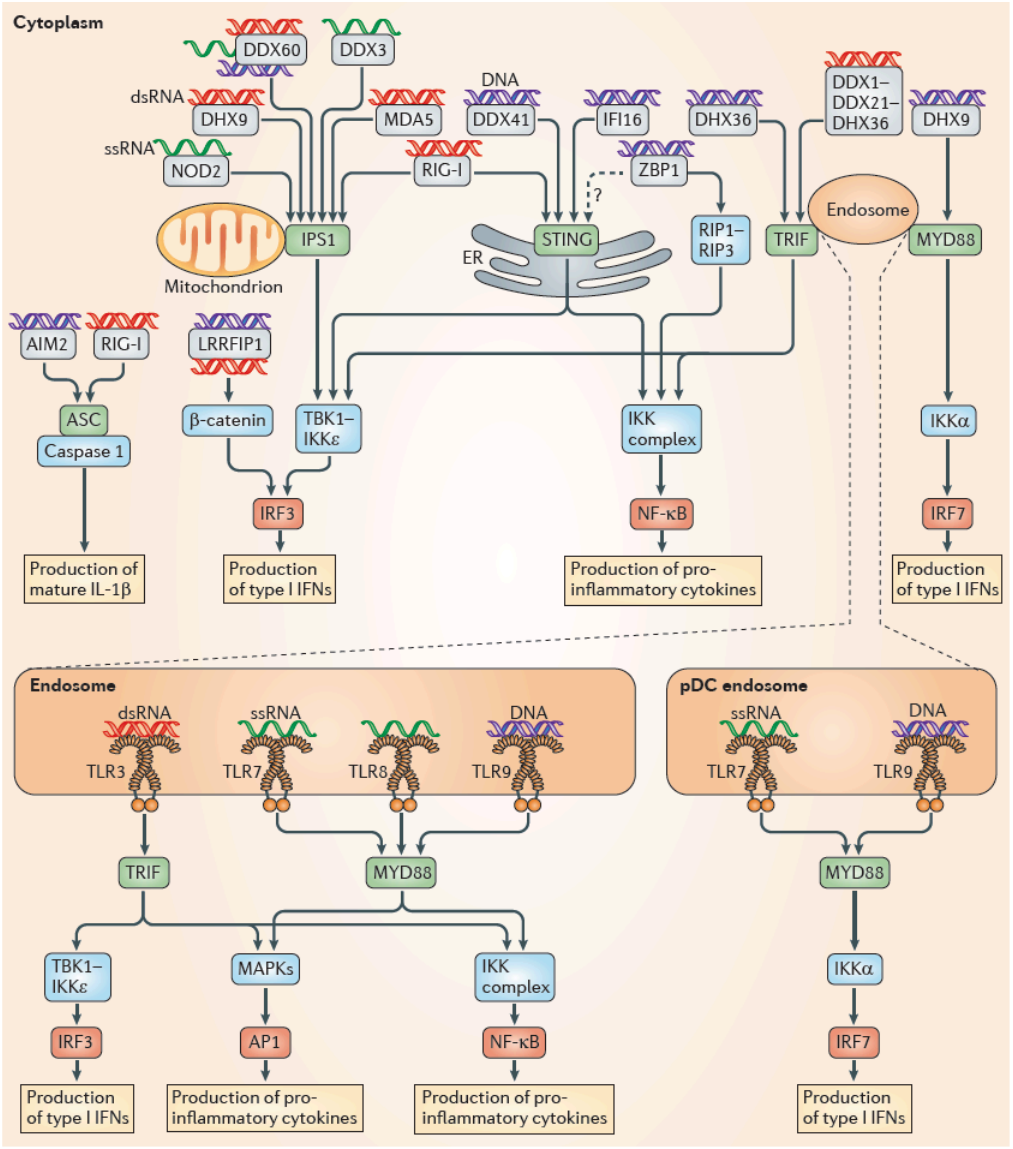

Figure 1.11 Overview of the nucleic acid sensing machinery.
Endosomal Toll-like receptor 7 (TLR7), TLR8 and TLR9 signal via the adaptor protein myeloid differentiation primary-response protein 88 (MYD88) in the cytosol, leading to the activation of mitogen-activated protein kinases (MAPKs) and the IκB kinase (IKK) complex subsequent activation of the transcription factors activator protein 1 (AP1) and nuclear factor-κB (NF-κB). Endosomal TLR3 signals through TIR-domain-containing adaptor protein inducing IFNβ (TRIF), which may activate IRF3 through TANK-binding kinase 1 (TBK1) and IKKε, resulting in the expression of type I IFNs. Various cytosolic receptors — including nucleotide-binding oligomerization domain protein 2 (NOD2), the RIG-I-like receptors (RLRs) retinoic acid-inducible gene I (RIG-I) and melanoma differentiation-associated protein 5 (MDA5), and some other DExD/H-box helicases — may promote the expression of pro-inflammatory cytokines and type I IFNs through the IFNB-promoter stimulator 1 (IPS1)-mediated activation of TBK1 and IKKε or through the activation of the IKK complex. The proposed cytosolic DNA receptors DDX41, IFNγ-inducible protein 16 (IFI16) and possibly Z-DNA-binding protein 1 (ZBP1) interact with stimulator of IFN genes (STING) to activate

TBK1, IKKε and the IKK complex. The helicases DDX1, DDX21 and DHX36 have been thought to form a TRIF-interacting complex, and LRRFIP1 (leucine-rich repeat flightless-interacting protein 1) was suggested to enhance IRF3 transcriptional activity through β-catenin. In pDCs, DHX36 and DHX9 activate TRIF-dependent and MYD88-dependent signalling, respectively. RIG-I and absent in melanoma 2 (AIM2) may increase inflammasome formation and caspase 1 activation through the adaptor protein ASC, leading to the release of mature interleukin-1β (IL-1β). dsRNA, double-stranded RNA; ER, endoplasmic reticulum; ssRNA, single-stranded RNA. Reprinted by permission from Macmillan Publishers Ltd: Nature Reviews Immunology (Desmet and Ishii, 2012), copyright 2012.

1.3.1 Role of cytosolic DNA sensors in tumorigenesis

Both IFI16 and AIM2, which are cytosolic DNA sensors belonging to the PYHIN family, have been proposed to function as tumour suppressor. The PYHIN (pyrin and HIN200 domain-containing proteins) family consists of the mouse IFN-inducible genes *Ifi200*, *p202a*, *p202b*, *p203*, *p204*, *myeloid cell nuclear differentiation antigen 1 (Mnda1)*, and *Aim2*, and the human HIN-200 genes *IFI16*, *MNDA*, *AIM2* and *PYHIN1* (Gariglio et al., 2011). Many PYHIN family members were also shown to modulate proliferation, differentiation, and transcriptional regulation (Asefa et al., 2004; Cresswell et al., 2005; Johnstone and Trapani, 1999).

Increased expression of IFI16 protein in normal human diploid fibroblasts and prostate epithelial cells had been linked to cellular senescence-associated permanent cell growth arrest (Choubey et al., 2008). In line with this finding, expression of IFI16 was downregulated in breast cancer tissue (Fujiuchi et al., 2004) and transcriptional silencing of IFI16 via histone deacetylase (HDAC) was found in human prostate cancer cell lines (Alimirah et al., 2007). IFI16 could negatively regulate p53 as inhibition of endogenous IFI16 expression by small interfering RNA (siRNA) induces $p21^{Waf1}$ mRNA and protein expression through p53 but does not induce pro-apoptotic p53

target genes (Kwak et al., 2003). Overexpression of IFI16 in cells inhibits cell proliferation by promoting the p53/p21- and RB/E2F-mediated inhibition of cell-cycle progression, and downregulation of IFI16 contributes to oncogenesis (Liao et al., 2011; Ludlow et al., 2005). IFI16 had been found to have *in vivo* anti-tumoral activity by promoting apoptosis of tumor cells, by inhibiting neo-vascularisation, and by increasing the recruitment of macrophages through the release of chemotactic factors through xenografts experiments using cell lines derived from head and neck squamous cell carcinoma (Mazibrada et al., 2010).

AIM2 was originally cloned in a functional screen to identify putative tumor suppressor genes present on chromosome 6, which is often mutated in human melanomas, colorectal carcinomas, gastric and endometrial cancers (DeYoung et al., 1997; Michel et al., 2010; Ray et al., 1996; Woerner et al., 2003; Woerner et al., 2005; Woerner et al., 2007). Extensive studies had been done on how overexpression of AIM2 suppressed proliferation and increased the rate of apoptosis of several cells ,similar to the effects of other members of the HIN-200 family of proteins (Asefa et al., 2006; Asefa et al., 2004; Chen et al., 2006; Choubey et al., 2000; Ding et al., 2004; Johnstone and Trapani, 1999; Landolfo et al., 1998; Patsos et al., 2010; Trapani et al., 1992). Restoration of AIM2 expression in AIM2-deficient colon cancer cells increased the mestastic potential of colorectal cancer (Chen et al., 2006; Patsos et al., 2010). Inhibition of AIM2 expression in human diploid fibroblasts leads to the activation of the DDR,thus implicating a role of AIM2 in the maintenance of genomic stability in cells which is one of the hallmarks of cancer (Duan et al., 2011). In addition, expression of AIM2 innibits cell

proliferation and mammory tumour growth in a mouse model (Chen et al., 2006). AIM2 are over-expressed in Epstein-Barr virus (EBV)-associated nasopharyngeal carcinoma (NPC), and the expression levels correlate with patient's survival (Chen et al., 2012). AIM2 is necessary for production of IL-1β induction by EBV genomic DNA and EBV-encoded small RNAs in tumour cells, and this tumour-derived IL-1β would inhibit tumour growth and promote survival through host responses (Chen et al., 2012).

LRRFIP1 recognize both cytosolic dsDNA and dsRNA in macrophages infected by *Listeria monocytogenes* and vesicular stomatitis virus (Yang et al., 2010). Upon activation, LRRFIP1 interacts with β-catenin and promotes β-catenin activation, which would enhance recruitment of the p300-histone acteyltransferase complex to the *Ifnb1* promoter through IRF3, leading to the transcription of *Ifnb*. LRRFIP1 has been shown to be upregulated in breast cancers and Burkitt lymphomas (Ariake et al., 2012; Rikiyama et al., 2003; Sjoblom et al., 2006) and it promotes colorectal cancer metastasis and liver invasion by regulating RhoA-induced cell adhesion, migration, and invasion of cancer cells (Rikiyama et al., 2003; Sjoblom et al., 2006). LRRFIP1 is also one of the targets of the microRNA-21 (miR-21), which is overexpressed in many cancers such as glioblastoma (Li et al., 2009b). Suppression of miR-21 could upregulate the expression of its LRRFIP1, which can inhibit NF-κB activation, and promotes the topoisomerase II inhibitor VM26-mediated cell death in glioblastoma multiforme cells (Li et al., 2009b). LRRFIP1 could contribute to resistance of cells to the topoisomerase II inhibitor VM-26 and the two genotoxic drugs cisplatin and doxorubicin (Li et al., 2009b; Shen et al., 2012).

HMGB1 is a highly versatile molecule that is involved in diverse functions such as recognition of cytosolic DNA, regulation of chromatin structure, transcription and DNA repair. It can bind both distorted and damaged DNA (Lange and Vasquez, 2009; Sims et al., 2010). HMGB1 expression has been found to be upregulated in several tumors and tumor endothelium (van Beijnum et al., 2009). The metastatic potential of cancer cells was found to correlate with HMGB1 expression, possibly due to its ability to modulate the adhesion of cells, the extracellular matrix and angiogenesis (Brezniceanu et al., 2003; Chung et al., 2009; Ellerman et al., 2007; Sparvero et al., 2009). HMGB1 can also promote endothelial cell proliferation *in vitro* and neovascularization *in vivo* (Schlueter et al., 2005). Consistent with a role for HMGB1 in cancer, inhibiting HMGB1 blocks proliferation of tumors and the ability to metastasize in a mouse model for lung cancer (Taguchi et al., 2000). In addition, HMGB1, which was released from tumor cells treated with different genotoxic agents, was found to enhance processing and cross-presentation of tumor antigens by dendritic cells (Apetoh et al., 2007).

1.3.2 ZBP1 (Z-DNA-binding protein 1)

ZBP1(Z-DNA-binding protein 1, also known as DNA-dependent activator of IRFs (DAI) or DLM1) is the first cytosolic DNA sensor identified (Takaoka et al., 2007). It has three DNA-binding domains in its N-terminal, Zα, Zβ and D3 (Figure 1.12). It shares similar DNA binding domains to ADAR1 (Adenosine deaminase acting on RNase 1), an RNA editing enzyme (Zα and Zβ) and the protein of vaccinia virus, E3L (Zα) (Vilaysane and Muruve, 2009). Its C-terminal contains multiple phosphorylation sites, which

may participate in various signal transduction pathways. ZBP1 is expressed ubiquitiously in various tissues such as the spleen, thymus, liver, lung and heart (Fu et al., 1999). Upon binding to dsDNA, ZBP1 would form a complex with TBK1 and IRF3 at its C terminal (Takaoka et al., 2007). IRF3 will be phosphorylated and it would form a dimer and translocate to the nucleus and induce the expression of type 1 interferons (IFNs) gene. Recent studies have also shown that ZBP1 is involved in the activation of NF-κB through interaction with RIP1 (receptor interacting protein kinase 1) and RIP3 via their RHIM (RIP homotypic interaction motif) domains (Kaiser et al., 2008). This result in the production of proinflammatory cytokines such as IL-6 and the induction of necrosis. ZBP1 could form a compex with RIP3 to mediate virus-induced necrosis that is targeted by murine cytomegalovirus infection (Upton et al., 2012). ZBP1 recognises DNA irrespective of the sequences, but the induction of IFN requries a minimum length requirement of 100bp (Vilaysane and Muruve, 2009).

ZBP1 is an interferon-inducible gene and the expression of ZBP1 can be upregulated by treatment with type I and II IFN (Takaoka and Taniguchi, 2008) and PAMPs, which include dsDNA and lipopolysaccharides (LPS). ZBP1 mainly resides in the cytoplasm and forms stress granules when cells are exposed to stress such as oxidative stress, viral infection or UV radiation (Takaoka and Taniguchi, 2008).

ZBP1 has been linked to autoimmune diesase. Expression of ZBP1 was increased in SLE patients as well as in lupus mice (Zhang et al., 2013). In

addition, ZBP1 was reported to promote lupus nephritis by activating the calcium pathway (Zhang et al., 2013).

A link of ZBP1 to cancer was suggested by the finding that *Zbp1* is highly upregulated in the peritoneal lining tissue of mice bearing ascites tumors (Fu et al., 1999). The role of ZBP1 in cancer still remains unclear and one of the aims of the study is to investigate the role of ZBP1 in the transgenic Eμ-*Myc* model, which developes spontaneous tumour.

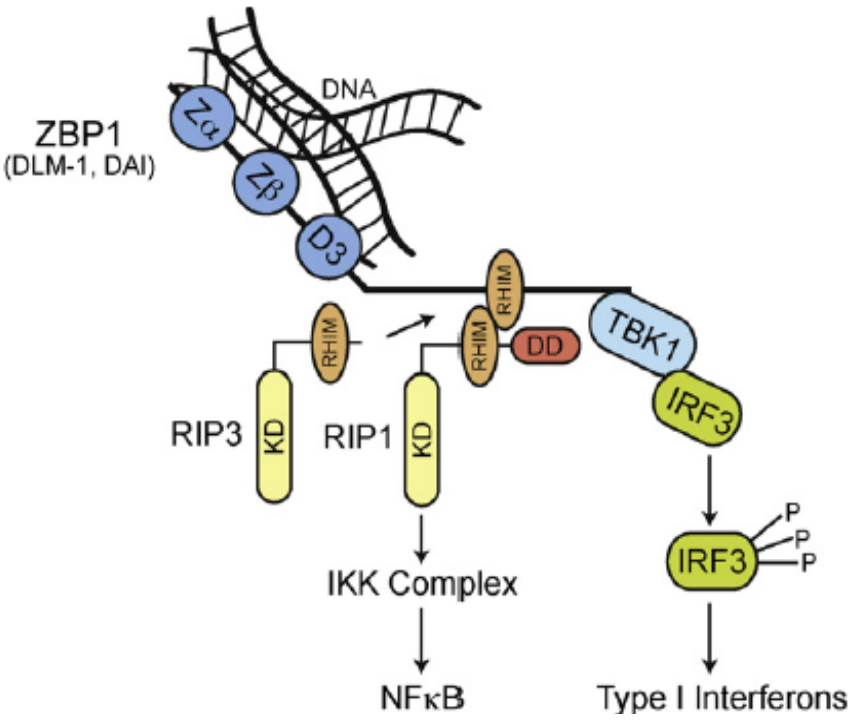

Figure 1.12 Schematic drawing of the main domains of ZBP1.
ZBP1 binds DNA via its Zα, Zβ and D3 domains. The RHIM domain interacts with RIP1 and RIP3. The carboxy-terminal of the protein is required for type1 interferon pathways involing TBK1 and IRF3. Reprinted from (Vilaysane and Muruve, 2009) with permission from Elsevier.

1.4 Eμ -*Myc* mouse model

In the Eμ-*Myc* transgenic mouse model, the Eμ-*Myc* mice express *c-Myc* on B cells under control of the immunoglobulin heavy chain enhancer (Eμ) and the mice develop Burkitt-like pre-B and B cell lymphomas (Adams et al., 1985). *Myc* is deregulated in 70% of all human malignancies (Meyer and Penn, 2008) and the genetics of the Eμ-*Myc* mice resembles that of acute lymphoblastic leukaemia (ALL) or non-Hodgkin's lymphomas in humans. Sustained expression of MYC has been shown to cause DNA damage in tumour cells through various mechanisms (Pusapati et al., 2006a; Ray et al., 2006; Vafa et al., 2002a). DNA damage and the ensuing DDR have been proposed to represent an anticancer barrier in early tumorigenesis (Bartek et al., 2007; Bartkova et al., 2005; Gorgoulis et al., 2005a).

There are at least two types of DNA damage associated with *Myc* overexpression. ROS production, which has been shown to increase where *Myc* is deregulated, can increase oxidative damage (Vafa et al., 2002b). Another source of *Myc*-induced DNA damage is replication stress, which represents the generation of aberrant DNA replication intermediates that lead to the accumulation of DDR markers at sites of active DNA replication. *Myc*-induced DDR are responsible for the genomic and chromosomal instability commonly linked with *Myc* hyper-activation. Various chromosomal abnormalities including translocations, dicentric chromosomes and tetraploidy have been reported upon *Myc* overexpression (Felsher and Bishop, 1999). ATM has been reported to regulate *Myc*-induced DDR (Maclean et al., 2007; Pusapati et al., 2006b; Reimann et al., 2007). Both DDR and apoptosis induced by *Myc* were reduced upon ATM loss, while tumorigenesis was

greatly accelerated in Eμ-*Myc* deficient in *Atm*. The role of ATM in regulating *Myc*-induced tumor suppressive DDR, was further confirmed in a mouse model of skin cancer suggesting that the relevance of this pathway in suppressing *Myc*-induced tumors suppression is not limited to hematological malignancies, but can be applied to solid tumors (Pusapati et al., 2006b). In support of these findings, genetic analysis of mice lacking wild-type p53-induced phosphatase 1 (WIP1), a protein phosphatase that negatively regulates ATM, suggest that loss of WIP1 protect against Eμ-*Myc* induced lymphomas (Shreeram et al., 2006). Similar results were reported for the haploinsufficient tumor suppressor histone acetyltransferase HTATIP (TIP60) (Gorrini et al., 2007), a histone acetyl transferase (HAT) that has been associated in the regulation of the DDR via activation of ATM (Sun et al., 2005) and of DNA repair through a multifunctional complex with HAT and chromatin remodeling activities. Loss of one TIP60 allele in Eμ-*Myc* transgenic mouse impaired ATM activation, p53 phosphorylation on Serine 18 and H2AX phosphorylation, thereby accelerating tumorigenesis.

Previous studies of Eμ-*Myc* mice demonstrated proliferating immature B cells appearing in the periphery after birth, followed by their disappearance after around 6 weeks of age and the appearance of B-cell lymphomas in 50% of mice by 15 to 20 weeks of age (Harris et al., 1988; Langdon et al., 1986; Sidman et al., 1993b). The mechanisms underlying their disappearance are poorly understood. Our lab has found that tumour cells in young Eμ-*Myc* mice undergo spontaneous rejection mediated by DNA-damage induced DNAM-1 ligand expression and the rejection of tumour cells depends on natural killer cells and T cells (Croxford et al., 2013).

1.5 Aims

Whether or how the DDR signaling pathway leading to NKG2D ligand expression intersects or interacts with signaling by PRRs has not been investigated in detail, though there are indications that PRRs can stimulate NKG2D ligand expression (Hamerman et al., 2004). One of the aims of the project is to investigate if molecules involved in the PRR can regulate NKG2D ligands. We would also like to investigate the role of one of the DNA sensors, ZBP1, in tumourigenesis using the Eμ-*Myc* mouse model.

Chapter 2: Materials and methods

2.1 Mice and cells

C57BL/6 mice were purchased from the Centre for Animal Resources at the National University of Singapore. Eμ-*Myc* transgenic mice were purchased from Jackson Laboratory (USA) and *Irf3*$^{-/-}$ mice were purchased from Riken (Japan). *Zbp1*$^{-/-}$ mice (*Zbp1*^{tm1Aki}) were kindly provided by Prof. K. Ishii (National Institute of Biomedical Innovation, NIBIO) and Prof. S. Akira (iFREC, Osaka University) (Ishii et al., 2008a). Mice were bred and housed according to the guidelines by the National University of Singapore. *Zbp1*$^{-/-}$ fibroblasts, TBK1$^{-/-}$IKKε$^{-/-}$ and TBK1$^{+/+}$IKKε$^{+/+}$ mouse embryonic fibroblasts (MEFs) were generated as described in (Ishii et al., 2006a). BC2 cells, which were derived from Eμ-*Myc* C57BL/6/129 mice, were a generous gift by L.M. Corcoran and EμM1 cells were generated from late stage Eμ-*Myc* C57BL/6 as described (Corcoran et al., 1999). Yac-1 cells were purchased from ATCC (USA). Cells were cultured in RPMI (Invitrogen, Carlsbad, USA) supplemented with 10% FCS (Thermo Scientific^{TM} HyClone^{TM}, Waltham, USA), 50 μM 2-mercaptoethanol, 100 μM asparagine (for BC2 cells), 2mM glutamine (Sigma-Aldrich, St. Louis, USA) and 1% pen/strep (Invitrogen, Carlsbad, USA).

Cells derived from C57BL/6 such as EμM1, MEFs and tumor cells in Eμ-*Myc* mice express RAE1βδ and/or RAE1ε. In contrast, cells derived from other strains of mice including BC2 (C57BL/6 and 129) and Yac-1 (A/Sn) can express RAE1α, RAE1β, RAE1γ and RAE1δ.

2.2 Reagents

Aphidicolin, CGK733, cytosine β-D-arabinofuranoside hydrochloride (Ara-C), DMSO, Poly A:U and Poly I:C were purchased from Sigma-Aldrich

(St Louis, USA). The ATM inhibitor KU55933 and KU60019 and the ATR inhibitor VE-821 were obtained from Tocris Bioscience (Bristol, UK) and Axon Medchem (Groningen, Netherlands) respectively.The murine TLR9 ligand ODN1585, ODN1668 control (ssDNA) and LPS were purchased from InvivoGen (San Diego, USA). 8 μg of MSCV-IRES-GFP plasmid, genomic DNA or ODN1668 control were conjugated to AF488 using the Ulysis nucleic acid staining kit according to manufacturer's instructions (Invitrogen, Carlsbad, USA). 4 μg labelled DNA was transfected into cells using TransFectin™ (Bio-Rad Laboratories Inc, Hercules, USA) according to manufacturer's instructions.

2.3 Flow cytometry

2.3.1 Stainings of NKG2D ligands

Cells were stained for different NKG2D ligands using pan-Rae1-, Rae1αβγ-, Rae1βδ- and Rae1ε- (R&D Systems, Minneapolis, USA) and rat IgG-coupled to APC-specific antibodies (eBioscience, San Diego, USA). Stained cells were analyzed by multicolor flow cytometry using FACSCalibur (BD Biosciences, San Jose, USA) and FlowJo. 8.8.6 (Treestar, Ashland, USA).

2.3.2 Intracellular staining

For intracellular staining, cells were fixed with 0.25% paraformaldehyde at 37°C for 10 min, followed by addition of -20°C methanol and incubation on ice for 20 min. After washing, cells were resuspended in 2% mouse serum and stained with 1/100 rabbit-anti-phospho-IRF3-Ser396 (Cell Signaling Technology Inc, Danvers, USA) and 1/25 AF647-conjugated anti-phospho-TBK1-Ser172 antibodies (BD Biosciences, San Jose, USA) followed

by AF-488-coupled rabbit IgG-specific antibodies (Invitrogen, Carlsbad, USA). Some cells were treated with 2 U/µl λ-phosphatase (NEB, Ipswich, USA) at 37°C for 90 min. before staining. Stained cells were analyzed by multicolor flow cytometry using FACSCalibur (BD Biosciences, San Jose, USA) and FlowJo. 8.8.6 (Treestar, Ashland, USA).

2.3.3 Determination of tumour load and stainings of surface makers on T and B cells

Blood was collected by facial bleeding and red blood cells were removed by red blood cells lysis. F_c receptors on blood cells were blocked by pre-incubating cells with CD16/CD32-specific antibodies for 10 min (eBioscience, San Diego, USA). Tumor cells were stained with combinations of anti-CD45R(B220), anti-IgM, anti-CD3, anti-CD4, anti-CD8 specific antibodies (eBioscience, San Diego, USA). Cells were stained for MHC class I (H-2K^b), CD80, CD86, CXCR4 CD62L, ICAM-1 (eBioscience, San Diego, USA), DNAM-1 and CD155 (Biolegend, San Diego, USA). Tumour load was calculated as follows: $\sum$ (% IgM$^-$B220^{low}) x % B220$^+$ + (IgM$^+$B220^{low}) x % B220$^+$. Concentration of tumour cells in the blood was calculated by multiplying the lymphocyte count determined using a Scil Vet abc animal blood cell counter (Horiba, Kyoto, Japan) by the % of B220^{low} cells in a FCS/SSC gate corresponding to lymphocytes as determined by flow cytometry. Stained cells were analyzed by multicolor flow cytometry using FACSCalibur (BD Biosciences, San Jose, USA) or LSRFortessa (BD Biosciences, San Jose, USA) and FlowJo. 8.8.6 (Treestar, Ashland, USA).

2.3.4 Stainings of surface markers for NK cell maturation

Spleen and bone marrow cells were harvested and red blood cells were removed by red blood cells lysis. F_c receptors were blocked by pre-incubating

cells with CD16/CD32-specific antibodies for 10 min. Cells were then stained with anti-CD122-eFluor®450, anti-CD43-FITC, anti-Cd11b-PerCP-Cy5.5, anti-CD49b/DX5-APC, anti-CD27, anti-CD3-eFluor®780, anti-NK1.1-PE-Cy7. Stained cells were analyzed by multicolor flow cytometry using LSRFortessa (BD Biosciences, San Jose, USA) and FlowJo. 8.8.6 (Treestar, Ashland, USA).

2.3.5 Proliferation and apoptosis assay

For cell cycle analysis mice were injected i.p. with 1 mg BrdU (BD Pharmingen, San Jose, USA) and spleen and bone marrow were harvested and analyzed 18 hours later according to the manufacturer's instructions. Briefly, 1 x 10^6 cells were stained with B220-FITC and IgM-PE-Cy7 before fixing in BD Cytofix/Cytoperm buffer. Cells were then resuspended with BD Cytoperm Plus buffer and re-fixed with BD Cytofix/Cytoperm, after which cells were treated with DNase to expose incorporated DNA before staining with anti-BrdU-APC. Finally, cells were resuspended in buffer containing 7AAD and analysed using LSRFortessa (BD Biosciences, San Jose, USA) and FlowJo. 8.8.6 (Treestar, Ashland, USA). Cell aggregates or doublets were gated out from plot of width of 7AAD fluorescence signal against height of 7AAD fluorescence signal.

For *ex vivo* Annexin-V (eBioscience, San Diego, USA) staining, harvested splenocytes and bone marrow cells were cultured for 30 min to remove adherent cells before staining. For *in vitro* staining, non-adherent cells were removed to a fresh flask and cultured at 37^{o}C for 3 hours before Annexin-V staining according to the manufacturer's instructions. Briefly, 1 x 10^6 cells were stained with B220-FITC and IgM-PE-Cy7 before incubating

with Annexin-V-APC. Cells were then resuspended in buffer containing propidium iodide and analysed using LSRFortessa (BD Biosciences, San Jose, USA) and FlowJo. 8.8.6 (Treestar, Ashland, USA).

2.4 shRNA retroviral constructs

Rig-I shRNA (5'-GCCCATTGAAACCAAGAAATT-3'), *Tbk1* shRNA (5'-GAAGCCGTCTGGTGCAATA-3'), *Ikke* shRNA (5'-CACTTCATCTACAAACAGT-3') and *Irf3* shRNA (5'-GCGGTTGGCTGTTGACAAT-3') target sequences were selected based on Dharmacon's siRNA Design Center algorithm (Dharmacon, Lafayette, USA). Control shRNAs included scrambled versions of the *Rig-I* shRNA (5'-GCCCATAGAAACCTAGAAATT-3'), *Tbk1* shRNA (5'-GAAGCCGTG TGCTGCAATA-3'), and *Irf3* shRNA (5'-GCGGTTCGTTGATGGCAAT-3'). The shRNAs constructs were subcloned in the MSCV/LTRmiR30-PIG vector (Open Biosystems Inc., Huntsville, USA) containing *Gfp* and the *PuroMycinR* gene according to manufacturer's instructions. *Irf3* (TRCN0000085239, TRCN0000085240, TRCN0000085241), *Sting* (V2MM_103338) and *Zbp1* (V2MM_47227)-specific shRNAs and the non-silencing control shRNAs were purchased from (Open Biosystems Inc, Huntsville, USA).

The shRNA plasmids were transiently transfected into 293T cells using TransFectin^{TM} according to the manufacturer's instructions (Bio-Rad Laboratories Inc, Hercules, USA). 48 h after transfection, BC2 or Yac-1 cells were transduced with the viral supernatant for 90 min at 34^{o}C. The cells were then selected using puromycin (Sigma-Aldrich, St. Louis, USA) or sorted for GFP using MoFlo XDP (Beckman Coulter Inc., Brea, USA) at 48h post-transduction.

2.5 Constructs and transduction of fibroblasts

Mouse *Irf3, Tbk1 and IKKε* were subcloned adjacent to the cytomegalovirus promoter in the pMSCV2.2-IRES-GFP proviral vector (gift of W. Sha, University of California, Berkeley). Human *IRF3-EGFP* and *IRF3A7-EGFP* were gifts of S. M. McWhirter (University of California, Berkeley). The chimeric constructs were subcloned into MSCV-IRES-GFP. Retroviral supernatants were generated as described (Diefenbach et al., 2003). WT and mutant *Sting* fibroblasts were kindly provided by Dr. R. Vance (University of California, Berkeley).

2.6 Quantitative real-time RT-PCR

Total RNA was isolated using the nucleospin RNA II kit (Macherey-Nagel, Düren, Germany). Total RNA was reverse transcribed with random hexamers using M-MLV Reverse Transcriptase (Promega, Fitchburg, USA). Each amplification mixture (25 µl) contained reverse transcribed RNA, 5 µM forward primer, 5 µM reverse primer and 12.5 µl of iTaq SYBR Green Supermix with ROX (Bio-Rad Laboratories Inc, Hercules, USA). PCRs were performed in triplicates using the ABI PRISM® 7700 Sequence Detection System (Applied Biosystems, Foster City, USA). PCR thermocycling parameters were 50°C for 2 min, 95°C for 3 min, and 40 cycles of 95°C for 15 sec and 60°C for 30 sec and 72°C for 45 sec. Samples were normalized to the signal generated from the housekeeping gene HPRT or GAPDH. The following primers were used: *Hprt*-5': ctttgctgacctgctggatt; *Hprt*-3': tatgtcccccgttgactgat; *Irf3*-5': gccggacgtgtcaacctgga; *Irf3*-3': cgcgcccctggagtcacaaa; *Ifna*-5': tgacctcaaagcctgtgtgatg, *Ifna*-3': aagtatttcctcacagccagcag; *Ifnb*-5': aatttctccagcactgggtg, *Ifnb*-3': tctcccacgtcaatctttcc; *Ip-10*-5': gctgcaactgcatccatatc, *Ip-10*-3':

tttcatcgtggcaatgatct; *Ccl5*-5': accactccctgctgctttgc, *Ccl5*-3': cacacttggcggttccttcg; *Pkr*-5': ccaaagagaaaggcaggctcc, *Pkr*-3': ttcctccctccctcctccattc; *Sting*-5': tggaaatcctgtggggccctgtc; *Sting*-3': ggcttctgaatggggagacagcag; *Bcl2l12*-5': cccccacccacggagaagga, *Bcl2l12*-3': gagttccacaaggcgggcga; *Ku70-5': attttgtggctttggtgccc, Ku70-3' : tccgcttgtcatcggcataa; Hr23b-5': agccagcttcaacaaccctg, Hr23b-3': ggagttccagtactcacagcc; Rad54-5' : tgtctccttttcggaagccc, Rad54-3' : agcccaggggaccttgataa; Rad50-5': tggatggttttgagcgtgga, Rad50-3': tgtctgtcaggtcgctcaag; Mre11-5': tctcagagaggccgagacac, Mre11-3': gaaggctgttgtcgggtaga; Xrcc1-5': tgtgcgtaaagagtgggtgc, Xrcc1-3': ttttggggaagcttgggagc; Brca1T1-5': atagccactttcgggtgctg, Brca1T1-3': gatgctcggtaaggaagtctca; Brca1T2-5': gccggattacctaacacttcc, Brca1T2-3': tctgaggaaagctcctcaaacc; Ku80-5': gattgagaggcgttccatgc, Ku80-5': tcttgcgtccacaactaccc; Wrn-5': gggctttggttctcagtcctc, Wrn-3': cgcaggccttttcttctgtag; Nbs1-5': atgccaagcagcacaagaaac, Nbs1-3': acatcaacaacgcaggttcc; LigaseIV-5': gggactgatttcaggtggca, LigaseIV-3': aaccctgccgaatgaaggag; c-Jun-5': ttgctatgactgcaaagatggaaacgaccttc, c-Jun-3' :tttcaaaacgtttgcaactgctgcgttagcatga ; TNF-α-5': ccacgtcgtagcaaaccacc, TNF-α-3': ccttgtcccttgaagagaacc. Gapdh-5': gaaggtcggtgtgaacgga, Gapdh-3': gttagtggggtctcgctcct.* Samples prepared without reverse-transcription served as negative control templates.

2.7 Immunocytochemistry

IRF3-GFP or IF3A7-GFP expressing BC2 cells or Yac-1 cells were fixed with 4% formaldehyde for 10 min., rinsed once with 1 x PBS and incubated in 70% ethanol in PBS for 1 h at -20°C. For DNA stainings, cells were fixed according to manufacturer's instructions (Merck Millipore,

Billerica, USA), washed once with 1 x PBS before addition of 2 mg/ml RNase A (Sigma-Aldrich, St. Louis, USA) for 30 min at 37°C. For single-standed DNA (ssDNA) stainings, some cells were incubated with 1000 U/ml S1 nuclease (Fermentas, Waltham, USA) for 1 h at 37°C. For double stranded DNA (dsDNA) stainings some cells were pretreated with 100 U/ml Dnase (Sigma-Aldrich, St. Louis, USA) for 1 h at 37°C. After washing with 1 x PBS, cells were stained with ssDNA- (clone F7-26, Merck Millipore, Billerica, USA) or dsDNA- (MAB1293, Merck Millipore, Billerica, USA) and Cox IV (Abcam, Cambridge, UK)-specific antibodies, followed by anti-mouse IgG coupled to Cy3 (Merck Millipore, Billerica, USA), anti-rabbit IgG coupled to dylight 488 (Jackson ImmunoResearch Laboratories Inc, West Grove, USA) or anti-mouse IgM coupled to Cy3 (Merck Millipore, Billerica, USA) antibodies. Cytospins were prepared and slides were stained with DNA fluorochrome DAPI (0.05 mg/ml in PBS) (Dako, Glostrup, Denmark) for 10 min. Slides were washed once in PBS before mounting with fluorescent mounting medium (Dako, Glostrup, Denmark).

For γH2AX, RAD51 and cleaved CASPASE 3 staining, cells were cytospined and fixed with 4% formaldehyde for 15 min, rinse once with 1 x PBS and block with 1% bovine serum albumin and 2% goat serum for 1 hour. Cells were stained with γH2AX (Cell Signaling Technology Inc, Danvers USA), RAD51 (Santa Cruz Biotechnology Inc, Dallas, USA) or cleaved CASPASE 3 (Cell Signaling Technology Inc., Danvers USA) overnight at 4^{o}C before incubating with anti-rabbit IgG-DyLight-488 (Jackson ImmunoResearch, West Grove, USA) antibodies. Cells were then stained with anti-CD45R(B220) (eBioscience, San Diego, USA) before incubating with

anti-rat IgG-AF647(Invitrogen, Carlsbad, USA). Cells were mounted in mounting medium containing 0.5 μg/ml DAPI (Dako, Glostrup, Denmark).

Pictures of cells were taken using a Zeiss Axio Imager Z1 fluorescent microscope equipped with AxioVision 4.8 software (Carl Zeiss MicroImaging, Oberkochen, Germany) or a confocal TCS SP5 (Leica, Wetzlar, Germany). Pictures were analyzed using ImageJ 1.46 or Adobe Photoshop CS5 (Adobe, San Jose, USA).

2.8 *In vivo* KU60019 injections

37-39 days of age *Zbp1*$^{+/+}$Eμ-*Myc* or *Zbp1*$^{-/-}$Eμ-*Myc* mice were separated into groups with similar tumor loads. Mice received 5 mg/kg i.p. KU60019 (Tocris Bioscience, Bristol, UK) or vehicle control at 37, 39, 47, 49, 57, 59, 67 and 69 days of age. Blood tumor load was measured at 37, 44, 54, 64 and 74 days of age. The mice were also tracked for survival.

2.9 Microarray

Total RNA was extracted using TRIzol (Invitrogen, Carlsbad, USA) and purified using RNAminelute kit (Qiagen, Venlo, Netherlands) according to the manufacturer's instructions. The quality of total RNA was evaluated using Agilent Bioanalyzer (Agilent Technologies, Santa Clara, USA); only samples with RNA integrity number >7.5 were analyzed. Gene expression analysis was performed using Affymetrix GeneChip® Mouse Genome 430 2.0 Array (Affymetrix, Santa Clara, USA). cRNA preparation, purification and labeling, array hybridization, and scanning were conducted as per the manufacturer's instructions.

2.10 Western blot

Whole cell extracts were prepared from purified B220^{+} cells (> 95% purity, CD19 positive selection kit (Stem Cell Technology, Vancouver,

Canada) from the spleen and bone marrow or from cell lines and electrophoresed in 10% SDS-PAGE or pre-cast gels, and blotted onto nitrocellulose membranes (Bio-Rad Laboratories Inc., Hercules, USA). For the preparation of whole-cell extracts, cells were lysed in Radio-Immunoprecipitation Assay (RIPA) buffer consisting of 150 mM NaCl, 1 mM EDTA, 50 mM Tris-HCl (pH 7.4), 1% NP-40 and 1% sodium deoxycholate (Sigma-Aldrich, St. Louis, USA). In addition, protease inhibitor cocktail set III and phosphatase inhibitor cocktail set V (Merck KGaA, Darmstadt, Germany) were added to the lysis buffer according to the manufacturer's instructions. Antibodies specific for phospho-H2AX-Ser139 (H2AX-P-Ser139), phospho-ATM-Ser1981 (ATM-P-Ser1981), ATM, phospho-CHK1-Ser345 (Chk1-P-Ser345), CHK1, CHK2, phospho-p53-Ser15 (p53-P-Ser15), p53, pRB, phospho-Rb-Ser608 (Rb-P-Ser608), CYCLIN D1, PUMA, c-*MYC*, IRF3, phospho-IRF3-Ser396 (IRF3-P-Ser396), TBK1, phospho-TBK1-Ser172 (TBK1-P-Ser172), CASPASE3, CASPASE8, CASPASE7, NF-κB p65/RelA, phospho-NF-κB p65-Ser536 (NF-κB p65-P-Ser536) (Cell Signaling Technology Inc., Danvers, USA), CYCLIN A, BCL2L12 (clone E-13, Santa Cruz Biotechnology Inc., Dallas, USA), phospho-CHK2-Thr68 (CHK2-P-Thr68) (Pierce Thermo Scientific, Waltham, USA) and GAPDH (Sigma-Aldrich, St. Louis, USA) specific antibodies and horseradish peroxidase-coupled second stage reagents were used to develop the blots (Thermo Fisher Scientific, Waltham, USA). Blots were exposed on X-ray film (Thermo Fisher Scientific, Waltham, USA) and densitometry analysis was performed using ImageJ 1.46.

2.11 Native PAGE and immunoblotting

Dimerization of IRF3 was detected using Native PAGE using a 7.5% gel. The gel was pre-run with 25 mm Tris and 192 mm glycine, pH 8.4 with and without 1% deoxycholate (DOC) in the cathode and anode chamber, respectively, for 30 min at 40 mA. Samples in the native sample buffer (30 μg protein, 62.5 mm Tris-Cl, pH 6.8, 15% glycerol and 1% DOC) were applied to the gel and electrophoresed for 60 min at 25 mA. Immunoblotting was performed as described in 2.10.

2.12 Measurement of NK cell activity

2.12.1 CD107a degranulation assay

Mouse NK cells were isolated from C57BL/6 mice spleens using an EasySep mouse NK cell enrichment kit following the manufacturer's instructions (Stem Cell Technology, Vancouver, Canada). NK cells were cultured for another 4 days in 1 x 10^3 units/ml recombinant human IL-2 (eBioscience, San Diego, USA) before co-incubation with target cells. NK cell purity was determined by flow cytometry to be >90% of $NK1.1^+CD3^-$ cells. For the degranulation assays, 6 x 10^4 NK cells were incubated for 5 hours with 2 x 10^4 Yac-1 tumor target cells in the presence of 4.0 μg/ml anti-CD107a-PE (eBioscience, San Diego, USA), 1.0 μg/ml GolgiPlug (BD Biosciences, San Jose, USA) and 2.0 μM GolgiStop (BD Biosciences, San Jose, USA) at 37^{o}C. Cells were stained for anti-NK1.1 (eBioscience, San Diego, USA), anti-CD3 (eBioscience, San Diego, USA) and intracellular IFN-γ (eBioscience, San Diego, USA) according to the manufacturer's protocol (BD Pharmingen, San Jose, USA).

2.12.2 *In vitro* activation of NK cells

96-well plate was pre-coated with either 10 μg/ml of anti-mouse

NKG2D (MI6, eBioscience, San Diego, USA) or rat IgG2a κ isotype control (eBioscience, San Diego, USA) overnight at 4°C as previously described (Guerra et al., 2008). Freshly isolated splenocytes were harvested and added to each well. Some splenocytes were incubated with Leukocyte Activation Cocktail with Golgi Plug (BD Biosciences, San Jose, USA) to serve as positive control. In summary, 1 x 10^6 cells/well were stimulated for 5 hr at 37°C in the presence of 1.0 μg/ml Golgi Plug (BD Biosciences, San Jose, USA) and 1 x 10^3 units/ml recombinant human IL-2 (eBioscience, San Diego, USA) before staining of surface markers and intracellular IFNγ as described above.

2.13 ELISA

The quantification of TNF-α was determined using ELISA kits (R&D systems, Minneapolis, USA), and quantification of IL-6 was determined using ELISA Ready Set Go kits (eBioscience, San Diego, USA) according to the manufacturer's instructions.

2.14 Statistical analyses

Mean percentages of tumor load between groups was compared using 2-tailed unpaired *t*-tests (GraphPad Prism 5.0, La Jolla, USA). Survival was represented by Kaplan-Meier curves and statistical analysis of survival was performed with the log rank Mantel-Cox Test and Gehan-Breslow-Wilcoxon Test. $P < 0.05$ denotes significance.

Chapter 3: TBK1 and IRF3 are necessary for RAE1 expression in response to DNA damage

3.1 IRF3 is activated upon DNA damage in BC2 cells

IRF3 was previously shown to be activated in response to DNA damaging agents (Kim et al., 1999a; Servant et al., 2002). We therefore investigated the role of IRF3 in the expression of NKG2DLs in cells exposed to DNA damaging agents. Phosphorylation of serine 396 (serine 388 of mouse IRF3) has been shown to be critical for the activation of IRF3 (Hiscott et al., 2003). Using flow cytometry to detect phosphorylation of IRF3S388, we observed increased phosphorylation of IRF3 after treatment with the DDR-inducing agents Ara-C or aphidicolin in BC2 cells, a cell lined derived from Eμ-*Myc* (Figure 3.1a). The relatively late kinetics of IRFS388 phosphorylation was similar to the kinetics we previously observed for upregulation of NKG2DLs in response to DNA damage (Gasser et al., 2005). We also saw increase phosphorylation of endogenous IRF3 and formation of endogeneous IRF3 dimer in response to Ara-C treatment in BC2 cells (Figure 3.1b), although not to the same degree as LPS, a known inducer of IRF3 (Stein and Falck-Pedersen, 2012). Treatment of BC2 cells with Ara-C also induced activated IRF3 characterized by nuclear translocation of overexpressed chimeric IRF3-GFP (Figure 3.1c and d) consistent with previous reports (Kim et al., 1999a; Servant et al., 2002). No nuclear translocation was observed with a kinase-dead mutant of IRF3 (IRF3A7-GFP) that is unable to be activated (Figure 3.1c and d). The data suggest activation of IRF3 in response to DNA damaging agents in BC2 cells.

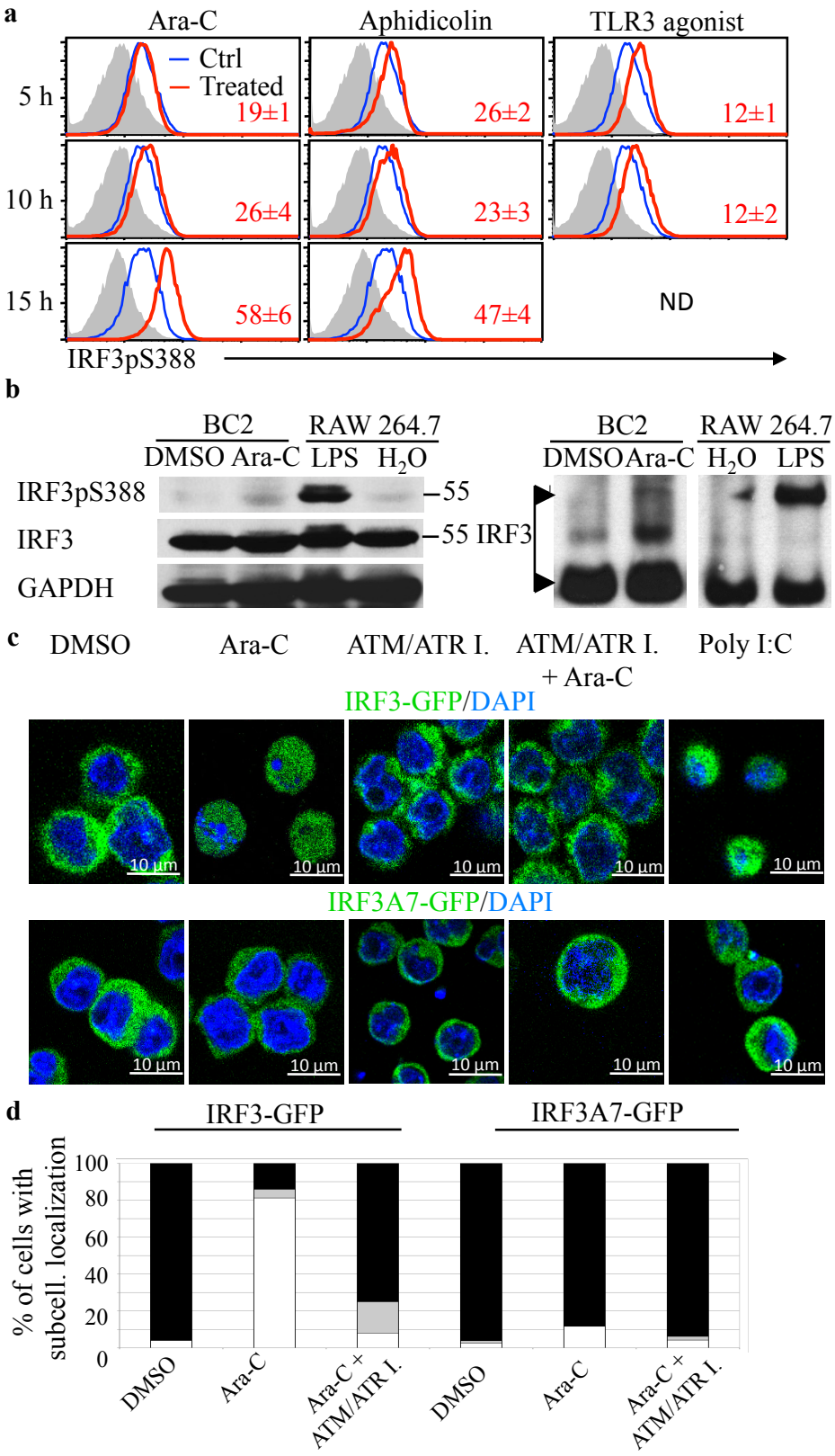
a
Ara-C
Aphidicolin
TLR3 agonist
Ctrl
Treated
5 h
10 h
15 h
19±1
26±2
12±1
26±4
23±3
12±2
58±6
47±4
ND
IRF3pS388
b
BC2
RAW 264.7
DMSO Ara-C LPS H2O
BC2
RAW 264.7
DMSO Ara-C H2O LPS
IRF3pS388
IRF3
GAPDH
55
55 IRF3
c
DMSO
Ara-C
ATM/ATR I.
ATM/ATR I. + Ara-C
Poly I:C
IRF3-GFP/DAPI
IRF3A7-GFP/DAPI
10 µm
d
IRF3-GFP
IRF3A7-GFP
% of cells with subcell. localization
100
80
60
40
20
0
DMSO
Ara-C
Ara-C + ATM/ATR I.
DMSO
Ara-C
Ara-C + ATM/ATR I.

Figure 3. 1 IRF3 is activated by the DDR in BC2.
(a) Kinetics of IRF3-S388 phosphorylation in BC2 cells treated with 10 μM Ara-c, 4 μM aphidicolin, 10 μg/ml TLR3 agonist Poly I: C (red lines) or DMSO (blue line) detected by flow cytometry. Filled histograms depict isotype staining of Ara-C treated cells. Median fluorescence intensity (MFI) ± SD of three independent experiments are shown. **(b)** Phosphorylation (left panel) and dimerization (right panel) of IRF3 in response to 14 hours of 10 μM Ara-C treatment detected by Western blotting and native gel respectively. For comparison, Raw 264.7 cells were treated with LPS, a known activator of IRF3 for 2 hours. Both the monomeric and dimeric IRF3 forms were detected by Western blotting using anti-IRF3 antibody and are indicated by arrows**. (c)** 10 μM Ara-C induces nuclear localization of transduced IRF3-GFP in BC2 cells. Cells treated with 10 μg/ml Poly I: C served as a positive control. Kinase-dead IRF3A7-GFP failed to undergo nuclear localization. Some cells were treated with 10 μM of the ATM/ATR-specific inhibitor CGK733, which prevented IRF3 nuclear localization. FACS sorted GFP^+ transductants were treated for 16 hours 9 days after transduction. Localization of IRF3 in DAPI stained cells was analyzed by confocal fluorescent microscopy. Representative image from 3 independent experiments are shown.**(d)** Quantification of DMSO, Ara-C and Ara-C with ATM/ATR inhibitor treated cells shown in (c). Nuclear (black), partial nuclear (grey) and cytoplasmic localization are indicated as stacked columns. >100 cells are counted for each treatment. Immunoblot data on phosphorylation of IRF3-S388 were kindly provided by Dr Nina Le Bert. All experiments were repeated at least three times

3.2 IRF3 is required for RAE1 expression in response to DNA damaging agents in BC2 cells

To test if IRF3 is required for DDR-mediated upregulation of NKG2DLs, we transduced BC2 cells with an *Irf3*-specific shRNA. Compared to a control shRNA, the *Irf3*-specific shRNA significantly inhibited the upregulation of RAE1 ligands of NKG2D, in response to Ara-C (Figure 3.2). No consistent effects were observed for the NKG2DLs MULT-1 and H60.

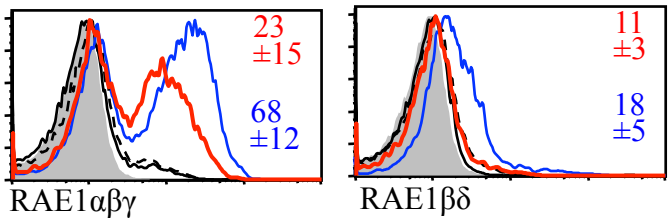

Figure 3.2 IRF3-specific shRNA inhibits RAE1 expression in BC2 cells treated with 10 µM Ara-C for 16 hours.
Cells were transduced with retroviral vectors encoding IRF3 shRNA and GFP (red line) or control shRNA and GFP (blue line), and cultured for 5 days before treatment. Gated GFP^+ (transduced) cells were analyzed. DMSO-treated IRF3 shRNA-transduced (dashed line) or control shRNA-transduced cells (dotted line) are also shown. Filled histograms depict isotype staining of Ara-C-treated BC2 cells. MFI ± SD of 3 independent experiments are indicated.

3.3 IRF3 is activated constitutively in Yac-1 cells

The DDR is constitutively activated in many tumor cell lines (Bartek and Lukas, 2003; Mills et al., 2003; Sieber et al., 2003). Activation of ATM and other components of the DDR pathway is also observed in precancerous lesions (Bartkova et al., 2005; Gorgoulis et al., 2005a). As a result many tumor cell lines constitutively express NKG2D ligands (Gasser and Raulet, 2006c; Raulet, 2003). As expected if the DDR is activated in tumor cells and stimulates IRF3, S388-phosphorylated IRF3 was readily detected in Yac-1 cells by intracellular staining (Figure 3.3a). The staining was specific for phosphorylated IRF3, because it was abrogated when the permeabilized Yac-1 cells were pretreated with λ-phosphatase before staining. Inhibition of IRF3 expression in Yac-1 cells by shRNA decreased the expression level of IRF3 target genes (Figure 3.3b). IRF3-GFP, when transduced into Yac-1 cells, was frequently localised to the nucleus, indicating that IRF3 is often activated in Yac-1 cells (Figure 3.3c). In contrast, kinase-dead IRF3A7 exhibited an exclusively cytoplasmic localization pattern in Yac-1 cells. In summary, the data suggest that IRF3 is constitutively activated in Yac-1 cells.

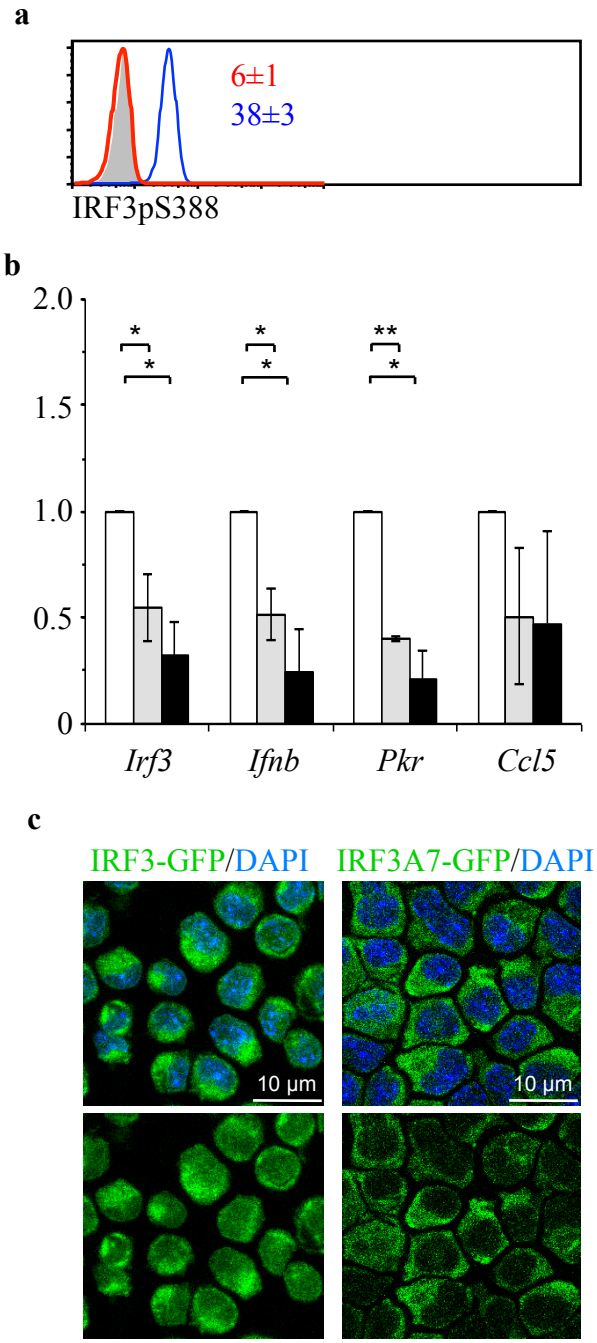

Figure 3. 3 IRF3 is activated constitutively in Yac-1 cells.
(a) Phosphorylation of IRF3-S388 in Yac-1 cells was detected by flow cytometry before (blue line) or after (red line) pre-treating the cells with λ-phosphatase. The filled histogram shows isotype-staining of untreated Yac-1 cells. MFI ± SD of 3 independent experiments are indicated. **(b)** Relative mRNA of indicated IRF3 target genes in Yac-1 cells transduced with different *Irf3*-specific shRNAs (grey and black bars) or control shRNA (white bar). mRNA levels of the indicated IRF3 target genes were analyzed by real-time PCR. Means ± SD of 3 independent experiments normalized to control shRNA-transduced cells are shown. p values are indicated as $^{*}p < 0.05$ and $^{**}p < 0.01$. Data was kindly provided by Dr Nina Le Bert. **(c)** Constitutive nuclear localization in Yac-1 cells of transduced IRF3-GFP but not IRF3A7-GFP. DAPI-stained cells were examined by confocal microscopy 7 days after FACS sorting of GFP^{+} cells. Bottom panels shown without DAPI staining. Representative images from 3 independent experiments are shown.

3.4 IRF3 is required for constitutive RAE1 expression in Yac-1 cells

To test whether IRF3 plays a role in maintaining constitutive Rae1 expression on tumor cell lines, we determined whether IRF3 shRNA inhibited ligand expression in these cells. Compared to control shRNA, the *Irf3*-specific shRNA caused a significant reduction in the amount of Rae1 displayed on the cell surface of Yac-1 cells (Figure 3.4). The incomplete reduction in cell surface RAE1 by IRF3 shRNA may reflect in part incomplete turnover of preformed RAE1. These data suggest that IRF3 is constitutively activated in several tumor cell lines and that the optimal expression of RAE1 requires IRF3 function.

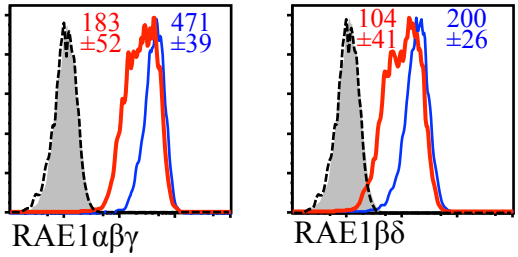

Figure 3.4 IRF3-specific shRNA inhibits constitutive RAE1 expression in Yac-1 cells.
Cells transduced with vectors encoding GFP and IRF3-specific shRNA (red line) or control shRNA (blue line) were selected for 5 days in puromycin. Transduced cells were examined by gating on GFP^+ cells. Isotype control staining of IRF3 shRNA (dotted line) or control shRNA (filled histogram) transduced cells is also shown. MFI ± SD of 3 independent experiments are indicated.

3.5 TBK1 is necessary for RAE1 expression in response to DNA damaging agents in BC2 cells

IRF3 is activated by the two IKK-related serine/threonine kinases, TBK1 and IKKε (Fitzgerald et al., 2003; Pomerantz and Baltimore, 1999; Sharma et al., 2003; Shimada et al., 1999), prompting us to examine the role of TBK1 and IKKε in RAE1 expression. We initially tested whether TBK1 was phosphorylated on serine 172 in response to DNA damage. Similar to results with IRF3, substantial TBK1 phosphorylation was detected after Ara-C or aphidicolin treatment, and phosphorylation occurred with relatively late kinetics over a 25-hour period (Figure 3.5). Induction of TBK1 phosphorylation by Poly I: C occurred much more rapidly, as expected. We have not similarly assessed IKKε phosphorylation due to the lack of available phospho-IKKε-specific antibodies.

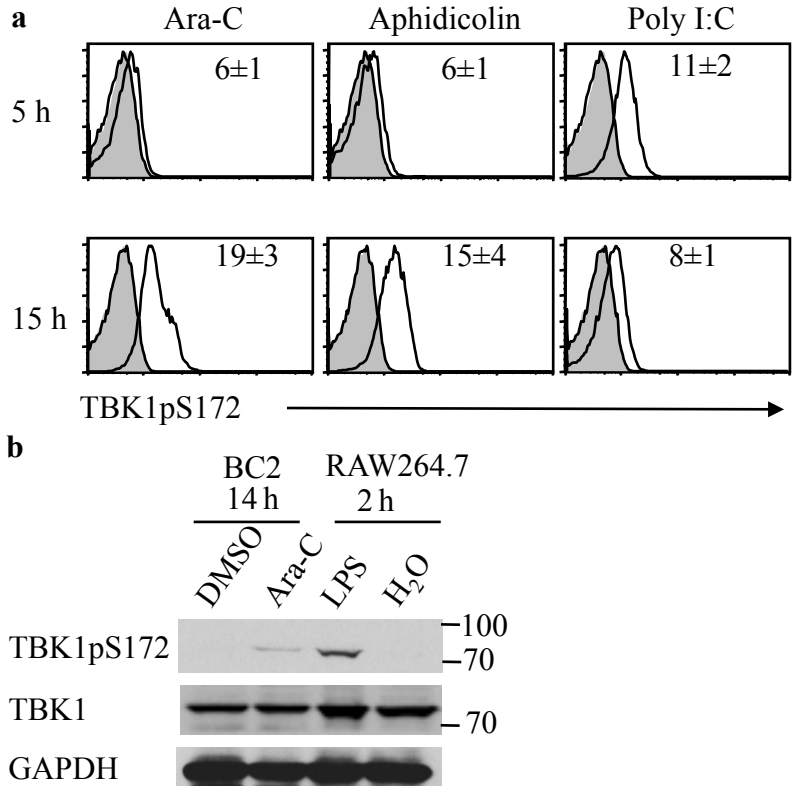

Figure 3.5 TBK1 is phosphorylated upon DNA damaging agents in BC2 cells. **(a)** BC2 cells were treated with 10 µM Ara-C, 4 µM aphidicolin, 10 µg/ml Poly I:C (bold lines) or DMSO (fine line) for the indicated time. Cells were stained for phosphorylation of S172 of TBK1. Filled histograms depict isotype staining of DMSO treated cells. MFI ± SD of 3 independent experiments are indicated. **(b)** Immunoblot analysis of TBK1S172 phosphorylation in BC2 cells treated with 10 µM Ara-C or DMSO for 14 hours. Raw 264.7 cells were treated with LPS for 4 hours for comparison. Immunoblot data was kindly provided by Dr Nina Le Bert.

BC2 cells transduced with TBK1 shRNA had significant reduction in RAE1 cell surface expression compared to BC2 cells tranduced with control shRNA upon treatment with Ara-C (Figure 3.6a). Inhibition was observed compared to untransduced (GFP^-) cells in the same cultures or compared to cells transduced with control shRNA (Figure 3.6a and data now shown). As an alternative approach, we employed mouse embryonic fibroblast (MEF) cell lines from mice in which both the TBK1 and IKKε genes were inactivated by gene targeting (Matsui et al., 2006). $TBK1^{-/-}IKK\varepsilon^{-/-}$ MEFs treated with Ara-C did not upregulate any of the NKG2D ligands tested (Figure 3.6bi). Genetic reconstitution of $TBK1^{-/-}IKK\varepsilon^{-/-}$ MEFs with either TBK1 or IKKε was sufficient to induce RAE1βδ and RAE1ε expression on a fraction of the cells (Figure 3.6bii and iii), and restore the capacity of the cells to upregulate RAE1 further in response to DNA damaging agent Ara-C (Figure 3.6bii and iii). The induction of RAE1 without Ara-C treatment in some cells may reflect overexpression of TBK1 or IKKε, which has been shown to result in unregulated activation of the pathway in other contexts (Buss et al., 2004; Fensterl et al., 2005; Parvatiyar et al., 2010). In summary, these data suggest that TBK1 (and/or the similarly functioning IKKε) is required for normal induction of NKG2D ligands in response to DNA damage.

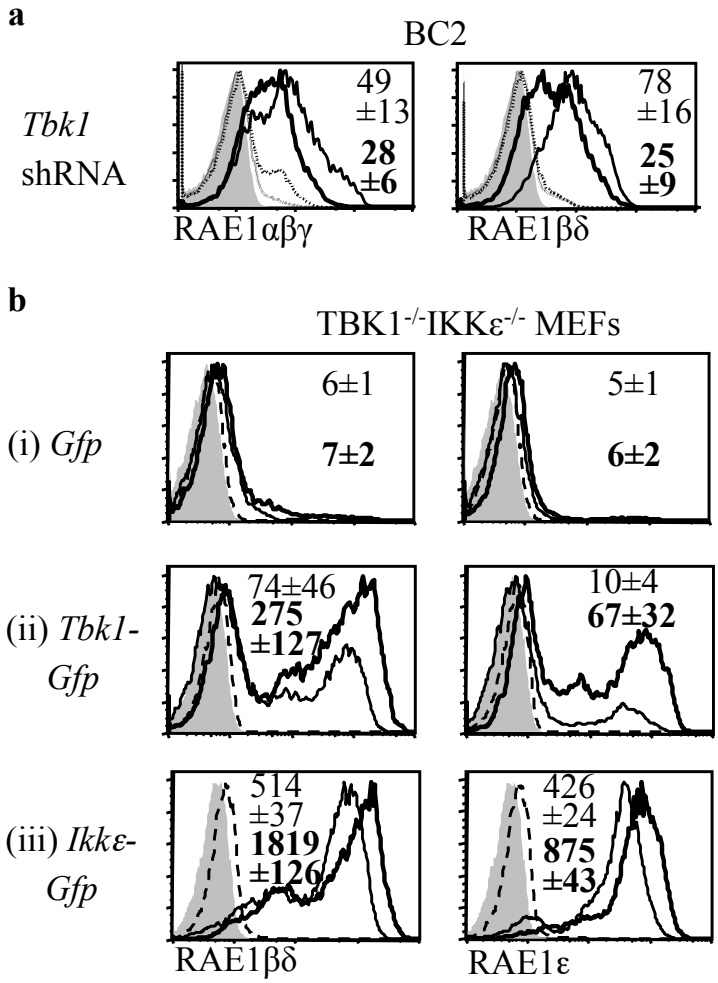

Figure 3.6 TBK1 is necessary for RAE1 expression in response to DNA damage.

(a) Inhibition of RAE1 upregulation in response to DNA damage by TBK1 shRNA. BC2 cells were transduced with retroviral vectors encoding TBK1 shRNA and GFP (bold lines in histograms) or control shRNA and GFP (fine lines), cultured for 5 days and treated with 10 μM Ara-C for 16 hours. Rae1 expression was determined by gating on transduced (GFP^+) cells. Dotted line: DMSO treated cells expressing TBK1-specific (dashed line) or control shRNA (dotted line) stained with RAE1-specific antibodies. Filled histogram: Ara-C treated cells stained with isotype controls. **(b)** $TBK1^{-/-}IKK\varepsilon^{-/-}$ MEFs were transduced with the retroviral vectors encoding TBK1-IRES-GFP (ii), IKKε-IRES-GFP (iii) or IRES-GFP (i). 8 days after selection cells were treated with DMSO (fine line) or 10 μM Ara-C for 18 hours (bold lines) and analyzed for indicated NKG2D ligand expression. Isotype staining of DMSO (filled histograms) or Ara-C treated (dashed line) is shown. MFI ±SD of 3 independent experiments are indicated.

3.6 TBK1 is necessary for constitutive RAE1 expression in Yac-1 cells

Given the constitutive activation of IRF3 in Yac-1 cells, we next tested whether TBK1 or IKKε are constitutively active in Yac-1 cells. TBK1 phosphorylated on serine 172 was readily detected in Yac-1 cells by intracellular staining (Figure 3.7a), which is to be contrasted with the undetectable level of phospho-TBK1 detected in unstimulated BC2 cells (Figure 3.6a).Treatment of the permeabilized Yac-1 cells with λ-phosphatase nearly abolished staining. Transduction of Yac-1 cells with TBK1 shRNA caused a significant but less complete reduction in RAE1 at the cell surface (Figure 3.7b).

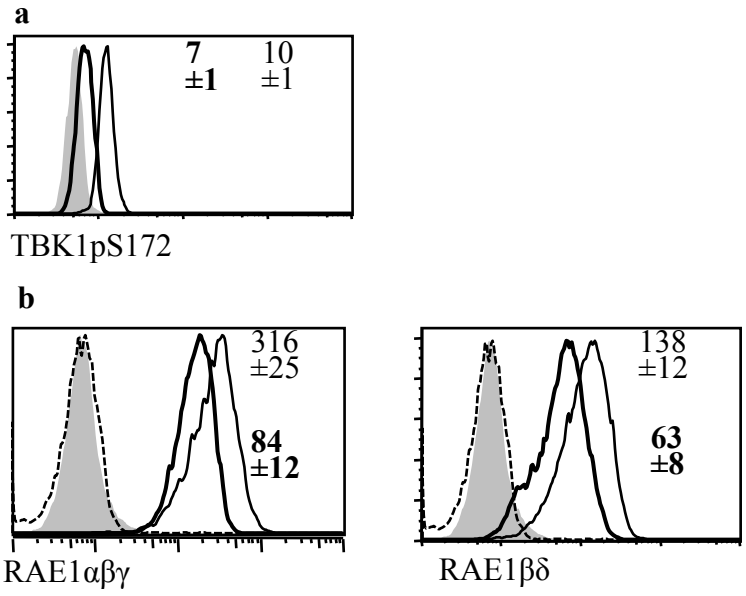

Figure 3.7 TBK1 is necessary for constitutive RAE1 expression in Yac-1 cells. **(a)** Phosphorylation on S172 of TBK1 was detected by flow cytometry (fine line). Some Yac-1 cells were pretreated with λ-phosphatase before staining (bold line). The filled histogram shows isotype-staining of untreated Yac-1 cells. **(b)** Yac-1 cells were transduced with retroviral vectors encoding *Tbk1*-specific shRNA and GFP (bold line) or control shRNA and GFP (fine line) and cultured for 5 days. RAE1 expression was determined by gating on transduced (GFP^+) cells. Isotype staining of *Tbk1*-specific shRNA (dashed lines) and control shRNA (filled histogram) transduced cells is shown. MFI ± SD of 3 independent experiments are indicated.

3.7 Phosphorylation of IRF3 and TBK1 in response to DNA Damage depends on ATR in BC2 cells

Activation of ATR versus ATM depends on the nature of DNA damage to which a cell is exposed. Treatment of cells with Ara-C, a nucleoside analogue, results in ssDNA breaks leading to the preferential activation of ATR, which in turn activates CHK1 (Covey et al., 1986; D'Incalci et al., 1985; Wang et al., 2008b). To address the role of ATM and ATR in the activation of TBK1 and IRF3, we utilised different chemical inhibitors to block ATM and ATR function. Induction of RAE1 expression in BC2 cells by Ara-C was inhibited by the combined treatment of cells with specific ATM and ATR inhibitors (Figure 3.8a). Inhibition of ATM and ATR also inhibited TBK1 and IRF3 phosphorylation (Figure 3.8b and c) and nuclear localization of chimeric IRF3-GFP (Figure 3.1c and d) in Ara-C-treated BC2 cells. The effects of ATM or ATR inhibition on NKG2DL expression and phosphorylation of TBK1 and IRF3 were less pronounced suggesting that ATM and ATR act redundantly (Figure 3.8).

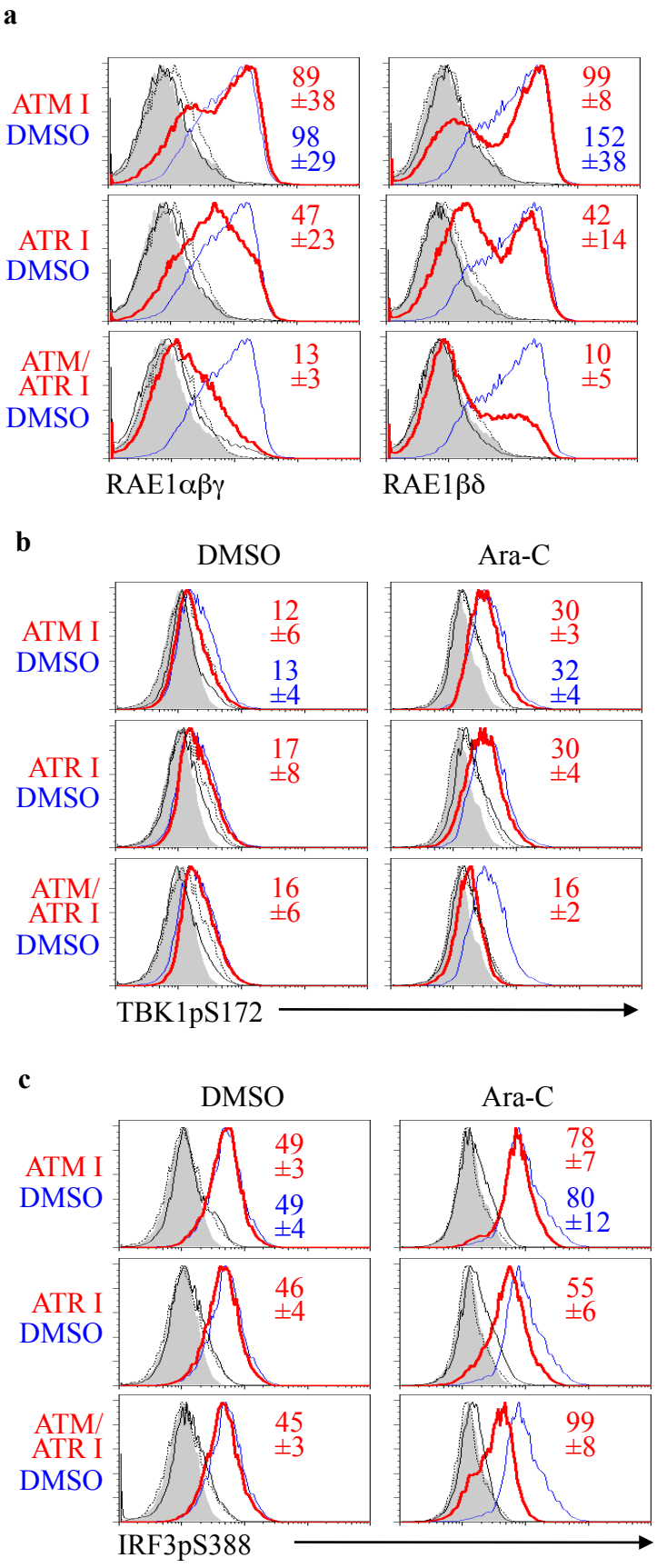
a
ATM I
DMSO
89
±38
98
±29
99
±8
152
±38
ATR I
DMSO
47
±23
42
±14
ATM/
ATR I
DMSO
13
±3
10
±5
RAE1αβγ
RAE1βδ
b
DMSO
Ara-C
ATM I
DMSO
12
±6
13
±4
30
±3
32
±4
ATR I
DMSO
17
±8
30
±4
ATM/
ATR I
DMSO
16
±6
16
±2
TBK1pS172
c
DMSO
Ara-C
ATM I
DMSO
49
±3
49
±4
78
±7
80
±12
ATR I
DMSO
46
±4
55
±6
ATM/
ATR I
DMSO
45
±3
99
±8
IRF3pS388

Figure 3.8 Phosphorylation of IRF3 and TBK1 in response to DNA Damage depends on ATR in BC2 cells.
(a) Analysis of RAE1 expression in BC2 cells pretreated with 10 µM of the ATM inhibitor KU55933, 10 µM of the ATR inhibitor VE-821, 10 µM of KU55933 and 10 µM of VE-821 (red line) or DMSO (blue line) and further incubated with 10 µM Ara-C for 16 hours. As controls, BC2 cells were pretreated with the same inhibitors (dashed line) or DMSO (fine line) before DMSO treatment for 16 hours. Filled histograms indicate isotype control staining. Phosphorylation of TBK1S172 (b) and IRF3S388 (c) in BC2 cells pretreated with 10 µM of the ATM inhibitor KU55933, 10 µM of the ATR inhibitor VE-821, 10 µM of KU55933 and 10 µM of VE-821 (red line) or DMSO (blue line) and further incubated with 10 µM Ara-C or DMSO for 16 hours. As controls, BC2 cells were pretreated with the same inhibitors (dashed line) or DMSO (fine line) before DMSO treatment for 16 hours. Filled histograms indicate isotype control staining. MFI ± SD of 3 independent experiments are indicated.

3.8 Phosphorylation of IRF3 and TBK1 depends on ATR in Yac-1 cells

The inhibition of ATR leads to a decrease in the constitutive RAE1 expression and phosphorylation of TBK1 and IRF3 in Yac-1 cells (Figure 3.9a and b). Nuclear localization of IRF3-GFP in Yac-1 cells was also suppressed by inhibition of ATM and ATR (Figure 3.9c). Thus, activation of TBK1 and IRF3 in Yac-1 cells depends on ATR suggesting that constitutive single-stranded (ss) DNA damage, which preferentially activates ATR (Sancar et al., 2004a), is present in Yac-1 cells.

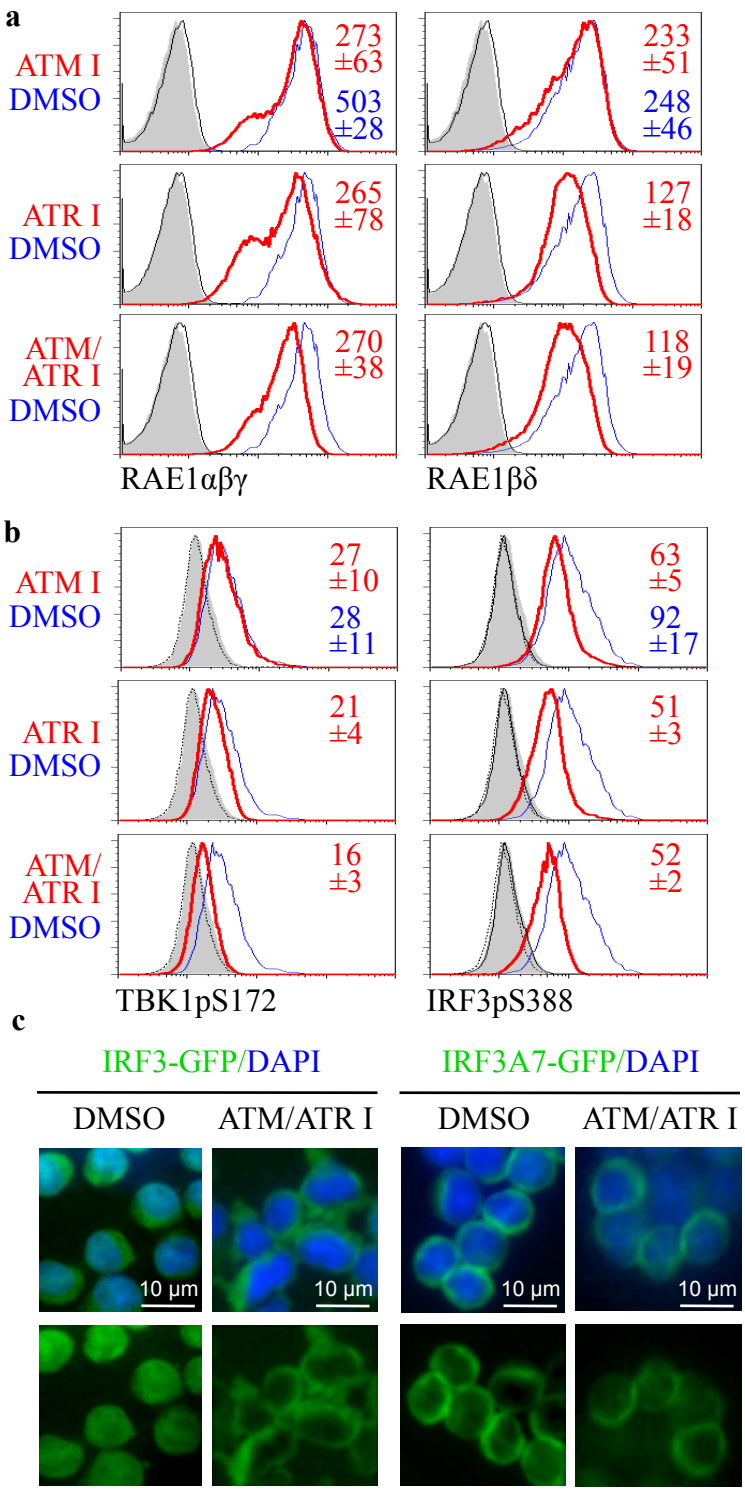

Figure 3.9 Phosphorylation of IRF3 and TBK1 depends on ATR in Yac-1 cells.

Yac-1 cells treated for 16 hours with ATM and/or ATR-specific inhibitors (red line) or DMSO (blue line) as indicated above and stained for RAE1 expression **(a),** TBK1pS172 (left panel) and IRF3pS388 (right panel) **(b).** Filled histograms depict isotype control staining. MFI ± SD of 3 independent experiments are indicated. **(c)** Yac-1 cells transduced with chimeric *IRF3-Gfp* or *IRF3A7-Gfp* encoding retroviral vectors were treated with 10 µM of KU55933 and 10 µM of VE-821 or DMSO for 14 hours. IRF3 expression was analyzed by fluorescent microscopy. DAPI staining was removed for better visualization of IRF3 expression in the lower panels. Representative image from 3 independent experiments are shown. .

3.9 Summary

The data provide evidence that IRF3 and TBK1 are activated in response to DNA damage via ATR. Both constitutive and inducible expressions of NKG2DLs are dependent on IRF3 and TBK1.

Chapter 4: Accumulation of cytosolic DNA in response to DNA damage

4.1 DNA damaging agents induce accumulation of cytosolic DNA

Recognition of cytosolic DNA by DNA sensors activates TBK1 and IKKε (Takeshita and Ishii, 2008; Yanai et al., 2009b). To test whether treatment of cells with DNA damaging agents leads to the accumulation of cytosolic DNA, we stained cells with antibodies specific for ssDNA or dsDNA. The specificity of DNA staining was determined by pretreating some cells with RNase and DNase to digest dsDNA or S1 nuclease to digest ssDNA before staining (Suzuki et al., 1997; Yang et al., 2007). In addition, we treated cells with RNase and stained for the mitochondrial marker COX IV to exclude mitochondrial DNA (Figure 4.1 and 4.2) (Khalimonchuk and Winge, 2008). Strikingly, we found that significant amounts of ssDNA and dsDNA accumulated in the cytosol after Ara-C treatment (Figure 4.1). Furthermore, we observed cytosolic ssDNA and dsDNA in untreated Yac-1 cells (Figure 4.2).

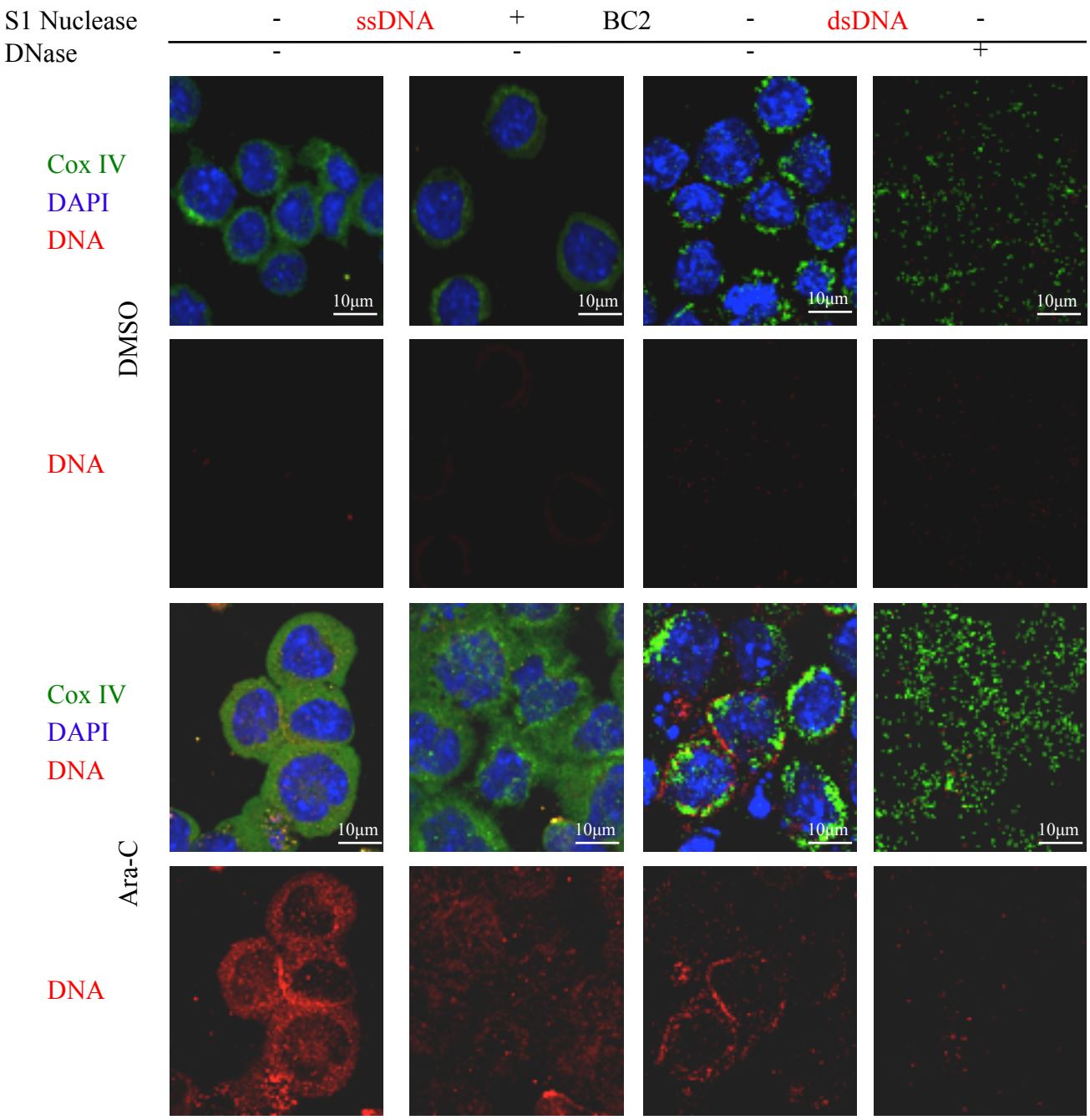

Figure 4.1 DNA damage results in accumulation of cytosolic DNA in BC2 cells.
(a) BC2 cells treated with 10 µM Ara-C or DMSO for 13 hours were fixed and stained with ssDNA or dsDNA-specific antibodies (red) and Cox-IV (green) in presence of RNase and DAPI (blue). Cells in the indicated panels were treated with S1 nuclease or DNase before staining. Representative image from 3 independent experiments are shown.

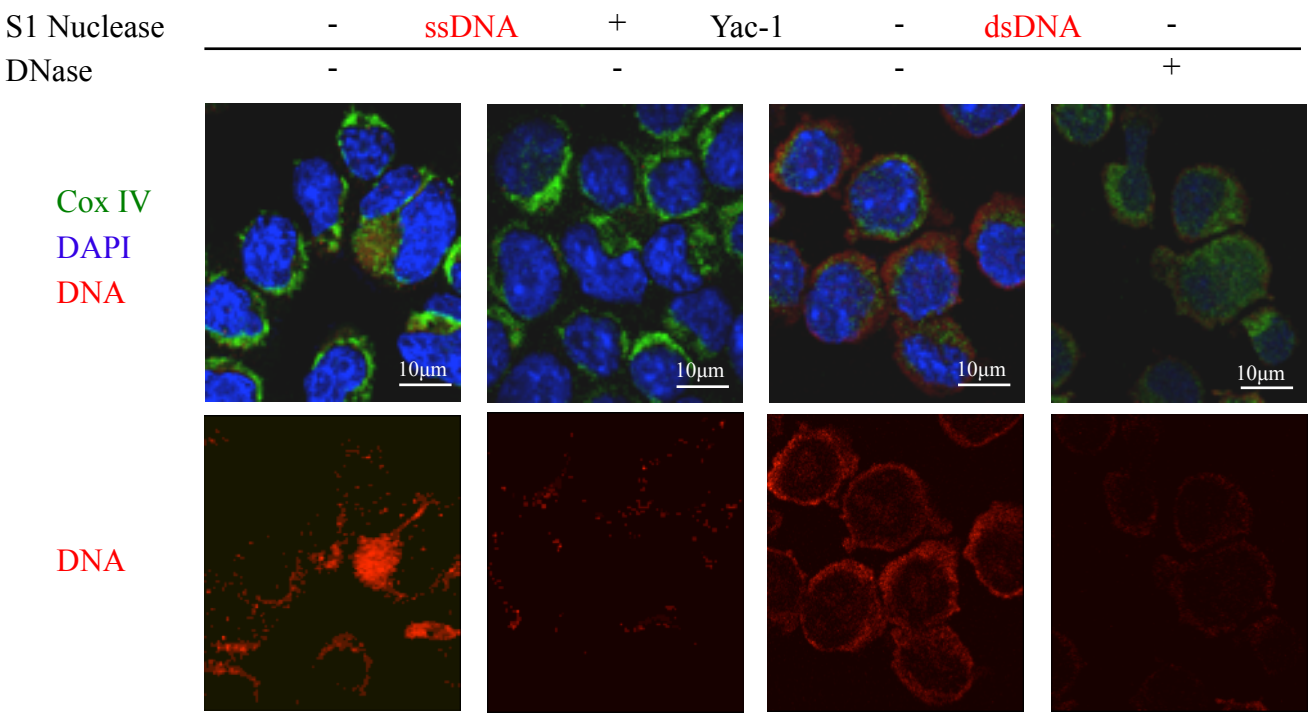

Figure 4.2 DNA damage results in accumulation of cytosolic DNA in Yac-1 cells. Yac-1 cells were fixed and stained with ssDNA or dsDNA-specific antibodies (red) and Cox-IV (green) in presence of RNase and DAPI (blue). Cells in the indicated panels were treated with S1 nuclease or DNase before staining. Representative image from 3 independent experiments are shown.

4.2 Expressions of RAE1 is dependent on DNA

The finding that DNA accumulates in the cytosol of cells exposed to DNA damage, coupled with the data showing that mediators that relay signals from DNA sensors (IRF3 and TBK1) are required for induction of NKG2D ligands, suggested that DNA sensors may play a role in the induction of NKG2D ligands. To test whether cytoplasmic DNA can induce RAE1 expression in BC2 cells we transfected cells with AF488-labelled plasmid DNA, genomic DNA or ssDNA. AF488-positive BC2 cells upregulated expression of NKG2D ligands, although to a lesser degree than cells treated with the DNA damaging agent Ara-C **(**Figure 4.3**)**. The findings that DNA accumulates in the cytoplasm of cells subjected to DNA damage and that DNA introduced into cells induces NKG2D ligands provide additional evidence that links the DNA sensing pathway to NKG2D ligand expression induced by the DDR.

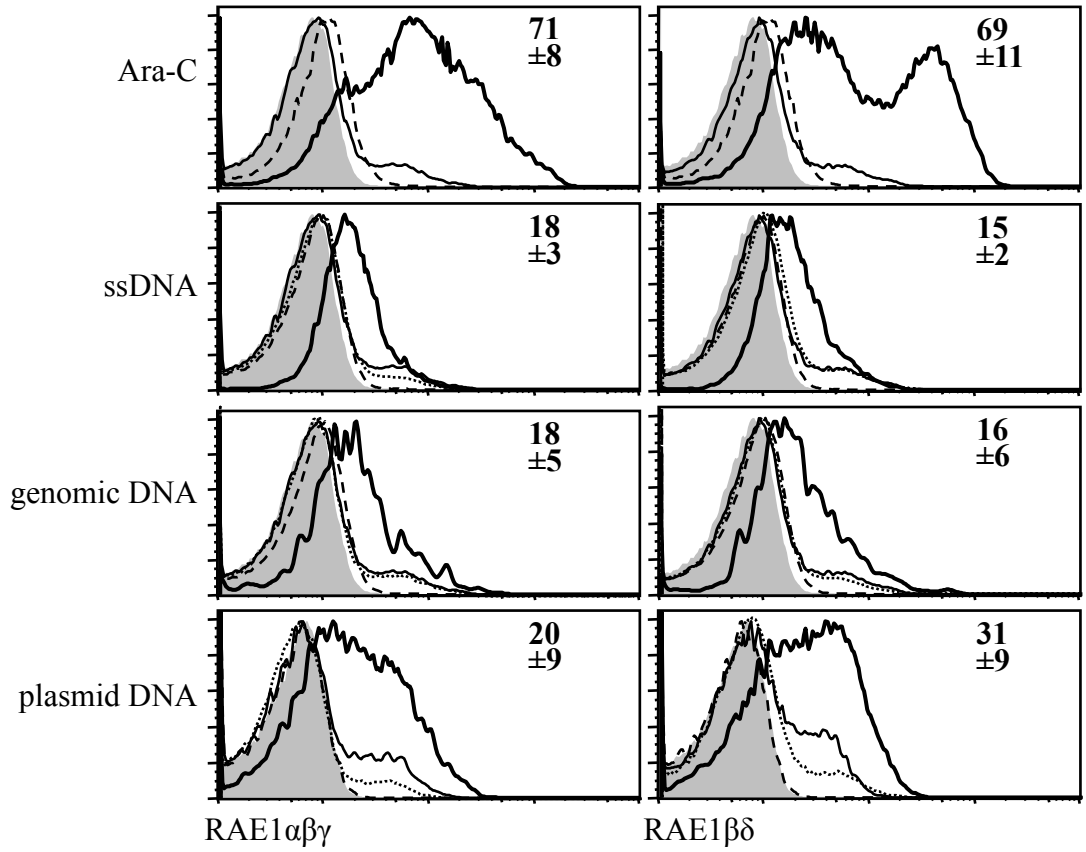

Figure 4.3 RAE1 expression is induced by DNA.
BC2 cells were transfected with 4 μg AF488-labelled MSCV-IRES-GFP, C57BL/6 genomic DNA or ssDNA (non-stimulatory control for ODN 1668). As controls, cells were treated with 10 μM Ara-C or DMSO. 18 hours after transfection or treatment, BC2 cells were stained for the indicated NKG2D ligands and analyzed by flow cytometry. Ara-C treated or gated DNA-transfected cells ($AF488^+$) are shown as bold lines. Control gated $AF488^-$ cells are indicated as dotted lines. DMSO treated cells are depicted as fine lines. Isotype staining of Ara-C treated or $AF488^+$ cells is shown as dashed lines. Filled histograms indicate DMSO treated cells stained with isotype controls. MFI ± SD of 3 independent experiments are indicated.

4.3 Expressions of RAE1 is dependent on STING

The presence of DNA in the cytosol activates endoplasmic reticulum-resident transmembrane protein stimulator of IFN genes (STING)-dependent DNA sensors leading to the activation of TBK1 and IRF3 (Ishikawa and Barber, 2008). We therefore tested whether STING is necessary for RAE1 expression induced in cells exposed to genotoxic stress. WT MEFs upregulated RAE1βδ in response to Ara-C, but this was abrogated in MEFs with a loss of function *Sting* mutation (Figure 4.4) (Burdette et al., 2011). Reconstitution of *Sting* expression by transduction resulted in restored inducibility of RAE1 in the cells. As another approach, BC2 cells expressing a *Sting*-specific shRNA showed reduced RAE1 induction by Ara-C as well (Figure 4.5a). Furthermore, *Sting* inhibition in Yac-1 cells resulted in reduced constitutive RAE1 expression levels (Figure 4.5b). These data support the conclusion that the STING-dependent DNA sensor pathway is necessary for induction of NKG2D ligands.

We next tested the requirement in RAE1 induction for one candidate STING-dependent DNA sensor that activates IRF3, ZBP1 (Takaoka et al., 2007). Knockdown of *Zbp1* partly inhibited the upregulation of RAE1αβγ in response to Ara-C, but had little effect on RAE1βδ (Figure 4.5a). In contrast, knockdown of *Zbp1* modestly inhibited RAE1βδ, but not RAE1αβγ, expression in Yac-1 cells (Figure 4.5b). Inhibition of *Rig-I*, a RNA sensor that may indirectly mediate responses to cytosolic DNA, had no effect on RAE1 expression in BC2 or Yac-1 cells (Figure 4.5). It is likely, therefore, that DNA sensors other than ZBP1 participate in inducing RAE1 expression in response to DNA damage, in line with other evidence suggesting the existence of DNA sensors redundant with ZBP1 (Ishii et al., 2008a). Taken together these data

suggest that cytosolic nucleic acid sensors regulate NKG2D ligand expression in cells exposed to DNA damage.

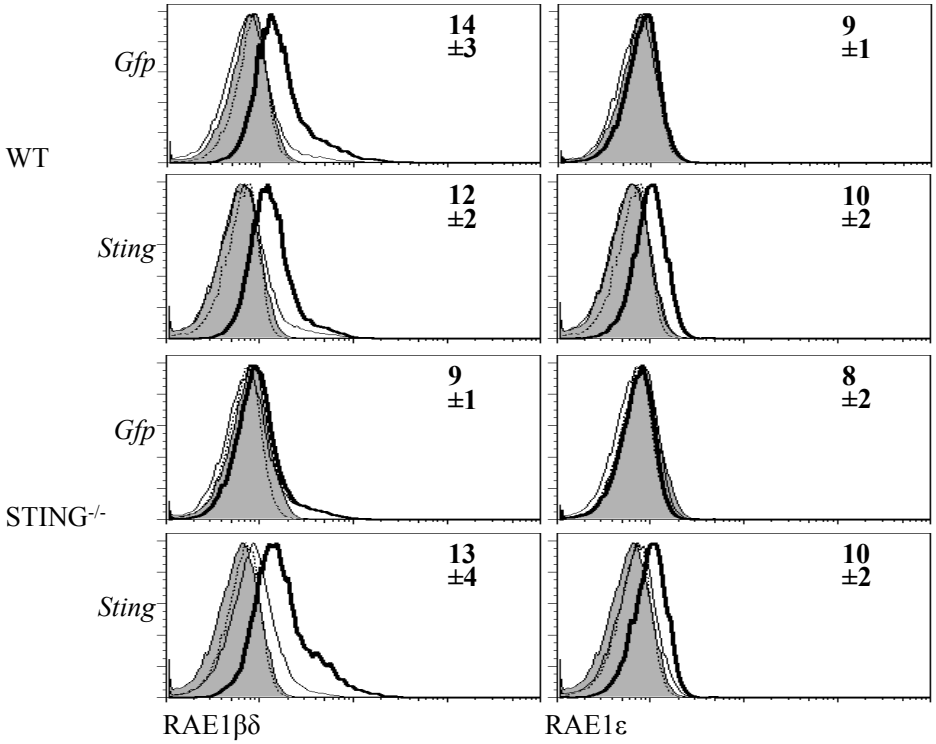

Figure 4.4 Expressions of RAE1 is dependent on STING.
WT MEFs or MEFs lacking functional STING were transduced with retroviral vectors encoding *Sting*-IRES-*Gfp* or IRES-*Gfp* and cultured for 5 days before treating with 10 μM Ara-C for 16 hours. RAE1 expression was determined by gating on transduced (GFP^+) cells. Ara-C treated (bold) and DMSO-treated (thin) cells were stained with the different RAE1 isoforms. Isotype controls for Ara-C treated (filled histogram) and DMSO-treated (dotted) cells were indicated. MFI ± SD of 3 independent experiments are indicated.

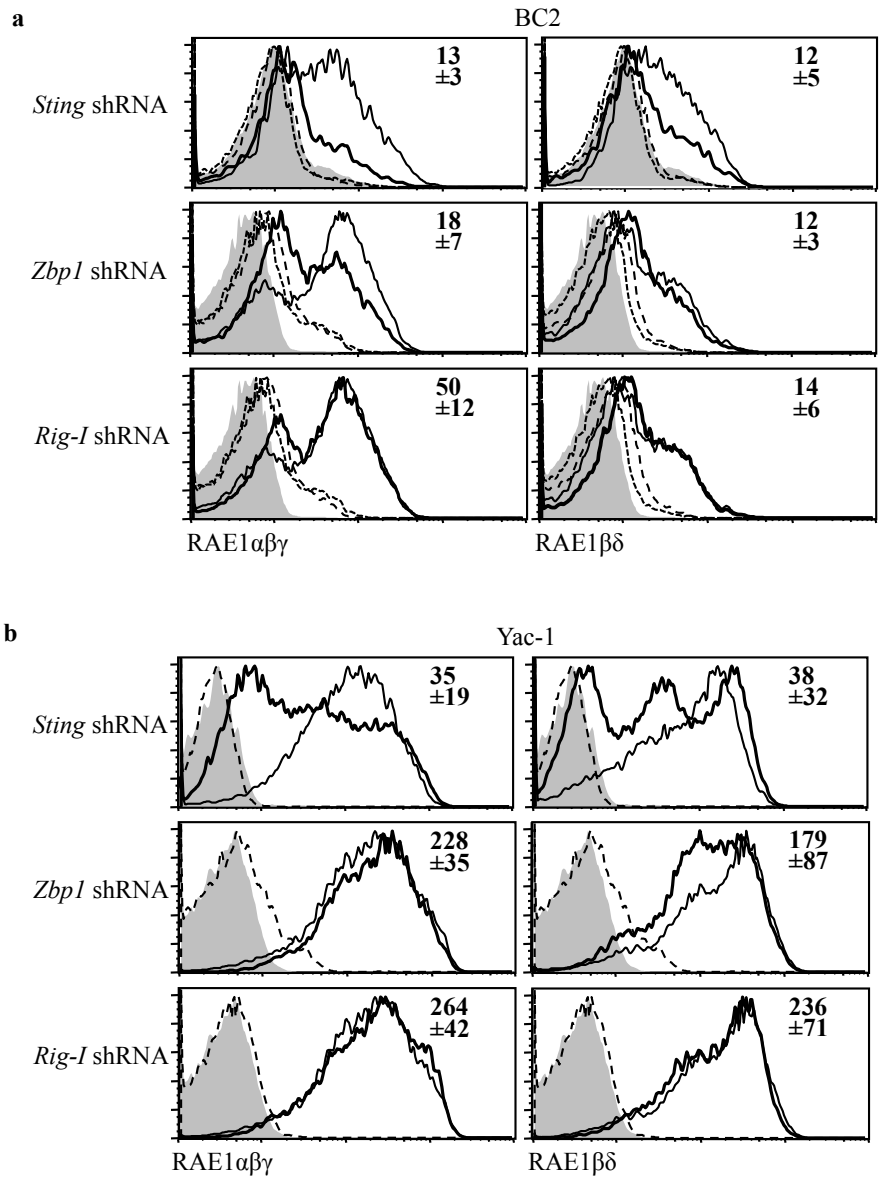

Figure 4.5 Knockdown of *Sting, Zbp1 and Rig-I* in BC2 and Yac-1 cells.
(a) BC2 cells were transduced with *Sting*, *ZBP1* and *Rig-I*-specific shRNAs (bold line) or control shRNAs (fine line) and treated with 10 μM Ara-C for 16 hours. As a control, BC2 cells were transduced with shRNA specific for the nucleic acid sensors (Dashed line) or control shRNAs and treated with DMSO (dotted line). NKG2D ligand expression was analyzed by flow cytometry. Isotype control stainings are shown as filled histograms. **(b)** Yac-1 cells were transduced with *Sting*, *Zbp1* and *Rig-I*-specific shRNAs (bold line) or control shRNAs (fine line). Isotype control staining of nucleic acid sensor-specific shRNA (dashed line) or control shRNA (filled histogram) is shown. MFI ± SD of 3 independent experiments are indicated.

4.4 Accumulation of cytosolic DNA in leukaemic B cells of Eμ-*Myc* mice

Our previous data suggested that cytosolic DNA may lead to the immune mediated rejection of immune cells. To study this *in vivo*, we used the Eμ-*Myc* murine model or B cell lymphoma (Harris et al., 1988). Eμ-*Myc* mice over-express murine c-*Myc* under the control of the Ig heavy chain enhancer region (Eμ), analogous to human Burkitt lymphoma (Harris et al., 1988). Early-stage Eμ-*Myc* disease is characterized by immature B cell leukaemia, which progresses to lymphoma terminal-stage disease (Harris et al., 1988). The tumour cells in Eμ-*Myc* mice can be identified in the blood by their surface expression markers B220 and IgM (Figure 4.6). Tumour cells in Eμ-*Myc* mice spontaneously regress at around day 40 of age and the regression is dependent on immune cells (Croxford et al., 2013). *Myc*-induced replication stress was shown to induce DNA damage in Eμ-*Myc* mice (Croxford et al., 2013; Reimann et al., 2007). Furthermore, NKG2D was reported to play a role in tumour surveillance in the Eμ-*Myc* mice (Guerra et al., 2008). To test if B cell tumors express ssDNA as a consequence of *Myc* expression, we stained B cells for the presence of cytosolic DNA. In agreement with our *in vitro* findings, we observed ssDNA in the cytoplasm of *ex vivo* leukaemic B cells purified from the spleen of young (< d42) Eμ-*Myc* mice (Figure 4.7a). Quantification analyses showed that 23.0 ± 1.4 % of the total B220 cells accumulate ssDNA (Figure 4.7b). This is in contrast to wild type B cells, which do not show cytosolic DNA.

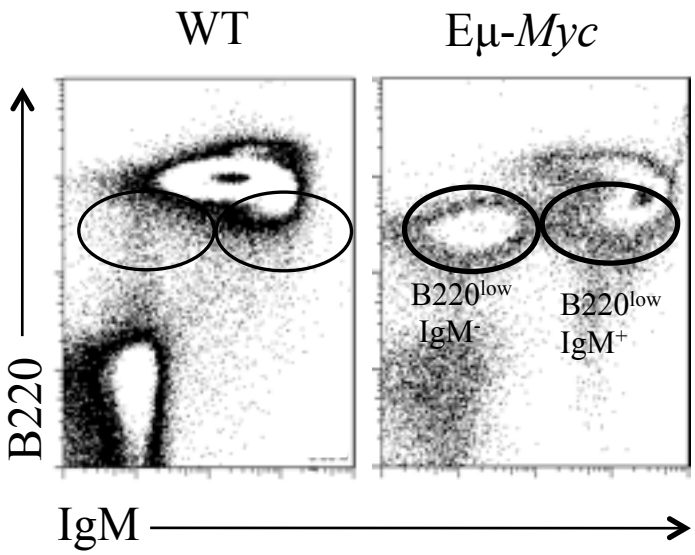

Figure 4.6 Tumour populations in Eμ-*Myc* and WT mice.
Cells derived from the peripheral blood were stained for anti-B220 and anti-IgM antibodies, and were subsequently assessed by flow cytometry. $B220^{low}$ populations in Eμ-*Myc* mice were identified by the oval gates. Adapted from (Croxford et al., 2013)

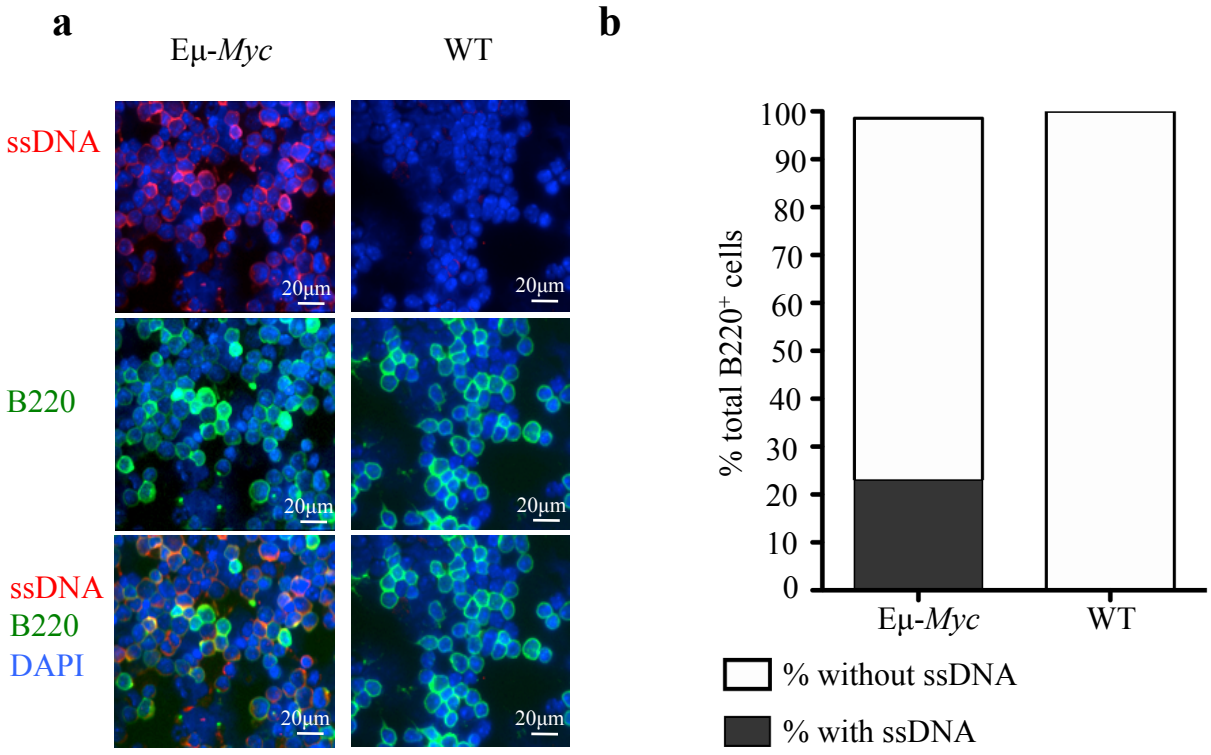

Figure 4.7 *Ex vivo* leukemia B cells accumulate ssDNA.
(a) Accumulation of ssDNA in early Eμ-*Myc* tumour cells compared to WT cells. Data is representative of 3 independent experiments. **(b)** Quantification of the percentage of total $B220^{+}$ cells with ssDNA. Error bar indicating SD was too small to be seen. > 100 cells were counted for each genotype.

4.5 Summary

We observed accumulation of cytosolic DNA in response to DNA damaging drugs in BC2 and constitutive expression of cytosolic DNA in Yac-1 cells. In addition, cytosolic DNA is also present in *ex vivo* tumour B cells from Eμ-*Myc* mice. We also showed that the expression of NKG2DLs is dependent on STING and cytosolic DNA.

Chapter 5: Decreased survival of Eμ-*Myc* mice deficient in *Irf3*

5.1 Decreased survival of Eμ-*Myc* mice heterozygous for *Irf3*

Our data raise the possibility that IRF3-dependent NKG2D ligand expression plays a critical role in immune surveillance of tumours. To analyse the effect of IRF3 on the progression of B cell lymphomas, *Irf3*-deficient mice were crossed with the Eμ-*Myc* mice. Survival analysis showed that *Irf3*$^{+/-}$Eμ-*Myc* mice (n= 17; median survival= 62 days) experienced a significantly reduced survival rate compared to *Irf3*$^{+/+}$Eμ-*Myc* mice (n= 25; median survival= 116 days) (***p<0.001 by Log-Rank test or by Gehan-Breslow-Wilcoxon Test) (Figure 5.1). No difference in survival rate between *Irf3*$^{-/-}$ or *Irf3*$^{+/+}$ non-Eμ-*Myc* mice was observed (n= 25; median survival= >250 days) (Figure 5.1). We were not able to generate *Irf3*$^{-/-}$Eμ-*Myc* mice because *Irf3*$^{+/-}$ Eμ-*Myc* mice failed to breed.

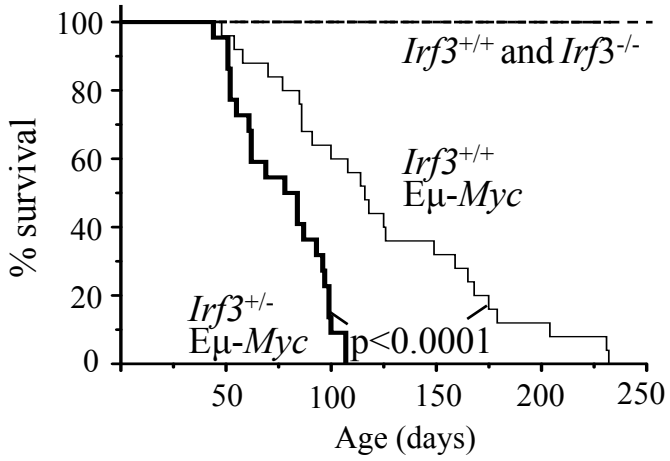

Figure 5.1 Accelerated onset of *Myc*-driven lymphomas in heterozygous IRF3 Eμ -*Myc* mice.

Irf3$^{+/-}$Eμ-*Myc* mice (thick line) exhibit decreased survival compared to *Irf3*$^{+/+}$Eμ-*Myc* (thin line) or non-transgenic *Irf3*$^{+/+}$ (dashed line) or *Irf3*$^{-/-}$ mice (dotted line). Kaplan-Meier analysis of survival of *Irf3*$^{+/+}$Eμ-*Myc* mice (n= 25; median survival= 116 days), *Irf3*$^{+/-}$Eμ-*Myc* mice (n= 17; median survival= 62 days) and *Irf3*$^{+/+}$ or *Irf3*$^{-/-}$ mice (n= 25; median survival= >250 days). ***p < 0.0001 by Log-Rank test or by Gehan-Breslow-Wilcoxon Test. Data were kindly provided by Dr John Ludovic Croxford and Ms Pan Meng Fei.

In addition, heterozygosity of *Irf3* in Eμ-*Myc* mice resulted in a 2.5-fold lower levels of IRF3 and reduced expression of IRF3 target genes in splenic B cell lymphomas when compared to *Irf3*$^{+/+}$Eμ-*Myc* mice (Figure 5.2).

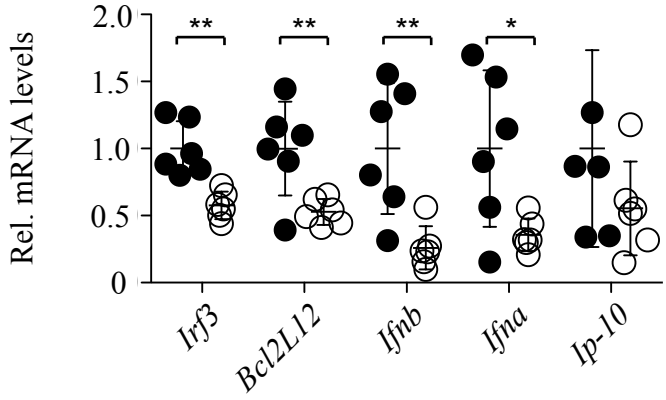

Figure 5.2 Reduced expression of IRF3 target genes.
Relative mRNA levels of indicated IRF3 target genes in purified tumor cells of *Irf3*$^{+/-}$Eμ-*Myc* (white) and *Irf3*$^{+/+}$Eμ-*Myc* (black) mice were measured by real-time PCR and normalized with HPRT. Error bar denotes SD. Data were kindly provided by Dr Nina Le Bert.

5.2 Lower expressions of RAE-1 isoforms in *Irf3*$^{+/-}$Eμ-*Myc* mice

To determine if the reduced IRF3 amounts impaired NKG2D ligand expression in Eμ-*Myc* mice we stained tumor cells for expression for RAE1ε, the only RAE1 family member detected on Eμ-*Myc* tumor cells (Unni et al., 2008). In Eμ-*Myc* mice, tumor cells exhibit the phenotypes of IgM^{-}B220^{low} and IgM^{+}B220^{low} cells in the blood or spleen (Figure 4.5) (Harris et al., 1988; Langdon et al., 1986; Sidman et al., 1993a; Yukawa et al., 1989), allowing them to be distinguished from normal B cells (IgM^{+}B220^{high}). RAE1ε expression was significantly reduced in tumor cells of *Irf3*$^{+/-}$Eμ-*Myc* (n = 3) mice when compared to *Irf3*$^{+/+}$Eμ-*Myc* mice (n = 3) (Figure 5.3).

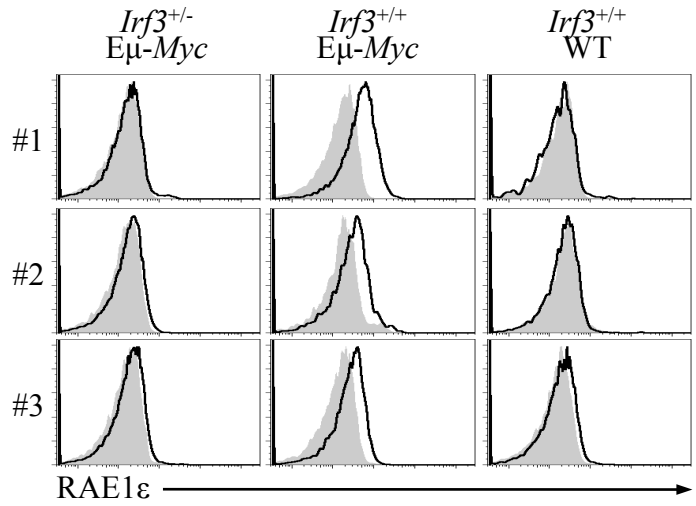

Figure 5.3 RAE1 ε expression in tumor cells of *Irf3*$^{+/-}$E μ -*Myc* mice.
B220^{low} tumor cells in blood of moribund *Irf3*$^{+/-}$Eμ-*Myc* (bold line) and *Irf3*$^{+/+}$Eμ-*Myc* (fine line) mice were stained for indicated NKG2DL expression. Filled histogram depicts isotype staining of B220^{low} tumor in *Irf3*$^{+/+}$Eμ-*Myc* mice. Flow histograms from 3 different mice are shown.

5.3 Altered survival curve in *Irf3/Bcl2l12*$^{+/-}$Eμ-*Myc* is due to decreased expression of IRF3, rather than changes in BCL2L12 expression

The null mutation introduced into the *Irf3* allele also resulted in the functional inactivation of the neighboring *Bcl2l12* gene (Nakajima et al., 2009). BCL2L12 was shown to promote or suppress tumorigenesis depending on the cellular context (Stegh et al., 2007). However, in contrast to IRF3, heterozyogosity of the gene-targeted locus did not result in reduced BCL2L12 protein levels (Figure 5.4).

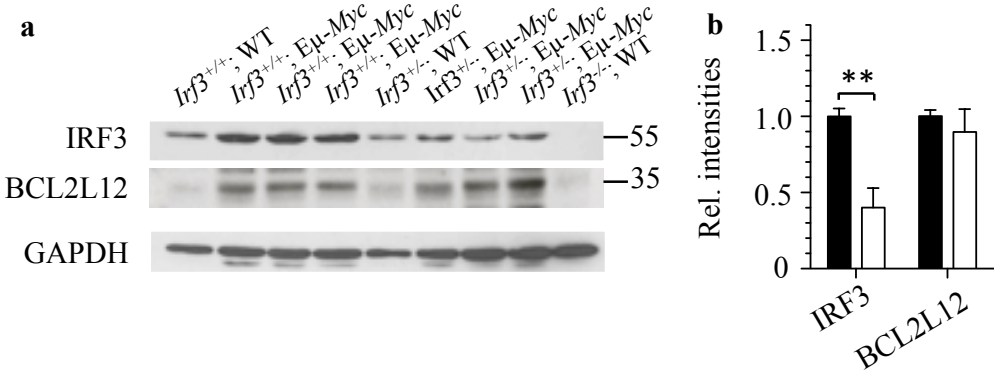

Figure 5.4 Reduced IRF3 but not BCL2L12 protein levels in *Irf3*$^{+/-}$Eμ-*Myc*.
(a) Immunoblot analysis of purified splenic B cell lymphomas (> 78% purity) from *Irf3*$^{+/-}$Eμ-*Myc*, *Irf3*$^{+/+}$Eμ-*Myc*, *Irf3*$^{+/+}$WT, *Irf3*$^{+/-}$WT and *Irf3*$^{-/-}$WT probed with antibodies for IRF3, BCL2L12 and GAPDH (left panel). **(b)** Densitometry of immunoblot analysis of IRF3, BCL2L12 expression in splenic B cells lymphomas from *Irf3*$^{+/-}$Eμ-*Myc* and *Irf3*$^{+/+}$Eμ-*Myc* mice. Mean ± SD of 3 mice are normalized to GAPDH levels. p values are indicated as **$p < 0.01$. Data were kindly provided by Dr Nina Le Bert.

To compare apoptosis rate in tumor cells of *Irf3*$^{+/-}$Eμ-*Myc* and *Irf3*$^{+/+}$Eμ-*Myc* mice, we cultured tumor cells for 2-4 hours *in vitro* (Figure 5.5a). We found no difference in the apoptosis rate of tumor cells derived from *Irf3*$^{+/-}$Eμ-*Myc* mice and *Irf3*$^{+/+}$Eμ-*Myc* mice. Tumor cells in *Irf3*$^{+/-}$ and *Irf3*$^{+/+}$Eμ-*Myc* mice also incorporated similar amounts of BrdU suggesting the proliferation rate of tumor cells is not changed by heterozygosity in the *Irf3* locus (Figure 5.5b).

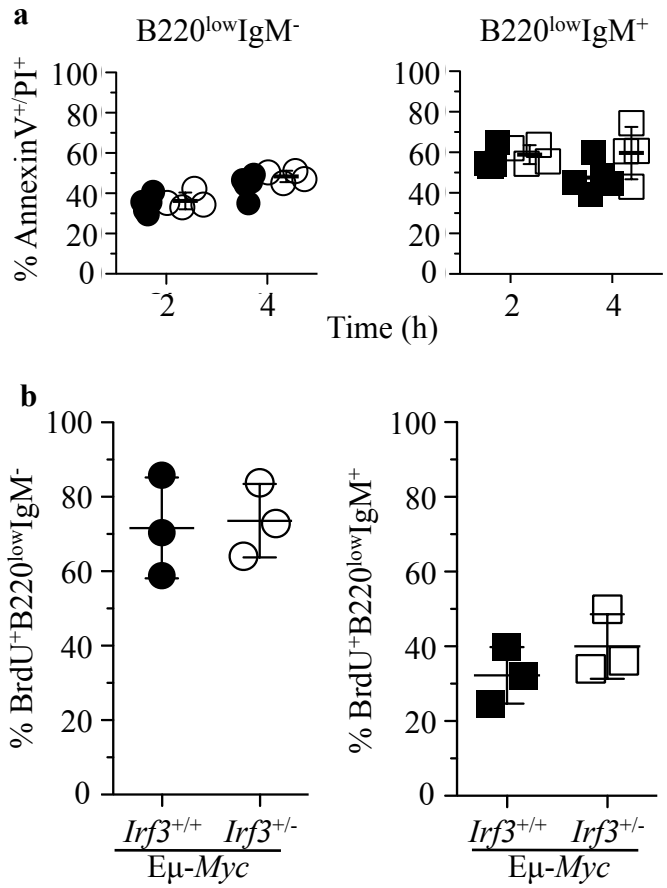

Figure 5.5 Rate of apoptosis and proliferation is not changed in tumors of *Irf3*$^{+/-}$Eμ-*Myc* mice.
(a) Tumor cells derived from the blood of day 27 of age *Irf3*$^{+/-}$Eμ-*Myc* (white) and *Irf3*$^{+/+}$Eμ-*Myc* (black*)* mice were cultured for 2 to 4 hrs before staining with B220, IgM, Propodium Iodide (PI) and Annexin-V. Annexin-V and PI positive cells were considered apoptotic. Data is represented as mean ± SD of 4 different mice for each genotype. **(b)** 37 days of age *Irf3*$^{+/+}$Eμ-*Myc* (black) and *Irf3*$^{+/-}$Eμ-*Myc* (white) mice were injected with 1 mg BrdU i.p. 18 hrs before B220^{low} blood cells were analysed for IgM expression and BrdU incorporation. Percentage of BrdU positive B220^{low}IgM^{-} (left panel) and B220^{low}IgM^{+} (right panel) in the blood of mice is shown. Data is represented as mean ± SD of 3 different mice for each genotype.

In BC2 and EμM1 cells, overexpression of *Bcl2l12* had no effect on proliferation or NKG2D ligand expression (Figure 5.6a and b). The rate of apoptosis was not also changed in BC2 cells overexpressing *Bcl2l12* when compared to empty vector transduced cells and marginally decreased

apoptosis in EμM1 cells (Figure 5.6c). In EμM1 cells, the percentage of Annexin V^+PI^+ cells was significantly higher in cells transduced with *Gfp* control (mean ± SD = 7.850 ± 0.752 %, n = 4) compared to cells transduced with *Bcl2l12* (mean ± SD = 5.213 ± 0.607 %, n = 4) (P = 0.0116). These data support the conclusion that the altered survival curve in *Irf3/Bcl2l12*$^{+/-}$Eμ-*Myc* is due to decreased expression of IRF3, rather than changes in BCL2L12 expression.

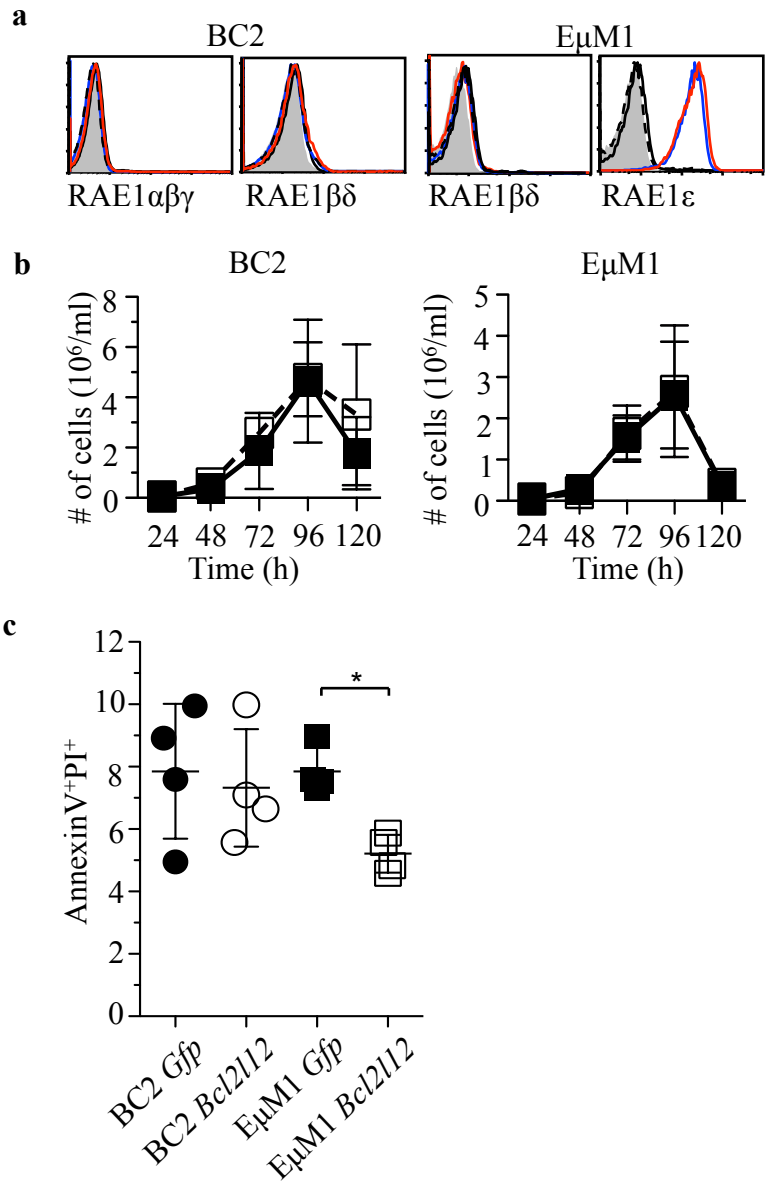

Figure 5.6 Overexpression of *Bcl2l12* in BC2 or EμM1 cells has little or no effect on RAE1 expressions, apoptosis or proliferation rate.

BC2 or EμM1 cells were transduced with retroviral vectors encoding *Bcl2l12*-IRES-*Gfp* (red line) or IRES-*Gfp* (blue line). **(a)** 3 days post transduction expression of indicated RAE1s was determined by flow cytometry. Filled histograms show isotype staining of *Bcl2l12*-IRES-*Gfp* transduced cells. Fine line indicates the isotype staining of IRES-*Gfp* expressing cells. **(b)** 0.5 x 10^5/ml MSCV-Bcl2L12 (open symbol) or MSCV-GFP (filled symbol) transduced BC2 cells (left panel) or EμM1 (right panel) were plated and living GFP^+ cells were counted every 24 hours for the next 5 days. Data is represented as means ± SD of 3 independent experiments. **(c)** The percentage of Annexin-V^+/PI^+ cells MSCV-Bcl2L12 (open symbol) or MSCV-GFP (filled symbol) transduced BC2 cells (circle) or EμM1 (black) was determined by flow cytometry. Statistical analyses were performed using student's t test. *$p<0.05$. Data represents means ± SD of 4 independent experiments.

5.4 Characterization of NK cells maturation and activity in *Irf3*$^{+/-}$Eμ-*Myc* mice

Our previous data showed that NK cells and T cell contribute to immunosurveillance in Eμ-*Myc* mice (Croxford et al., 2013). *Irf3* deficiency has no impact on NK and T cell numbers (Sato et al., 2000). To address if there is any difference in NK cells activation in the *Irf3*$^{+/-}$Eμ-*Myc* mice, we performed a CD107a degranulation assay. Several studies had established that degranulation of CD107a in NK cells correlate with its cytotoxicity activity and could be used as a sensitive marker for NK cell activity (Aktas et al., 2009; Alter et al., 2004). Besides being expressed on nearly all cytokine-secreting cells, CD107a was also expressed on a large subset of NK cells that did not secrete cytokine following stimulation. Thus, this facilitates identification of a large fraction of activated NK cells that may degranulate without cytokine secretion. We did not observe any difference in percentage of CD107a^{+} NK cells between *Irf3*$^{+/-}$Eμ-*Myc* (n = 9, mean ± SD = 21.489 ± 4.589%) and *Irf3*$^{+/+}$Eμ-*Myc* mice (n = 7, mean ± SD = 23.400 ± 7.528%) when co-incubation with Yac-1 in a 3:1 target to effector ratio (Figure 5.7a). Similarly, the percentage of IFNγ^{+} NK cells were not significantly different between *Irf3*$^{+/-}$ Eμ-*Myc* (n = 9, mean ± SD = 4.901 ± 1.371%) and *Irf3*$^{+/+}$Eμ-*Myc* mice (n = 7, mean ± SD = 4.751 ± 2.288%) (Figure 5.7a).

To investigate if there is any difference in NK cells activity upon stimulation of the NKG2D receptor, we took freshly isolated splenocytes and stimulated *in vitro* for 5 hours on plates pre-coated with anti-NKG2D or isotype control antibody. We did not observe any difference in percentage of IFNγ^{+} NK cells between *Irf3*$^{+/-}$ Eμ-*Myc* (n = 4, mean ± SD = 20.350 ±

6.360%) and *Irf3*$^{+/+}$Eμ-*Myc* mice (n = 4, mean ± SD = 28.625 ± 12.156%) upon *in vitro* stimulation by anti-NKG2D antibody (Figure 5.7b).

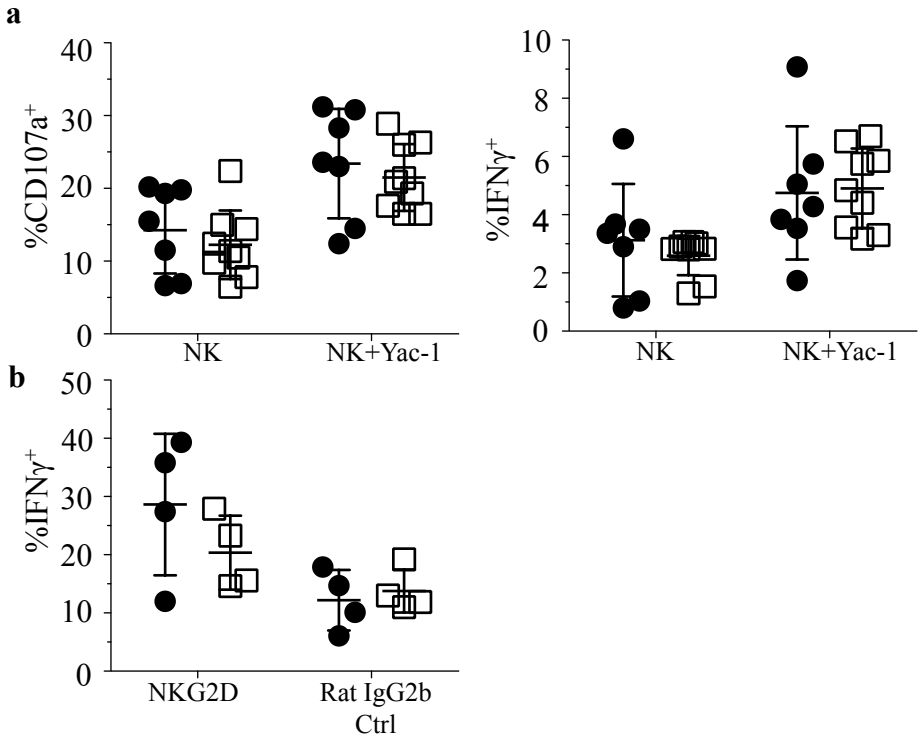

Figure 5.7 NK cells from *Irf3*$^{+/-}$ Eμ-*Myc* and *Irf3*$^{+/+}$Eμ-*Myc* showed similar activation.

(a) IL-2–activated NK cells derived from *Irf3*$^{+/-}$Eμ-*Myc* (white squares, n= 8) and *Irf3*$^{+/+}$Eμ-*Myc* (black circles, n= 7) mice were incubated with Yac-1 cells at an effector: target ratio of 3:1. After 4 hrs, the percentage of CD107a and IFN-γ-expressing NK1.1^{+}CD3^{-} cells was determined by flow cytometry (left and right panel). **(b)** Freshly isolated splenocytes of *Irf3*$^{+/-}$Eμ-*Myc* (white squares, n= 4) and *Irf3*$^{+/+}$Eμ-*Myc* (black circles, n= 4) mice were stimulated *in vitro* for 5 hrs on plates coated with NKG2D-specific antibodies (MI-6, 10 μg/ml), or isotype control (10 μg/ml) in the presence of GolgiPlug and 1 x 10^3 units/ml recombinant human IL-2 before staining and analysis. Intracellular IFN-γ was detected by flow cytometry on electronically gated NK1.1^{+}CD3^{-} cells. Data is represented as mean ± SD.

In addition, we did not observe a significant difference in the development of NK cells from *Irf3*$^{+/-}$Eμ-*Myc* and *Irf3*$^{+/+}$Eμ-*Myc* mice (Figure 5.8). NKG2D deficiency increases the tumor load of Eμ-*Myc* mice, but has not impact on the survival (Guerra et al., 2008). Hence, it is possible that additional *Irf3*-mediated effects are responsible for the shortened survival of *Irf3*$^{+/-}$Eμ-*Myc* mice.

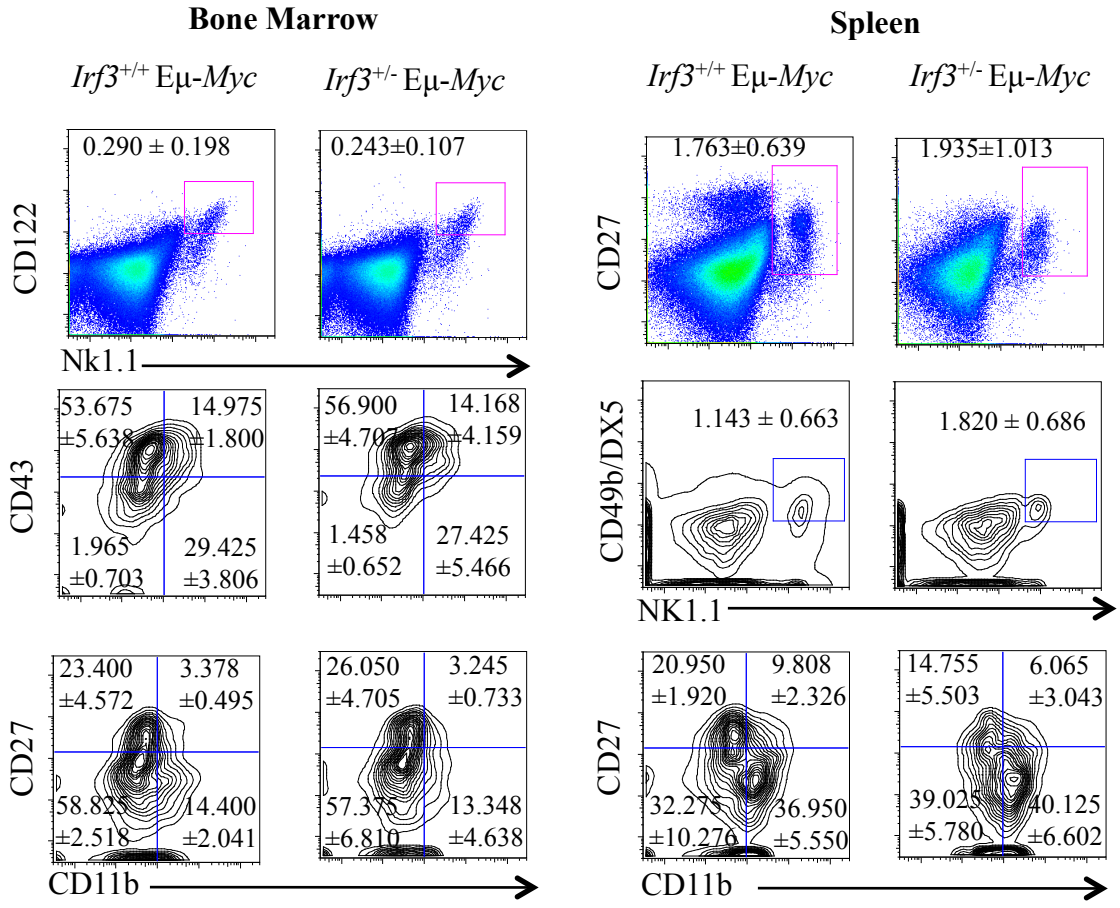

Figure 5.8 NK cell development is preserved in *Irf3*$^{+/-}$Eμ-*Myc* mice.
Analysis of NK subsets in the bone marrow (n= 4; left panel) and spleen (n= 4; right panel) of *Irf3*$^{+/+}$Eμ-*Myc* mice (left columns) and *Irf3*$^{+/-}$Eμ-*Myc* mice (right columns). The top groups represent gated CD3^{-} cells, whereas the remaining panels represent gated NK1.1^{+}CD3^{-} cells. The numbers represent mean percentages (±SD) of cells expressing the indicated markers.

5.5 Summary

Eμ-*Myc* mice heterozygous for *Irf3* exhibit decreased survival and reduced expression of RAE1ε. The null mutation introduced into the *Irf3* allele also resulted in the functional inactivation of the neighboring *Bcl2l12* gene. *Bcl2l12* in BC2 or EμM1 cells has little or no effect on RAE1 expressions, apoptosis or proliferation rate, thus suggesting that the altered survival curve in *Irf3/Bcl2l12*$^{+/-}$Eμ-*Myc* is due to decreased expression of IRF3, rather than changes in BCL2L12 expression. The activity and maturation of NK cells are not deficient in Eμ-*Myc* mice heterozygous for *Irf3*.

Chapter 6: Increased survival of Eμ-*Myc* mice deficient in *Zbp1*

6.1 Increased survival of Eμ-*Myc* mice deficient in *Zbp1*

To study the potential role of cytosolic DNA sensors in tumorigenesis, we bred mice deficient for *Zbp1* (*Zbp1*$^{-/-}$) to Eμ-*Myc* mice. Surprisingly, the survival of complete knockout of *Zbp1*-deficient Eμ-*Myc* mice (*Zbp1*$^{-/-}$Eμ-*Myc*) showed a significant increase in survival (median survival of 174 days, n = 57) when compared to *Zbp1*$^{+/+}$Eμ-*Myc* (median survival of 111 days, n = 38) (P = 0.003 by Log-Rank(Mantel-Cox) Test or P = 0.016 by Gehan-Breslow-Wilcoxon Test) and *Zbp1*$^{+/-}$Eμ-*Myc* mice (median survival of 111 days, n= 32) (P < 0.001 by Log-Rank (Mantel-Cox) Test or P = 0.008 by Gehan-Breslow-Wilcoxon Test) (Figure 6.1).

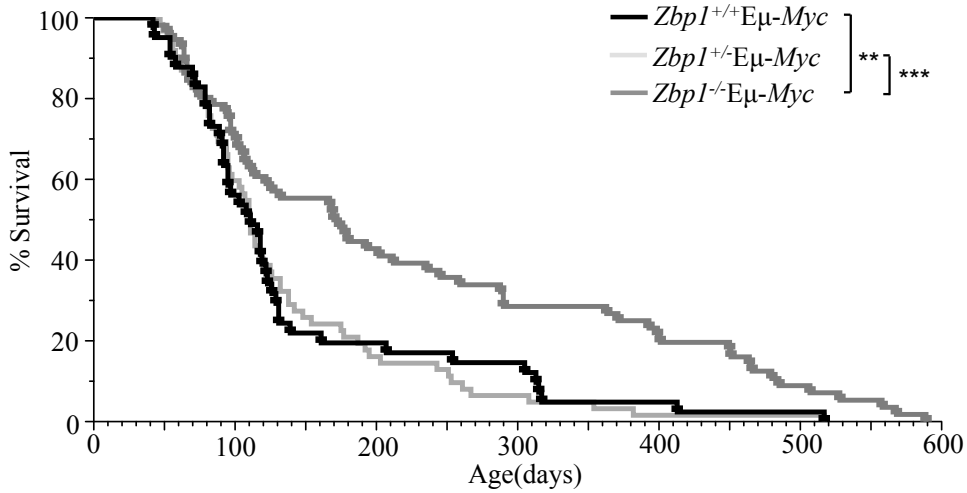

Figure 6.1 Survival is increased in Eμ-*Myc* mice deficient in *Zbp1*.
Zbp1$^{-/-}$Eμ-*Myc* mice (dark grey) exhibit increased survival compared to *Zbp1*$^{+/-}$Eμ-*Myc* (light grey) and *Zbp1*$^{+/+}$Eμ-*Myc* mice (black) using Kaplan-Meier analysis of survival. **p < 0.010 or *** p< 0.001 by Log-Rank (Mantel-Cox) Test.

6.2 Eμ-*Myc* mice deficient in *Zbp1* had reduced tumour load

The tumour cells in Eμ-*Myc* mice can be identified in the blood by their surface expression markers B220 and IgM (Figure 4.5). The prolonged survival of *Zbp1*$^{-/-}$Eμ-*Myc* mice correlated with a lower blood tumor load in the blood between day 21-40 (n = 152, mean tumor load ± SD = 39.570 ± 12.020%) and day 41-65 (n = 106, mean tumor load ± SD = 25.860 ± 15.800%) ($P < 0.001$) (Figure 6.2a and b). However, we did not observe similar regression in *Zbp1*$^{+/+}$Eμ-*Myc* between day 21-40 (n = 120, mean tumour load ± SD = 39.410 ± 26.280%) and day 41-65 (n = 80, mean tumour load ± SD = 37.540 ± 24.220%) (Figure 6.2a and b). Similarly, *Zbp1*$^{+/-}$Eμ-*Myc* mice showed no significant decrease in blood tumour load between day 21-40 (n = 173, mean tumour load ± SD = 45.940 ± 14.980%) and day 41-65 (n = 127, mean tumour load ± SD = 36.460 ± 21.030%) (Figure 6.2a and b). Expectedly, the tumour load of WT mice remains low (mean tumour load< 20%).

At day 41-65, the tumour load for *Zbp1*$^{-/-}$Eμ-*Myc* mice (n = 106, mean tumor load ± SD = 25.860 ± 15.800%) was significantly lower than *Zbp1*$^{+/-}$ Eμ-*Myc* (n = 80, mean tumour load ± SD = 37.540 ± 24.220%) ($P < 0.001$) and *Zbp1*$^{+/+}$Eμ-*Myc* mice (n = 80, mean tumour load ± SD= 37.540 ± 24.220%) ($P < 0.001$) (Figure 6.2a and b). At greater than 65 days of age, the tumour load for *Zbp1*$^{+/+}$ Eμ-*Myc* mice (n = 88, mean tumor load ± SD = 39.580 ± 29.950%) was significantly higher than *Zbp1*$^{-/-}$Eμ-*Myc* mice (n = 215, mean tumor load ± SD = 24.830 ± 21.500%) (Figure 6.2a and b).

We also measured the absolute number of B220^{low} cells in the blood by multiplying the number of blood lymphocytes measured by scil Vet abc with

percentage of blood tumor load assessed by flow cytometry. We observed a significant decreease in the number of $B220^{low}$ cells in the blood between day 31-40 (n = 14, mean ± SD = 2.597 ± 1.649 x 10^3 cells per µl) and day 51-65 (n = 14, mean ± SD = 1.395 ± 0.187 x 10^3 cells per µl) (P = 0.0187) in *Zbp1*$^{-/-}$ Eµ-*Myc* mice (Figure 6.2c). We did not observe a difference in the number of $B220^{low}$ cells in the blood between day 31-40 (n = 15, mean ± SD = 2.646 ± 1.379 x 10^3 cells per µl) and day 51-65 (n = 15, mean ± SD = 2.490 ± 2.681 x 10^3 cells per µl) in *Zbp1*$^{+/+}$Eµ-*Myc* mice (Figure 6.2c).

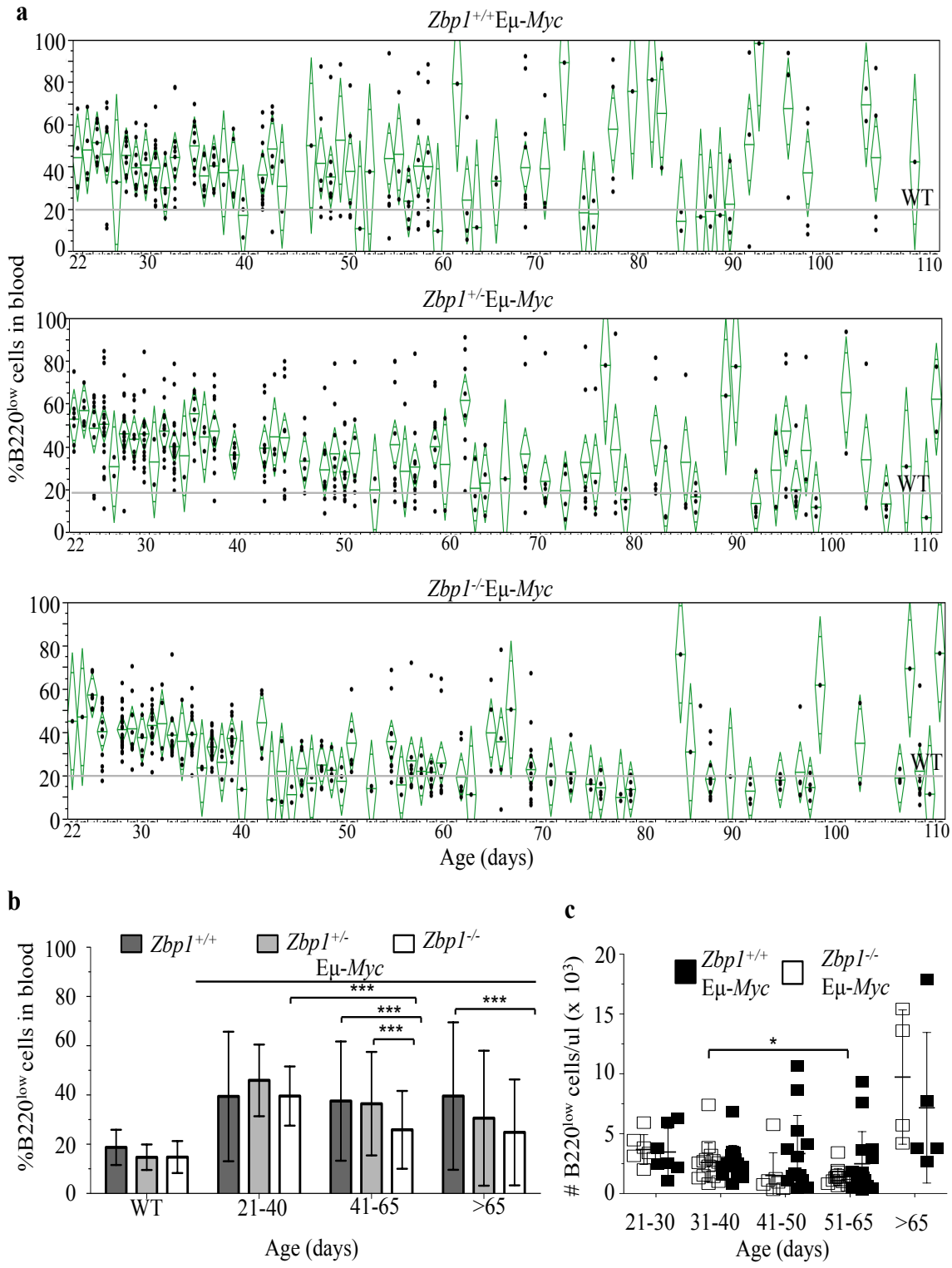
a
Zbp1+/+Eμ-Myc
Zbp1+/-Eμ-Myc
Zbp1-/-Eμ-Myc
WT
%B220low cells in blood
Age (days)
b
Zbp1+/+
Zbp1+/-
Zbp1-/-
Eμ-Myc
***
%B220low cells in blood
WT
21-40
41-65
>65
Age (days)
c
Zbp1+/+ Eμ-Myc
Zbp1-/- Eμ-Myc
*
B220low cells/ul (x 10³)
21-30
31-40
41-50
51-65
>65
Age (days)

Figure 6.2 Eμ-*Myc* mice deficient in *Zbp1* had reduced tumour load.
(a) and (b) Longitudinal analysis of tumor load in peripheral blood of Eμ-*Myc* or WT mice by flow cytometric analysis. Each point (·) represents percentage of $B220^{low}$ cells in the blood of individual Eμ-*Myc* mice. Mice were sacrificed after developing signs of disease. Diamond represents mean tumor load per time-point and 95% confidence limit. Mean percentage of $B220^{low}$ cells in the blood of WT mice is represented by black line. Summary of data in **(a)** is shown in **(b)**. Data represent average tumour cells ± SD. Statistical analyses were performed using one-way ANOVA. *** $p<0.001$. (**c)** Number of $B220^{low}$ cells in the peripheral blood of *Zbp1*$^{-/-}$Eμ-*Myc* (black circle) and *Zbp1*$^{+/+}$Eμ-*Myc* mice (white square) is calculated by multiplying the number of blood lymphocytes measured by scil Vet abc with percentage of blood tumor load assessed by flow cytometry. Data represent mean tumor load per time-point ± SD. Statistical analyses were performed using student's t test. *$p<0.05$.

6.3 Difference in regression was not due to altered trafficking of tumour cells

A similar decrease was observed in the tumor load in the spleen and lymph nodes at 41-65 days of age in the *Zbp1*$^{-/-}$Eμ-*Myc* mice (Figure 6.3). In the spleen of *Zbp1*$^{-/-}$Eμ-*Myc* mice, there was a significant decrease in the percentage of IgM^{-} B220^{low} cells from day 21-40 (n = 39, mean ± SD = 48.350 ± 14.831%) to day 41-65(n = 10, mean ± SD = 24.518 ± 24.939%) ($P < 0.001$) (Figure 6.3). However, in the spleen of *Zbp1*$^{+/+}$Eμ-*Myc* mice, the percentage of IgM^{-} B220^{low} cells from day 21-40 (n = 32, mean ± SD = 47.241 ± 16.923%) to day 41-65(n = 15, mean ± SD = 39.654 ± 29.086%) remains relatively constant.

In the lymph nodes of *Zbp1*$^{-/-}$Eμ-*Myc* mice, there was a significant decrease in the percentage of IgM^{-} B220^{low} cells from day 21-40 (n = 22, mean ± SD = 42.145 ± 17.682%) to day 41-65(n = 7, mean ± SD = 14.454 ± 25.382%) ($P = 0.003$) (Figure 6.3). However, in the spleen of *Zbp1*$^{+/+}$Eμ-*Myc* mice, the percentage of IgM^{-} B220^{low} cells from day 21-40 (n = 19, mean ± SD = 43.053 ± 16.733%) to day 41-65(n = 11, mean ± SD = 37.818 ± 32.657%) remains relatively constant (Figure 6.3). The percentage of tumor cells in the bone marrow in both *Zbp1*$^{+/+}$Eμ-*Myc* and *Zbp1*$^{-/-}$Eμ-*Myc* was comparable and was roughly constant at all stages of disease (Figure 6.3).

No tumor cell invasion of the thymus was detected except at the very late stage of disease in mice older than 120 days of age. As expected, no tumors were detected in WT mice (background staining was < 20%) ((Figure 6.3). Our data suggest that the decrease of tumor cells in the blood was not a consequence of altered trafficking of tumor cells to other organs.

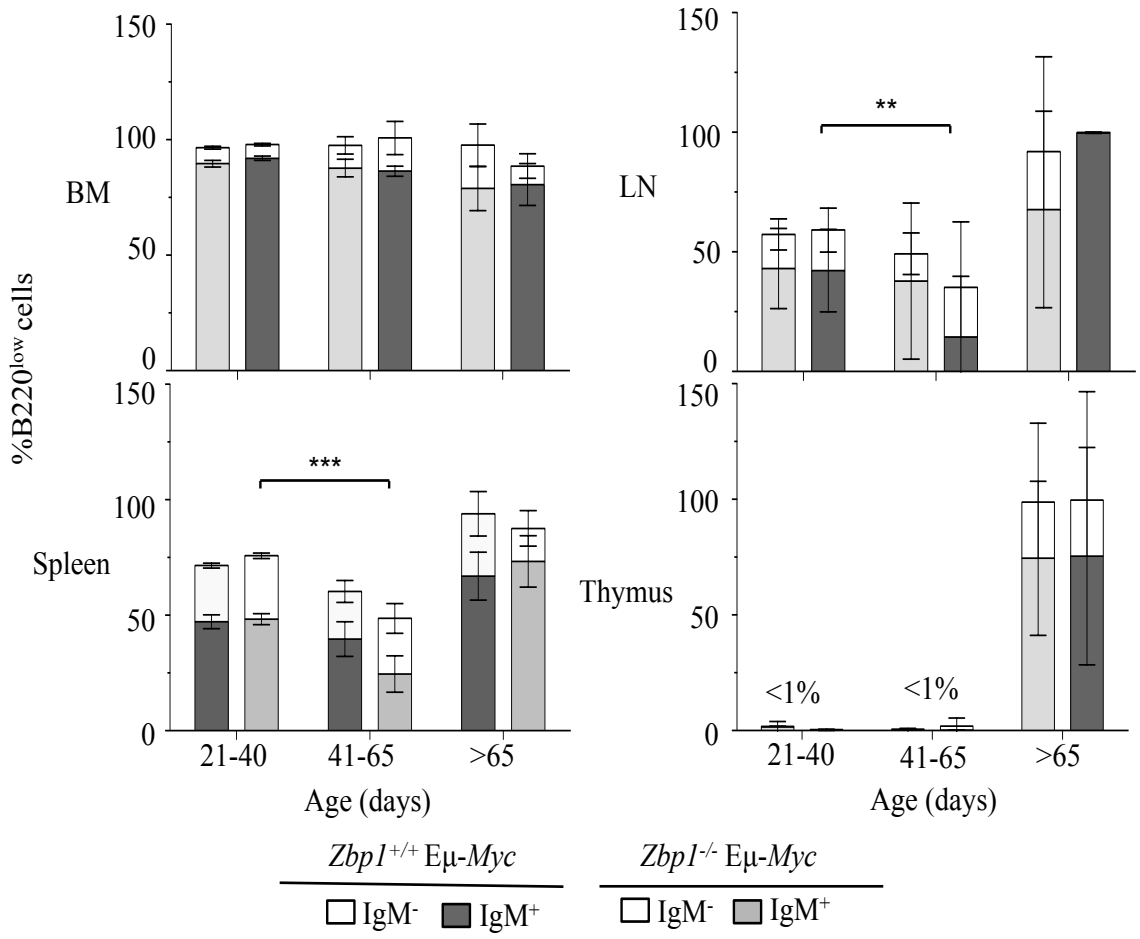

Figure 6.3 Difference in regression was not due to altered trafficking of tumour cells.

Longitudinal analysis of the $B220^{low}$ cells in spleen, thymus, bone marrow and lymph node of $Zbp1^{-/-}$Eμ-*Myc* (light grey column) and $Zbp1^{+/+}$Eμ-*Myc* mice (dark grey column). Mean percentage ± SD of $IgM^{-}B220^{low}$ (grey bars), $IgM^{+}B220^{low}$ (white bars) cells in the indicated organs of $Zbp1^{-/-}$ Eμ-*Myc* mice (n≥ 7 per time-point) before 41 days of age (early), between 41 and 65 days of age (regression) and post 65 days of age (late) are shown. Statistical analyses were performed using student's t test. **p<0.010, ***p<0.001.

6.4 B220^{low} cells from *Zbp1*$^{+/+}$E μ -*Myc* and *Zbp1*$^{-/-}$E μ -*Myc* mice showed similar rate of proliferation

KI-67 protein is present during all active phases of the cell cycle (G (1), S, G (2), and mitosis), but is absent from resting cells (G (0)), thus, its expression is strictly associated with cell proliferation (Gerdes, 1990). Anti-KI-67 protein antibodies had been used in diagnostics of human tumours and the fraction of KI-67-positive tumor cells or the KI-67 labeling index often correlates with the clinical course of the disease (Gerdes, 1990; Scholzen and Gerdes, 2000). Therefore, we compared the percentage of KI-67 positive b220^{low} tumour cells in the blood of *Zbp1*$^{-/-}$Eμ-*Myc*, *Zbp1*$^{+/+}$Eμ-*Myc, Zbp1*$^{-/-}$ and *Zbp1*$^{+/+}$ mice by intracellular flow cytometry. As expexted, pre-regression B220^{low} cells from both *Zbp1*$^{-/-}$Eμ-*Myc* and *Zbp1*$^{+/+}$Eμ-*Myc* mice expressed high levels of KI-67 compared to WT cells (Figure 6.4). However, we did not observe any difference in the percentage of KI-67 high cells between B220^{low} cells from both *Zbp1*$^{-/-}$Eμ-*Myc* (n = 9, mean ± SD = 67.678 ± 9.910%) and *Zbp1*$^{+/+}$Eμ-*Myc* mice (n = 9, mean ± SD = 67.811 ± 10.712%) (Figure 6.4).

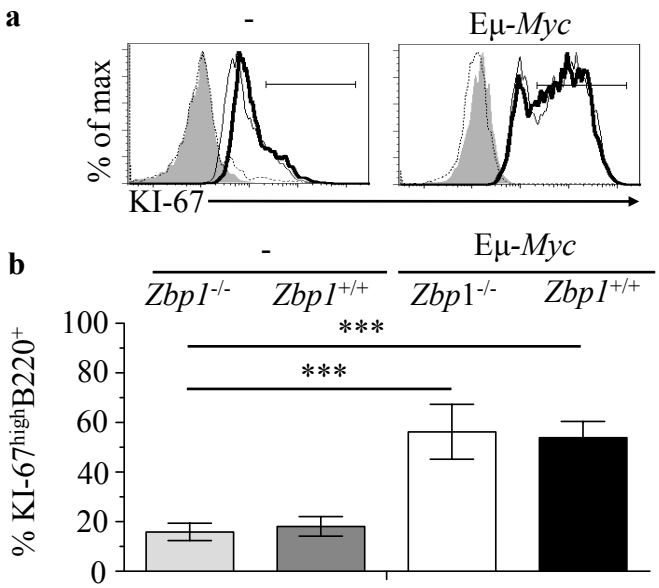

Figure 6.4 Similar levels of KI-67 in B220^{low} cells from *Zbp1*$^{-/-}$Eμ-*Myc* and *Zbp1*$^{+/+}$Eμ-*Myc* mice.

(a) B220^{low} cells from blood of *Zbp1*$^{+/+}$ (black bold) and *Zbp1*$^{-/-}$ (grey bold) mice were assessed for intracellular KI-67 expression. Isotype controls for *Zbp1*$^{+/+}$ (filled grey) and *Zbp1*$^{-/-}$(black) were as shown. Representative FACS histograms with gatings for KI-67^{high} cells are shown. **(b)** Mean percentage of B220^{low} cells that were KI-67^{high} ± SD for each genotype (≥ 4n each) were plotted. Statistical analyses were performed using student's t test and *** denotes $p < 0.001$.

We also compared the proliferation rate of the tumour cells by BrdU incorporation and DNA content. Analysis of BrdU incorporation and DNA content revealed that pre-regression (before 40 days of age) $B220^{low}$ cells of *Zbp1*$^{+/+}$Eμ-*Myc* and *Zbp1*$^{-/-}$Eμ-*Myc* mice incorporated similar amount of BrdU in both the spleen and the bone marrow (Figure 6.5). As expected, the rate of proliferation was higher for *Zbp1*$^{+/+}$Eμ-*Myc* compared to *Zbp1*$^{+/+}$ and for *Zbp1*$^{-/-}$Eμ-*Myc* compared to *Zbp1*$^{-/-}$ in both the spleen and bone marrow (Figure 6.5). In the bone marrow, the percentage of $B220^{low}$ cells in S-phase was higher for *Zbp1*$^{+/+}$Eμ-*Myc* (n = 5, mean ± SD = 55.940 ± 10.650%) compared to *Zbp1*$^{+/+}$ (n = 3, mean ± SD = 25.333 ± 1.604%) (P = 0.0402) and for *Zbp1*$^{-/-}$Eμ-*Myc* (n = 9, mean ± SD = 48.633 ± 11.745%) compared to *Zbp1*$^{-/-}$ (n = 4, mean ± SD = 24.675 ± 4.577%) (P = 0.0026) (Figure 6.5). In the spleen, the percentage of $B220^{low}$ cells in S-phase was higher for *Zbp1*$^{+/+}$Eμ-*Myc* (n = 5, mean ± SD = 33.320 ± 12.747%) compared to *Zbp1*$^{+/+}$ (n = 5, mean ± SD = 9.652 ± 7.113%) (P = 0.0067) and for *Zbp1*$^{-/-}$Eμ-*Myc* (n = 5, mean ± SD = 27.500 ± 10.487%) compared to *Zbp1*$^{-/-}$ (n = 3, mean ± SD = 11.360 ± 3.323%) (P = 0.0454) (Figure 6.5).

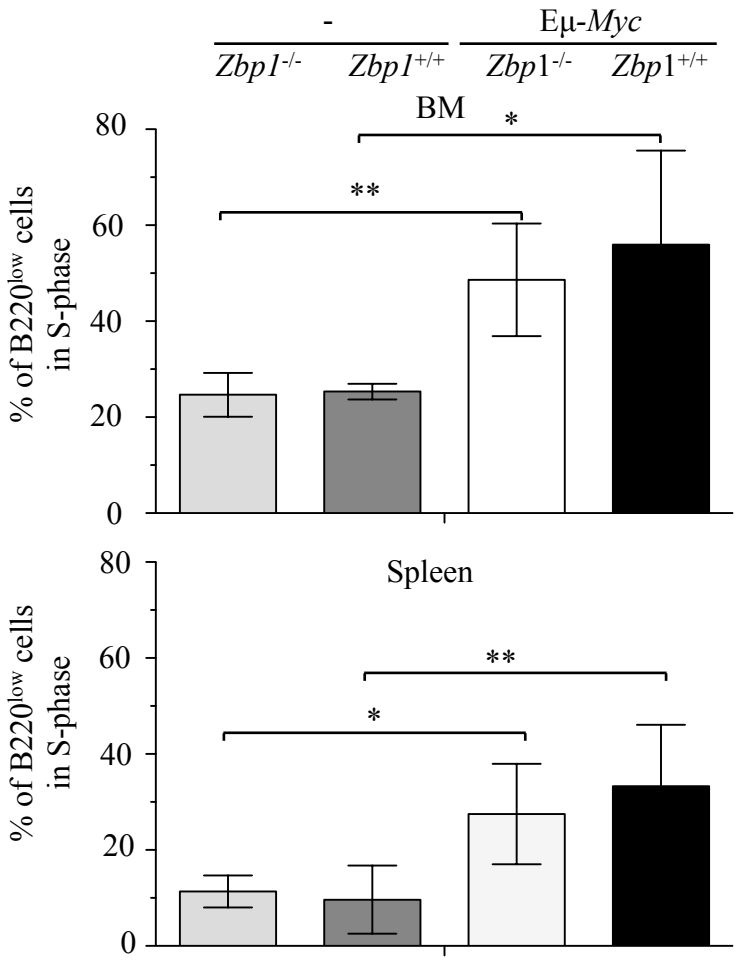

Figure 6.5 B220^{low} cells from *Zbp1*$^{-/-}$Eμ-*Myc* and *Zbp1*$^{+/+}$Eμ-*Myc* mice displayed similar proliferation rate.

Spleen (bottom panel) and bone marrow (BM) (top panel) from day 31-40 were analysed for BrdU incorporation and DNA content. Data represent mean percentages of B220^{low} cells in S-phase ± SD. Statistical analyses were performed using Student's t test. * denotes $p < 0.05$ and ** denotes $p < 0.01$. $n \geq 3$ mice were analysed for each genotype.

As expected for tumor cells, proteins important for S-phase entry such as CYCLIN D1, CYCLIN A, phosphorylated pRB and CDK2 were upregulated in B220^{low} cells of Eμ-*Myc* mice when compared to WT cells (Figure 6.6). However, we did not observe a significant difference in the expression levels of S-phase associated proteins in pre- regression B220^{low} cells between *Zbp1*$^{+/+}$Eμ-*Myc* and *Zbp1*$^{-/-}$Eμ-*Myc* (Figure 6.6). This support the conclusion that proliferation rate might not account for the difference in regression.

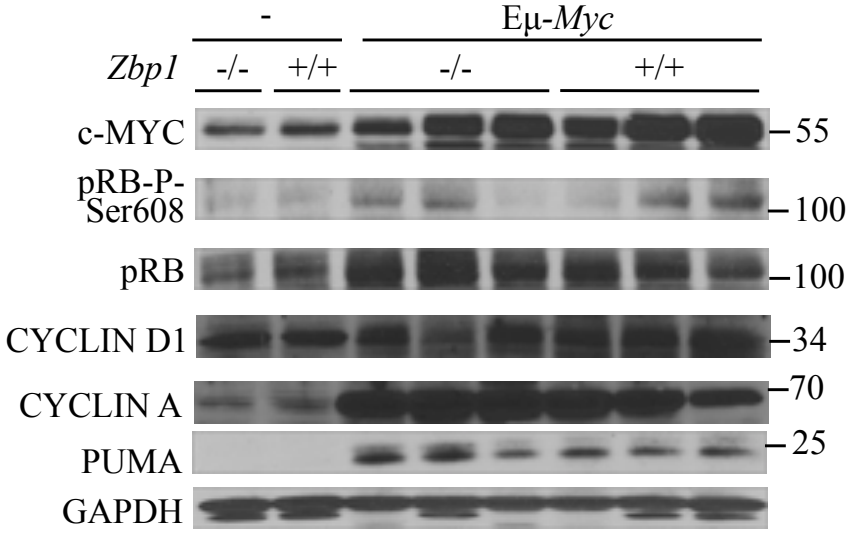

Figure 6.6 Immunoblot of cell cycle proteins.
Expression levels of cell cycle-related proteins in purified splenic B220^{+} cells of *Zbp1*$^{+/+}$Eμ-*Myc*, *Zbp1*$^{-/-}$Eμ-*Myc*, *Zbp1*$^{+/+}$ and *Zbp1*$^{-/-}$ from 31-40 days of age. Representative immunoblots from 3 independent experiments are shown.

6.5 B220^{low} cells from *Zbp1*$^{-/-}$Eμ-*Myc* mice have higher apoptosis rate than *Zbp1*$^{+/+}$Eμ-*Myc* mice

To compare the rates of apoptosis, we analyzed pre-regression (before 40 days of age), regression (between 41-65 days of age) and WT B220^{low} cells for Annexin-V expression and propidium iodide (PI) uptake. The percentage of apoptotic cells (Annexin-V^{+} and/or PI^{+}) was significantly increased in B220^{low} cells from 41-65 day of age bone marrow of *Zbp1*$^{-/-}$Eμ-*Myc* mice (n = 8, mean ± SD = 84.454 ± 6.655%) compared to *Zbp1*$^{+/+}$Eμ-*Myc* mice (n = 7, mean ± SD = 70.000 ± 15.443%) (P = 0.0276), *Zbp1*$^{+/+}$ mice (n = 4, mean ± SD = 55.225 ± 9.944%) (P < 0.001) or *Zbp1*$^{-/-}$ mice (n = 4, mean ± SD = 50.351 ± 8.829%) (P < 0.001) after 3 hours in culture (Figure 6.7b). The rate of apoptosis in B220^{low} cells from bone marrow of *Zbp1*$^{+/+}$Eμ-*Myc* mice (n = 7, mean ± SD = 70.000 ± 15.443%) was significantly higher than *Zbp1*$^{-/-}$ mice (n = 4, mean ± SD = 50.351 ± 8.829%) (P = 0.039) but not significant when compared to *Zbp1*$^{+/+}$ mice (n = 4, mean ± SD = 55.225 ± 9.944%)(Figure 6.7b). This could be due to insufficient number of mice.

The percentage of apoptotic cells was significantly increased in B220^{low} cells from 41-65 day of age bone marrow of *Zbp1*$^{-/-}$Eμ-*Myc* mice (n = 8, mean ± SD = 84.454 ± 6.655%)compared to 31-40 days of age bone marrow (n = 7, mean ± SD = 51.858 ± 26.801%) (P = 0.005) (Figure 6.7b). This is consistent with the observation that regression of B220^{low} occurs after day 41 in *Zbp1*$^{-/-}$ Eμ-*Myc* mice.

We did not observe any significant difference in percentage of apoptotic cells in *ex vivo* B220^{low} cells from the spleen or bone marrow and in spleenic B220^{low} cells that had been cultured for 3 hours of each genotype (Figure6.7).

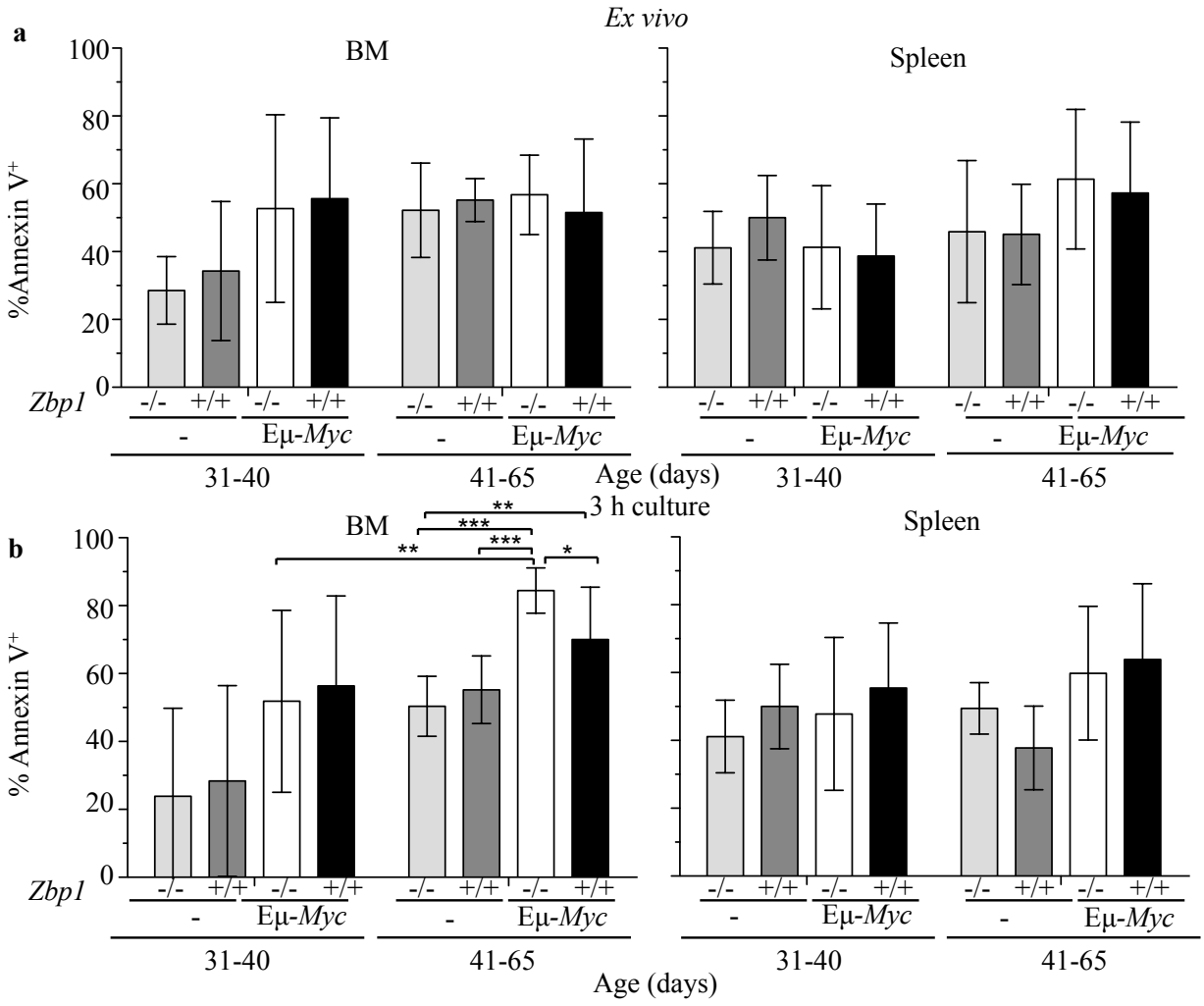

Figure 6.7 Increase apoptosis of B220^{low} cells from the bone marrow of *Zbp1*$^{-/-}$Eμ-*Myc*.

Annexin-V staining of B220^{low} cells from spleen (right panel) or bone marrow (left panel) of *Zbp1*$^{+/+}$Eμ-*Myc* (black columns), *Zbp1*$^{-/-}$Eμ-*Myc* (white column), *Zbp1*$^{+/+}$ (light grey column) and *Zbp1*$^{-/-}$ (dark grey column)(≥ 4n each). Annexin-V staining was done on *ex vivo* cells **(a)** or cells kept in culture for 3 hours **(b)**. Data were represented as mean percentage of Annexin V^{+} cells ± SD. Student's t test was used to perform statistical analysis and *p* values are indicated as **p* < 0.05, **p<0.01. n ≥ 4 mice were analysed for each genotype.

Caspases play a major role in the apoptotic response (Shi, 2002; Thornberry and Lazebnik, 1998). Caspases are cysteine proteases that cleave after an aspartate residue in their substrates and belong to a conserved family of enzymes that irreversibly commit a cell to die (Riedl and Shi, 2004). There are two classes of apoptotic caspases: the initiator caspases, which include caspase-2, -8, -9 and -10 and the effector caspases, which include caspases-3, -6 and -7 in mammals (Riedl and Shi, 2004). All caspases exist in cells as catalytically inactive precursor and must undergo proteolytic activation during apoptosis. The activation of an effector caspase is carried out by an initiator caspase through cleavage at specific internal Asp residues that would produce the large (~p20) and small (~p10) subunits. By contrast, the initiator caspases are auto-activated in a tightly regulated process.

To investigate if there are differences in the activation of caspases, we purified B cells from the mice and performed an immunblot analysis using antibodies specific for CASPASE7 and CASPASE3. We observed presence of cleaved CASPASE 7 in all 3 *Zbp1*$^{-/-}$Eμ-*Myc* mice but only 1 out of 3 *Zbp1*$^{+/+}$ Eμ-*Myc* mice showed presence of cleaved CASPASE 7 (Figure 6.8a). Similarly, we saw presence of cleaved CASPASE 3 in all 3 *Zbp1*$^{-/-}$Eμ-*Myc* mice but only 1 out of 3 *Zbp1*$^{+/+}$Eμ-*Myc* mice showed presence of cleaved CASPASE 3 (Figure 6.8a). The ratio of the relative intensity of cleaved CASPASE 3 to CASPASE 3 was significantly higher in *Zbp1*$^{-/-}$Eμ-*Myc* mice (n = 3, mean ± SD = 1.446 ± 0.747) compared to *Zbp1*$^{+/+}$ Eμ-*Myc* mice (n = 3, mean ± SD = 0.140 ± 0.150) (P = 0.041) (Figure 6.8b). Similarly, the ratio of the relative intensity of cleaved CASPASE 7 to CASPASE 7 was significantly

higher in *Zbp1*$^{-/-}$Eμ-*Myc* mice (n = 6, mean ± SD = 0.660 ± 0.490) compared to *Zbp1*$^{+/+}$ Eμ-*Myc* mice (n = 6, mean ± SD = 0.157 ± 0.246) (P = 0.049) (Figure 6.8b). The data is in line with the finding that B220^{+} cells in *Zbp1*$^{-/-}$ Eμ-*Myc* mice have increased apoptosis.

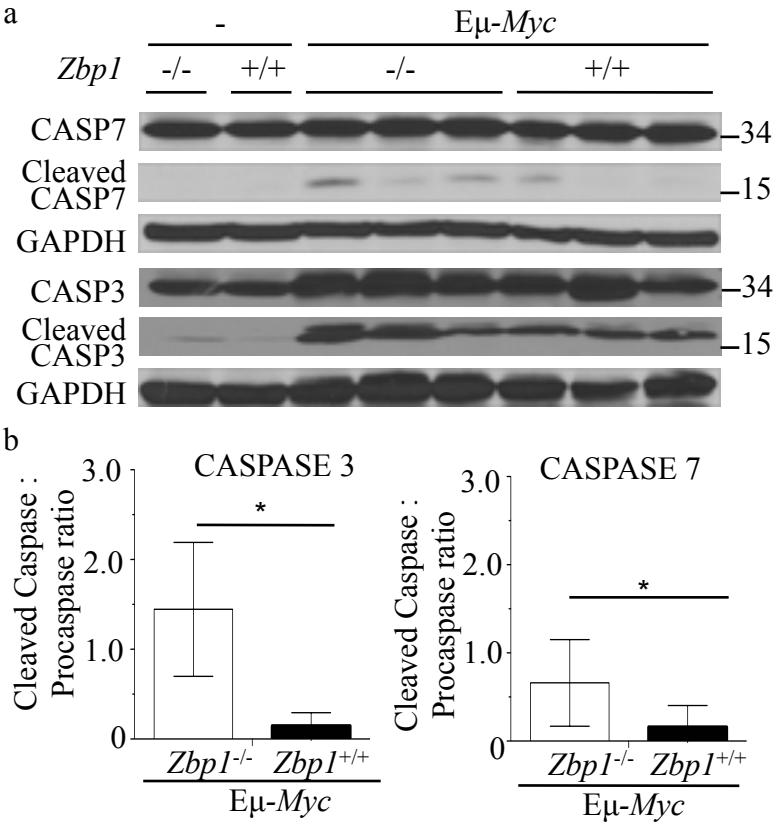

Figure 6.8 Increased activation of CASPASE7 and CASPASE3 in B220^{+} cells of *Zbp1*$^{-/-}$Eμ-*Myc* mice.
(a) Expression levels of CASPASE7, cleaved CASPASE7, CASPASE3 and cleaved CASPASE3 in purified bone marrow B220^{+} cells of *Zbp1*$^{+/+}$Eμ-*Myc*, *Zbp1*$^{-/-}$Eμ-*Myc*, *Zbp1*$^{+/+}$ and *Zbp1*$^{-/-}$ mice. Representative blots from 3 independent experiments are shown. **(b)** The ratio of the intensity of cleaved caspase to procaspase from the immunoblot in (a) was plotted as mean ± SD. n ≥ 3 mice were analysed for each genotype. Student's t test was used to perform statistical analysis and *p* values are indicated as *$p < 0.05$.

Using immunocytochemistry, we used antibody specific for cleaved CASPASE 3 to probe for activated CASPASE 3 in the bone marrow and spleen of *Zbp1*$^{-/-}$Eμ-*Myc* and *Zbp1*$^{+/+}$Eμ-*Myc* mice. We observed more B220^{+} cells with cleaved CASPASE3 in the bone marrow of *Zbp1*$^{-/-}$Eμ-*Myc* compared to the bone marrow of *Zbp1*$^{+/+}$Eμ-*Myc* mice (Figure 6.9). We observed presence of cleaved CASPASE 3 in the spleen of 2 out of 3 *Zbp1*$^{-/-}$ Eμ-*Myc* mice in contrast to only 1 out of 3 *Zbp1*$^{+/+}$Eμ-*Myc* mice/*Zbp1*$^{+/-}$Eμ-*Myc* mice (Figure 6.9).

These data support the conclusion that *Zbp1*$^{-/-}$Eμ-*Myc* tumor cells were more prone to apoptosis possibly due to increased levels of p53 upregulated modulator of apoptosis (PUMA) (Figure 6.6) and increases in cleaved CASPASE 3 and cleaved CASPASE 7 (Figure 6.8 and 6.9). In summary, our analysis revealed that differences in cell intrinsic apoptosis pathways might contribute to differences in regression between the *Zbp1*$^{+/+}$E*μ*-*Myc* and *Zbp1*$^{-/-}$ Eμ-*Myc* mice.

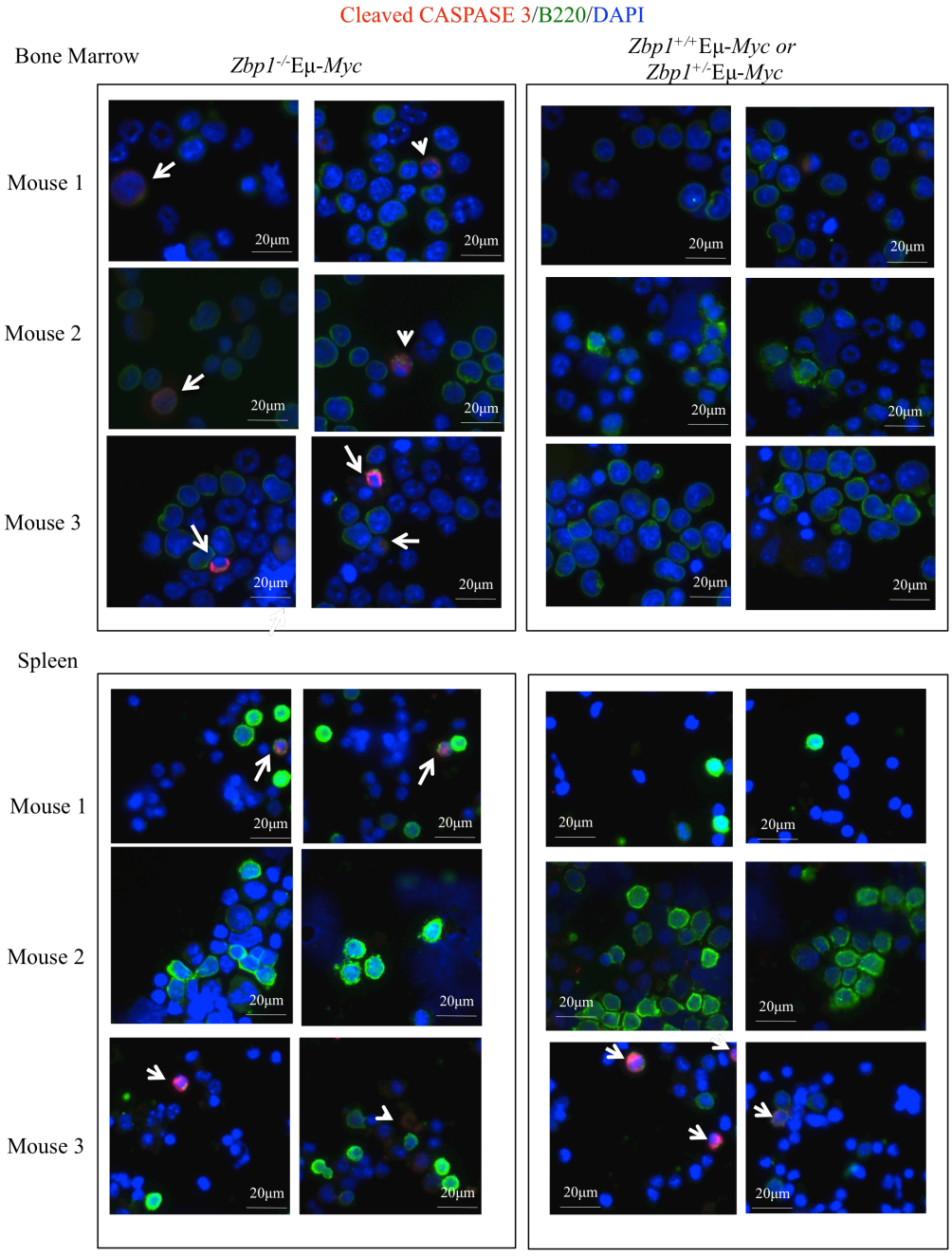
Cleaved CASPASE 3/B220/DAPI
Bone Marrow
Zbp1-/-Eμ-Myc
Zbp1+/+Eμ-Myc or
Zbp1+/-Eμ-Myc
Mouse 1
Mouse 2
Mouse 3
Spleen
Mouse 1
Mouse 2
Mouse 3
20μm

Figure 6.9 Immunocytochemistry of cleaved CASPASE 3 in bone marrow and spleen.
Splenocytes and bone marrow cells from 40-65 days of age *Zbp1*$^{-/-}$Eμ-*Myc* (n=3) mice or *Zbp1*$^{+/+}$Eμ-*Myc* mice/*Zbp1*$^{+/-}$Eμ-*Myc* mice (n=3) were cytospined and probed for antibody specific for cleaved CASPASE3 (red), B220^{+}(green) and DAPI (blue). Arrows point to cells positive for both B220 and cleaved CASPASE 3. For each cytospun slides, 5 different fields were observed under the microscrope and >100 cells were being examined. Representative immunofluorescence images are shown for each mouse.

6.6 No difference in expressions of T cells activation markers in *Zbp1*$^{-/-}$Eμ-*Myc* and *Zbp1*$^{+/+}$Eμ-*Myc* mice

We have previously reported that regression of tumour cells in the peripheral is dependent on T and NK cells (Croxford et al., 2013). Regression correlated with upregulation of the DNAM-1 ligand CD155 and the downregulation of H-2K^{b} on tumour cells and the downregulation of CD62L on T cells.

CD62L/L-selectin is a marker found on naïve T cells and further differentiates central memory (T_{cm}, CD62L^{+}) from effector memory (T_{em}, CD62L^{-}) T cells (Yang et al., 2011). CD62L is shed from the cell membrane following T cell activation and it can be used as a marker for T cell activation (Yang et al., 2011). The percentage of CD62L^{low} CD4^{+} T cells was not significantly different between *Zbp1*$^{-/-}$Eμ-*Myc* and *Zbp1*$^{+/+}$E*μ-Myc* mice during 21-40 days of age (n = 10, mean ± SD = 17.591 ± 11.382% versus n = 10, mean ± SD = 17.584 ± 12.500%) and during 41-65 days of age (n = 10, mean ± SD = 21.165 ± 10.504% versus n = 10, mean ± SD = 27.770 ± 11.700%) (Figure 6.10a). Furthermore, we did not observe any significant difference in CD62L^{low} CD8^{+} T cells between *Zbp1*$^{-/-}$Eμ-*Myc* and *Zbp1*$^{+/+}$E*μ-Myc* mice during 21-40 days of age (n = 10, mean ± SD = 13.069 ± 11.679% versus n = 10, mean ± SD = 12.874 ± 9.436%) and during 41-65 days of age

(n = 10, mean ± SD = 19.084 ± 14.177% versus n = 10, mean ± SD = 23.847 ± 15.767%) (Figure 6.10a).

DNAM-1 is an adhesion molecule involved in the cytolytic function of T lymphocytes (Shibuya et al., 1996). We did not observe any significant difference in DNAM-1 expressions on CD4+ T cells from *Zbp1*$^{-/-}$Eμ-*Myc* and *Zbp1*$^{+/+}$E*μ*-*Myc* mice during 21-40 days of age (n = 10, mean MFI ± SD = 4.805 ± 0.887 and n = 10, mean MFI ± SD = 5.033 ± 0.974 respectively) and during 41-65 days of age (n = 10, mean MFI ± SD = 3.478 ± 1.126 and n = 10, mean ± SEM MFI = 3.455 ± 2.701 respectively) (Figure 6.10b). There was no significant difference in DNAM-1 expressions on CD8^{+} T cells from *Zbp1*$^{-/-}$ Eμ-*Myc* and *Zbp1*$^{+/+}$E*μ*-*Myc* mice during 21-40 days of age (n = 10, mean MFI ± SD = 27.940 ± 3.199 and n = 10, mean MFI ± SD = 30.085 ± 3.706 respectively) and during 41-65 days of age (n = 10, mean MFI ± SD = 20.389 ± 8.087 and n = 10, mean MFI ± SD = 21.597 ± 12.618 respectively) (Figure 6.10b).

The observations are in contrast to previous report from our lab that implicates the role of T cells and NK cells in spontaneous regressions (Croxford et al., 2013). As tumour-specific T cells might only constitute a small percentage of the total population, it would be difficult to detect any significant difference in T cells activation between *Zbp1*$^{-/-}$Eμ-*Myc* and *Zbp1*$^{+/+}$E*μ*-*Myc* mice, thus explaining the discrepancies in observations.

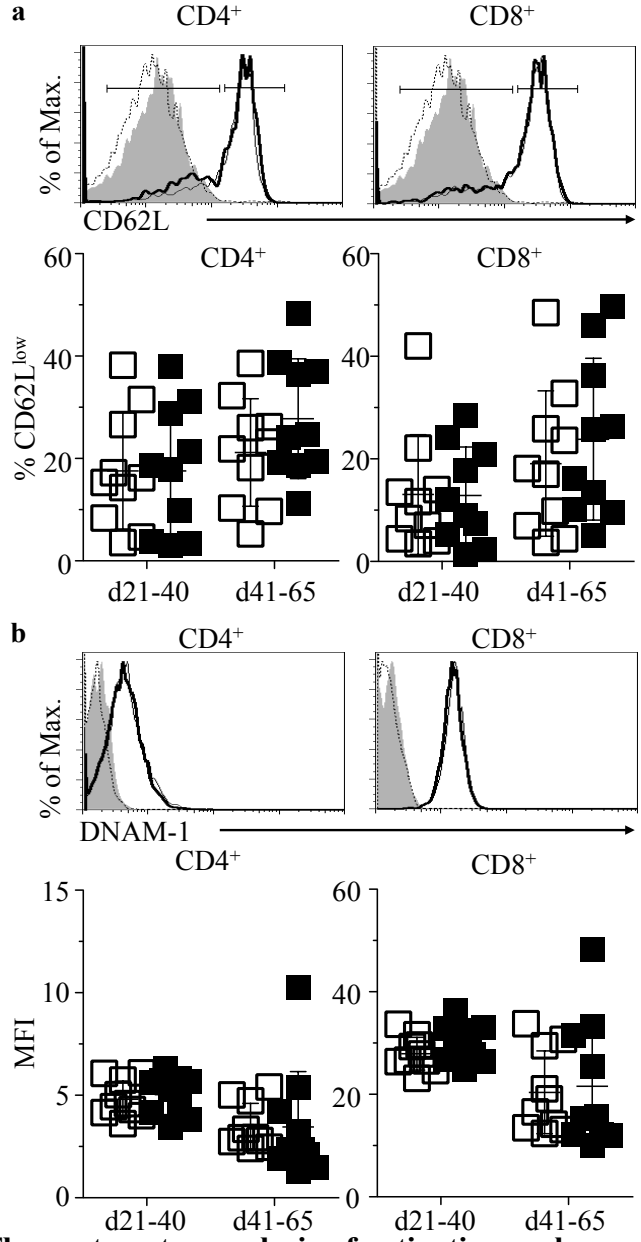

Figure 6.10 Flow cytometry analysis of activation makers on CD8$^+$ and CD4$^+$ T cells from the blood.

(a) Top panel: Representative FACS plot showing CD62L levels on CD4$^+$ and CD8$^+$ T cells from the blood of regression mice (d41-d65) from both *Zbp1*$^{+/+}$Eμ-*Myc* (bold lines) and *Zbp1*$^{-/-}$Eμ-*Myc* (thin lines). Isotype control for *Zbp1*$^{+/+}$Eμ-*Myc* (filled histogram) and *Zbp1*$^{-/-}$Eμ-*Myc* (dashed lines) and gates indicating CD62L^{low} and CD62L^{high} populations are also shown. Bottom panel: Mean percentage ± SD of CD62L ^{low} cells on CD4$^+$ or CD8$^+$ T cells from blood of *Zbp1*$^{+/+}$Eμ-*Myc* (black) and *Zbp1*$^{-/-}$Eμ-*Myc* (white) from pre-regression (d21-40) and regression (d41-65) mice. n= 10 for each genotype. **(b)** Top panel: Representative FACS plot showing DNAM-1 levels on CD4$^+$ and CD8$^+$ T cells from the blood of regression mice (d41-d65) from both *Zbp1*$^{+/+}$Eμ-*Myc* (bold lines) and *Zbp1*$^{-/-}$Eμ-*Myc* (thin lines). Isotype control for *Zbp1*$^{+/+}$Eμ-*Myc* (filled histogram) and *Zbp1*$^{-/-}$Eμ-*Myc* (dashed lines) Bottom panel: mean MFI ± SD of DNAM-1 levels on CD4$^+$ or CD8$^+$ T cells from blood of *Zbp1*$^{+/+}$Eμ-*Myc* (black) and *Zbp1*$^{-/-}$Eμ-*Myc* (white) from pre-regression (d21-40) and regression (d41-65) mice. n= 10 for each genotype. Statistical analyses were performed using Student's t test.

6.7 Similar expressions of co-stimulatory molecules on B220^{low} cells from *Zbp1*$^{-/-}$Eμ-*Myc* and *Zbp1*$^{+/+}$Eμ-*Myc* mice

Poliovirus receptor (CD155) and Nectin-2 (CD112) have been identified as ligands for DNAM-1, with CD155 appearing to have a major role in inducing DNAM-1-dependent responses (Bottino et al., 2003). CD155 is widely expressed on normal cells and overexpressed on many tumor types (Bottino et al., 2003; Carlsten et al., 2007; Castriconi et al., 2004; El-Sherbiny et al., 2007; Pende et al., 2006; Reymond et al., 2004; Sloan et al., 2005). The DNAM-1/CD155 interaction is important for recognition and elimination of tumour cells by NK cells (Carlsten et al., 2007). We did not observe any significant difference in CD155 expressions on B220^{low} cells from *Zbp1*$^{-/-}$Eμ-*Myc* and *Zbp1*$^{+/+}$E*μ-Myc* mice during 21-40 days of age (n = 10, mean MFI ± SD = 2.241 ± 1.719 and n = 10, mean MFI ± SD = 1.913 ± 1.137 respectively) and during 41-65 days of age (n = 10, mean MFI ± SD = 2.683 ± 1.195 and n= 10, mean MFI ± SD = 3.191 ± 1.368 respectively) (Figure 6.11a and b). We also did not see any significant difference in CD155 expressions when we compare *Zbp1*$^{-/-}$Eμ-*Myc* or *Zbp1*$^{+/+}$E*μ-Myc* between 21-40 days of age and 41-65 days of age.

Engagement of CD28 on naive T cells by either CD80 or CD86 ligands on antigen-presenting cells provides a strong costimulatory signal to T cells activated through their T cell receptor (Carreno and Collins, 2002). This leads to induction of IL-2 transcription, expression of CD25, proliferation and provides critical survival signals to the T cells. We did not observe any significant difference in CD80 expressions on B220^{low} cells from *Zbp1*$^{-/-}$Eμ-*Myc* and *Zbp1*$^{+/+}$E*μ-Myc* mice during 21-40 days of age (n = 10, mean MFI ± SD = 0.264 ± 0.403 and n = 10, mean MFI ± SD = 0.130 ± 0.172

respectively) and during 41-65 days of age (n= 10, mean MFI ± SD = 0.096 ± 0.166 and n= 10 and mean MFI ± SD = 0.125 ± 0.297 respectively) (Figure 6.11a and b). Similarly, we did not observe any significant difference in CD86 expressions on $B220^{low}$ cells from *Zbp1*$^{-/-}$Eμ-*Myc* and *Zbp1*$^{+/+}$E*μ*-*Myc* mice during 21-40 days of age (n = 10, mean MFI ± SD = 1.365 ± 0.243 and n = 10, mean MFI ± SD = 1.463 ± 0.561 respectively) and during 41-65 days of age (n= 10, mean MFI ± SD = 1.082 ± 0.578 and n= 10 and mean MFI ± SD = 1.689 ± 1.525 respectively) (Figure 6.11a and b). We also did not see any significant difference in CD80 or CD86 expressions when we compare *Zbp1*$^{-/-}$ Eμ-*Myc* or *Zbp1*$^{+/+}$E*μ*-*Myc* between 21-40 days of age and 41-65 days of age.

ICAM-1 is an integral membrane glycoprotein possessing an extracellular domain containing five tandem Ig-like domains, a transmembrane domain, and a short cytoplasmic tail (Staunton et al., 1988). ICAM-1 provides enough costimulatory signals to induce T cell activation and IL-2 gene expression in a CD28-independent mechanism, and is the main, essential costimulatory molecule required for the activation of T cells in the absence of B7/CD28 costimulation (Salomon and Bluestone, 1998; Zuckerman et al., 1998). We did not observe any significant difference in ICAM-1 expressions on $B220^{low}$ cells from *Zbp1*$^{-/-}$Eμ-*Myc* and *Zbp1*$^{+/+}$E*μ*-*Myc* mice during 21-40 days of age (n = 10, mean MFI ± SD = 21.223 ± 5.601 and n = 10 and mean MFI ± SD = 20.801 ± 7.513 respectively) and during 41-65 days of age (n = 10, mean MFI ± SD = 18.905 ± 6.222 and n= 10 and mean MFI ± SD = 21.678 ± 10.103 respectively) (Figure 6.11a and b). We also did not observe any significant difference in ICAM-1 expressions when

we compare *Zbp1*$^{-/-}$Eμ-*Myc* or *Zbp1*$^{+/+}$E*μ*-*Myc* between 21-40 days of age and 41-65 days of age.

The chemokine receptor type 4 (CXCR4), which binds to the chemokine stromal cell-derived factor (SDF)-1 (CXCL12), is involved in lymphocyte trafficking. CXCR4 had also been found to be a prognostic marker in different cancers, including leukemia and breast cancer. There is increasing evidence that CXCR4 expression and function in hematopoietic malignancies have an important role on disease progression. CXCR4 levels are significantly increased in B-cell chronic lymphocytic leukemia (Mohle et al., 1999), B-cell but not T-cell acute lymphoblastic leukemia (Bradstock et al., 2000; Dialynas et al., 2001), multiple myeloma (Hideshima and Anderson, 2002), and acute myeloid leukaemia (Tavor et al., 2004). We observe a significant decrease in CXCR4 expressions on B220^{low} cells from *Zbp1*$^{-/-}$Eμ-*Myc* between 21-40 days of age (n = 10, mean MFI ± SD = 14.244 ± 8.232) and 41-65 days of age (n = 10, mean MFI ± SD = 6.49 ± 1.33) (P = 0.016) (Figure 6.11a and b). However, expressions of CXCR4 on B220^{low} cells remain high in *Zbp1*$^{+/+}$Eμ-*Myc* mice during 21-40 days of age (n = 10, mean MFI ± SD = 12.147 ± 8.587) and during 41-65 days of age (n = 10, mean MFI ± SD = 18.580 ± 26.613) (Figure 6.11a and b). These correlated with the increased in malignancy of the tumours, as CXCR4/CXCL12 signaling is critically involved in the survival and trafficking of normal and malignant B-lymphocytes.

It had been reported that tumour cells could lose MHC class 1 molecules through a variety of mechanisms, resulting in escape from immune surveillance (Khong and Restifo, 2002). Consistent with the earlier report by

Croxford et al. (2013), we saw a similar decrease in expressions of MHC class I H-2K^{b} molecules on B220^{low} cells in the blood in *Zbp1*$^{-/-}$Eμ-*Myc* mice between 21-40 days of age (n = 22, mean MFI ± SD = 70.160 ± 22.093) and 41-65 days of age (n = 19, mean MFI ± SD = 49.422 ± 22.295) (P = 0.005) (Figure 6.11a and b). We also observe a significant decrease in MFI intensity in *Zbp1*$^{+/+}$Eμ-*Myc* mice between 21-40 days of age (n = 16, mean MFI ± SD = 62.801 ± 18.575) and 41-65 days of age (n = 15, mean MFI ± SD = 44.663 ± 20.042) (P = 0.014) (Figure 6.11a and b). However, when we compare the MFI of H-2K^{b} of *Zbp1*$^{-/-}$Eμ-*Myc* and *Zbp1*$^{+/+}$Eμ-*Myc* mice within each age group, we did not observe any significant difference, suggesting that the expression levels of H-2K^{b} were similar for *Zbp1*$^{-/-}$Eμ-*Myc* and *Zbp1*$^{+/+}$Eμ-*Myc* in each age group.

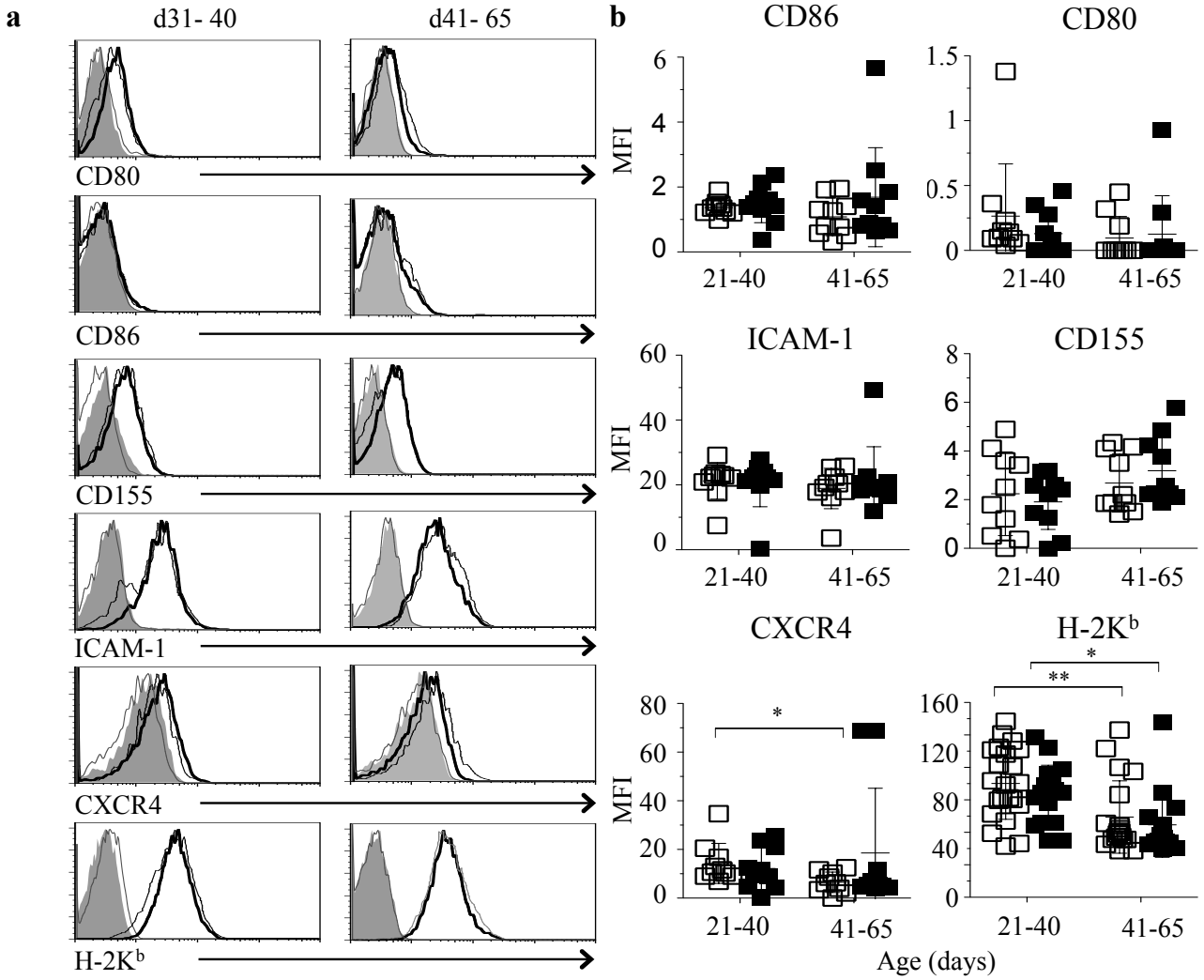

Figure 6.11 Flow cytometry analysis of surface makers on B220^{low} cells from the blood of *Zbp1*$^{-/-}$Eμ-*Myc* and *Zbp1*$^{+/+}$Eμ-*Myc* mice.
(a) Representative FACS plot showing expressions of CD80, CD86, CD155, ICAM-1, CXCR4 and H-2K^{b} in both *Zbp1*$^{+/+}$Eμ-*Myc* (black bold lines) and *Zbp1*$^{-/-}$Eμ-*Myc* (black dash lines) on B220^{low} cells from the blood of pre-regression (d31-40) and regression mice (d41-65). Isotype controls were either tinted (*Zbp1*$^{+/+}$Eμ-*Myc*) or dashed (*Zbp1*$^{-/-}$Eμ-*Myc*). **b)** Mean MFI ± SD of CD80, CD86, CD155, ICAM-1, CXCR4 and H-2K^{b} on both *Zbp1*$^{+/+}$Eμ-*Myc* (black) and *Zbp1*$^{-/-}$Eμ-*Myc* (white) in B220^{low} cells from the blood. n= 10 each for *Zbp1*$^{+/+}$Eμ-*Myc* and *Zbp1*$^{-/-}$Eμ-*Myc*. Statistical analyses were performed using Student's t test. *p<0.05 and **p<0.01.

6.8 Summary

Eμ-*Myc* mice deficient in *Zbp1* had increased survival and reduced tumour load. The reduced tumour load is not due to altered trafficking of the tumour cells to other organs or dicrepancies in proliferation rate. Eμ-*Myc* mice deficient in *Zbp1* had higher expressions of cleaved CASPASE3 and cleaved CASPASE7 and increased apoptosis rate which might account for the reduced tumour burden.

Chapter 7: Increased DNA damage in Eμ-*Myc* mice deficient in *Zbp1*

7.1 Whole genome microarray revealed increase expression of genes involved in the DNA repair pathways in *Zbp1*$^{-/-}$Eμ-*Myc*

We performed a whole genome microarray on sorted B220^{low} cells from pre-regression spleens of both *Zbp1*$^{+/+}$Eμ-*Myc* (n= 3) and *Zbp1*$^{-/-}$Eμ-*Myc* (n= 3) mice. Interestingly, we saw upregulation of various genes involved in the DNA damage repair pathways in B220^{low} cells in the *Zbp1*$^{-/-}$Eμ-*Myc* mice compared to the *Zbp1*$^{+/+}$Eμ-*Myc* mice (Figure 7.1). This is consistent with our previous study which indicated that DDR plays a role in tumorigenesis (Croxford et al., 2013) .

Key genes invovled in HRR such as *Brca2*, *Rad50*, *Rad54* were upregulated in all 3 *Zbp1*$^{-/-}$Eμ-*Myc* mice compared to *Zbp1*$^{+/+}$Eμ-*Myc* mice; *Mre11* and *Nbs1* were upregulated in 2 out of 3 *Zbp1*$^{-/-}$Eμ-*Myc* mice compared to *Zbp1*$^{+/+}$Eμ-*Myc* mice from the microarray analyses (Figure 7.1a). We validated these genes using real time PCR and we observed slightly higher fold change of *Brca2* transcript variant 1 (n = 3, mean fold change ± SD = 1.689 ± 0.432), *Brca2* transcript variant 2 (n = 3, mean fold change ± SD = 1.536 ± 0.444), *Rad54* (n = 3, mean fold change ± SD = 2.659 ± 0.680) and *Nbs1* (n = 3, mean fold change ± SD = 1.410 ± 1.342) in B220^{low} cells from *Zbp1*$^{-/-}$Eμ-*Myc* mice compared to *Zbp1*$^{+/+}$Eμ-*Myc* (Figure 7.1b). However, we did not observe much difference in the fold change of *Rad50* (n = 3, mean fold change ± SD = 1.071 ± 0.230) and *Mre11* (n = 3, mean fold change ± SD = 0.910 ± 0.141) (Figure 7.1b).

In the NER pathway, *Hr23b, Xpg* and *Csa* were upregulated in all 3 *Zbp1*$^{-/-}$Eμ-*Myc* mice compared to *Zbp1*$^{+/+}$Eμ-*Myc* mice from the microarray results (Figure 7.1a). We validated *Hr23b* with real time PCR as *Hr23b* was one of the top few genes that were upregulated in *Zbp1*$^{-/-}$Eμ-*Myc* mice.

Consistent with the microarray analyses, we observed significantly higher fold change of *Hr23b* (n = 3, mean fold change ± SD = 2.133 ± 0.198) (P = 0.010) in real time PCR in $B220^{low}$ cells from *Zbp1*$^{-/-}$Eμ-*Myc* mice compared to *Zbp1*$^{+/+}$Eμ-*Myc* mice (Figure 7.1b).

From the microarary analyses, *Ku70, Dna ligase II, Atm* from the NHEJ pathway were upregulated in all 3 *Zbp1*$^{-/-}$Eμ-*Myc* mice while *Ku80, Xrcc1, Dna ligase IV* and *Wrn* were upregulated in 2 out of 3 *Zbp1*$^{-/-}$Eμ-*Myc* mice (Figure 7.1a). In the real-time PCR analyses, we observed significantly higher fold change of *Ku70* (n = 3, mean fold change ± SD = 1.635 ± 0.177) (P = 0.025), *Ku80* (n = 3, mean fold change ± SD = 1.461 ± 0.101) (P = 0.016) and *Xrcc1* (n = 3, mean fold change ± SD = 1.171 ± 0.051) (P = 0.029) in $B220^{low}$ cells from *Zbp1*$^{-/-}$Eμ-*Myc* mice compared to *Zbp1*$^{+/+}$Eμ-*Myc* mice (Figure 7.1b). We observed slightly higher fold change of *Atm* (n = 3, mean fold change ± SD = 1.531 ± 0.365), *Dna ligase IV* (n = 3, mean fold change ± SD = 1.671 ± 1.197) and *Wrn* (n = 3, mean fold change ± SD = 1.556 ± 0.788) in $B220^{low}$ cells from *Zbp1*$^{-/-}$Eμ-*Myc* mice compared to *Zbp1*$^{+/+}$Eμ-*Myc* mice(Figure 7.1b).

c-Jun , which had role in apoptosis and cell cycle, was one of the top genes that were downregulated in *Zbp1*$^{-/-}$Eμ-*Myc* mice from the microarray results (Figure 7.1a). From the real-time PCR, we also observed significant downregulation of *c-Jun* (n = 3, mean fold change ± SD = 0.477 ± 0.082) (P = 0.0081) in $B220^{low}$ cells from *Zbp1*$^{-/-}$Eμ-*Myc* mice (Figure 7.1b). TNF-α is a major inflammatory cytokine that was first identified to induce rapid haemorrhagic necrosis of experimental cancers (Balkwill, 2009). TNF-α can be pro- or anti- tumour and it is important in cancer biology. From the

microarray results, *Tnf-α* was upregulated in 2 out of 3 *Zbp1*$^{-/-}$Eμ-*Myc* mice (Figure 7.1a). Consistent with the microarray results, we observed higher fold change of *Tnf-α* (n = 3, mean fold change ± SD = 1.998 ± 0.486) in B220^{low} cells from *Zbp1*$^{-/-}$Eμ-*Myc* mice compared to *Zbp1*$^{+/+}$Eμ-*Myc* mice (Figure 7.1b).

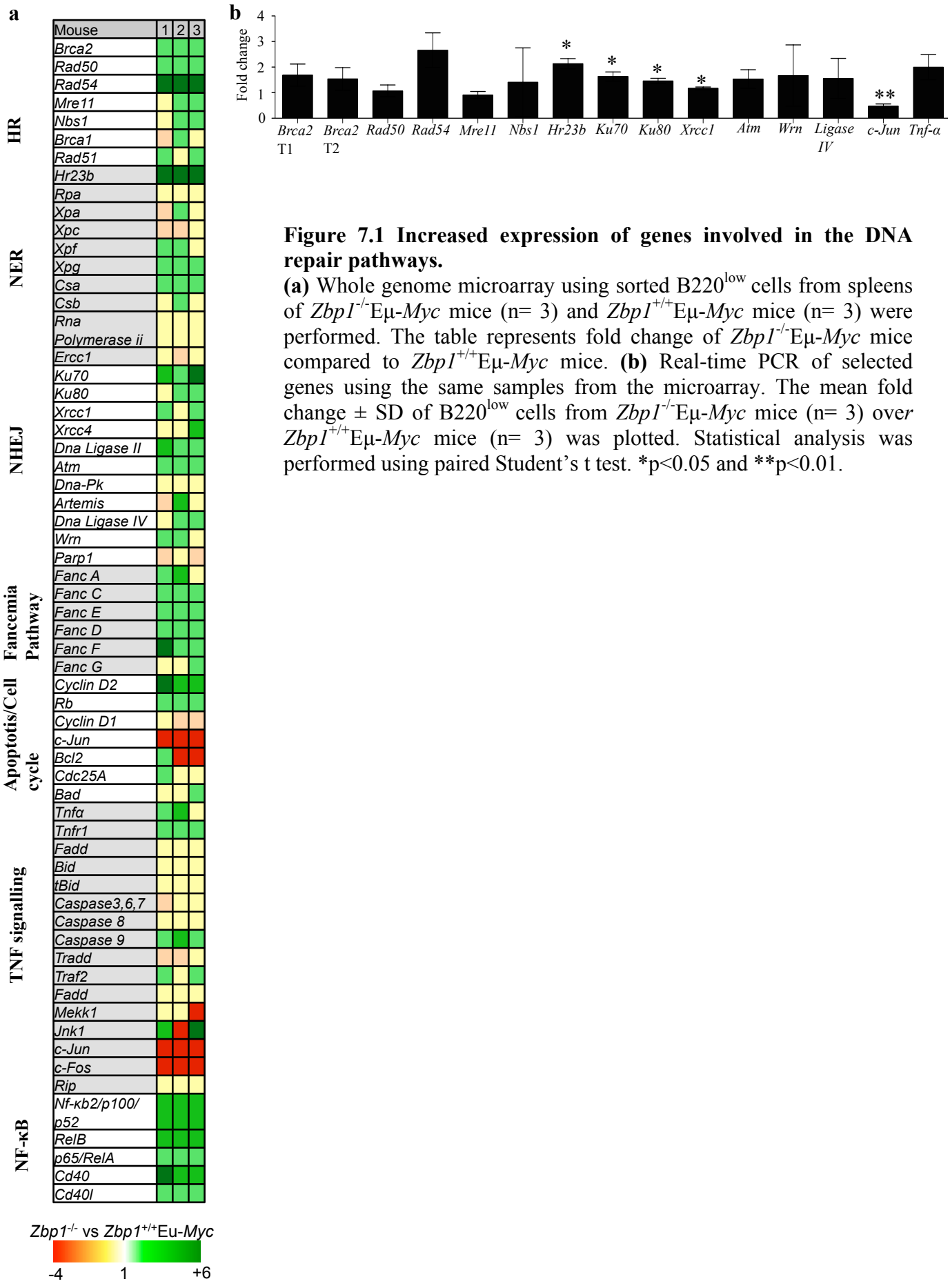

Figure 7.1 Increased expression of genes involved in the DNA repair pathways.

(a) Whole genome microarray using sorted B220^{low} cells from spleens of *Zbp1*$^{-/-}$Eμ-*Myc* mice (n= 3) and *Zbp1*$^{+/+}$Eμ-*Myc* mice (n= 3) were performed. The table represents fold change of *Zbp1*$^{-/-}$Eμ-*Myc* mice compared to *Zbp1*$^{+/+}$Eμ-*Myc* mice. **(b)** Real-time PCR of selected genes using the same samples from the microarray. The mean fold change ± SD of B220^{low} cells from *Zbp1*$^{-/-}$Eμ-*Myc* mice (n= 3) over *Zbp1*$^{+/+}$Eμ-*Myc* mice (n= 3) was plotted. Statistical analysis was performed using paired Student's t test. *p<0.05 and **p<0.01.

7.2 Enhanced DDR in tumour cells from *Zbp1*$^{-/-}$Eμ-*Myc* mice

Most proteins in the DDR pathway are phosphorylated upon activation; therefore, we investigated the phosphorylation status of some of the key molecules in the DDR pathway. B220^{+} splenocytes of *Zbp1*$^{-/-}$Eμ-*Myc* mice expressed higher levels of phosphorylated H2AX (γH2AX), a DNA damage marker, when compared to *Zbp1*$^{+/+}$Eμ-*Myc* mice (n = 3) (Figure 7.2). Western blot analysis of B cells from the spleen revealed higher levels of phosphorylated p53, phosphorylated CHK1, phosphorylated CHK2 and phosphorylated ATM in *Zbp1*$^{-/-}$Eμ-*Myc* mice compared to the *Zbp1*$^{+/+}$Eμ-*Myc* mice, providing further evidence that the loss of *Zbp1* potentiates the DDR (Figure 7.2). The presence of γH2AX acts as a sensitive marker for DNA double-strand breaks (DSBs) (Bonner et al., 2008), which are predominantly repaired by NHEJ or HRR. Both the Western blot data and the microarray data are consistent with the suggestion that there are persistent DSB breaks in the tumour cells in *Zbp1*$^{-/-}$Eμ-*Myc* mice.

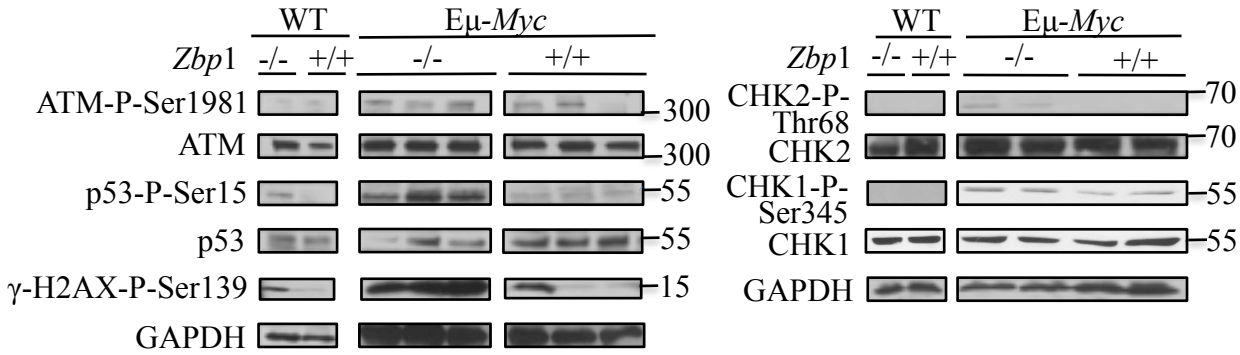

Figure 7.2 Enhanced DNA damage response in tumour cells from *Zbp1*$^{-/-}$ Eμ-*Myc* mice.
Immunoblot analysis of splenic B220^{+} cells (> 98% purity) from day 31- 40 *Zbp1*$^{+/+}$, *Zbp1*$^{-/-}$, *Zbp1*$^{+/+}$Eμ-*Myc*, and *Zbp1*$^{-/-}$Eμ-*Myc* mice were probed with antibodies for indicated DNA damage response markers. Representative blots from 3 independent experiments are shown.

In an alternative approach, we stained blood cells of mice with γH2AX and B220 specific antibodies and DAPI (nuclear stain). Immunofluorescence microscopy provided further evidence that there were significantly higher number of tumour cells of *Zbp1*$^{-/-}$Eμ-*Myc* mice (n = 3, mean ± SD = 93.110 ± 9.602%) with γH2AX as compared to *Zbp1*$^{+/+}$Eμ-*Myc* mice (n = 4, mean ± SD = 14.020 ± 11.080%) ($P < 0.001$) (Figure 7.3a).

Additionally, we stained for RAD51, a molecule that acts to transduce DNA damage signals to promote DSB repair via HRR (Suwaki et al., 2011). In addition, a recent study has identified *RAD51* as a potential tumour suppressor gene (Bric et al., 2009). As expected, we observed accumulation of higher number of RAD51 foci in the nucleus of B cells in *Zbp1*$^{-/-}$Eμ-*Myc* mice. Quantitative analysis of microscopy data showed that there was significantly higher percentage of B cells in *Zbp1*$^{-/-}$Eμ-*Myc* mice (n = 3, mean ± SD = 83.460 ± 19.40%) with more than three foci as compared to *Zbp1*$^{+/+}$Eμ-*Myc* mice (n = 3, mean ± SD = 14.010 ± 12.37%) ($P = 0.0064$) (Figure 7.3b). The greater activation of RAD51 observed in *Zbp1*$^{-/-}$Eμ-*Myc* mice indicated higher levels of DNA repair occurring through HRR, which probably exert a greater tumour suppressor effect.

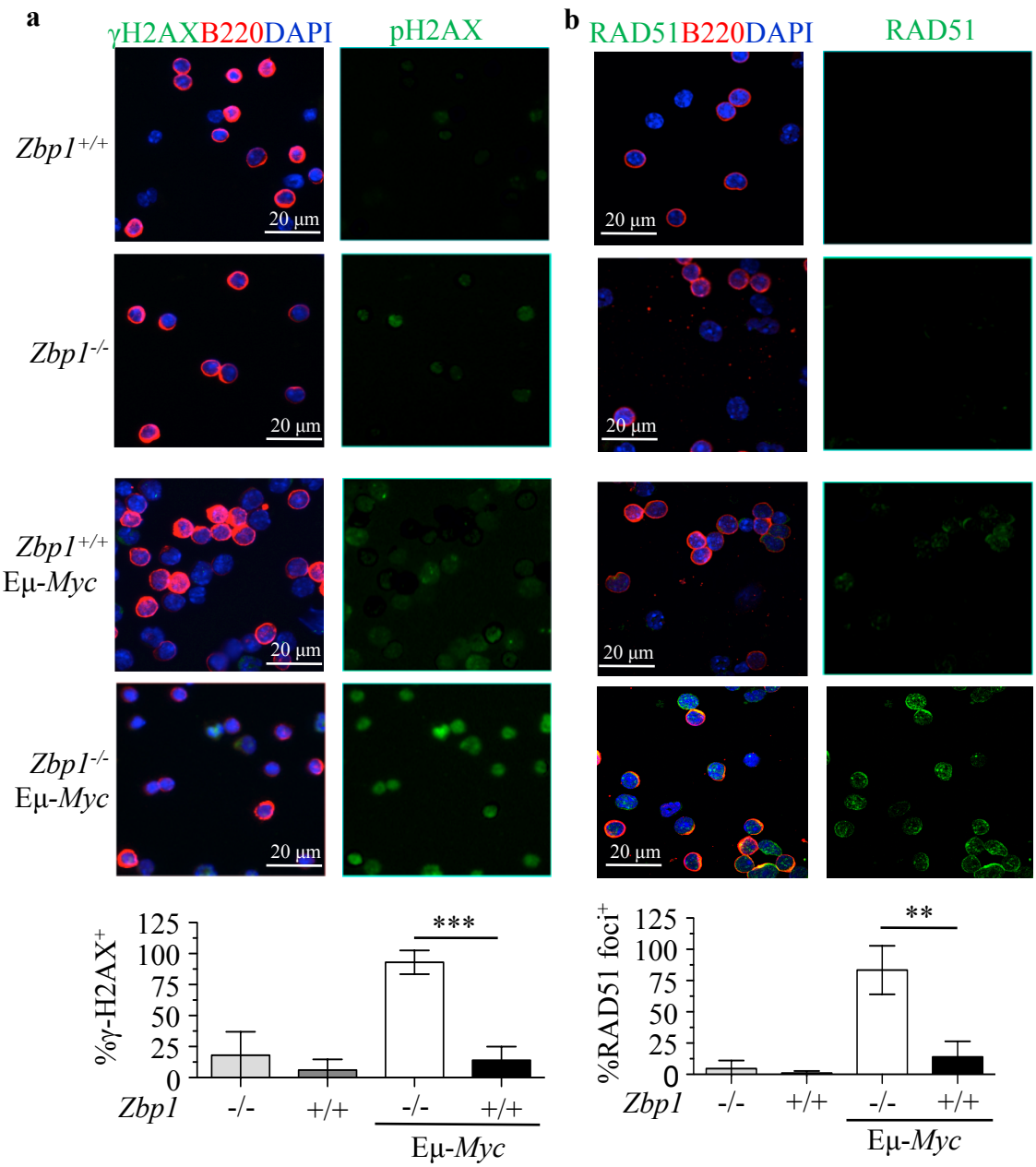

Figure 7.3 Increased γ H2AX and RAD51 foci in B220$^+$ cells of *Zbp1*$^{-/-}$Eμ-*Myc* mice.

Costaining of B cells from blood of *Zbp1*$^{+/+}$ (n=2), *Zbp1*$^{-/-}$ (n=2), *Zbp1*$^{+/+}$Eμ-*Myc* (n≥3) and *Zbp1*$^{-/-}$Eμ-*Myc* (n=3) mice for expression of γH2AX **(a)** and RAD51 **(b)** and the B cell marker B220 (red) in presence of DAPI (blue). The percentage of B220$^+$ that are positive for γH2AX (**a**, bottom panel) and having more than 3 RAD51 foci (**b,** bottom panel) were plotted. Statistical analyses were performed using Student's t test and error bar denotes SD. **p<0.01 and ***p<0.001. Representative images from 3 independent experiments are shown. Data was kindly provided by Ms Munirah.

7.3 Enhanced DNA damage in *in vitro* cell lines derived from *Zbp1*$^{-/-}$Eμ-*Myc* mice

Late stage Eμ-*Myc* mice developed enlarged lymph nodes. We derived an *in vitro* cell line, EμM1, from enlarged lymph nodes from late stage *Zbp1*$^{+/+}$Eμ-*Myc* (*Zbp1*$^{+/+}$ EμM1) and *Zbp1*$^{-/-}$Eμ-*Myc* (*Zbp1*$^{-/-}$ EμM1) mice (see Materials and methods section 2.1). We saw higher expression of γH2AX in DMSO treated *Zbp1*$^{-/-}$ EμM1 compared to *Zbp1*$^{+/+}$ EμM1 (Figure 7.4). There is no significant difference in γH2AX levels in *Zbp1*$^{-/-}$ EμM1 cells treated with Ara-C compared to *Zbp1*$^{+/+}$ EμM1 cells (Figure 7.4). This is consistent with the findings that tumour cells in the *Zbp1*$^{-/-}$Eμ-*Myc* mice had enhanced DNA damage. Cell cycle analysis of *Zbp1*$^{-/-}$ EμM1 cells revealed that these cells contain more than 2n DNA (Figure 7.5a), which might explain why these cells have more DNA damage.

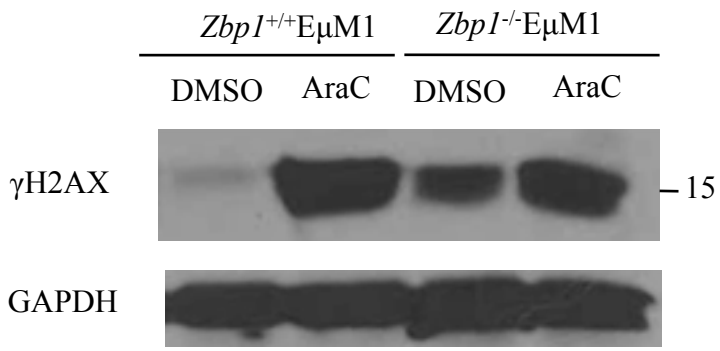

Figure 7.4 Enhanced DNA damage in *in vitro* cell lines derived from *Zbp1*$^{-/-}$ Eμ-*Myc* mice.
Zbp1$^{+/+}$ EμM1 cells and *Zbp1*$^{-/-}$ EμM1 cells were treated with DMSO or 10 μM Ara-C for 16 hours and probed for γH2AX. Representative blots from 3 independent experiments are shown.

7.4 *Zbp1*$^{-/-}$ EμM1 cells and *Zbp1*$^{+/+}$ EμM1 cells showed no difference in proliferation and apoptosis rate

We compared the proliferation rate of *Zbp1*$^{-/-}$ EμM1 cells compared to *Zbp1*$^{+/+}$ EμM1 cells by BrdU incorporation (Figure 7.5). We did not find any significant difference in percentage of cells that were BrdU^{+} in *Zbp1*$^{-/-}$ EμM1 cells (n = 3, mean ± SD = 61.050 ± 8.839%) and *Zbp1*$^{+/+}$ EμM1 cells (n = 3, mean ± SD= 65.350 ± 2.899 %) (Figure 7.5b).

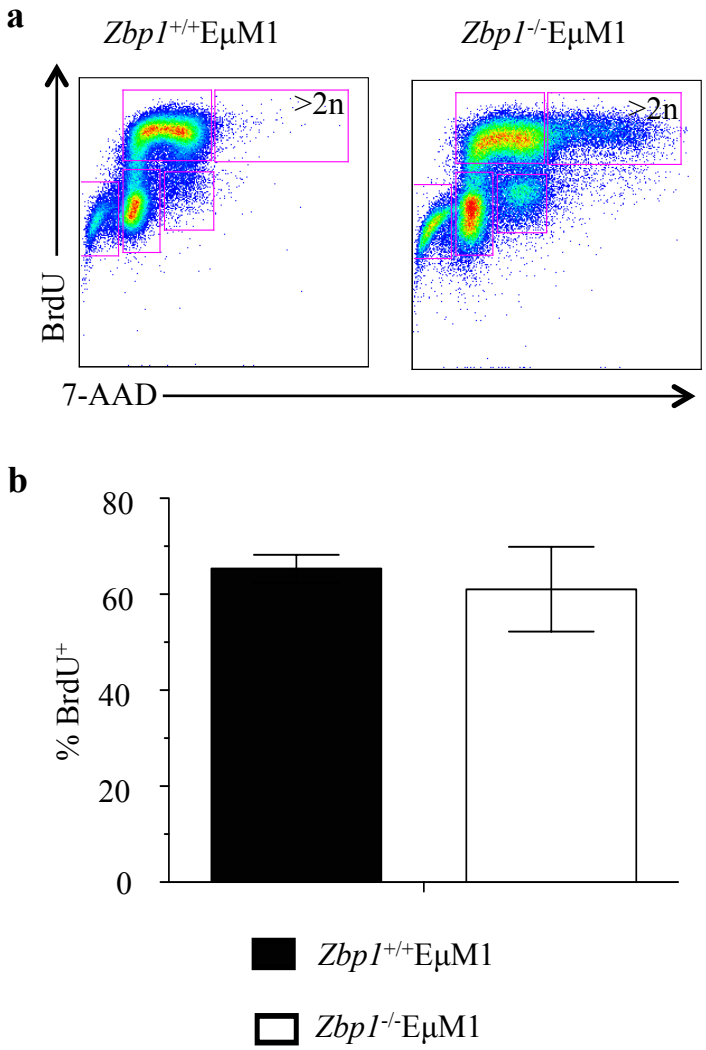

Figure 7.5 No difference in proliferation rate in *Zbp1*$^{-/-}$ EμM1 cells compared to *Zbp1*$^{+/+}$ EμM1 cells.
(a) Cell cycle analysis of *Zbp1*$^{-/-}$ EμM1 cells compared to *Zbp1*$^{+/+}$ EμM1 cells using BrdU incorporation. The population of cells with >2n DNA were indicated. Results in **(a)** were quantified as percentage of BrdU^{+} cells in **(b)**. Statistical comparisons were conducted using Student's t test and the results were expressed as means ± SD of 3 independent experiments.

We also investigated the apoptosis rate of *Zbp1*$^{-/-}$ EμM1 cells compared to *Zbp1*$^{+/+}$ EμM1 cells by Annexin V and PI staining. We did not find any significant difference in early apoptotic cells, defined as being Annexin V^{+} and PI^{-} between *Zbp1*$^{-/-}$ EμM1 cells (mean ± SEM= 5.10 ± 0.710%) and *Zbp1*$^{+/+}$ EμM1 cells (mean ± SEM= 7.24 ± 0.66%) (Figure 7.6). We also did not find any significant difference in Annexin V^{+} and PI^{+} between *Zbp1*$^{-/-}$ EμM1 cells (mean ± SEM= 1.95 ± 0.210%) and *Zbp1*$^{+/+}$EμM1 cells (mean ± SEM= 1.99 ± 0.025%) (Figure 7.6).

Although we observed higher γH2AX in *Zbp1*$^{-/-}$EμM1 cells compared to *Zbp1*$^{+/+}$EμM1 cells, we did not observe any difference in apoptosis or proliferation. This could likely be because these cells are derived from late stage tumour that might have been selected for their ability to circumvent the tumour suppressor effects of the DDR pathways.

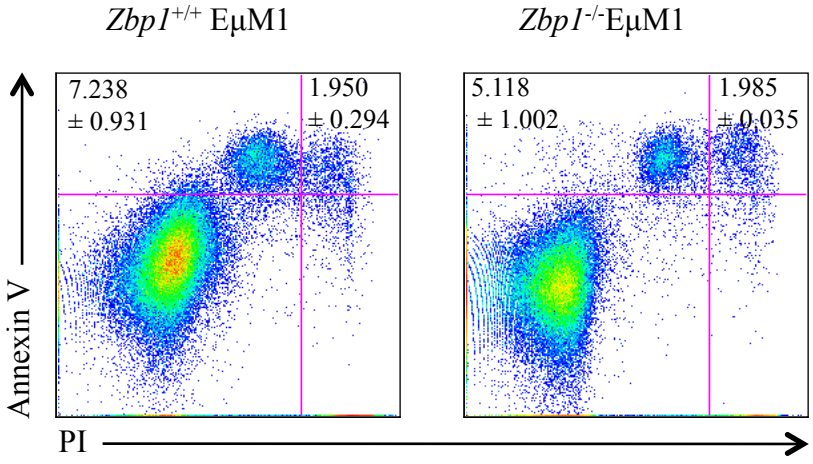

Figure 7.6 No difference in apoptosis rate in *Zbp1*$^{-/-}$EμM1 and *Zbp1*$^{+/+}$EμM1 cells.
Cell cycle analysis of *Zbp1*$^{-/-}$ EμM1 cells compared to *Zbp1*$^{+/+}$ EμM1 cells using Annexin V/PI staining. Data are represented as mean percentage of cells ± SD of 3 independent experiments.

7.5 Knockdown of *Zbp1* increased γH2AX in BC2 cells

To address the relationships between *Zbp1* and the DDR, *Zbp1* expression was knocked down using shRNA in BC2 cells. Inhibition of *Zbp1* expression by shRNA in BC2 cells increased the expression of γH2AX (Figure 7.7). The expression of γH2AX in *Zbp1*-expressing BC2 was comparable to the γH2AX expression in BC2 cells treated with the DNA-damage-inducing agents Ara-C and Aphidicolin (Figure 7.7a). This further suggests that higher levels of DDR activation were seen in BC2 cells with *Zbp1* knockdown.

To address if ZBP1 could directly regulate the DDR, we reconstituted *Zbp1* in *Zbp1*$^{-/-}$ EμM1 cells and treated the cells with Ara-C or DMSO for 16 hours before performing an intracellular flow staining of γH2AX. However, *Zbp1*$^{-/-}$ EμM1 cells reconstituted with *Zbp1-Gfp* or *Ctrl-Gfp* showed similar response to DMSO or Ara-C treatment (Figure 7.7b). This suggests that ZBP1 might be inhibiting an irreversible form of damage in the cells, which could not be reversed by reconstituting *Zbp1*.

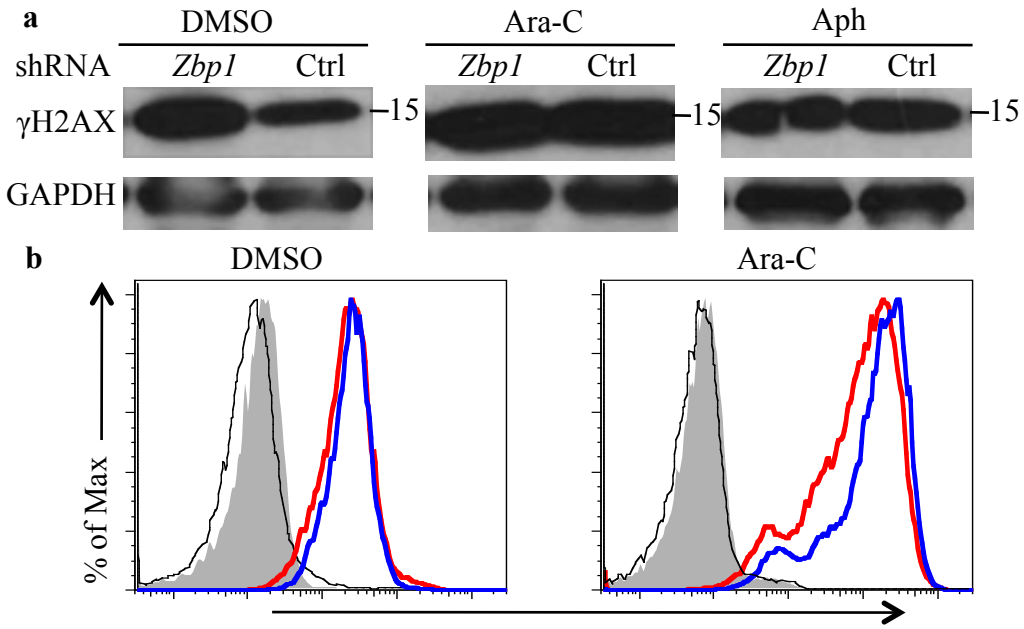

Figure 7.7 Knockdown of *Zbp1* increased γH2AX.
(a) Immunoblot analysis of BC2 cells transduced with retroviral vectors encoding *Zbp1* shRNA and *Gfp* or control shRNA and *Gfp*, and cultured for 5 days before treatment with DMSO, 10 μM Ara-C or 4 μM aphidicolin. Data were kindly provided by Ms Munirah. Representative immunoblots from 3 indpendent experiments are shown. **(b)** *Zbp1*$^{-/-}$ EμM1 cells were transduced with retroviral vectors encoding *Zbp1-Gfp* (blue line) *or* with *Ctrl-Gfp* (red line). 5 days after transduction, cells were treated with 10 μM Ara-C (right panel) or DMSO (left panel) for 16 hrs and analyzed for the expression of γH2AX on GFP^{+} cells. Isotype stainings of *Zbp1*$^{-/-}$ EμM1 cells transduced with *Zbp1-Gfp* (black line) or *Ctrl-Gfp* (filled histogram) are shown. Representative histograms from 3 independent experiments are shown.

7.6 Regression is dependent on ATM in *Zbp1*$^{-/-}$Eμ-*Myc* mice

We have previously shown that the ATM-dependent DNA damage contributes to the regression of B220^{low} tumor cells in the blood of Eμ-*Myc* mice (Croxford et al., 2013). To establish if ATM-dependent DNA damage contributes to the regression of B220^{low} tumor cells in the *Zbp1*$^{-/-}$Eμ-*Myc* mice, we injected both *Zbp1*$^{+/+}$Eμ-*Myc* mice and *Zbp1*$^{-/-}$Eμ-*Myc* mice with the ATM inhibitor, KU60019, or DMSO control. We observed earlier survival in the *Zbp1*$^{-/-}$Eμ-*Myc* mice in the KU60019 group (n = 8, median age = 106) compared to the DMSO group (n = 5, median age = undefined) (P = 0.029 by Log-rank (Mantel-Cox) Test and P = 0.401 by Gehan-Breslow-Wilcoxon Test) (Figure 7.8a). In contrast, the survival of *Zbp1*$^{+/+}$Eμ-*Myc* mice in the KU60019 group (n =10, median age = 115.5) was not significantly different from the DMSO group (n = 6, median age = 138.5) (Figure 7.8a). In the DMSO control group of *Zbp1*$^{-/-}$Eμ-*Myc* mice, there is a significant decrease in the absolute number of B220^{low} cells in the blood between day 21-40 (n = 5, mean ± SD = 2.607 ± 0.925 10^3 per μl) and day 61-70 (n = 5, mean ± SD = 0.927 ± 0.515 10^3 per μl) (P = 0.008) and between day 21-40 and day 71-80 (n = 5, mean ± SD = 0.356 ± 0.185 10^3 per μl) (P < 0.001) (Figure 7.8b). In contrast, in the KU60019 group of *Zbp1*$^{-/-}$Eμ-*Myc* mice, the absolute number of B220^{low} cells in the blood remains relatively constant and we did not observe a decrease in B220^{low} cells in the blood between the different age groups (Figure 7.8b). In the *Zbp1*$^{+/+}$Eμ-*Myc* mice, there was no significant difference in the absolute number of B220^{low} cells in the blood between the KU60019-treated and DMSO-treated mice within each age group (Figure 7.8b). The data support the importance of ATM-dependent DDR pathway in mediating regression in *Zbp1*$^{-/-}$Eμ-*Myc* mice.

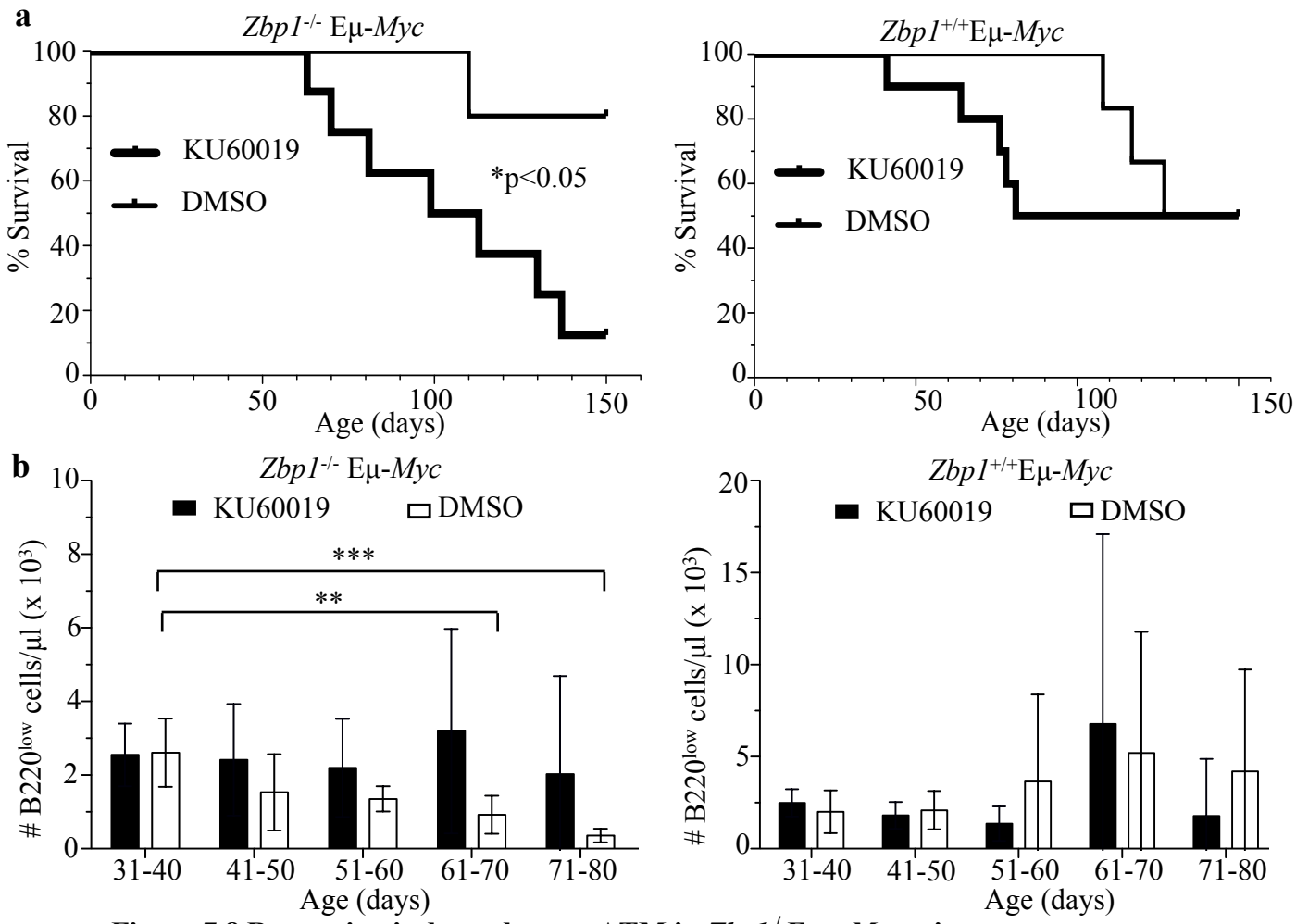

Figure 7.8 Regression is dependent on ATM in *Zbp1*$^{-/-}$E μ *-Myc* mice.

Zbp1$^{-/-}$Eμ-*Myc* (left panel) and *Zbp1*$^{+/+}$Eμ-*Myc* mice (right panel) were injected i.p. with 5 mg/kg of the ATM inhibitor, KU60019 (bold) or DMSO (thin) at 37, 39, 47, 49, 57, 59, 67 and 69 days of age. The survival of the mice was plotted using Kaplan-Meier survival analysis **(a)** and the number of B220^{low} cells in the blood was measured at 37, 44, 54, 64 and 74 days of age **(b)**. Statistical comparisons were conducted using Log-rank (Mantel-Cox) Test and Gehan-Breslow-Wilcoxon Test **(a)** and Student's t test **(b).** In **(b)**, the results are expressed as mean ± SD. At least 5 mice were analysed for each treatment. *** $p < 0.001$, ** $p < 0.01$ and *$p<0.05$.

7.7 Enhanced NF-κB activation in *Zbp1*$^{-/-}$Eμ-*Myc* mice

p65/RelA is a member of the NF-κB family that includes other proteins such as c-Rel, RelB, NF-κB1 (p105/p50), and NF-κB2 (p100/p52). Heterodimers of RelA/p65 and p50 are the most common in most cells, and the term NF-κB is frequently used to refer to this complex (Janssens and Tschopp, 2006). NF-κB can be activated in response to genotoxic stress via a highly regulated process involving ATM, NF-κB essential modulator (NEMO) and IKK (Wu et al., 2006). Western blot analyses revealed higher levels of phosphorylated NF-κB p65/RelA in B220^{+} cells from the spleen of *Zbp1*$^{-/-}$Eμ-*Myc* compared to *Zbp1*$^{+/+}$ Eμ-*Myc* mice (Figure 7.9), which is consistent with the data that there are higher DDR in *Zbp1*$^{-/-}$Eμ-*Myc* mice.

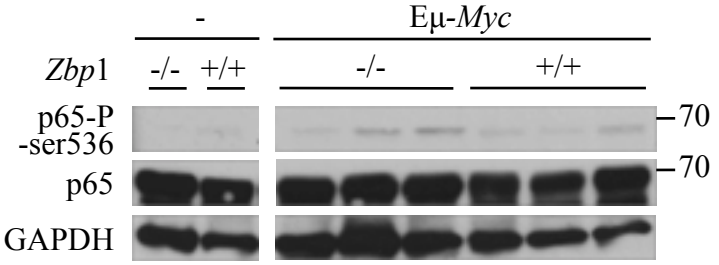

Figure 7.9 Enhanced activation of NF-κB in *Zbp1*$^{-/-}$Eμ-*Myc* mice.
Splenic B220^{+} cells (> 98% purity) from day 31-40 *Zbp1*$^{+/+}$, *Zbp1*$^{-/-}$, *Zbp1*$^{+/+}$Eμ-*Myc* and *Zbp1*$^{-/-}$Eμ-*Myc* mice were probed with antibodies for phosphorylated NF-κB p65 subunit and NF-κB p65 subunit. Representative blots from 3 independent experiments are shown.

Several NF-κB target genes, including the pro-inflammatory cytokines TNF-α and IL-6, are associated with tumor development and progression in humans and mice (Karin and Greten, 2005). We measured the serum levels of IL-6 and TNF-α in *Zbp1*$^{+/+}$, *Zbp1*$^{-/-}$, *Zbp1*$^{+/+}$Eμ-*Myc* and *Zbp1*$^{-/-}$Eμ-*Myc* mice.

We did not observe any significant difference in serum IL-6 levels between *Zbp1*$^{+/+}$Eμ-*Myc* (n = 13, mean ± SD = 52.283 ± 80.564 pg/ml) and *Zbp1*$^{-/-}$Eμ-*Myc* (n = 13, mean ± SD = 122.429 ± 206.522 pg/ml) mice in 31-40 days of age (Figure 7.10a). In mice bearing lymphomas, we did not observe any significant difference in serum IL-6 levels between *Zbp1*$^{+/+}$Eμ-*Myc* (n = 7, mean ± SD = 141.100 ± 115.522 pg/ml) and *Zbp1*$^{-/-}$Eμ-*Myc* (n = 6, mean ± SD = 44.727 ± 45.683 pg/ml) mice (Figure 7.10a). Serum IL-6 levels in lymphomas bearing *Zbp1*$^{+/+}$Eμ-*Myc* was siginificantly higher than *Zbp1*$^{+/+}$ (n = 5, mean ± SD = 12.757 ± 10.435 pg/ml) (P = 0.035) and *Zbp1*$^{-/-}$ (n = 7, mean ± SD = 14.618 ± 15.573 pg/ml) (P = 0.014) (Figure 7.10a).

We were unable to detect serum TNF-α levels in *Zbp1*$^{+/+}$, *Zbp1*$^{-/-}$, *Zbp1*$^{+/+}$Eμ-*Myc* and *Zbp1*$^{-/-}$Eμ-*Myc* mice during 31-40 days of age. Serum levels of TNF-α was not significantly different between *Zbp1*$^{+/+}$Eμ-*Myc* (n = 5, mean ± SD = 29.465 ± 15.415 pg/ml) and *Zbp1*$^{-/-}$Eμ-*Myc* (n = 5, mean ± SD = 85.975 ± 89.064 pg/ml) mice bearing lymphoma (Figure 7.10b).

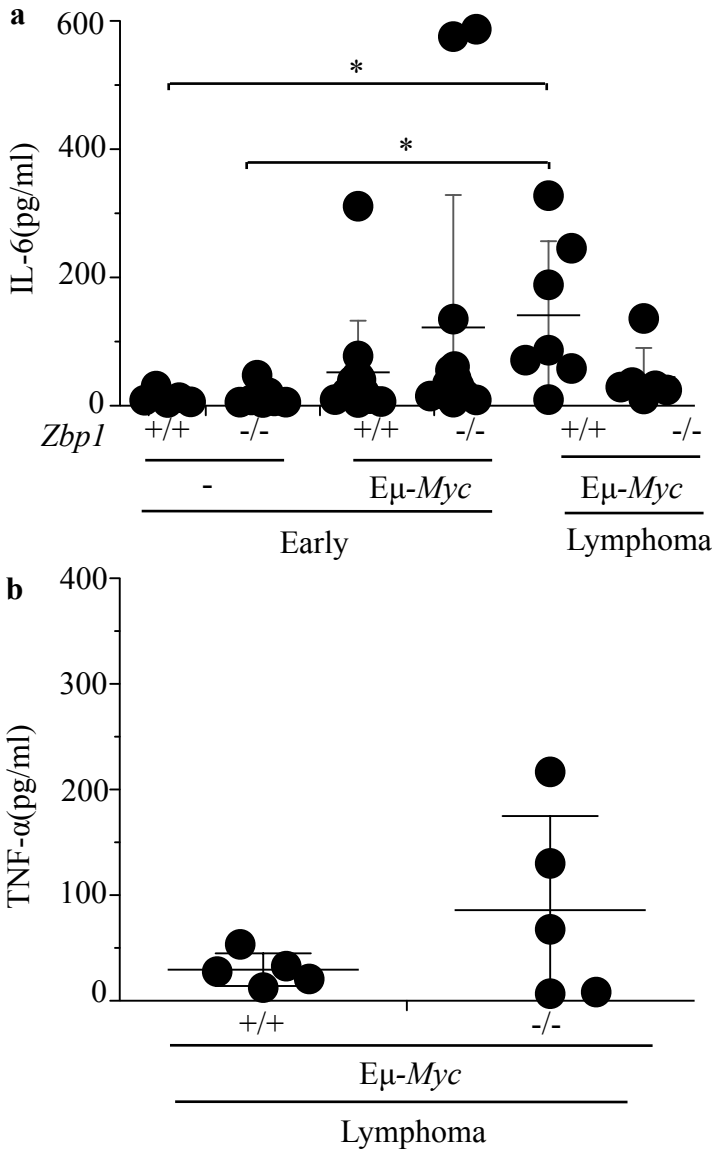

Figure 7.10 Serum levels of IL-6 and TNF-α.
(a) ELISA of serum levels of IL-6 in *Zbp1*$^{+/+}$ (n = 5), *Zbp1*$^{-/-}$(n = 7), *Zbp1*$^{+/+}$Eμ-*Myc* (n = 13) and *Zbp1*$^{-/-}$Eμ-*Myc* (n = 13) mice in early stage of the disease (31-40 days of age) and *Zbp1*$^{+/+}$Eμ-*Myc* (n = 7) and *Zbp1*$^{-/-}$Eμ-*Myc* (n = 6) mice bearing lymphomas. Statistical comparisons were conducted using Student's t test and data are represented as means ± SD. * denote $p < 0.05$. **(b)** ELISA of serum levels of TNF-α in *Zbp1*$^{+/+}$Eμ-*Myc* (n = 5) and *Zbp1*$^{-/-}$Eμ-*Myc* (n = 5) mice bearing lymphomas.

The effects of cytokines on tumour cells could occur in the tumour microenvironment. In an alternative method, we sorted B220^{low} cells from lymphoma bearing *Zbp1*$^{+/+}$Eμ-*Myc* and *Zbp1*$^{-/-}$Eμ-*Myc* mice and performed real-time PCR to determine the expression levels of TNF-α levels. The mRNA level of TNF-α was significantly higher in *Zbp1*$^{-/-}$Eμ-*Myc* (n = 3, mean ± SD = 1.329 ± 0.680) compared to *Zbp1*$^{+/+}$Eμ-*Myc* (n = 3, mean ± SD = 0.091 ± 0.045) (P = 0.035) (Figure 7.11). This is consistent with the data that there are higher DNA damage and more activation of NF-κB in *Zbp1*$^{-/-}$Eμ-*Myc* mice .

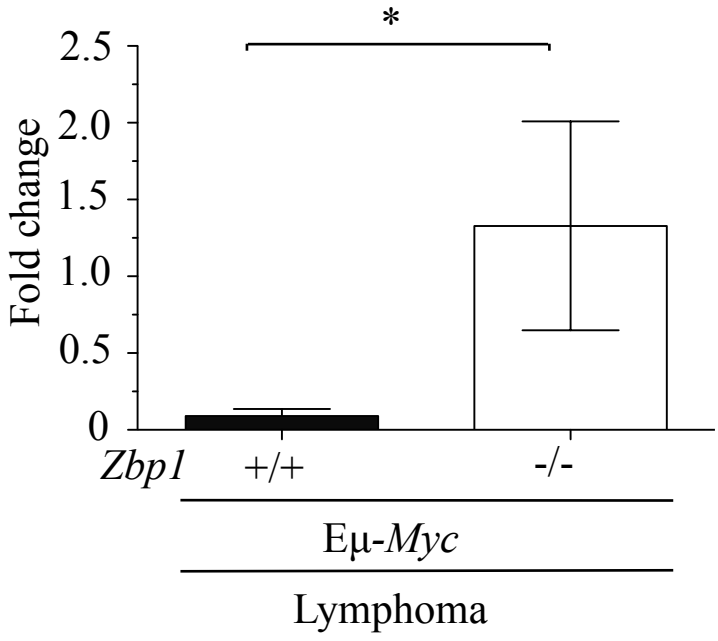

Figure 7.11 Higer mRNA expressions of *Tnf- α* in *Zbp1*$^{-/-}$Eμ-*Myc*.
Real-time PCR of TNF-α levels in sorted B220^{low} cells from lymphoma bearing *Zbp1*$^{+/+}$Eμ-*Myc* (n = 3) and *Zbp1*$^{-/-}$Eμ-*Myc* (n = 3) mice. Data were normalised to B220^{low} cells in WT bone marrow. *Gapdh* was used as internal control. Statistical comparisons were conducted using Student's t test and the results are expressed as mean ± SD. * denote $p < 0.05$.

7.8 Increased cleaved CASPASE 8 in *Zbp1*$^{-/-}$Eμ-*Myc* mice

We observe higher expressions of *Tnf-α* in sorted B220^{+} cells of the *Zbp1*$^{-/-}$Eμ-*Myc* mice compared to *Zbp1*$^{+/+}$Eμ-*Myc* mice in both microarray (Figure 7.1) and real-time PCR (Figure 7.11). TNF-α produced may bind to TNFR1 on the tumour cells and activate caspase-8 which could result in apoptosis (Balkwill, 2009). To investigate presence of TNF-α mediated apoptosis, we performed an immunoblot using purified B220^{+} cells from bone marrows of day 41-65 *Zbp1*$^{+/+}$, *Zbp1*$^{-/-}$, *Zbp1*$^{+/+}$Eμ-*Myc*, and *Zbp1*$^{-/-}$Eμ-*Myc* mice. We observed an increase in cleaved CASPASE 8 in *Zbp1*$^{-/-}$Eμ-*Myc* mice compared to *Zbp1*$^{+/+}$Eμ-*Myc* mice (Figure 7.12). The data is consistent with the idea that tumour cells in the *Zbp1*$^{-/-}$Eμ-*Myc* mice produced more TNF-α leading to apoptosis triggered by caspase-8 activation.

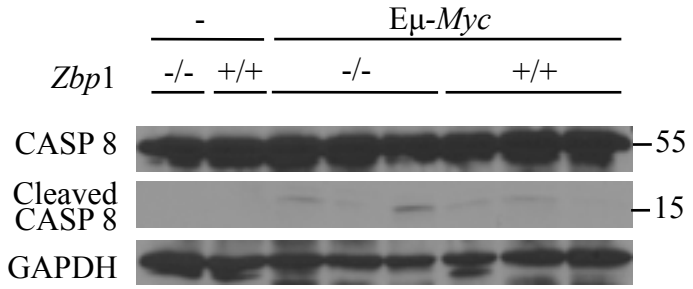

Figure 7.12 Increased cleaved CASPASE 8 in *Zbp1*$^{-/-}$Eμ-*Myc* mice.
Bone marrow B220^{+} cells (> 98% purity) from day 41-65 *Zbp1*$^{+/+}$, *Zbp1*$^{-/-}$, *Zbp1*$^{+/+}$Eμ-*Myc* and *Zbp1*$^{-/-}$Eμ-*Myc* mice were probed with antibodies for CASPASE 8. Representative blots from 3 different experiments are shown.

7.9 Overexpression of *ZBP1* in human cancer cells

According to the data deposited in the *ZBP1* gene expression profile database from Oncomine Research, the mRNA levels of *ZBP1* are significantly higher in human leukemia and head and neck cancer samples compared to normal samples (Figure 7.13). This is consistent with the potential role of ZBP1 as a tumour promoter from our data. As loss of *ZBP1* might potentiate the DDR leading to apoptosis in the tumour cells, tumour cells might undergo selection pressure to upregulate *ZBP1* expressions. However, more experiments had to be performed to verify the expression status of ZBP1 in various human cancer samples.

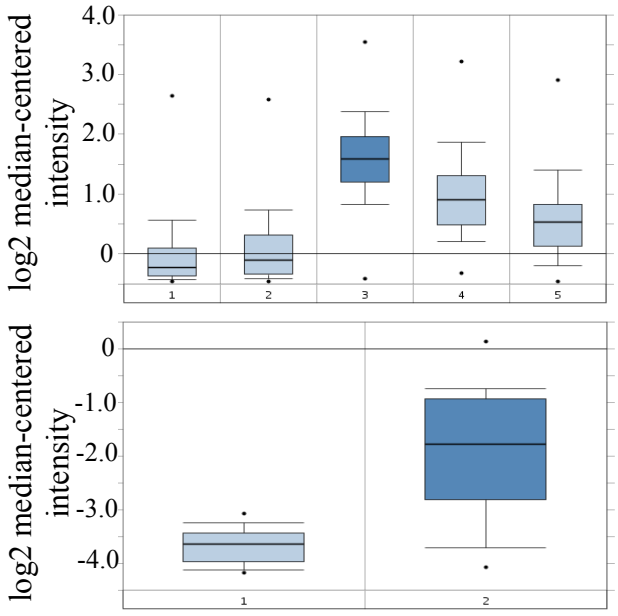

Figure 7.13 Overexpression of *ZBP1* in human cancer cells.
ZBP1 mRNA expression in B cell leukemia samples (left panel) and in head and neck cancer samples (right panel) compared to normal human sample. The graphs were derived from published data available through the ONCOMINE database (http://www.oncomine.org) (Haferlach et al., 2010; Peng et al., 2011).

7.10 Summary

Zbp1$^{-/-}$Eμ-*Myc* mice had enhanced DDR response based on data from microarray, immunoblotting and immunocytochemistry analyses. *In vivo* inhibition of ATM shortened the survival and reversed the regression in *Zbp1*$^{-/-}$Eμ-*Myc* mice. *In vitro* cell lines derived from late stage *Zbp1*$^{-/-}$Eμ-*Myc* mice displayed enhanced DNA damage. Knockdown of *Zbp1* using shRNA increased the expressions of γH2AX. Consistent with enhanced DDR in *Zbp1*$^{-/-}$Eμ-*Myc* mice, we observed enhanced activation of NF-κB and increased expression of TNF-α in *Zbp1*$^{-/-}$Eμ-*Myc* mice. The presence of cleaved CASPASE 8 suggested a role of TNF-α signalling in mediating apoptosis in *Zbp1*$^{-/-}$Eμ-*Myc* mice. Deposited data from Oncomine Research suggest overexpression of ZBP1 in human cnacer cells.

Chapter 8: Discussions and future perspectives

8.1 Summary of key findings

In the present study, we investigated the pathway linking the DDR to the induction of NKG2D ligands. The results show that the DDR is associated with the accumulation of DNA in the cytoplasm of affected cells, the phosphorylation of TBK1 and IRF3, nuclear localization of IRF3 and the production of interferon and certain cytokines in damaged cells. Furthermore, ligand induction by the DDR requires the action of TBK1 and IRF3, and transfection of undamaged cells with cytoplasmic DNA induces the expression of NKG2D ligands. Mice heterozygous for IRF3 had shortened survival and reduced levels of RAE1ε expressions. We proposed a model based on our findings (Figure 8.1).

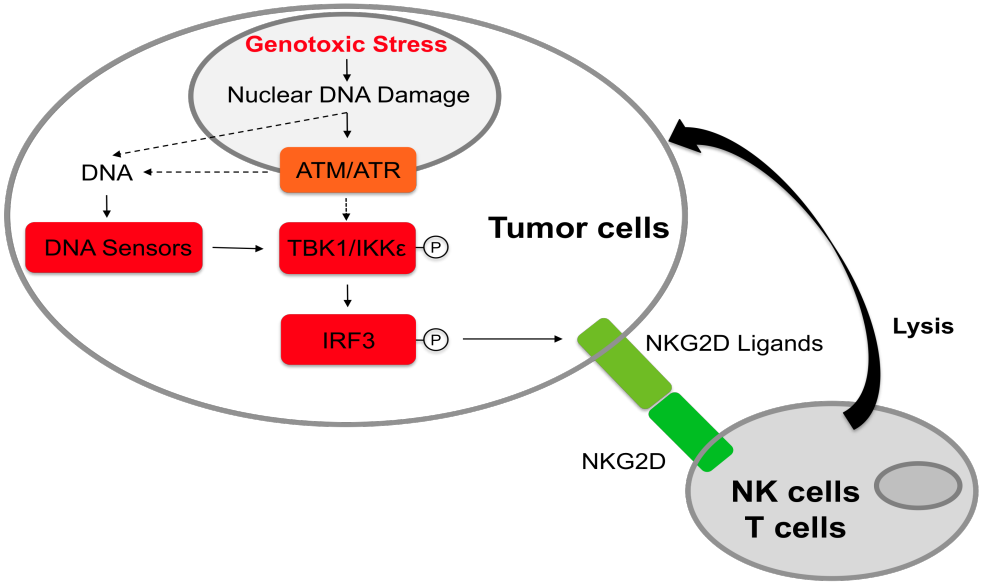

Figure 8.1 Proposed model of regulation of NKG2D ligands.
Genotoxic stress results in increased nuclear DNA damage, which would activate the ATM/ATR pathway. The increased nuclear DNA damage might result in accumulation of cytosolic DNA, which would be sensed by DNA sensors. This would activate STING, which would in turn activate TBK1/IKKε, leading to phosphorylation of IRF3. Activated IRF3 would increase NKG2D ligands expressions on tumor cells, facilitating the killing of the tumour cells by NK cells and T cells.

To investigate the *in vivo* function of DNA sensors in lymphomagenesis, we cross mice deficient in *Zbp1* with Eμ-*Myc* mice, a mouse model for Burkitt lymphomas. We made the surprising discovery that loss of ZBP1 prolongs the survival of Eμ-*Myc* mice significantly. In the absence of ZBP1, tumor cells accumulate DNA damage in the nucleus leading to the activation of ATM and the downstream DDR. Consequently, tumour cells deficient in ZBP1 undergo apoptosis, resulting in suppression of tumorigenesis and contributes to the increased survival of *Zbp1*$^{-/-}$Eμ-*Myc* mice. Our findings reveal a novel role for ZBP1 in Eμ-*Myc* malignancy.

8.2 Linkage of DNA sensing pathway with regulation of NKG2D ligands

8.2.1 Regulation of NKG2D ligands by STING/TBK1/IRF3

Our previous results provided evidence that genotoxic stress provides signals that induce NKG2D ligands and thus activate immune responses. As genotoxic stress is associated with both infections and cancer, these findings suggested a new scheme exploited by the immune system to discriminate between diseased or normal tissues or cells from normal ones. Although ATR/ATM and CHK1 were shown to play a role in the induction of NKG2D ligands downstream of DNA damage, little else was known about the pathway.

The results herein link the DDR to the STING/TBK1/IRF3 signaling molecules, which constitute critical components of a major pathway common to many innate immune receptors, including TLRs and sensors that detect the cytosolic DNA and RNA introduced into cells by pathogens (Palm and Medzhitov, 2009; Takeuchi and Akira, 2010). The convergence of signaling by these pattern recognition receptors and the DDR enables diverse signals associated with disease, specifically pathogen constituents and disease-

induced stress pathways, to provide a common output for immune activation. Previous studies provided indications that the DDR could induces IRF3 phosphorylation and that certain Toll-like receptor ligands could induce *Rae1* gene expression in peritoneal macrophages (Hamerman et al., 2004; Kim et al., 1999b) (though not in several other cell types tested, data not shown), but the linkage of these pathways had not been explored.

Previous studies demonstrated that many tumor cell lines and precancerous lesions exhibit constitutive activation of the DDR. The data herein demonstrated that Yac-1 tumor cells contain detectable cytosolic DNA and exhibit constitutive activation of TBK1/IRF3, thus providing at least a partial explanation for the constitutive expression of NKG2D ligands by these and other tumor cell lines. Whereas IRF3 activation is necessary for optimal cell surface expression of RAE1, it is unlikely to be sufficient, because we failed to observe reproducible cell surface expression in macrophages or dendritic cells exposed to various TLR agonists that activate IRF3 (data not shown).

A key question is how the DDR induces TBK1 and IRF3. A most interesting finding in the present study was that cells subjected to DNA damaging agents accumulate DNA in the cytoplasm, suggesting that cytosolic DNA is a trigger leading to DNA damage-dependent activation of TBK1/IRF3 and ultimately the expression of NKG2D ligands. It is well established that DNA sensor pathways activate STING/TBK1/IRF3 (Stetson and Medzhitov, 2006; Takaoka et al., 2007; Yang et al., 2010). Additional support for the interpretation that cytoplasmic DNA induces RAE1 comes from the finding that transfection of DNA into cells resulted in the induction of RAE1 on the

cell surface. Most striking was the finding that NKG2D ligand expression critically depended on expression of Sting, a crucial mediator of DNA sensors (Goubau et al., 2010). Finally, induction of RAE1 by Ara-C partially relied on ZBP1. ZBP1 is a candidate sensor that is reported to activate TBK1/IRF3 (Takaoka et al., 2007). However, additional TBK1-activating DNA sensors exist since MEFs from *Zbp1*$^{-/-}$-deficient mice mount a normal type-I IFN response to DNA (Ishii et al., 2008b; Takaoka et al., 2007). These sensors may be required for constitutive NKG2D ligand expression in Yac-1 cells. Hence, unidentified DNA sensors may play a predominant role in Yac-1 cells, or may function redundantly with ZBP1, in the induction of RAE1. How DNA damage and the DDR influence the accumulation of DNA in the cytosol and the subsequent biological response remains to be elucidated and worked out in detail, though it is possible that some of the cytosolic DNA corresponds to products of DNA repair, which is enhanced in cells in which the DDR is activated.

It remains uncertain whether cytoplasmic DNA sensing is the sole mechanism for the activation of TBK1 and IRF3 in cells subjected to DNA damage. It is possible that the DDR contributes more directly to TBK1 or IRF3 activation by phosphorylating critical residues in these molecules. Although TBK1 and IRF3 were not identified as DDR-induced ATR or ATM substrates in a recent large-scale proteomic analysis (Matsuoka et al., 2007), it remains possible that CHK1 or another DDR effector kinases downstream of ATR will play such a role.

Taken together, the *in vitro* study suggests that DNA damaging agents or tumorigenesis leads to the accumulation of cytoplasmic ssDNA and

dsDNA, one or both of which are recognized by DNA sensor pathways that activate STING/TBK1/IRF3. STING/TBK1/IRF3 activation, in turn, induces interferon and other cytokines and is required for the optimal expression of NKG2D ligands such as RAE1. RAE1 displayed on tumor cells or damaged cells can trigger the activation of innate immune cells, particularly NK cells, and enhance the responses of various T cell subsets.

8.2.2 Nature of the cytosolic DNA in tumour cells

Cytosolic DNA has been shown to accumulate in cells upon viral and bacterial infection or the uptake of apoptotic host cells (Ishii and Akira, 2006). Our data show the presence of cytosolic DNA in uninfected tumor cells. An intriguing question is where cytosolic DNA originates from and the mechanism leading to cytosolic DNA accumulation in tumor cells.

There are several reports that suggest the release of mitochondrial DNA (mtDNA) in the cytoplasm during cellular stress. Oxidized mtDNA released during apoptosis could activate the NLRP3 inflammasome, resulting in the production of IL-1β (Shimada et al., 2012). IL-5- or IFN-γ–primed eosinophils could release mitochondrial DNA in a reactive oxygen species (ROS)–dependent manner, but independent of eosinophil death and the release of DNA happened rapidly in a catapult-like manner (Yousefi et al., 2008). Neutrophils were also found to release mitochondrial DNA in a similar manner (Yousefi et al., 2009).

It is also possible that the cytosolic DNA is derived from the genome. Cytosolic dsDNA could be generated during the DDR-dependent DNA repair of retroelements that can result in deletion of genomic DNA (Hedges and Deininger, 2007). Finally, it is possible that long tandem repeats,

retrotransposon elements and inverted repeats cause replication fork stalling resulting in dsDNA breaks, repair and the accumulation of cytosolic DNA (Brown et al., 2012). It is unclear if such deletions of DNA from the genome would result in increase genomic instability and if these DNA would integrate back into the genome as the constant removal of portions of the genome might be deleterious to the cell.

It would be interesting to clone and sequence the DNA from the cytoplasm to verify its origins as outlined by the method in (Stetson et al., 2008). This might provide insights in the mechanism leading to cytosolic DNA accumulation in tumour cells. Current literature suggests that the recognition of DNA in the cystoplasm occurs in a sequence independent but length dependent manner (Hornung and Latz, 2010). However, the sequence of the DNA might affect the efficiency of transcription of type 1 IFNs. The homo-copolymer poly (dA: dT) was the stongest activator of IRF3 transcription while other homo-copolymers such as poly (dG: dC) or poly (dI: dC) were much less potent IFN inducers (Ishii et al., 2006a). As such, determining the length and sequence of the cytosolic DNA might provide information on the efficiency of IRF3 activation.

The exact nature of the DNA ligand that is recognised by cells during an innate immune response is not known. DNA isolated from viruses, bacteria or mammals appears to be recognised equally well when transfected into responsive cells, so long as the DNA fragments are of sufficient length (Ablasser et al., 2009; Ishii et al., 2006b; Unterholzner et al., 2010b). An exception is the dsDNA mimic poly (dA-dT), which is specifically transcribed to dsRNA by RNA polymerase III (Ablasser et al., 2009; Chiu et al., 2009;

Unterholzner et al., 2010b). While all the cytosolic DNA sensors have been shown to bind DNA, only a handful have well-described DNA binding specificities. The crystal structure of the IFI16 HINb domain in a complex with DNA corresponds well with the observed sequence-independence of DNA recognition, as the binding occurs speficificty with the sugar-phosphate backbone of the DNA (Jin et al., 2012). A similar sequence-independent interaction has been seen in the structure of cGAS with DNA (Civril et al., 2013; Gao et al., 2013). However, this does not provide further insights into why a mimumum length of dsDNA fragments are needed to elicit an IFN response in cells.

Nucleic acids, especially DNA ligand, are emerging as key activators of the innate immune system in several situations beside viral infection. Intracellular DNA is a crucial PAMP during infection with intracellular bacteria, such as Mycobacterium tuberculosis (Manzanillo et al., 2012), Listeria monocytogenes (Rathinam et al., 2010; Stetson and Medzhitov, 2006; Stockinger et al., 2004), and Francisella tularensis (Atianand et al., 2011; Jones et al., 2010; Rathinam et al., 2010), and the protozoan Plasmodium falciparum (Sharma et al., 2011). DNA can also act as endogenous 'danger' signal during conditions of sterile inflammation and in autoimmune diseases such as SLE (Ablasser et al., 2013). It is thought that DNA from dead cells that is not effectively cleared by DNases, DNase I in the extracellular space, DNase II in lysosomes and TREX1 (three prime repair exonuclease 1) in the cytoplasm, could activate the DNA sensing pathways. DNA from dying cells has also been shown to be a 'danger' signal during the immune response to the vaccine adjuvant alum (Marichal et al., 2011). The proper

compartmentalization of DNA is important for the survival of the cell as the presence of DNA, both foreign and self, in the cytoplasm would trigger an innate immune response. Our data suggest that presence of cytosolic DNA in the tumour cells could act as endogenous "danger" signal that might trigger an immune response.

8.2.3 Role of STING/TBK1/IRF3 in cancer

STING is a transmembrane protein that is expressed in the endoplasmic reticulum and interacts with SSR2 signal sequence receptor 2 (SSR2), a member of the translocon-associated protein (TRAP) complex (Ishikawa and Barber, 2008, 2011) that is associated with the exocyst complex (Heider and Munson, 2012). In the presence of cytosolic DNA, STING relocalizes with TBK1 from the endoplasmic reticulum to perinuclear vesicles that contain the exocyst component Sec5A (Ishikawa et al., 2009). STING could function as an adaptor in the DNA-induced IFN response, but as a receptor in the recognition of bacterial signalling molecules such as cyclic di-AMP and di-GMP (Burdette et al., 2011). The role of STING in tumorigenesis has not been elucidated, but STING was found to induce apoptosis and possibly inhibit proliferation of B cell lymphoma cells (Jin et al., 2008). Many cancer cells have elevated cellular levels of ROS and it was reported that ROS could inhibit STING induction of IFNβ (Jin et al., 2010). Given the crucial role of STING in the activation of type I IFN in a variety of DNA virus infections, it is possible that STING may act as a tumor suppressor by preventing infection of cells by oncoviruses (Heiber and Barber, 2012).

We have established a role of STING in regulating the expressions of NKG2D ligands. As mentioned in the introduction, NKG2D ligands were

thought to play an important role in immunesurveillance of tumours. Our data suggest that STING might play a role in regulating the immunesurveillance of tumours through regulation of NKG2D ligands expressions. Further experiments have to be done to investigate the relationship of STING in cancer. One possible experiment would be to cross mice deficient in *Sting* to Eμ-*Myc* mice.

Both TBK1 and IKKε have been implicated in cancer. Recent findings suggest a role for TBK1 and IKKε in RAS-induced transformation of cells (Chien et al., 2006; Clement et al., 2008; Ou et al., 2011). TBK1 is recruited and activated by a RalB-Sec5 effector complex that is needed for RAS-mediated transformation. In addition, TBK1 was necessary to inhibit apoptosis in response to RAS activation possibly by activating the v-akt murine thymoma viral oncogene homolog (AKT) survival pathway (Barbie et al., 2009; Chien et al., 2006; Chien and White, 2008; Ou et al., 2011). IKKε was identified as an effector of the phosphatidylinositol 3-kinase (PI3K)-AKT pathway and works with MAP kinase-ERK kinase (MEK) to promote transformation. siRNA-mediated inhibition of IKKε expression blocked proliferation, adhesion, and invasiveness of several tumor cell lines (Hsu et al., 2012; Qin and Cheng, 2010). In patients with prostate cancer, there was a correlation between IKKε expression levels and malignancy of the cancer (Peant et al., 2011).

We have established a role of TBK1/IKKε in regulating the expressions of NKG2D ligands. This additional function of TBK1/IKKε might contribute to their implicated roles in cancer. TBK1/IKKε has been previously thought to influence cancer progression through their effects on cell intrinsic

survival pathway, however, our results hint that TBK1/IKKε might also play a role in immunesurveillance of tumours through regulation of NKG2D expressions.

IRF3 is one of the main regulators of type I IFN production needed for an effective anti-viral response (Taniguchi et al., 2001). Upon phosphorylation by TBK1 or IKKε in the cytoplasm, IRF3 forms a homodimer, translocate into the nucleus, and form part of an IFN enhanceosome consisting of IRF3, NF-κB and activating transcription factor 2 (ATF2)-c-JUN heterodimers that recruit the histone acetyltransferase CREB-binding protein (CBP) to the *IFNB* promoter (Barber, 2011; Falvo et al., 2000; Merika et al., 1998). IRF3 also binds to the *IFNA* promoter in humans and *Ifna4* promoter in mice (Civas et al., 2006).

IRFs and IFNs have been implicated in eliciting anti-tumor effects (Taniguchi et al., 2001). Expression of a dominant-negative mutant form of IRF3 in tumor cells increased their ability to form tumors in nude mice, while overexpression of IRF3 inhibited cell proliferation and increased apoptosis due to activation of p53 (Kim et al., 2007b) and possibly secretion of type I IFNs (Kim et al., 2003). 5,6-dimethylxanthenone-4-acetic acid (DMXAA), which was found to activate the TBK1-IRF3 pathway (Roberts et al., 2007), is currently in clinical trials for use as a chemotherapeutic drug against lung, ovarian and prostate cancer activates. However, some human lung cancer express constitutively activated IRF3 (Tokunaga et al., 2010). A study using high throughput screening of genes to identify factors that would stimulate human umbilical vein endothelial cell (HUVEC) proliferation, found that the TBK1-IRF3 axis was involved in the production of factors such as chemokine

(C-C motif) ligand 5 (CCL5) and IL-8 that can promote angiogenesis and tumor growth (Korherr et al., 2006).

Consistent with the proposed tumour suppressor effects of IRF3, we observed shortened survival of Eμ-*Myc* mice heterozygous for IRF3. Although the *Irf3* mutation also suppresses expression of the neighboring *Bcl2l12* gene, numerous experiments we performed argued that heterozygosity of that locus did not account for the observed effects. IRF3 is known to have tumor suppressor activities that are linked to its effect on apoptosis by transactivating genes, such as *Isg56*, *Trail*, and *Noxa* in a p53-independent manner (Grandvaux et al., 2002; Guo et al., 2000; Kirshner et al., 2005; Lallemand et al., 2007; Weaver et al., 2001). We observed no difference in the rates of apoptosis or proliferation comparing the WT and heterozygous tumor cells. These data support the conclusion that the accelerated tumorigenesis of heterozygous *Irf3/Bcl2l12* Eμ-*Myc* mice is not due to effects of IRF3 or BCL2L12 on cell intrinsic apoptosis or proliferation. In addition, we observed lower expressions of IRF3 target genes in $Irf3^{+/-}$Eμ-*Myc* mice compated to $Irf3^{+/+}$Eμ-*Myc* mice, suggesting reduced activation of IRF3 and its tartget genes in $Irf3^{+/-}$Eμ-*Myc* mice. This might contribute to the quickened survival in $Irf3^{+/-}$Eμ-*Myc* mice due to less efficient removal of tumours.

8.3 Role of ZBP1 in tumourigenesis

8.3.1 A novel role of ZBP1 in B cell cancer

Having established a role for STING/TBK1/IRF3 in cancer using *in vitro* system, we would like to investigate the potential role of the cytosolic DNA sensing pathway *in vivo*. We crossed mice deficient in *Zbp1* to the Eμ-

Myc and found that the loss of ZBP1 in Eμ-*Myc* mice promotes survival of the mice significantly.

ZBP1 was the first cytoplasmic DNA sensor to be identified through studies done using *in vitro* system (Takaoka et al., 2007). However, cells derived from *Zbp1*-deficient mice responded normally to poly (dA: dT) and plasmid DNA and they did not display defects in immune function after infection with a DNA virus (Ishii et al., 2008a; Wang et al., 2008a). ZBP1 was also reported to interact with RIP3 to induced necrosis upon murine cytomegalovirus infection. Most of the studies done on ZBP1 were in the context of pathogen recognition and it is unclear if it plays a role in other systems. The only link of ZBP1 to cancer was suggested by the finding that ZBP1 is highly upregulated in the peritoneal lining tissue of mice bearing ascites tumors (Fu et al., 1999). Here, we provided evidence of a novel role of ZBP1 as loss of ZBP1 prolongs the survival of Eμ-*Myc* mice, a mouse model for Burkitt lymphomas, significantly.

Although there are some reports that suggested an association between DNA sensors and tumorigenesis, much remains to be done to elucidate the physiological relationships as most of the study was performed using in vitro cell lines, transplantable tumours or induced tumour mice models (Chen et al., 2006; Liao et al., 2011; Ludlow et al., 2005; Mazibrada et al., 2010). In addition, the exact mechanism of how these DNA sensors promote tumorigenesis remains to be elucidated.

Activation of the intracellular DNA sensing pathways lead to the production of type I IFNs, which have both antiviral and antitumour activities.

Type I IFNs, which are pleiotropic in nature, consist of IFN-α, IFN-β, IFN-ω, IFN-ε and IFN-κ. Type 1 IFNs have been linked to suppression of tumorigenesis in both hematological and solid tumors (Dunn et al., 2006). *Ifnar1*-deficient mice are more susceptible to carcinogen-induced tumors and transplanted syngeneic tumors (Dunn et al., 2005). The inactivation of IFN-consensus-sequence binding protein (ICSBP), a transcription factor involved in the regulation of IFN-stimulated genes, results in a chronic myeloid leukemia (CML)-like disease and many patients with untreated CML have low ICSBP levels (Schmidt et al., 1998). In addition, type I IFNs can enhance cells susceptibility to p53-mediated apoptosis (Takaoka et al., 2003). The production of endogenous IFN-α/β has been shown to reject tumour formation of sarcomas and carcinogen-induced tumours in immunocompetent mice (Kim et al., 2007a). IFN-α/β has also been shown to increase NK cells cytotoxic activity through activation of tumour necrosis factor related apoptosis-inducing ligand (TRAIL) (Swann et al., 2007). In addition, it can also activate dendritic cells (DCs). Furthermore, tumour cells that express IFN-α induce anti-tumour immunity whereby it prevents apoptosis of tumour-specific T cells after stimulation.

Activation of the intracellular DNA sensing pathways could activate NF-κB, which is a major transcription factor responsible for inflammation and driving the expression of various cytokines, chemokines and receptors needed for antigen presentation or immune recognition (Pahl, 1999). Deregulation of NF-κB plays an important role in supporting pro-survival properties of tumor cells. The classical and non-canonical pathway can activate NF-κB. In the classical pathway, bacterial and viral infections, as well as pro-inflammatory

cytokines, activate the IKK complex and target IκBα for proteasomal degradation, releasing NF-κB dimers that are made up of REL-A/p65, REL/c-REL and p50 subunits to translocate to the nucleus and mediate transcription of target genes (Karin and Greten, 2005). Certain TNF-family members can activate the non-canonical pathway leading to the phosphorylation of p100 by IKK-α and the degradation of its carboxy-terminal half by the proteasome in an IKK-β- independent and IKK-γ-independent manner (Karin and Greten, 2005). This results in nuclear translocation of p52/REL-B dimers. The role of the classical pathway in cancer is more extensively studied than the alternate pathway. Somatic copy number alteration analysis of multiple human cancer samples identified NF-κB regulators such as TRAF6, IKBKB, IKBKG, and RIPK1 to be amplified (Beroukhim et al., 2010), consistent with its emerging importance in tumorigenesis. Studies have shown that NF-κB is constitutively activated in various tumor cells and inhibition of NF-κB in tumor cells induces apoptosis (Sovak et al., 1997).

It remains unclear if these pathways are deregulated in *Zbp1*$^{-/-}$Eμ-*Myc.* However, the anti-tumour activities of type 1 IFNs contrasted with the increased survival that we observed in *Zbp1*$^{-/-}$Eμ-*Myc.* In addition, we reported a decreased in survival of the *Irf3*$^{+/-}$Eμ-*Myc* mice compared to the *Irf3*$^{+/+}$Eμ-*Myc* mice, which is opposite to the phenotype we saw in *Zbp1*-deficient Eμ-*Myc* mice. It is unknown why there is a divergent in the phenotypes observed for *Zbp1*$^{-/-}$Eμ-*Myc* and *Irf3*$^{+/-}$Eμ-*Myc* mice. It is likely that ZBP1 might be involved in other functions in addition to its IFN-dependent antiviral role. In addition, redundancy in the DNA sensors suggests that other sensors could play a role in mediating the phenotype observed in *Irf3*$^{+/-}$Eμ-*Myc* mice. It

would be interesting to investigate the role of STING, which is a key adaptor molecule in the DNA sensing pathway, in Eμ-*Myc* lymphomagenesis.

It remains to be investigated if ZBP1 has a unique role in B cell cancer or if it plays a crucial role in other forms of cancer. In addition, the other DNA sensors have not been crossed with Eμ-*Myc* mice and it remains to be seen if other DNA sensors also play a similar role as ZBP1 in Eμ-*Myc* lymphomagenesis.

8.3.2 Role of ZBP1 in DDR

Constitutive DNA damage and DDR signalling is found in most tumour cells including those of the bladder, breast and colon (Bartkova et al., 2005). In the Eμ-*Myc* mouse model, expression of c-*Myc* in B cells under control of the immunoglobulin heavy chain enhancer (Eμ) results in a sustained *Myc* expression, which promotes DNA damage in tumour cells by increasing ROS production and replication stress, thus resulting in more DNA DSB (Pusapati et al., 2006a; Ray et al., 2006; Vafa et al., 2002a).

We found that *Zbp1*$^{-/-}$Eμ-*Myc* mice showed higher levels of γH2AX in splenocytes from B cells using two separate techniques, thus indicating sustained DNA DSB. In addition, there was a corresponding increase in RAD51 foci in tumour B cells of *Zbp1*$^{-/-}$Eμ-*Myc* mice. RAD51 is involved in DSB repair via homologous recombination and presence of its distinct foci indicates ongoing DNA repair (Suwaki et al., 2011). In addition, a recent study has identified Rad51 as a potential tumour suppressor gene (Bric et al., 2009). As such, an increased RAD51 foci in *Zbp1*$^{-/-}$Eμ-*Myc* mice, indicates higher levels of DNA repair occurring through HRR and which might contribute in suppressing tumours.

There are hints of a link between viral infection, DNA damage and the innate immune response based on previous reports on the ability of DNA viruses to induce and regulate the DDR (Weitzman et al., 2010), and the finding that DNA damage can result in the production of IFNs (Karpova et al., 2002; Kim et al., 1999b; Weitzman et al., 2010). However, several molecules involved in the DDR such as the catalytic subunit of DNA-PK (DNA-PKcs), its binding partners KU70 and KU80 and ATM were shown to be dispensable for the IFN response to intracellular DNA in murine bone marrow-derived macrophages (Stetson and Medzhitov, 2006). Since then, other molecules in the DDR have been implicated in the STING-dependent response to intracellular DNA in other cell types.

During DNA damage, a complex consisting of DNA-PKcs, KU70 and KU80 binds to DNA breaks and activates cell cycle arrest and the repair of damaged DNA. In addition, DNA-PKcs, KU70 and KU80 have been implicated in the IFN-dependent anti-viral response. KU70 has been linked to the DNA-induced production of IFN-λ (Zhang et al., 2011a). DNA-PKcs, KU70 and KU80 are required for the production of IFN-β following DNA transfection into mouse and human fibroblasts (Ferguson et al., 2012). Furthermore, DNA-PKcs, KU70 and KU80 were also involved in the response to the DNA viruses HSV-1 and Modified Vaccinia Ankara (MVA) in mouse embryonic fibroblasts (MEFs) and in mouse intradermal infection models *in vivo*.

Recently, MRE11, an important molecule in the DDR, has been implicated in the sensing of cytosolic DNA (Kondo et al., 2013). MRE11 and the DNA-PKcs/KU70/KU80 complex are involved in HRR and NHEJ, which

are the two major repair pathways for dsDNA breaks. MRE11 was shown to be required for the DNA-induced IFN response in mouse bone marrow derived dendritic cells, MEFs and in a human cell line lacking MRE11 (Kondo et al., 2013). MRE11 was specifically involved in the detection of transfected dsDNA, but not in the recognition of pathogens such as HSV-1 and Listeria (Kondo et al., 2013). The physiological role of MRE11 during infection with other pathogens or during conditions of sterile inflammation remains to be investigated.

ZBP1 had not been implicated in the DNA repair pathways. ZBP might have an effect on the two major repair pathways for dsDNA breaks in addition to its role as intracellular DNA sensor. Interestingly, ZBP1 is predominantly cytosolic and it is unclear how it could affect the nuclear DDR. In IFN or leptomycin B (LMB)-treated cells, ZBP1 can form foci in the nucleus that overlap with PML oncogenic domains or nuclear bodies (Pham et al., 2006). It remains to be seen if ZBP1 could translocate to the nucleus of the cell upon DNA damage and if it does, the exact role of ZBP1 in the nucleus. One of the cytosolic DNA sensors, IFI16, had been reported to shuttle between the nuclear and the cytoplasm (Unterholzner, 2013). Alternatively, there is increasing evidence for a cytoplasmic pool of ATM or extranuclear shuttling of ATM (Boehrs et al., 2007; Kim et al., 2010; Li et al., 2009a; Lim et al., 1998; McCool and Miyamoto, 2012; Watters et al., 1999). Loss of ATM could also affect various cytoplasmic signalling pathways, such as calcium and potassium ion mobilization (Chiesa et al., 2000; Famulski et al., 2003; Rhodes et al., 1998). In addition, in response to DNA damage, ATM was reported to regulate *de novo* synthesis of ceramide, which occurs in the

endoplasmic reticulum (Liao et al., 1999). It is possible that ZBP1 could interact with ATM in the cytoplasm and the relationship between ZBP1 and ATM remains to be investigated.

8.3.3 Cell intrinsic versus cell extrinsic factors

Oncogenic stress created by sustained *MYC* expression was shown to induce DNA damage in tumors cells of Eμ-*Myc* transgenic mice through DNA DSB and increased ROS, leading to cell cycle arrest or apoptosis. Previous study reported that $B220^{+}$ cells in Eμ-*Myc* mice underwent apoptosis (Jacobsen et al., 1994; Sidman et al., 1993b), which could be triggered via cell intrinsic or cell extrinsic pathways. Our data shows increase activation of the DDR and the subsequent activation of p53 and PUMA in Eμ-*Myc* mice deficient in ZBP1, suggesting that changes in cell intrinsic pathways trigger the induction of apoptosis in these mice.

In line with this idea, we observed an increase in apoptosis of $B220^{low}$ cells from bone marrow of *Zbp1*$^{-/-}$Eμ-*Myc* mice from 41-64 days of age after incubating them in culture for 3 hours. We also observed increase activation of CASPASE 3, 7 and 8 in tumour cells of *Zbp1*$^{-/-}$Eμ-*Myc* mice by immunoblot analysis. Because of the speed with which apoptotic cells are cleared by resident phagocytes *in vivo*, the analysis of Annexin V^{+}/PI^{+} or PI^{-} by flow cytometry can give only a semi-quantitative comparison of the true magnitude of apoptosis among B-lineage cells. Western blot analyses of cleaved CASPASE 3, 7 and 8 suggest that apoptosis may occur in higher frequency *in vivo*. This may explain why we did not observe any significant differences in apoptosis in both *ex vivo* bone marrow and spleen by Annexin V^{+}/PI^{+} or PI^{-} assay.

We observed a more pronounced activation of CASPASE 7 compared to CASPASE 3 by immunoblot analysis. Caspases-3 and -7 are activated by the same upstream activators and share overlapping substrate specificity. It is not clear the extent to which caspase-3 and caspase-7 share functions. However, there are some differences in their regulation, probably due to their divergent amino-terminal sequences. Removal of the amino terminus sequences of caspase-7 present only in the pro-enzyme and not the mature enzyme seem to potentiate caspase-7 activity. The authors speculate that these residues may play an undefined role in sequestering the enzyme from its upstream activators (Denault and Salvesen, 2003). Therefore, it is currently unknown why caspase-7 may be preferentially activated in *Zbp1*$^{-/-}$Eμ-*Myc* mice.

In addition, we did not find any significant differences in proliferation in both the bone marrow and spleen by immunoblot analysis of key cell cycle proteins, intracellular KI-67 staining and BrdU incorporation. These data support the finding that tumour cells from *Zbp1*$^{-/-}$Eμ-*Myc* mice have increased DNA damage and thus are more prone to apoptosis either through ATM-dependent apoptosis or TRAIL-induced apoptosis. Increase in apoptosis of tumour B cells in the bone marrow may lead to decrease in tumour load in the periphery, which is consistent with the observed regression of tumour cells.

We have previously reported a role of T and NK cells in mediating regression in the Eμ-*Myc* mice (Croxford et al., 2013). We did not observe any difference in T cells activation markers in *Zbp1*$^{-/-}$Eμ-*Myc* and *Zbp1*$^{+/+}$Eμ-*Myc* and in co-stimulatory molecules important for T cells activation in *Zbp1*$^{-/-}$Eμ-*Myc* and *Zbp1*$^{+/+}$Eμ-*Myc* mice. The percentage of tumour specific T cells

could be less than 1%; therefore it might be difficult to observe any significant difference in *Zbp1*$^{-/-}$Eμ-*Myc* and *Zbp1*$^{+/+}$Eμ-*Myc* mice. While we could not conclude that the immune system does not play a role in mediating the difference between *Zbp1*$^{-/-}$Eμ-*Myc* and *Zbp1*$^{+/+}$Eμ-*Myc* mice, our data suggest that differences in the cell intrinsic pathway might play a dominant role in the phenotype that we observed for *Zbp1*$^{-/-}$Eμ-*Myc* mice. To conclusively delineate the effects of the immune system, one could perform a bone marrow chimera experiment (Iwasaki, 2006). It would also be useful to perform a transfer experiment where we transfer tumour cells from the Eμ-*Myc* mice to the severe combined immunodeficiency (SCID) common γ chain$^{-/-}$ mice (Bosma and Carroll, 1991), which lack functional T and B cells, and monitor survival of the mice. If T cells play a role, there should be no difference in survival of the SCID injected with tumour cells from either *Zbp1*$^{-/-}$Eμ-*Myc* mice or *Zbp1*$^{+/+}$Eμ-*Myc* mice.

8.3.4 DNA-damaged induced NF-κB activation

ZBP1 could interact with RIP1 and RIP3 to activate NF-κB (Kaiser et al., 2008; Rebsamen et al., 2009), but we did not observe an increase in NF-κB activation in tumour cells from *Zbp1*$^{-/-}$Eμ-*Myc* mice. In contrast, we saw higher phosphorylated p65/RELA in tumour cells from *Zbp1*$^{-/-}$Eμ-*Myc* mice, which are most likely activated as part of the DDR (Wu et al., 2006). NF-κB is usually thought of as a pro-survival factor; however, recent papers suggest that NF-κB can contribute to genotoxic stressed-induced apoptosis (Bian et al., 2001; Campbell et al., 2001; Campbell et al., 2004; Kaltschmidt et al., 2000; Ryan et al., 2000; Wang et al., 2002). Genetic activation of the NF-κB pathway could induce apoptosis in mouse and human c-MYC transformed

lymphomas (Klapproth et al., 2009). Overexpression of c-MYC could sensitize cells to NF-κB-induced apoptosis, and persistent inactivity of NF-κB signaling is a prerequisite for *Myc*-induced tumorigenesis (Klapproth et al., 2009).

The tumour suppressor status of a cell plays a decisive role in the functional outcome of NF-κB, thereby explaining the apparent dual role of NF-κB (Rocha et al., 2003a; Rocha et al., 2003b; Webster and Perkins, 1999). As NF-κB is a pro-survival factor and promote cellular proliferation, and p53 induces cell cycle arrest or apoptosis, mechanisms that integrate the activities of both pathways in conditions when they are activated simultaneously must exist (such as genotoxic stress treatment). p53 could oppose NF-κB function by blocking its transcriptional activity through competition for coactivators or through conversion of Rel members from activators to repressors (Culmsee et al., 2003; Ravi et al., 1998). p53 could promote a switch from p52–Bcl-3 activator complexes to p52–HDAC1 complexes (Rocha et al., 2003b) and another tumour suppressor gene ARF could induce phosphorylation of Thr505 on RelA, resulting in its association with HDAC1, thereby inhibiting its transcriptional activity (Rocha et al., 2003a). Both effects could explain why p53-induced NF-κB activation is not transcriptionally active and leads to apoptosis, most likely through p53-mediated repression of NF-κB induced antiapoptotic gene expression (Ryan et al., 2000). In addition, other p53-independent mechanisms must exist to play a role in NF-κB 's proapoptotic functions (Campbell et al., 2004).

Several NF-κB target genes, including the pro-inflammatory cytokines TNF-α and IL-6, are associated with tumor development and progression in

humans and mice (Karin and Greten, 2005). These cytokines can promote proliferation, survival or apoptosis of tumor cells in an auto- and paracrine fashion (Grivennikov et al., 2010).

IL-6 was found to promote or inhibit lymphoma progression depending on their development stage (Gilbert and Hemann, 2012). In the bone marrow, IL-6 signaling suppresses the development of B cell lymphomas by promoting differentiation of B cells, while IL-6 stimulates survival of transformed B cells. IL-6 also supports the survival of colitis-associated cancers in mice and promotes the growth of hepatocellular carcinomas (HCCs) (Bollrath et al., 2009; Grivennikov et al., 2009; Naugler et al., 2007). In humans, serum levels of IL-6 predict the HCC development in patients with chronic hepatitis B (Wong et al., 2009). We did not find any difference in IL-6 between *Zbp1*$^{+/+}$Eμ-*Myc* and *Zbp1*$^{-/-}$Eμ-*Myc* mice, suggesting that the effects of IL-6 might not explain the phenotype observed.

Low concentrations of TNF-α released from tumor-associated inflammatory cells augment tumor proliferation and progression, while high concentrations of TNF can induce necrosis of tumor cells (Karin and Greten, 2005; Luo et al., 2004). *In vivo* the latter function of TNF-α may be more relevant as *Tnfa*-deficient mice and *Tnfr1*-deficient mice are resistant to carcinogen-induced tumors (Arnott et al., 2004; Moore et al., 1999). TNF-α could have pro- or anti- tumour effect depending on the status of the cell. The default pathway is induction of genes involved in inflammation and cell survival. Upon binding to TNF-α, the activated TNFR1 induces a range of inflammatory mediators and growth factors through the AP1 transcription factors or IKKs which would activate NF-κB (Balkwill, 2009). Notably, NF-

κB activation induces negative regulators of apoptosis such as FLIPL (also known as CFLAR), BCL-2 and superoxide dismutase. If NF-κB activation is insufficient, apoptosis occurs through caspase-8 and, through accumulation of intracellular reactive oxygen, sustained Jun amino-terminal kinase (JNK) activation and mitochondrial pathways (Balkwill, 2009). Apoptosis is a late response to TNF, unlike the rapid apoptosis that is induced by other members of the TNF superfamily such as FAS ligand (FASL) and TRAIL (also known as TNFRSF10C).

Consistent with the notion that there are increased DNA damage and increased NF-κB activation in the *Zbp1*$^{-/-}$Eμ-*Myc* mice, we observed an increase in mRNA expressions of *Tnf-α* in *Zbp1*$^{-/-}$Eμ-*Myc* mice and increased in caspase-8 activation in *Zbp1*$^{-/-}$Eμ-*Myc* mice. This suggests that TNF-α induced apoptosis that is mediated through caspase-8 may contribute to the increase in apoptosis seen in *Zbp1*$^{-/-}$Eμ-*Myc* mice. However, further experiments had to be done to determine the importance of this pathway in *Zbp1*$^{-/-}$Eμ-*Myc* lymphomagenesis. We could inhibit TNF-α *in vivo* using antibodies or small molecule inhibitors and obrserve the effects on regression or survival. In addition, we could cross mice deficient in TNF-α with Eμ-*Myc* mice and monitor disease progression.

8.4 Future work

In light of the phenotype that we observed for *Zbp1*$^{-/-}$Eμ-*Myc* and *Irf3*$^{+/-}$Eμ-*Myc*, it would be worthwhile to cross mice deficient in STING with Eμ-*Myc*. STING is an important adaptor molecule that links signals from the cytosolic DNA sensors to downstream effectors such as TBK1 and IRF3. In

addition, STING could act as a direct sensor of cyclic di-GMP (Burdette et al., 2011).

An outstanding question is the mechanism of actions of ZBP1 in potentiating the DDR in Eμ-*Myc* lymphomagenesis. It would be interesting to identify potential interacting partners of ZBP1 by performing a co-immunoprecipitate experiment with antibody against ZBP1. This might provide insights on the mechanism of actions of ZBP1 and if it interacts directly with any of the proteins that are involved in the DDR. In addition, it would be interesting to investigate the role of ZBP1 in other mouse models of cancer. Genome instability is one of the hallmarks of cancer (Hanahan and Weinberg, 2011). If ZBP1 could affect the DDR response, ZBP1 could presumably play an important role in different contexts of cancer.

It would be worthwhile to investigate if loss of ZBP1 could potentiate the DDR in human cancer cell lines. With the advent of clustered regularly interspaced short palindromic repeats (CRISPR)/CRISPR-associated (Cas) system as an efficient gene-targeting technology (de Souza, 2013; Jinek et al., 2012), it might be possible to utilise the system to generate ZBP1 knockout human cells and test if it affects the DDR in these cells.

8.5 Conclusion

Together our findings link genotoxic stress to cytoplasmic DNA sensor pathways and the induction of NKG2D ligands. The response to cytoplasmic DNA could provide a common trigger for NKG2D ligand induction in cancerous and infected cells, linking together protective NKG2D-mediated responses to infections, malignant transformation and cells with genomic damage (Gasser and Raulet, 2006c; Weitzman et al., 2004). We also link IRF3

and ZBP1, which are involved in the intracellular DNA sensing pathway, to B cell lymphomagenesis, thus providing new targets for therapy.

Bibliography

Ablasser, A., Bauernfeind, F., Hartmann, G., Latz, E., Fitzgerald, K.A., and Hornung, V. (2009). RIG-I-dependent sensing of poly(dA:dT) through the induction of an RNA polymerase III-transcribed RNA intermediate. Nat Immunol *10*, 1065-1072.

Ablasser, A., Hertrich, C., Wassermann, R., and Hornung, V. (2013). Nucleic acid driven sterile inflammation. Clin Immunol *147*, 207-215.

Adams, J.M., Harris, A.W., Pinkert, C.A., Corcoran, L.M., Alexander, W.S., Cory, S., Palmiter, R.D., and Brinster, R.L. (1985). The c-myc oncogene driven by immunoglobulin enhancers induces lymphoid malignancy in transgenic mice. Nature *318*, 533-538.

Aktas, E., Kucuksezer, U.C., Bilgic, S., Erten, G., and Deniz, G. (2009). Relationship between CD107a expression and cytotoxic activity. Cell Immunol *254*, 149-154.

Alimirah, F., Chen, J., Davis, F.J., and Choubey, D. (2007). IFI16 in human prostate cancer. Mol Cancer Res *5*, 251-259.

Alter, G., Malenfant, J.M., and Altfeld, M. (2004). CD107a as a functional marker for the identification of natural killer cell activity. J Immunol Methods *294*, 15-22.

Apetoh, L., Ghiringhelli, F., Tesniere, A., Obeid, M., Ortiz, C., Criollo, A., Mignot, G., Maiuri, M.C., Ullrich, E., Saulnier, P*., et al.* (2007). Toll-like receptor 4-dependent contribution of the immune system to anticancer chemotherapy and radiotherapy. Nat Med *13*, 1050-1059.

Ariake, K., Ohtsuka, H., Motoi, F., Douchi, D., Oikawa, M., Rikiyama, T., Fukase, K., Katayose, Y., Egawa, S., and Unno, M. (2012). GCF2/LRRFIP1 promotes colorectal cancer metastasis and liver invasion through integrin-dependent RhoA activation. Cancer Lett *325*, 99-107.

Arnott, C.H., Scott, K.A., Moore, R.J., Robinson, S.C., Thompson, R.G., and Balkwill, F.R. (2004). Expression of both TNF-alpha receptor subtypes is essential for optimal skin tumour development. Oncogene *23*, 1902-1910.

Asefa, B., Dermott, J.M., Kaldis, P., Stefanisko, K., Garfinkel, D.J., and Keller, J.R. (2006). p205, a potential tumor suppressor, inhibits cell proliferation via multiple pathways of cell cycle regulation. FEBS Lett *580*, 1205-1214.

Asefa, B., Klarmann, K.D., Copeland, N.G., Gilbert, D.J., Jenkins, N.A., and Keller, J.R. (2004). The interferon-inducible p200 family of proteins: a perspective on their roles in cell cycle regulation and differentiation. Blood Cells Mol Dis *32*, 155-167.

Atianand, M.K., Duffy, E.B., Shah, A., Kar, S., Malik, M., and Harton, J.A. (2011). Francisella tularensis reveals a disparity between human and mouse NLRP3 inflammasome activation. J Biol Chem *286*, 39033-39042.

Balkwill, F. (2009). Tumour necrosis factor and cancer. Nat Rev Cancer *9*, 361-371.

Barber, G.N. (2011). Cytoplasmic DNA innate immune pathways. Immunol Rev *243*, 99-108.

Barbie, D.A., Tamayo, P., Boehm, J.S., Kim, S.Y., Moody, S.E., Dunn, I.F., Schinzel, A.C., Sandy, P., Meylan, E., Scholl, C.*, et al.* (2009). Systematic RNA interference reveals that oncogenic KRAS-driven cancers require TBK1. Nature *462*, 108-112.

Barlow, C., Hirotsune, S., Paylor, R., Liyanage, M., Eckhaus, M., Collins, F., Shiloh, Y., Crawley, J.N., Ried, T., Tagle, D.*, et al.* (1996). Atm-deficient mice: a paradigm of ataxia telangiectasia. Cell *86*, 159-171.

Bartek, J., Bartkova, J., and Lukas, J. (2007). DNA damage signalling guards against activated oncogenes and tumour progression. Oncogene *26*, 7773-7779.

Bartek, J., Falck, J., and Lukas, J. (2001). CHK2 kinase--a busy messenger. Nat Rev Mol Cell Biol *2*, 877-886.

Bartek, J., and Lukas, J. (2003). Chk1 and Chk2 kinases in checkpoint control and cancer. Cancer Cell *3*, 421-429.

Bartkova, J., Horejsi, Z., Koed, K., Kramer, A., Tort, F., Zieger, K., Guldberg, P., Sehested, M., Nesland, J.M., Lukas, C.*, et al.* (2005). DNA damage response as a candidate anti-cancer barrier in early human tumorigenesis. Nature *434*, 864-870.

Bartkova, J., Rezaei, N., Liontos, M., Karakaidos, P., Kletsas, D., Issaeva, N., Vassiliou, L.-V.F., Kolettas, E., Niforou, K., Zoumpourlis, V.C.*, et al.* (2006). Oncogene-induced senescence is part of the tumorigenesis barrier imposed by DNA damage checkpoints. Nature *444*, 633-637.

Bensimon, A., Schmidt, A., Ziv, Y., Elkon, R., Wang, S.Y., Chen, D.J., Aebersold, R., and Shiloh, Y. (2010). ATM-dependent and -independent dynamics of the nuclear phosphoproteome after DNA damage. Sci Signal *3*, rs3.

Beroukhim, R., Mermel, C.H., Porter, D., Wei, G., Raychaudhuri, S., Donovan, J., Barretina, J., Boehm, J.S., Dobson, J., Urashima, M.*, et al.* (2010). The landscape of somatic copy-number alteration across human cancers. Nature *463*, 899-905.

Bian, X., McAllister-Lucas, L.M., Shao, F., Schumacher, K.R., Feng, Z., Porter, A.G., Castle, V.P., and Opipari, A.W., Jr. (2001). NF-kappa B activation mediates doxorubicin-induced cell death in N-type neuroblastoma cells. J Biol Chem *276*, 48921-48929.

Boehrs, J.K., He, J., Halaby, M.J., and Yang, D.Q. (2007). Constitutive expression and cytoplasmic compartmentalization of ATM protein in differentiated human neuron-like SH-SY5Y cells. J Neurochem *100*, 337-345.

Boissel, N., Rea, D., Tieng, V., Dulphy, N., Brun, M., Cayuela, J.M., Rousselot, P., Tamouza, R., Le Bouteiller, P., Mahon, F.X.*, et al.* (2006). BCR/ABL oncogene directly controls MHC class I chain-related molecule A expression in chronic myelogenous leukemia. J Immunol *176*, 5108-5116.

Bollrath, J., Phesse, T.J., von Burstin, V.A., Putoczki, T., Bennecke, M., Bateman, T., Nebelsiek, T., Lundgren-May, T., Canli, O., Schwitalla, S.*, et al.* (2009). gp130-mediated Stat3 activation in enterocytes regulates cell survival and cell-cycle progression during colitis-associated tumorigenesis. Cancer Cell *15*, 91-102.

Bonner, W.M., Redon, C.E., Dickey, J.S., Nakamura, A.J., Sedelnikova, O.A., Solier, S., and Pommier, Y. (2008). GammaH2AX and cancer. Nat Rev Cancer *8*, 957-967.

Borghesani, P.R., Alt, F.W., Bottaro, A., Davidson, L., Aksoy, S., Rathbun, G.A., Roberts, T.M., Swat, W., Segal, R.A., and Gu, Y. (2000). Abnormal development of Purkinje cells and lymphocytes in Atm mutant mice. Proc Natl Acad Sci U S A *97*, 3336-3341.

Bosma, M.J., and Carroll, A.M. (1991). The SCID mouse mutant: definition, characterization, and potential uses. Annu Rev Immunol *9*, 323-350.

Bottino, C., Castriconi, R., Pende, D., Rivera, P., Nanni, M., Carnemolla, B., Cantoni, C., Grassi, J., Marcenaro, S., Reymond, N.*, et al.* (2003). Identification of PVR (CD155) and Nectin-2 (CD112) as cell surface ligands for the human DNAM-1 (CD226) activating molecule. J Exp Med *198*, 557-567.

Bradstock, K.F., Makrynikola, V., Bianchi, A., Shen, W., Hewson, J., and Gottlieb, D.J. (2000). Effects of the chemokine stromal cell-derived factor-1 on the migration and localization of precursor-B acute lymphoblastic leukemia cells within bone marrow stromal layers. Leukemia *14*, 882-888.

Brezniceanu, M.L., Volp, K., Bosser, S., Solbach, C., Lichter, P., Joos, S., and Zornig, M. (2003). HMGB1 inhibits cell death in yeast and mammalian cells and is abundantly expressed in human breast carcinoma. FASEB J *17*, 1295-1297.

Bric, A., Miething, C., Bialucha, C.U., Scuoppo, C., Zender, L., Krasnitz, A., Xuan, Z., Zuber, J., Wigler, M., Hicks, J.*, et al.* (2009). Functional identification of tumor-suppressor genes through an in vivo RNA interference screen in a mouse lymphoma model. Cancer Cell *16*, 324-335.

Brown, J.D., Mitchell, S.E., and O'Neill, R.J. (2012). Making a long story short: noncoding RNAs and chromosome change. Heredity (Edinb) *108*, 42-49.

Burdette, D.L., Monroe, K.M., Sotelo-Troha, K., Iwig, J.S., Eckert, B., Hyodo, M., Hayakawa, Y., and Vance, R.E. (2011). STING is a direct innate immune sensor of cyclic di-GMP. Nature *478*, 515-518.

Buss, H., Dorrie, A., Schmitz, M.L., Hoffmann, E., Resch, K., and Kracht, M. (2004). Constitutive and interleukin-1-inducible phosphorylation of p65 NF-{kappa}B at serine 536 is mediated by multiple protein kinases including I{kappa}B kinase (IKK)-{alpha}, IKK{beta}, IKK{epsilon}, TRAF family member-associated (TANK)-binding kinase 1 (TBK1), and an unknown kinase and couples p65 to TATA-binding protein-associated factor II31-mediated interleukin-8 transcription. J Biol Chem *279*, 55633-55643.

Campbell, K.J., Chapman, N.R., and Perkins, N.D. (2001). UV stimulation induces nuclear factor kappaB (NF-kappaB) DNA-binding activity but not transcriptional activation. Biochem Soc Trans *29*, 688-691.

Campbell, K.J., Rocha, S., and Perkins, N.D. (2004). Active repression of antiapoptotic gene expression by RelA(p65) NF-kappa B. Mol Cell *13*, 853-865.

Campisi, J., and D'adda Di Fagagna, F. (2007). Cellular senescence: when bad things happen to good cells. Nat Rev Mol Cell Biol *8*, 729-740.

Carlsten, M., Bjorkstrom, N.K., Norell, H., Bryceson, Y., van Hall, T., Baumann, B.C., Hanson, M., Schedvins, K., Kiessling, R., Ljunggren, H.G.*, et al.* (2007).

DNAX accessory molecule-1 mediated recognition of freshly isolated ovarian carcinoma by resting natural killer cells. Cancer Res *67*, 1317-1325.

Carreno, B.M., and Collins, M. (2002). The B7 family of ligands and its receptors: new pathways for costimulation and inhibition of immune responses. Annu Rev Immunol *20*, 29-53.

Castriconi, R., Dondero, A., Corrias, M.V., Lanino, E., Pende, D., Moretta, L., Bottino, C., and Moretta, A. (2004). Natural killer cell-mediated killing of freshly isolated neuroblastoma cells: critical role of DNAX accessory molecule-1-poliovirus receptor interaction. Cancer Res *64*, 9180-9184.

Cerboni, C., Zingoni, A., Cippitelli, M., Piccoli, M., Frati, L., and Santoni, A. (2007). Antigen-activated human T lymphocytes express cell-surface NKG2D ligands via an ATM/ATR-dependent mechanism and become susceptible to autologous NK- cell lysis. Blood *110*, 606-615.

Chen, I.F., Ou-Yang, F., Hung, J.Y., Liu, J.C., Wang, H., Wang, S.C., Hou, M.F., Hortobagyi, G.N., and Hung, M.C. (2006). AIM2 suppresses human breast cancer cell proliferation in vitro and mammary tumor growth in a mouse model. Mol Cancer Ther *5*, 1-7.

Chen, L.C., Wang, L.J., Tsang, N.M., Ojcius, D.M., Chen, C.C., Ouyang, C.N., Hsueh, C., Liang, Y., Chang, K.P., and Chang, Y.S. (2012). Tumour inflammasome-derived IL-1beta recruits neutrophils and improves local recurrence-free survival in EBV-induced nasopharyngeal carcinoma. EMBO Mol Med *4*, 1276-1293.

Chien, Y., Kim, S., Bumeister, R., Loo, Y.M., Kwon, S.W., Johnson, C.L., Balakireva, M.G., Romeo, Y., Kopelovich, L., Gale, M., Jr.*, et al.* (2006). RalB GTPase-mediated activation of the IkappaB family kinase TBK1 couples innate immune signaling to tumor cell survival. Cell *127*, 157-170.

Chien, Y., and White, M.A. (2008). Characterization of RalB-Sec5-TBK1 function in human oncogenesis. Methods Enzymol *438*, 321-329.

Chiesa, N., Barlow, C., Wynshaw-Boris, A., Strata, P., and Tempia, F. (2000). Atm-deficient mice Purkinje cells show age-dependent defects in calcium spike bursts and calcium currents. Neuroscience *96*, 575-583.

Chiu, Y.H., Macmillan, J.B., and Chen, Z.J. (2009). RNA polymerase III detects cytosolic DNA and induces type I interferons through the RIG-I pathway. Cell *138*, 576-591.

Choi, S., Gamper, A.M., White, J.S., and Bakkenist, C.J. (2010). Inhibition of ATM kinase activity does not phenocopy ATM protein disruption: implications for the clinical utility of ATM kinase inhibitors. Cell Cycle *9*, 4052-4057.

Choubey, D., Deka, R., and Ho, S.M. (2008). Interferon-inducible IFI16 protein in human cancers and autoimmune diseases. Front Biosci *13*, 598-608.

Choubey, D., Walter, S., Geng, Y., and Xin, H. (2000). Cytoplasmic localization of the interferon-inducible protein that is encoded by the AIM2 (absent in melanoma) gene from the 200-gene family. FEBS Lett *474*, 38-42.

Chung, H.W., Lee, S.G., Kim, H., Hong, D.J., Chung, J.B., Stroncek, D., and Lim, J.B. (2009). Serum high mobility group box-1 (HMGB1) is closely associated with the clinical and pathologic features of gastric cancer. J Transl Med *7*, 38.

Civas, A., Genin, P., Morin, P., Lin, R., and Hiscott, J. (2006). Promoter organization of the interferon-A genes differentially affects virus-induced expression and responsiveness to TBK1 and IKKepsilon. J Biol Chem *281*, 4856-4866.

Civril, F., Deimling, T., de Oliveira Mann, C.C., Ablasser, A., Moldt, M., Witte, G., Hornung, V., and Hopfner, K.P. (2013). Structural mechanism of cytosolic DNA sensing by cGAS. Nature *498*, 332-337.

Cleaver, J.E., Lam, E.T., and Revet, I. (2009). Disorders of nucleotide excision repair: the genetic and molecular basis of heterogeneity. Nat Rev Genet *10*, 756-768.

Clement, J.F., Meloche, S., and Servant, M.J. (2008). The IKK-related kinases: from innate immunity to oncogenesis. Cell Res *18*, 889-899.

Corcoran, L.M., Tawfilis, S., and Barlow, L.J. (1999). Generation of B lymphoma cell lines from knockout mice by transformation in vivo with an Emu-myc transgene. J Immunol Methods *228*, 131-138.

Coudert, J.D., and Held, W. (2006). The role of the NKG2D receptor for tumor immunity. Semin Cancer Biol *16*, 333-343.

Covey, J.M., D'Incalci, M., Tilchen, E.J., Zaharko, D.S., and Kohn, K.W. (1986). Differences in DNA damage produced by incorporation of 5-aza-2'-deoxycytidine or 5,6-dihydro-5-azacytidine into DNA of mammalian cells. Cancer Res *46*, 5511-5517.

Cresswell, K.S., Clarke, C.J., Jackson, J.T., Darcy, P.K., Trapani, J.A., and Johnstone, R.W. (2005). Biochemical and growth regulatory activities of the HIN-200 family member and putative tumor suppressor protein, AIM2. Biochem Biophys Res Commun *326*, 417-424.

Croxford, J.L., Tang, M.L., Pan, M.F., Huang, C.W., Kamran, N., Phua, C.M., Chng, W.J., Ng, S.B., Raulet, D.H., and Gasser, S. (2013). ATM-dependent spontaneous regression of early Emu-myc-induced murine B-cell leukemia depends on natural killer and T cells. Blood *121*, 2512-2521.

Culmsee, C., Siewe, J., Junker, V., Retiounskaia, M., Schwarz, S., Camandola, S., El-Metainy, S., Behnke, H., Mattson, M.P., and Krieglstein, J. (2003). Reciprocal inhibition of p53 and nuclear factor-kappaB transcriptional activities determines cell survival or death in neurons. J Neurosci *23*, 8586-8595.

D'Incalci, M., Covey, J.M., Zaharko, D.S., and Kohn, K.W. (1985). DNA alkali-labile sites induced by incorporation of 5-aza-2'-deoxycytidine into DNA of mouse leukemia L1210 cells. Cancer Res *45*, 3197-3202.

Daniel, J.A., Pellegrini, M., Lee, B.S., Guo, Z., Filsuf, D., Belkina, N.V., You, Z., Paull, T.T., Sleckman, B.P., Feigenbaum, L.*, et al.* (2012). Loss of ATM kinase activity leads to embryonic lethality in mice. J Cell Biol *198*, 295-304.

David, S.S., O'Shea, V.L., and Kundu, S. (2007). Base-excision repair of oxidative DNA damage. Nature *447*, 941-950.

de Souza, N. (2013). RNA-guided gene editing. Nat Methods *10*, 189.

Denault, J.B., and Salvesen, G.S. (2003). Human caspase-7 activity and regulation by its N-terminal peptide. J Biol Chem *278*, 34042-34050.

Desmet, C.J., and Ishii, K.J. (2012). Nucleic acid sensing at the interface between innate and adaptive immunity in vaccination. Nat Rev Immunol *12*, 479-491.

DeYoung, K.L., Ray, M.E., Su, Y.A., Anzick, S.L., Johnstone, R.W., Trapani, J.A., Meltzer, P.S., and Trent, J.M. (1997). Cloning a novel member of the human interferon-inducible gene family associated with control of tumorigenicity in a model of human melanoma. Oncogene *15*, 453-457.

Dialynas, D.P., Shao, L., Billman, G.F., and Yu, J. (2001). Engraftment of human T-cell acute lymphoblastic leukemia in immunodeficient NOD/SCID mice which have been preconditioned by injection of human cord blood. Stem Cells *19*, 443-452.

Diefenbach, A., Hsia, J.K., Hsiung, M.Y., and Raulet, D. (2003). A novel ligand for the NKG2D receptor activates NK cells and macrophages and induces tumor immunity. Eur J Immunol *33*, 381-391.

Diefenbach, A., Jamieson, A.M., Liu, S.D., Shastri, N., and Raulet, D. (2000). Ligands for the murine NKG2D receptor: expression by tumor cells and activation of NK cells and macrophages. Nat Immunol *1*, 119-126.

Ding, Y., Wang, L., Su, L.K., Frey, J.A., Shao, R., Hunt, K.K., and Yan, D.H. (2004). Antitumor activity of IFIX, a novel interferon-inducible HIN-200 gene, in breast cancer. Oncogene *23*, 4556-4566.

Duan, X., Ponomareva, L., Veeranki, S., Panchanathan, R., Dickerson, E., and Choubey, D. (2011). Differential roles for the interferon-inducible IFI16 and AIM2 innate immune sensors for cytosolic DNA in cellular senescence of human fibroblasts. Mol Cancer Res *9*, 589-602.

Dunn, G.P., Bruce, A.T., Sheehan, K.C., Shankaran, V., Uppaluri, R., Bui, J.D., Diamond, M.S., Koebel, C.M., Arthur, C., White, J.M.*, et al.* (2005). A critical function for type I interferons in cancer immunoediting. Nat Immunol *6*, 722-729.

Dunn, G.P., Koebel, C.M., and Schreiber, R.D. (2006). Interferons, immunity and cancer immunoediting. Nat Rev Immunol *6*, 836-848.

El-Sherbiny, Y.M., Meade, J.L., Holmes, T.D., McGonagle, D., Mackie, S.L., Morgan, A.W., Cook, G., Feyler, S., Richards, S.J., Davies, F.E.*, et al.* (2007). The requirement for DNAM-1, NKG2D, and NKp46 in the natural killer cell-mediated killing of myeloma cells. Cancer Res *67*, 8444-8449.

Ellerman, J.E., Brown, C.K., de Vera, M., Zeh, H.J., Billiar, T., Rubartelli, A., and Lotze, M.T. (2007). Masquerader: high mobility group box-1 and cancer. Clin Cancer Res *13*, 2836-2848.

Elson, A., Wang, Y., Daugherty, C.J., Morton, C.C., Zhou, F., Campos-Torres, J., and Leder, P. (1996). Pleiotropic defects in ataxia-telangiectasia protein-deficient mice. Proc Natl Acad Sci U S A *93*, 13084-13089.

Falvo, J.V., Parekh, B.S., Lin, C.H., Fraenkel, E., and Maniatis, T. (2000). Assembly of a functional beta interferon enhanceosome is dependent on ATF-2-c-jun heterodimer orientation. Mol Cell Biol *20*, 4814-4825.

Famulski, K.S., Al-Hijailan, R.S., Dobler, K., Pienkowska, M., Al-Mohanna, F., and Paterson, M.C. (2003). Aberrant sensing of extracellular Ca2+ by cultured ataxia telangiectasia fibroblasts. Oncogene *22*, 471-475.

Felsher, D.W., and Bishop, J.M. (1999). Transient excess of MYC activity can elicit genomic instability and tumorigenesis. Proc Natl Acad Sci U S A *96*, 3940-3944.

Fensterl, V., Grotheer, D., Berk, I., Schlemminger, S., Vallbracht, A., and Dotzauer, A. (2005). Hepatitis A virus suppresses RIG-I-mediated IRF-3 activation to block induction of beta interferon. J Virol *79*, 10968-10977.

Ferguson, B.J., Mansur, D.S., Peters, N.E., Ren, H., and Smith, G.L. (2012). DNA-PK is a DNA sensor for IRF-3-dependent innate immunity. Elife *1*, e00047.

Fionda, C., Soriani, A., Malgarini, G., Iannitto, M.L., Santoni, A., and Cippitelli, M. (2009). Heat shock protein-90 inhibitors increase MHC class I-related chain A and B ligand expression on multiple myeloma cells and their ability to trigger NK cell degranulation. J Immunol *183*, 4385-4394.

Fitzgerald, K.A., McWhirter, S.M., Faia, K.L., Rowe, D.C., Latz, E., Golenbock, D.T., Coyle, A.J., Liao, S.M., and Maniatis, T. (2003). IKKepsilon and TBK1 are essential components of the IRF3 signaling pathway. Nature immunology *4*, 491-496.

Fu, Y., Comella, N., Tognazzi, K., Brown, L.F., Dvorak, H.F., and Kocher, O. (1999). Cloning of DLM-1, a novel gene that is up-regulated in activated macrophages, using RNA differential display. Gene *240*, 157-163.

Fujiuchi, N., Aglipay, J.A., Ohtsuka, T., Maehara, N., Sahin, F., Su, G.H., Lee, S.W., and Ouchi, T. (2004). Requirement of IFI16 for the maximal activation of p53 induced by ionizing radiation. J Biol Chem *279*, 20339-20344.

Gao, P., Ascano, M., Wu, Y., Barchet, W., Gaffney, B.L., Zillinger, T., Serganov, A.A., Liu, Y., Jones, R.A., Hartmann, G.*, et al.* (2013). Cyclic [G(2',5')pA(3',5')p] is the metazoan second messenger produced by DNA-activated cyclic GMP-AMP synthase. Cell *153*, 1094-1107.

Gariglio, M., Mondini, M., De Andrea, M., and Landolfo, S. (2011). The multifaceted interferon-inducible p200 family proteins: from cell biology to human pathology. J Interferon Cytokine Res *31*, 159-172.

Garrido, C., Brunet, M., Didelot, C., Zermati, Y., Schmitt, E., and Kroemer, G. (2006). Heat shock proteins 27 and 70: anti-apoptotic proteins with tumorigenic properties. Cell Cycle *5*, 2592-2601.

Gasser, S., Orsulic, S., Brown, E.J., and Raulet, D.H. (2005). The DNA damage pathway regulates innate immune system ligands of the NKG2D receptor. Nature *436*, 1186-1190.

Gasser, S., and Raulet, D. (2006a). The DNA damage response, immunity and cancer. Semin Cancer Biol *16*, 344-347.

Gasser, S., and Raulet, D.H. (2006b). Activation and self-tolerance of natural killer cells. Immunol Rev *214*, 130-142.

Gasser, S., and Raulet, D.H. (2006c). The DNA damage response arouses the immune system. Cancer research *66*, 3959-3962.

Gerdes, J. (1990). Ki-67 and other proliferation markers useful for immunohistological diagnostic and prognostic evaluations in human malignancies. Semin Cancer Biol *1*, 199-206.

Gilbert, L.A., and Hemann, M.T. (2012). Context-specific roles for paracrine IL-6 in lymphomagenesis. Genes Dev *26*, 1758-1768.

Gorgoulis, V., Vassiliou, L., Karakaidos, P., Zacharatos, P., Kotsinas, A., Liloglou, T., Venere, M., Ditullio, R., Kastrinakis, N., Levy, B.*, et al.* (2005a). Activation of the DNA damage checkpoint and genomic instability in human precancerous lesions. Nature *434*, 907-913.

Gorgoulis, V.G., Vassiliou, L.V., Karakaidos, P., Zacharatos, P., Kotsinas, A., Liloglou, T., Venere, M., Ditullio, R.A., Jr., Kastrinakis, N.G., Levy, B.*, et al.* (2005b). Activation of the DNA damage checkpoint and genomic instability in human precancerous lesions. Nature *434*, 907-913.

Gorrini, C., Squatrito, M., Luise, C., Syed, N., Perna, D., Wark, L., Martinato, F., Sardella, D., Verrecchia, A., Bennett, S.*, et al.* (2007). Tip60 is a haplo-insufficient tumour suppressor required for an oncogene-induced DNA damage response. Nature *448*, 1063-1067.

Goubau, D., Rehwinkel, J., and Sousa, C.R.e. (2010). PYHIN proteins: center stage in DNA sensing. Nature Publishing Group *11*, 984-986.

Gourzi, P., Leonova, T., and Papavasiliou, F.N. (2006). A Role for activation-induced cytidine deaminase in the host response against a transforming retrovirus. Immunity *24*, 779-786.

Grandvaux, N., Servant, M.J., tenOever, B., Sen, G.C., Balachandran, S., Barber, G.N., Lin, R., and Hiscott, J. (2002). Transcriptional profiling of interferon regulatory factor 3 target genes: direct involvement in the regulation of interferon-stimulated genes. J Virol *76*, 5532-5539.

Grivennikov, S., Karin, E., Terzic, J., Mucida, D., Yu, G.Y., Vallabhapurapu, S., Scheller, J., Rose-John, S., Cheroutre, H., Eckmann, L.*, et al.* (2009). IL-6 and Stat3 are required for survival of intestinal epithelial cells and development of colitis-associated cancer. Cancer Cell *15*, 103-113.

Grivennikov, S.I., Greten, F.R., and Karin, M. (2010). Immunity, inflammation, and cancer. Cell *140*, 883-899.

Groh, V., Bahram, S., Bauer, S., Herman, A., Beauchamp, M., and Spies, T. (1996). Cell stress-regulated human major histocompatibility complex class I gene expressed in gastrointestinal epithelium. Proc Natl Acad Sci U S A *93*, 12445-12450.

Guerra, N., Tan, Y., Joncker, N., Choy, A., Gallardo, F., Xiong, N., Knoblaugh, S., Cado, D., Greenberg, N., and Raulet, D. (2008). NKG2D-Deficient Mice Are

Defective in Tumor Surveillance in Models of Spontaneous Malignancy. Immunity *28*, 571-580.

Guo, Z., Kumagai, A., Wang, S., and Dunphy, W. (2000). Requirement for Atr in phosphorylation of Chk1 and cell cycle regulation in response to DNA replication blocks and UV-damaged DNA in Xenopus egg extracts. Genes Dev *14*, 2745-2756.

Haferlach, T., Kohlmann, A., Wieczorek, L., Basso, G., Kronnie, G.T., Bene, M.C., De Vos, J., Hernandez, J.M., Hofmann, W.K., Mills, K.I.*, et al.* (2010). Clinical utility of microarray-based gene expression profiling in the diagnosis and subclassification of leukemia: report from the International Microarray Innovations in Leukemia Study Group. J Clin Oncol *28*, 2529-2537.

Halazonetis, T., Gorgoulis, V., and Bartek, J. (2008a). An Oncogene-Induced DNA Damage Model for Cancer Development. Science *319*, 1352-1355.

Halazonetis, T.D., Gorgoulis, V.G., and Bartek, J. (2008b). An oncogene-induced DNA damage model for cancer development. Science *319*, 1352-1355.

Hamerman, J.A., Ogasawara, K., and Lanier, L.L. (2004). Cutting edge: Toll-like receptor signaling in macrophages induces ligands for the NKG2D receptor. J Immunol *172*, 2001-2005.

Hanahan, D., and Weinberg, R.A. (2011). Hallmarks of cancer: the next generation. Cell *144*, 646-674.

Harris, A.W., Pinkert, C.A., Crawford, M., Langdon, W.Y., Brinster, R.L., and Adams, J.M. (1988). The E mu-myc transgenic mouse. A model for high-incidence spontaneous lymphoma and leukemia of early B cells. J Exp Med *167*, 353-371.

Hedges, D.J., and Deininger, P.L. (2007). Inviting instability: Transposable elements, double-strand breaks, and the maintenance of genome integrity. Mutat Res *616*, 46-59.

Heiber, J.F., and Barber, G.N. (2012). Evaluation of innate immune signaling pathways in transformed cells. Methods Mol Biol *797*, 217-238.

Heider, M.R., and Munson, M. (2012). Exorcising the exocyst complex. Traffic *13*, 898-907.

Heinemann, A., and Paschen, A. (2012). Tumor suppressors control ULBP2, an innate surface ligand of the lymphocyte immune receptor NKG2D. Oncoimmunology *1*, 535-536.

Heinemann, A., Zhao, F., Pechlivanis, S., Eberle, J., Steinle, A., Diederichs, S., Schadendorf, D., and Paschen, A. (2012). Tumor suppressive microRNAs miR-34a/c control cancer cell expression of ULBP2, a stress-induced ligand of the natural killer cell receptor NKG2D. Cancer Res *72*, 460-471.

Helleday, T., Petermann, E., Lundin, C., Hodgson, B., and Sharma, R.A. (2008). DNA repair pathways as targets for cancer therapy. Nat Rev Cancer *8*, 193-204.

Hemmi, H., Takeuchi, O., Sato, S., Yamamoto, M., Kaisho, T., Sanjo, H., Kawai, T., Hoshino, K., Takeda, K., and Akira, S. (2004). The roles of two IkappaB kinase-

related kinases in lipopolysaccharide and double stranded RNA signaling and viral infection. J Exp Med *199*, 1641-1650.

Hideshima, T., and Anderson, K.C. (2002). Molecular mechanisms of novel therapeutic approaches for multiple myeloma. Nat Rev Cancer *2*, 927-937.

Hiscott, J., Grandvaux, N., Sharma, S., Tenoever, B.R., Servant, M.J., and Lin, R. (2003). Convergence of the NF-kappaB and interferon signaling pathways in the regulation of antiviral defense and apoptosis. Ann N Y Acad Sci *1010*, 237-248.

Honda, K., and Taniguchi, T. (2006). IRFs: master regulators of signalling by Toll-like receptors and cytosolic pattern-recognition receptors. Nat Rev Immunol *6*, 644-658.

Hornung, V., Ablasser, A., Charrel-Dennis, M., Bauernfeind, F., Horvath, G., Caffrey, D.R., Latz, E., and Fitzgerald, K.A. (2009). AIM2 recognizes cytosolic dsDNA and forms a caspase-1-activating inflammasome with ASC. Nature *458*, 514-518.

Hornung, V., and Latz, E. (2010). Intracellular DNA recognition. Nat Rev Immunol *10*, 123-130.

Hsu, S., Kim, M., Hernandez, L., Grajales, V., Noonan, A., Anver, M., Davidson, B., and Annunziata, C.M. (2012). IKK-epsilon coordinates invasion and metastasis of ovarian cancer. Cancer Res *72*, 5494-5504.

Ishii, K., Kawagoe, T., Koyama, S., Matsui, K., Kumar, H., Kawai, T., Uematsu, S., Takeuchi, O., Takeshita, F., Coban, C.*, et al.* (2008a). TANK-binding kinase-1 delineates innate and adaptive immune responses to DNA vaccines. Nature *451*, 725-729.

Ishii, K.J., and Akira, S. (2006). Innate immune recognition of, and regulation by, DNA. Trends Immunol *27*, 525-532.

Ishii, K.J., Coban, C., Kato, H., Takahashi, K., Torii, Y., Takeshita, F., Ludwig, H., Sutter, G., Suzuki, K., Hemmi, H.*, et al.* (2006a). A Toll-like receptor-independent antiviral response induced by double-stranded B-form DNA. Nature immunology *7*, 40-48.

Ishii, K.J., Coban, C., Kato, H., Takahashi, K., Torii, Y., Takeshita, F., Ludwig, H., Sutter, G., Suzuki, K., Hemmi, H.*, et al.* (2006b). A Toll-like receptor-independent antiviral response induced by double-stranded B-form DNA. Nat Immunol *7*, 40-48.

Ishii, K.J., Kawagoe, T., Koyama, S., Matsui, K., Kumar, H., Kawai, T., Uematsu, S., Takeuchi, O., Takeshita, F., Coban, C.*, et al.* (2008b). TANK-binding kinase-1 delineates innate and adaptive immune responses to DNA vaccines. Nature *451*, 725-729.

Ishikawa, H., and Barber, G.N. (2008). STING is an endoplasmic reticulum adaptor that facilitates innate immune signalling. Nature *455*, 674-678.

Ishikawa, H., and Barber, G.N. (2011). The STING pathway and regulation of innate immune signaling in response to DNA pathogens. Cell Mol Life Sci *68*, 1157-1165.

Ishikawa, H., Ma, Z., and Barber, G.N. (2009). STING regulates intracellular DNA-mediated, type I interferon-dependent innate immunity. Nature *461*, 788-792.

Iwasaki, A. (2006). The use of bone marrow-chimeric mice in elucidating immune mechanisms. Methods Mol Med *127*, 281-292.

Jacobsen, K.A., Prasad, V.S., Sidman, C.L., and Osmond, D.G. (1994). Apoptosis and macrophage-mediated deletion of precursor B cells in the bone marrow of E mu-myc transgenic mice. Blood *84*, 2784-2794.

Janssens, S., and Tschopp, J. (2006). Signals from within: the DNA-damage-induced NF-kappaB response. Cell Death Differ *13*, 773-784.

Jin, L., Lenz, L.L., and Cambier, J.C. (2010). Cellular reactive oxygen species inhibit MPYS induction of IFNbeta. PLoS One *5*, e15142.

Jin, L., Waterman, P.M., Jonscher, K.R., Short, C.M., Reisdorph, N.A., and Cambier, J.C. (2008). MPYS, a novel membrane tetraspanner, is associated with major histocompatibility complex class II and mediates transduction of apoptotic signals. Mol Cell Biol *28*, 5014-5026.

Jin, T., Perry, A., Jiang, J., Smith, P., Curry, J.A., Unterholzner, L., Jiang, Z., Horvath, G., Rathinam, V.A., Johnstone, R.W.*, et al.* (2012). Structures of the HIN domain:DNA complexes reveal ligand binding and activation mechanisms of the AIM2 inflammasome and IFI16 receptor. Immunity *36*, 561-571.

Jinek, M., Chylinski, K., Fonfara, I., Hauer, M., Doudna, J.A., and Charpentier, E. (2012). A programmable dual-RNA-guided DNA endonuclease in adaptive bacterial immunity. Science *337*, 816-821.

Jiricny, J. (2006). The multifaceted mismatch-repair system. Nat Rev Mol Cell Biol *7*, 335-346.

Johnstone, R.W., and Trapani, J.A. (1999). Transcription and growth regulatory functions of the HIN-200 family of proteins. Mol Cell Biol *19*, 5833-5838.

Jones, J.W., Kayagaki, N., Broz, P., Henry, T., Newton, K., O'Rourke, K., Chan, S., Dong, J., Qu, Y., Roose-Girma, M.*, et al.* (2010). Absent in melanoma 2 is required for innate immune recognition of Francisella tularensis. Proc Natl Acad Sci U S A *107*, 9771-9776.

Jung H, H.B., Procyk E, Raulet DH. (2012). E2F Transcription Factors Regulate Expression of RAE1 Ligands for NKG2D, an Immune Cell Receptor Implicated in Tumor Surveillance. submitted.

Jung, H., Hsiung, B., Pestal, K., Procyk, E., and Raulet, D.H. (2012). RAE-1 ligands for the NKG2D receptor are regulated by E2F transcription factors, which control cell cycle entry. J Exp Med.

Kaiser, W.J., Upton, J.W., and Mocarski, E.S. (2008). Receptor-interacting protein homotypic interaction motif-dependent control of NF-kappa B activation via the DNA-dependent activator of IFN regulatory factors. J Immunol *181*, 6427-6434.

Kaltschmidt, B., Kaltschmidt, C., Hofmann, T.G., Hehner, S.P., Droge, W., and Schmitz, M.L. (2000). The pro- or anti-apoptotic function of NF-kappaB is determined by the nature of the apoptotic stimulus. Eur J Biochem *267*, 3828-3835.

Karin, M., and Greten, F.R. (2005). NF-kappaB: linking inflammation and immunity to cancer development and progression. Nat Rev Immunol *5*, 749-759.

Karpova, A.Y., Trost, M., Murray, J.M., Cantley, L.C., and Howley, P.M. (2002). Interferon regulatory factor-3 is an in vivo target of DNA-PK. Proc Natl Acad Sci U S A *99*, 2818-2823.

Khalimonchuk, O., and Winge, D. (2008). Function and redox state of mitochondrial localized cysteine-rich proteins important in the assembly of cytochrome c oxidase. Biochim Biophys Acta *1783*, 618-628.

Khong, H.T., and Restifo, N.P. (2002). Natural selection of tumor variants in the generation of "tumor escape" phenotypes. Nat Immunol *3*, 999-1005.

Kim, R., Emi, M., and Tanabe, K. (2007a). Cancer immunoediting from immune surveillance to immune escape. Immunology *121*, 1-14.

Kim, S.T., Lim, D.S., Canman, C.E., and Kastan, M.B. (1999a). Substrate specificities and identification of putative substrates of ATM kinase family members. J Biol Chem *274*, 37538-37543.

Kim, T., Kim, T.Y., Song, Y.H., Min, I.M., Yim, J., and Kim, T.K. (1999b). Activation of interferon regulatory factor 3 in response to DNA-damaging agents. J Biol Chem *274*, 30686-30689.

Kim, T., Lee, W.G., and Yim, J. (2000). Chemotherapeutic DNA-damaging drugs activate interferon regulatory factor-7 by the mitogen-activated protein kinase kinase-4-cJun NH2-terminal kinase pathway. Cancer Res *60*, 1153-1156.

Kim, T.K., Lee, J.S., Oh, S.Y., Jin, X., Choi, Y.J., Lee, T.H., Lee, E., Choi, Y.K., You, S., Chung, Y.G.*, et al.* (2007b). Direct transcriptional activation of promyelocytic leukemia protein by IFN regulatory factor 3 induces the p53-dependent growth inhibition of cancer cells. Cancer Res *67*, 11133-11140.

Kim, T.S., Kawaguchi, M., Suzuki, M., Jung, C.G., Asai, K., Shibamoto, Y., Lavin, M.F., Khanna, K.K., and Miura, Y. (2010). The ZFHX3 (ATBF1) transcription factor induces PDGFRB, which activates ATM in the cytoplasm to protect cerebellar neurons from oxidative stress. Dis Model Mech *3*, 752-762.

Kim, T.Y., Lee, K.H., Chang, S., Chung, C., Lee, H.W., Yim, J., and Kim, T.K. (2003). Oncogenic potential of a dominant negative mutant of interferon regulatory factor 3. J Biol Chem *278*, 15272-15278.

Kirshner, J.R., Karpova, A.Y., Kops, M., and Howley, P.M. (2005). Identification of TRAIL as an interferon regulatory factor 3 transcriptional target. J Virol *79*, 9320-9324.

Klapproth, K., Sander, S., Marinkovic, D., Baumann, B., and Wirth, T. (2009). The IKK2/NF-{kappa}B pathway suppresses MYC-induced lymphomagenesis. Blood *114*, 2448-2458.

Kondo, T., Kobayashi, J., Saitoh, T., Maruyama, K., Ishii, K.J., Barber, G.N., Komatsu, K., Akira, S., and Kawai, T. (2013). DNA damage sensor MRE11 recognizes cytosolic double-stranded DNA and induces type I interferon by regulating STING trafficking. Proc Natl Acad Sci U S A *110*, 2969-2974.

Korherr, C., Gille, H., Schafer, R., Koenig-Hoffmann, K., Dixelius, J., Egland, K.A., Pastan, I., and Brinkmann, U. (2006). Identification of proangiogenic genes and pathways by high-throughput functional genomics: TBK1 and the IRF3 pathway. Proc Natl Acad Sci U S A *103*, 4240-4245.

Kwak, J.C., Ongusaha, P.P., Ouchi, T., and Lee, S.W. (2003). IFI16 as a negative regulator in the regulation of p53 and p21(Waf1). J Biol Chem *278*, 40899-40904.

Lallemand, C., Blanchard, B., Palmieri, M., Lebon, P., May, E., and Tovey, M.G. (2007). Single-stranded RNA viruses inactivate the transcriptional activity of p53 but induce NOXA-dependent apoptosis via post-translational modifications of IRF-1, IRF-3 and CREB. Oncogene *26*, 328-338.

Landolfo, S., Gariglio, M., Gribaudo, G., and Lembo, D. (1998). The Ifi 200 genes: an emerging family of IFN-inducible genes. Biochimie *80*, 721-728.

Langdon, W., Harris, A., Cory, S., and Adams, J. (1986). The c-myc oncogene perturbs B lymphocyte development in E-mu-myc transgenic mice. Cell *47*, 11-18.

Lange, S.S., and Vasquez, K.M. (2009). HMGB1: the jack-of-all-trades protein is a master DNA repair mechanic. Mol Carcinog *48*, 571-580.

Li, H., Lakshmikanth, T., Garofalo, C., Enge, M., Spinnler, C., Anichini, A., Szekely, L., Karre, K., Carbone, E., and Selivanova, G. (2011). Pharmacological activation of p53 triggers anticancer innate immune response through induction of ULBP2. Cell Cycle *10*, 3346-3358.

Li, J., Han, Y.R., Plummer, M.R., and Herrup, K. (2009a). Cytoplasmic ATM in neurons modulates synaptic function. Curr Biol *19*, 2091-2096.

Li, Y., Li, W., Yang, Y., Lu, Y., He, C., Hu, G., Liu, H., Chen, J., He, J., and Yu, H. (2009b). MicroRNA-21 targets LRRFIP1 and contributes to VM-26 resistance in glioblastoma multiforme. Brain Res *1286*, 13-18.

Liao, J.C., Lam, R., Brazda, V., Duan, S., Ravichandran, M., Ma, J., Xiao, T., Tempel, W., Zuo, X., Wang, Y.X*., et al.* (2011). Interferon-inducible protein 16: insight into the interaction with tumor suppressor p53. Structure *19*, 418-429.

Liao, W.C., Haimovitz-Friedman, A., Persaud, R.S., McLoughlin, M., Ehleiter, D., Zhang, N., Gatei, M., Lavin, M., Kolesnick, R., and Fuks, Z. (1999). Ataxia telangiectasia-mutated gene product inhibits DNA damage-induced apoptosis via ceramide synthase. J Biol Chem *274*, 17908-17917.

Lim, D.S., Kirsch, D.G., Canman, C.E., Ahn, J.H., Ziv, Y., Newman, L.S., Darnell, R.B., Shiloh, Y., and Kastan, M.B. (1998). ATM binds to beta-adaptin in cytoplasmic vesicles. Proc Natl Acad Sci U S A *95*, 10146-10151.

Liu, X.V., Ho, S.S., Tan, J.J., Kamran, N., and Gasser, S. (2012). Ras activation induces expression of raet1 family NK receptor ligands. J Immunol *189*, 1826-1834.

Lord, C.J., and Ashworth, A. (2012). The DNA damage response and cancer therapy. Nature *481*, 287-294.

Ludlow, L.E., Johnstone, R.W., and Clarke, C.J. (2005). The HIN-200 family: more than interferon-inducible genes? Exp Cell Res *308*, 1-17.

Luo, J.L., Maeda, S., Hsu, L.C., Yagita, H., and Karin, M. (2004). Inhibition of NF-kappaB in cancer cells converts inflammation- induced tumor growth mediated by TNFalpha to TRAIL-mediated tumor regression. Cancer Cell *6*, 297-305.

Maclean, K.H., Kastan, M.B., and Cleveland, J.L. (2007). Atm deficiency affects both apoptosis and proliferation to augment Myc-induced lymphomagenesis. Mol Cancer Res *5*, 705-711.

Mallette, F.A., and Ferbeyre, G. (2007). The DNA damage signaling pathway connects oncogenic stress to cellular senescence. Cell Cycle *6*, 1831-1836.

Manzanillo, P.S., Shiloh, M.U., Portnoy, D.A., and Cox, J.S. (2012). Mycobacterium tuberculosis activates the DNA-dependent cytosolic surveillance pathway within macrophages. Cell Host Microbe *11*, 469-480.

Marichal, T., Ohata, K., Bedoret, D., Mesnil, C., Sabatel, C., Kobiyama, K., Lekeux, P., Coban, C., Akira, S., Ishii, K.J.*, et al.* (2011). DNA released from dying host cells mediates aluminum adjuvant activity. Nat Med *17*, 996-1002.

Matsui, K., Kumagai, Y., Kato, H., Sato, S., Kawagoe, T., Uematsu, S., Takeuchi, O., and Akira, S. (2006). Cutting edge: Role of TANK-binding kinase 1 and inducible IkappaB kinase in IFN responses against viruses in innate immune cells. J Immunol *177*, 5785-5789.

Matsuoka, S., Ballif, B.A., Smogorzewska, A., McDonald, E.R., Hurov, K.E., Luo, J., Bakalarski, C.E., Zhao, Z., Solimini, N., Lerenthal, Y.*, et al.* (2007). ATM and ATR substrate analysis reveals extensive protein networks responsive to DNA damage. Science *316*, 1160-1166.

Mazibrada, J., De Andrea, M., Ritta, M., Borgogna, C., Dell'eva, R., Pfeffer, U., Chiusa, L., Gariglio, M., and Landolfo, S. (2010). In vivo growth inhibition of head and neck squamous cell carcinoma by the Interferon-inducible gene IFI16. Cancer Lett *287*, 33-43.

McCool, K.W., and Miyamoto, S. (2012). DNA damage-dependent NF-kappaB activation: NEMO turns nuclear signaling inside out. Immunol Rev *246*, 311-326.

Merika, M., Williams, A.J., Chen, G., Collins, T., and Thanos, D. (1998). Recruitment of CBP/p300 by the IFN beta enhanceosome is required for synergistic activation of transcription. Mol Cell *1*, 277-287.

Meyer, N., and Penn, L.Z. (2008). Reflecting on 25 years with MYC. Nat Rev Cancer *8*, 976-990.

Michel, S., Kloor, M., Singh, S., Gdynia, G., Roth, W., von Knebel Doeberitz, M., Schirmacher, P., and Blaker, H. (2010). Coding microsatellite instability analysis in microsatellite unstable small intestinal adenocarcinomas identifies MARCKS as a common target of inactivation. Mol Carcinog *49*, 175-182.

Mills, K.D., Ferguson, D.O., and Alt, F.W. (2003). The role of DNA breaks in genomic instability and tumorigenesis. Immunol Rev *194*, 77-95.

Mistry, A.R., and O'Callaghan, C.A. (2007). Regulation of ligands for the activating receptor NKG2D. Immunology *121*, 439-447.

Mohle, R., Failenschmid, C., Bautz, F., and Kanz, L. (1999). Overexpression of the chemokine receptor CXCR4 in B cell chronic lymphocytic leukemia is associated with increased functional response to stromal cell-derived factor-1 (SDF-1). Leukemia *13*, 1954-1959.

Moore, R.J., Owens, D.M., Stamp, G., Arnott, C., Burke, F., East, N., Holdsworth, H., Turner, L., Rollins, B., Pasparakis, M.*, et al.* (1999). Mice deficient in tumor necrosis factor-alpha are resistant to skin carcinogenesis. Nat Med *5*, 828-831.

Mu, J.J., Wang, Y., Luo, H., Leng, M., Zhang, J., Yang, T., Besusso, D., Jung, S.Y., and Qin, J. (2007). A proteomic analysis of ataxia telangiectasia-mutated (ATM)/ATM-Rad3-related (ATR) substrates identifies the ubiquitin-proteasome system as a regulator for DNA damage checkpoints. J Biol Chem *282*, 17330-17334.

Nakajima, A., Nishimura, K., Nakaima, Y., Oh, T., Noguchi, S., Taniguchi, T., and Tamura, T. (2009). Cell type-dependent proapoptotic role of Bcl2L12 revealed by a mutation concomitant with the disruption of the juxtaposed Irf3 gene. Proc Natl Acad Sci U S A *106*, 12448-12452.

Naugler, W.E., Sakurai, T., Kim, S., Maeda, S., Kim, K., Elsharkawy, A.M., and Karin, M. (2007). Gender disparity in liver cancer due to sex differences in MyD88-dependent IL-6 production. Science *317*, 121-124.

Norman, J.M., Mashiba, M., McNamara, L.A., Onafuwa-Nuga, A., Chiari-Fort, E., Shen, W., and Collins, K.L. (2011). The antiviral factor APOBEC3G enhances the recognition of HIV-infected primary T cells by natural killer cells. Nat Immunol *12*, 975-983.

Okita, R., Mougiakakos, D., Ando, T., Mao, Y., Sarhan, D., Wennerberg, E., Seliger, B., Lundqvist, A., Mimura, K., and Kiessling, R. (2012). HER2/HER3 signaling regulates NK cell-mediated cytotoxicity via MHC class I chain-related molecule A and B expression in human breast cancer cell lines. J Immunol *188*, 2136-2145.

Ou, Y.H., Torres, M., Ram, R., Formstecher, E., Roland, C., Cheng, T., Brekken, R., Wurz, R., Tasker, A., Polverino, T.*, et al.* (2011). TBK1 directly engages Akt/PKB survival signaling to support oncogenic transformation. Mol Cell *41*, 458-470.

Pahl, H.L. (1999). Activators and target genes of Rel/NF-kappaB transcription factors. Oncogene *18*, 6853-6866.

Palm, N.W., and Medzhitov, R. (2009). Pattern recognition receptors and control of adaptive immunity. Immunol Rev *227*, 221-233.

Parekh, B.S., and Maniatis, T. (1999). Virus infection leads to localized hyperacetylation of histones H3 and H4 at the IFN-beta promoter. Mol Cell *3*, 125-129.

Parvatiyar, K., Barber, G.N., and Harhaj, E.W. (2010). TAX1BP1 and A20 inhibit antiviral signaling by targeting TBK1/IKKi kinases. Journal of Biological Chemistry, 1-21.

Patsos, G., Germann, A., Gebert, J., and Dihlmann, S. (2010). Restoration of absent in melanoma 2 (AIM2) induces G2/M cell cycle arrest and promotes invasion of colorectal cancer cells. Int J Cancer *126*, 1838-1849.

Peant, B., Forest, V., Trudeau, V., Latour, M., Mes-Masson, A.M., and Saad, F. (2011). IkappaB-Kinase-epsilon (IKKepsilon/IKKi/IkappaBKepsilon) expression and localization in prostate cancer tissues. Prostate *71*, 1131-1138.

Pende, D., Castriconi, R., Romagnani, P., Spaggiari, G.M., Marcenaro, S., Dondero, A., Lazzeri, E., Lasagni, L., Martini, S., Rivera, P.*, et al.* (2006). Expression of the DNAM-1 ligands, Nectin-2 (CD112) and poliovirus receptor (CD155), on dendritic cells: relevance for natural killer-dendritic cell interaction. Blood *107*, 2030-2036.

Peng, C.H., Liao, C.T., Peng, S.C., Chen, Y.J., Cheng, A.J., Juang, J.L., Tsai, C.Y., Chen, T.C., Chuang, Y.J., Tang, C.Y.*, et al.* (2011). A novel molecular signature identified by systems genetics approach predicts prognosis in oral squamous cell carcinoma. PLoS One *6*, e23452.

Perry, A.K., Chow, E.K., Goodnough, J.B., Yeh, W.C., and Cheng, G. (2004). Differential requirement for TANK-binding kinase-1 in type I interferon responses to toll-like receptor activation and viral infection. The Journal of experimental medicine *199*, 1651-1658.

Pham, H.T., Park, M.Y., Kim, K.K., Kim, Y.G., and Ahn, J.H. (2006). Intracellular localization of human ZBP1: Differential regulation by the Z-DNA binding domain, Zalpha, in splice variants. Biochem Biophys Res Commun *348*, 145-152.

Polo, S.E., and Jackson, S.P. (2011). Dynamics of DNA damage response proteins at DNA breaks: a focus on protein modifications. Genes Dev *25*, 409-433.

Pomerantz, J.L., and Baltimore, D. (1999). NF-kappaB activation by a signaling complex containing TRAF2, TANK and TBK1, a novel IKK-related kinase. Embo J *18*, 6694-6704.

Popa, N., Cedile, O., Pollet-Villard, X., Bagnis, C., Durbec, P., and Boucraut, J. (2011). RAE-1 is expressed in the adult subventricular zone and controls cell proliferation of neurospheres. Glia *59*, 35-44.

Pusapati, R., Rounbehler, R., Hong, S., Powers, J., Yan, M., Kiguchi, K., McArthur, M., Wong, P., and Johnson, D. (2006a). ATM promotes apoptosis and suppresses tumorigenesis in response to Myc. Proc Natl Acad Sci U S A *103*, 1446-1451.

Pusapati, R.V., Rounbehler, R.J., Hong, S., Powers, J.T., Yan, M., Kiguchi, K., McArthur, M.J., Wong, P.K., and Johnson, D.G. (2006b). ATM promotes apoptosis and suppresses tumorigenesis in response to Myc. Proc Natl Acad Sci U S A *103*, 1446-1451.

Qin, B., and Cheng, K. (2010). Silencing of the IKKepsilon gene by siRNA inhibits invasiveness and growth of breast cancer cells. Breast Cancer Res *12*, R74.

Rabinovich, B., Li, J., Shannon, J., Hurren, R., Chalupny, J., Cosman, D., and Miller, R. (2003). Activated, but not resting, T cells can be recognized and killed by syngeneic NK cells. J Immunol *170*, 3572-3576.

Rathinam, V.A., Jiang, Z., Waggoner, S.N., Sharma, S., Cole, L.E., Waggoner, L., Vanaja, S.K., Monks, B.G., Ganesan, S., Latz, E.*, et al.* (2010). The AIM2 inflammasome is essential for host defense against cytosolic bacteria and DNA viruses. Nat Immunol *11*, 395-402.

Raulet, D. (2003). Roles of the NKG2D immunoreceptor and its ligands. Nat Rev Immunol *3*, 781-790.

Raulet, D.H., Gasser, S., Gowen, B.G., Deng, W., and Jung, H. (2013). Regulation of ligands for the NKG2D activating receptor. Annu Rev Immunol *31*, 413-441.

Raulet, D.H., and Guerra, N. (2009). Oncogenic stress sensed by the immune system: role of natural killer cell receptors. Nature reviews Immunology *9*, 568-580.

Ravi, R., Mookerjee, B., van Hensbergen, Y., Bedi, G.C., Giordano, A., El-Deiry, W.S., Fuchs, E.J., and Bedi, A. (1998). p53-mediated repression of nuclear factor-kappaB RelA via the transcriptional integrator p300. Cancer Res *58*, 4531-4536.

Ray, M.E., Su, Y.A., Meltzer, P.S., and Trent, J.M. (1996). Isolation and characterization of genes associated with chromosome-6 mediated tumor suppression in human malignant melanoma. Oncogene *12*, 2527-2533.

Ray, S., Atkuri, K., Deb-Basu, D., Adler, A., Chang, H., Herzenberg, L., and Felsher, D. (2006). MYC can induce DNA breaks in vivo and in vitro independent of reactive oxygen species. Cancer Res *66*, 6598-6605.

Rebsamen, M., Heinz, L.X., Meylan, E., Michallet, M.C., Schroder, K., Hofmann, K., Vazquez, J., Benedict, C.A., and Tschopp, J. (2009). DAI/ZBP1 recruits RIP1 and RIP3 through RIP homotypic interaction motifs to activate NF-kappaB. EMBO Rep *10*, 916-922.

Reimann, M., Loddenkemper, C., Rudolph, C., Schildhauer, I., Teichmann, B., Stein, H., Schlegelberger, B., Dorken, B., and Schmitt, C.A. (2007). The Myc-evoked DNA damage response accounts for treatment resistance in primary lymphomas in vivo. Blood *110*, 2996-3004.

Renwick, A., Thompson, D., Seal, S., Kelly, P., Chagtai, T., Ahmed, M., North, B., Jayatilake, H., Barfoot, R., Spanova, K.*, et al.* (2006). ATM mutations that cause ataxia-telangiectasia are breast cancer susceptibility alleles. Nat Genet *38*, 873-875.

Reymond, N., Imbert, A.M., Devilard, E., Fabre, S., Chabannon, C., Xerri, L., Farnarier, C., Cantoni, C., Bottino, C., Moretta, A.*, et al.* (2004). DNAM-1 and PVR regulate monocyte migration through endothelial junctions. J Exp Med *199*, 1331-1341.

Rhodes, N., D'Souza, T., Foster, C.D., Ziv, Y., Kirsch, D.G., Shiloh, Y., Kastan, M.B., Reinhart, P.H., and Gilmer, T.M. (1998). Defective potassium currents in ataxia telangiectasia fibroblasts. Genes Dev *12*, 3686-3692.

Riedl, S.J., and Shi, Y. (2004). Molecular mechanisms of caspase regulation during apoptosis. Nat Rev Mol Cell Biol *5*, 897-907.

Rikiyama, T., Curtis, J., Oikawa, M., Zimonjic, D.B., Popescu, N., Murphy, B.A., Wilson, M.A., and Johnson, A.C. (2003). GCF2: expression and molecular analysis of repression. Biochim Biophys Acta *1629*, 15-25.

Roberts, Z.J., Goutagny, N., Perera, P.Y., Kato, H., Kumar, H., Kawai, T., Akira, S., Savan, R., van Echo, D., Fitzgerald, K.A.*, et al.* (2007). The chemotherapeutic agent DMXAA potently and specifically activates the TBK1-IRF-3 signaling axis. J Exp Med *204*, 1559-1569.

Rocha, S., Campbell, K.J., and Perkins, N.D. (2003a). p53- and Mdm2-independent repression of NF-kappa B transactivation by the ARF tumor suppressor. Mol Cell *12*, 15-25.

Rocha, S., Martin, A.M., Meek, D.W., and Perkins, N.D. (2003b). p53 represses cyclin D1 transcription through down regulation of Bcl-3 and inducing increased association of the p52 NF-kappaB subunit with histone deacetylase 1. Mol Cell Biol *23*, 4713-4727.

Routes, J., Ryan, S., Morris, K., Takaki, R., Cerwenka, A., and Lanier, L. (2005). Adenovirus serotype 5 E1A sensitizes tumor cells to NKG2D-dependent NK cell lysis and tumor rejection. J Exp Med *202*, 1477-1482.

Ryan, K.M., Ernst, M.K., Rice, N.R., and Vousden, K.H. (2000). Role of NF-kappaB in p53-mediated programmed cell death. Nature *404*, 892-897.

Salomon, B., and Bluestone, J.A. (1998). LFA-1 interaction with ICAM-1 and ICAM-2 regulates Th2 cytokine production. J Immunol *161*, 5138-5142.

Sancar, A., Lindsey-Boltz, L.A., Unsal-Kaccmaz, K., and Linn, S. (2004a). Molecular mechanisms of mammalian DNA repair and the DNA damage checkpoints. Annu Rev Biochem *73*, 39-85.

Sancar, A., Lindsey-Boltz, L.A., Unsal-Kacmaz, K., and Linn, S. (2004b). Molecular mechanisms of mammalian DNA repair and the DNA damage checkpoints. Annu Rev Biochem *73*, 39-85.

Sato, M., Suemori, H., Hata, N., Asagiri, M., Ogasawara, K., Nakao, K., Nakaya, T., Katsuki, M., Noguchi, S., Tanaka, N.*, et al.* (2000). Distinct and essential roles of transcription factors IRF-3 and IRF-7 in response to viruses for IFN-alpha/beta gene induction. Immunity *13*, 539-548.

Savitsky, K., Bar-Shira, A., Gilad, S., Rotman, G., Ziv, Y., Vanagaite, L., Tagle, D.A., Smith, S., Uziel, T., Sfez, S.*, et al.* (1995). A single ataxia telangiectasia gene with a product similar to PI-3 kinase. Science *268*, 1749-1753.

Schlueter, C., Weber, H., Meyer, B., Rogalla, P., Roser, K., Hauke, S., and Bullerdiek, J. (2005). Angiogenetic signaling through hypoxia: HMGB1: an angiogenetic switch molecule. Am J Pathol *166*, 1259-1263.

Schmidt, M., Nagel, S., Proba, J., Thiede, C., Ritter, M., Waring, J.F., Rosenbauer, F., Huhn, D., Wittig, B., Horak, I.*, et al.* (1998). Lack of interferon consensus sequence binding protein (ICSBP) transcripts in human myeloid leukemias. Blood *91*, 22-29.

Scholzen, T., and Gerdes, J. (2000). The Ki-67 protein: from the known and the unknown. J Cell Physiol *182*, 311-322.

Servant, M.J., Grandvaux, N., and Hiscott, J. (2002). Multiple signaling pathways leading to the activation of interferon regulatory factor 3. Biochem Pharmacol *64*, 985-992.

Sharma, S., DeOliveira, R.B., Kalantari, P., Parroche, P., Goutagny, N., Jiang, Z., Chan, J., Bartholomeu, D.C., Lauw, F., Hall, J.P.*, et al.* (2011). Innate immune recognition of an AT-rich stem-loop DNA motif in the Plasmodium falciparum genome. Immunity *35*, 194-207.

Sharma, S., tenOever, B.R., Grandvaux, N., Zhou, G.P., Lin, R., and Hiscott, J. (2003). Triggering the interferon antiviral response through an IKK-related pathway. Science *300*, 1148-1151.

Shen, D.W., Pouliot, L.M., Gillet, J.P., Ma, W., Johnson, A.C., Hall, M.D., and Gottesman, M.M. (2012). The transcription factor GCF2 is an upstream repressor of the small GTPAse RhoA, regulating membrane protein trafficking, sensitivity to doxorubicin, and resistance to cisplatin. Mol Pharm *9*, 1822-1833.

Shi, Y. (2002). Mechanisms of caspase activation and inhibition during apoptosis. Mol Cell *9*, 459-470.

Shibuya, A., Campbell, D., Hannum, C., Yssel, H., Franz-Bacon, K., McClanahan, T., Kitamura, T., Nicholl, J., Sutherland, G.R., Lanier, L.L.*, et al.* (1996). DNAM-1, a novel adhesion molecule involved in the cytolytic function of T lymphocytes. Immunity *4*, 573-581.

Shiloh, Y., and Ziv, Y. (2013). The ATM protein kinase: regulating the cellular response to genotoxic stress, and more. Nat Rev Mol Cell Biol *14*, 197-210.

Shimada, K., Crother, T.R., Karlin, J., Dagvadorj, J., Chiba, N., Chen, S., Ramanujan, V.K., Wolf, A.J., Vergnes, L., Ojcius, D.M.*, et al.* (2012). Oxidized mitochondrial DNA activates the NLRP3 inflammasome during apoptosis. Immunity *36*, 401-414.

Shimada, T., Kawai, T., Takeda, K., Matsumoto, M., Inoue, J., Tatsumi, Y., Kanamaru, A., and Akira, S. (1999). IKK-i, a novel lipopolysaccharide-inducible kinase that is related to IkappaB kinases. Int Immunol *11*, 1357-1362.

Shreeram, S., Hee, W.K., Demidov, O.N., Kek, C., Yamaguchi, H., Fornace, A.J., Jr., Anderson, C.W., Appella, E., and Bulavin, D.V. (2006). Regulation of ATM/p53-dependent suppression of myc-induced lymphomas by Wip1 phosphatase. J Exp Med *203*, 2793-2799.

Sidman, C.L., Denial, T.M., Marshall, J.D., and Roths, J.B. (1993a). Multiple mechanisms of tumorigenesis in E mu-myc transgenic mice. Cancer research *53*, 1665-1669.

Sidman, C.L., Shaffer, D.J., Jacobsen, K., Vargas, S.R., and Osmond, D.G. (1993b). Cell populations during tumorigenesis in Eu-myc transgenic mice. Leukemia *7*, 887-895.

Sieber, O.M., Heinimann, K., and Tomlinson, I.P. (2003). Genomic instability--the engine of tumorigenesis? Nat Rev Cancer *3*, 701-708.

Sims, G.P., Rowe, D.C., Rietdijk, S.T., Herbst, R., and Coyle, A.J. (2010). HMGB1 and RAGE in inflammation and cancer. Annu Rev Immunol *28*, 367-388.

Sjoblom, T., Jones, S., Wood, L.D., Parsons, D.W., Lin, J., Barber, T.D., Mandelker, D., Leary, R.J., Ptak, J., Silliman, N.*, et al.* (2006). The consensus coding sequences of human breast and colorectal cancers. Science *314*, 268-274.

Sloan, K.E., Stewart, J.K., Treloar, A.F., Matthews, R.T., and Jay, D.G. (2005). CD155/PVR enhances glioma cell dispersal by regulating adhesion signaling and focal adhesion dynamics. Cancer Res *65*, 10930-10937.

Soriani, A., Zingoni, A., Cerboni, C., Iannitto, M.L., Ricciardi, M.R., Di Gialleonardo, V., Cippitelli, M., Fionda, C., Petrucci, M.T., Guarini, A.*, et al.* (2009). ATM-ATR-dependent up-regulation of DNAM-1 and NKG2D ligands on multiple myeloma cells by therapeutic agents results in enhanced NK-cell susceptibility and is associated with a senescent phenotype. Blood *113*, 3503-3511.

Sovak, M.A., Bellas, R.E., Kim, D.W., Zanieski, G.J., Rogers, A.E., Traish, A.M., and Sonenshein, G.E. (1997). Aberrant nuclear factor-kappaB/Rel expression and the pathogenesis of breast cancer. J Clin Invest *100*, 2952-2960.

Sparvero, L.J., Asafu-Adjei, D., Kang, R., Tang, D., Amin, N., Im, J., Rutledge, R., Lin, B., Amoscato, A.A., Zeh, H.J.*, et al.* (2009). RAGE (Receptor for Advanced Glycation Endproducts), RAGE ligands, and their role in cancer and inflammation. J Transl Med *7*, 17.

Staunton, D.E., Marlin, S.D., Stratowa, C., Dustin, M.L., and Springer, T.A. (1988). Primary structure of ICAM-1 demonstrates interaction between members of the immunoglobulin and integrin supergene families. Cell *52*, 925-933.

Stegh, A.H., Kim, H., Bachoo, R.M., Forloney, K.L., Zhang, J., Schulze, H., Park, K., Hannon, G.J., Yuan, J., Louis, D.N.*, et al.* (2007). Bcl2L12 inhibits post-mitochondrial apoptosis signaling in glioblastoma. Genes Dev *21*, 98-111.

Stein, S.C., and Falck-Pedersen, E. (2012). Sensing adenovirus infection: activation of interferon regulatory factor 3 in RAW 264.7 cells. J Virol *86*, 4527-4537.

Stern-Ginossar, N., Gur, C., Biton, M., Horwitz, E., Elboim, M., Stanietsky, N., Mandelboim, M., and Mandelboim, O. (2008). Human microRNAs regulate stress-induced immune responses mediated by the receptor NKG2D. Nat Immunol.

Stetson, D.B., Ko, J.S., Heidmann, T., and Medzhitov, R. (2008). Trex1 prevents cell-intrinsic initiation of autoimmunity. Cell *134*, 587-598.

Stetson, D.B., and Medzhitov, R. (2006). Recognition of cytosolic DNA activates an IRF3-dependent innate immune response. Immunity *24*, 93-103.

Stiff, T., O'Driscoll, M., Rief, N., Iwabuchi, K., Lobrich, M., and Jeggo, P.A. (2004). ATM and DNA-PK function redundantly to phosphorylate H2AX after exposure to ionizing radiation. Cancer Res *64*, 2390-2396.

Stockinger, S., Reutterer, B., Schaljo, B., Schellack, C., Brunner, S., Materna, T., Yamamoto, M., Akira, S., Taniguchi, T., Murray, P.J.*, et al.* (2004). IFN regulatory factor 3-dependent induction of type I IFNs by intracellular bacteria is mediated by a TLR- and Nod2-independent mechanism. J Immunol *173*, 7416-7425.

Stratton, M.R., Campbell, P.J., and Futreal, P.A. (2009). The cancer genome. Nature *458*, 719-724.

Sulli, G., Di Micco, R., and d'Adda di Fagagna, F. (2012). Crosstalk between chromatin state and DNA damage response in cellular senescence and cancer. Nat Rev Cancer *12*, 709-720.

Sun, L., Wu, J., Du, F., Chen, X., and Chen, Z.J. (2013). Cyclic GMP-AMP synthase is a cytosolic DNA sensor that activates the type I interferon pathway. Science *339*, 786-791.

Sun, Y., Jiang, X., Chen, S., Fernandes, N., and Price, B.D. (2005). A role for the Tip60 histone acetyltransferase in the acetylation and activation of ATM. Proc Natl Acad Sci U S A *102*, 13182-13187.

Suwaki, N., Klare, K., and Tarsounas, M. (2011). RAD51 paralogs: roles in DNA damage signalling, recombinational repair and tumorigenesis. Seminars in cell & developmental biology *22*, 898-905.

Suzuki, T., Fujikura, K., Higashiyama, T., and Takata, K. (1997). DNA staining for fluorescence and laser confocal microscopy. J Histochem Cytochem *45*, 49-53.

Swann, J.B., Hayakawa, Y., Zerafa, N., Sheehan, K.C., Scott, B., Schreiber, R.D., Hertzog, P., and Smyth, M.J. (2007). Type I IFN contributes to NK cell homeostasis, activation, and antitumor function. J Immunol *178*, 7540-7549.

Swift, M., Reitnauer, P.J., Morrell, D., and Chase, C.L. (1987). Breast and other cancers in families with ataxia-telangiectasia. N Engl J Med *316*, 1289-1294.

Taguchi, A., Blood, D.C., del Toro, G., Canet, A., Lee, D.C., Qu, W., Tanji, N., Lu, Y., Lalla, E., Fu, C.*, et al.* (2000). Blockade of RAGE-amphoterin signalling suppresses tumour growth and metastases. Nature *405*, 354-360.

Takaoka, A., Hayakawa, S., Yanai, H., Stoiber, D., Negishi, H., Kikuchi, H., Sasaki, S., Imai, K., Shibue, T., Honda, K.*, et al.* (2003). Integration of interferon-alpha/beta signalling to p53 responses in tumour suppression and antiviral defence. Nature *424*, 516-523.

Takaoka, A., and Taniguchi, T. (2008). Cytosolic DNA recognition for triggering innate immune responses. Adv Drug Deliv Rev *60*, 847-857.

Takaoka, A., Wang, Z., Choi, M., Yanai, H., Negishi, H., Ban, T., Lu, Y., Miyagishi, M., Kodama, T., Honda, K.*, et al.* (2007). DAI (DLM-1/ZBP1) is a cytosolic DNA sensor and an activator of innate immune response. Nature *448*, 501-505.

Takeda, K., and Akira, S. (2005). Toll-like receptors in innate immunity. Int Immunol *17*, 1-14.

Takeshita, F., and Ishii, K.J. (2008). Intracellular DNA sensors in immunity. Current Opinion in Immunology.

Takeuchi, O., and Akira, S. (2010). Pattern recognition receptors and inflammation. Cell *140*, 805-820.

Taniguchi, T., Ogasawara, K., Takaoka, A., and Tanaka, N. (2001). IRF family of transcription factors as regulators of host defense. Annu Rev Immunol *19*, 623-655.

Tavor, S., Petit, I., Porozov, S., Avigdor, A., Dar, A., Leider-Trejo, L., Shemtov, N., Deutsch, V., Naparstek, E., Nagler, A.*, et al.* (2004). CXCR4 regulates migration and development of human acute myelogenous leukemia stem cells in transplanted NOD/SCID mice. Cancer Res *64*, 2817-2824.

Textor, S., Fiegler, N., Arnold, A., Porgador, A., Hofmann, T.G., and Cerwenka, A. (2011). Human NK cells are alerted to induction of p53 in cancer cells by upregulation of the NKG2D ligands ULBP1 and ULBP2. Cancer research *71*, 5998-6009.

Thornberry, N.A., and Lazebnik, Y. (1998). Caspases: enemies within. Science *281*, 1312-1316.

Tokunaga, T., Naruke, Y., Shigematsu, S., Kohno, T., Yasui, K., Ma, Y., Chua, K.J., Katayama, I., Nakamura, T., Hishikawa, Y.*, et al.* (2010). Aberrant expression of interferon regulatory factor 3 in human lung cancer. Biochem Biophys Res Commun *397*, 202-207.

Trapani, J.A., Browne, K.A., Dawson, M.J., Ramsay, R.G., Eddy, R.L., Show, T.B., White, P.C., and Dupont, B. (1992). A novel gene constitutively expressed in human lymphoid cells is inducible with interferon-gamma in myeloid cells. Immunogenetics *36*, 369-376.

Tsukerman, P., Stern-Ginossar, N., Gur, C., Glasner, A., Nachmani, D., Bauman, Y., Yamin, R., Vitenshtein, A., Stanietsky, N., Bar-Mag, T.*, et al.* (2012). MiR-10b downregulates the stress-induced cell surface molecule MICB, a critical ligand for cancer cell recognition by natural killer cells. Cancer Res.

Unni, A.M., Bondar, T., and Medzhitov, R. (2008). Intrinsic sensor of oncogenic transformation induces a signal for innate immunosurveillance. Proc Natl Acad Sci U S A *105*, 1686-1691.

Unterholzner, L. (2013). The interferon response to intracellular DNA: why so many receptors? Immunobiology *218*, 1312-1321.

Unterholzner, L., Keating, S.E., Baran, M., Horan, K.A., Jensen, S.B., Sharma, S., Sirois, C.M., Jin, T., Latz, E., Xiao, T.S.*, et al.* (2010a). IFI16 is an innate immune sensor for intracellular DNA. Nat Immunol.

Unterholzner, L., Keating, S.E., Baran, M., Horan, K.A., Jensen, S.B., Sharma, S., Sirois, C.M., Jin, T., Latz, E., Xiao, T.S.*, et al.* (2010b). IFI16 is an innate immune sensor for intracellular DNA. Nat Immunol *11*, 997-1004.

Upton, J.W., Kaiser, W.J., and Mocarski, E.S. (2012). DAI/ZBP1/DLM-1 complexes with RIP3 to mediate virus-induced programmed necrosis that is targeted by murine cytomegalovirus vIRA. Cell host & microbe *11*, 290-297.

Vafa, O., Wade, M., Kern, S., Beeche, M., Pandita, T., Hampton, G., and Wahl, G. (2002a). c-Myc can induce DNA damage, increase reactive oxygen species, and mitigate p53 function: a mechanism for oncogene-induced genetic instability. Mol Cell *9*, 1031-1044.

Vafa, O., Wade, M., Kern, S., Beeche, M., Pandita, T.K., Hampton, G.M., and Wahl, G.M. (2002b). c-Myc can induce DNA damage, increase reactive oxygen species, and mitigate p53 function: a mechanism for oncogene-induced genetic instability. Mol Cell *9*, 1031-1044.

van Beijnum, J.R., Petersen, K., and Griffioen, A.W. (2009). Tumor endothelium is characterized by a matrix remodeling signature. Front Biosci (Schol Ed) *1*, 216-225.

Venkataraman, G.M., Suciu, D., Groh, V., Boss, J.M., and Spies, T. (2007a). Promoter region architecture and transcriptional regulation of the genes for the MHC class I-related chain A and B ligands of NKG2D. Journal of immunology *178*, 961-969.

Venkataraman, G.M., Suciu, D., Groh, V., Boss, J.M., and Spies, T. (2007b). Promoter region architecture and transcriptional regulation of the genes for the MHC class I-related chain A and B ligands of NKG2D. J Immunol *178*, 961-969.

Vilaysane, A., and Muruve, D.A. (2009). The innate immune response to DNA. Semin Immunol *21*, 208-214.

Wang, S., Kotamraju, S., Konorev, E., Kalivendi, S., Joseph, J., and Kalyanaraman, B. (2002). Activation of nuclear factor-kappaB during doxorubicin-induced apoptosis in endothelial cells and myocytes is pro-apoptotic: the role of hydrogen peroxide. Biochem J *367*, 729-740.

Wang, Z., Choi, M.K., Ban, T., Yanai, H., Negishi, H., Lu, Y., Tamura, T., Takaoka, A., Nishikura, K., and Taniguchi, T. (2008a). Regulation of innate immune responses by DAI (DLM-1/ZBP1) and other DNA-sensing molecules. Proc Natl Acad Sci U S A *105*, 5477-5482.

Wang, Z., Zhou, Z.J., Liu, D.P., and Huang, J.D. (2008b). Double-stranded break can be repaired by single-stranded oligonucleotides via the ATM/ATR pathway in mammalian cells. Oligonucleotides *18*, 21-32.

Ward, I.M., and Chen, J. (2001). Histone H2AX is phosphorylated in an ATR-dependent manner in response to replicational stress. J Biol Chem *276*, 47759-47762.

Ward, J., Davis, Z., DeHart, J., Zimmerman, E., Bosque, A., Brunetta, E., Mavilio, D., Planelles, V., and Barker, E. (2009). HIV-1 Vpr triggers natural killer cell-mediated lysis of infected cells through activation of the ATR-mediated DNA damage response. PLoS Pathog *5*, e1000613.

Watters, D., Kedar, P., Spring, K., Bjorkman, J., Chen, P., Gatei, M., Birrell, G., Garrone, B., Srinivasa, P., Crane, D.I*., et al.* (1999). Localization of a portion of extranuclear ATM to peroxisomes. J Biol Chem *274*, 34277-34282.

Weaver, B.K., Ando, O., Kumar, K.P., and Reich, N.C. (2001). Apoptosis is promoted by the dsRNA-activated factor (DRAF1) during viral infection independent of the action of interferon or p53. Faseb J *15*, 501-515.

Webster, G.A., and Perkins, N.D. (1999). Transcriptional cross talk between NF-kappaB and p53. Mol Cell Biol *19*, 3485-3495.

Weitzman, M.D., Carson, C.T., Schwartz, R.A., and Lilley, C.E. (2004). Interactions of viruses with the cellular DNA repair machinery. DNA Repair (Amst) *3*, 1165-1173.

Weitzman, M.D., Lilley, C.E., and Chaurushiya, M.S. (2010). Genomes in conflict: maintaining genome integrity during virus infection. Annu Rev Microbiol *64*, 61-81.

Woerner, S.M., Benner, A., Sutter, C., Schiller, M., Yuan, Y.P., Keller, G., Bork, P., Doeberitz, M., and Gebert, J.F. (2003). Pathogenesis of DNA repair-deficient cancers: a statistical meta-analysis of putative Real Common Target genes. Oncogene *22*, 2226-2235.

Woerner, S.M., Kloor, M., Mueller, A., Rueschoff, J., Friedrichs, N., Buettner, R., Buzello, M., Kienle, P., Knaebel, H.P., Kunstmann, E.*, et al.* (2005). Microsatellite instability of selective target genes in HNPCC-associated colon adenomas. Oncogene *24*, 2525-2535.

Woerner, S.M., Kloor, M., Schwitalle, Y., Youmans, H., Doeberitz, M., Gebert, J., and Dihlmann, S. (2007). The putative tumor suppressor AIM2 is frequently affected by different genetic alterations in microsatellite unstable colon cancers. Genes Chromosomes Cancer *46*, 1080-1089.

Wong, V.W., Yu, J., Cheng, A.S., Wong, G.L., Chan, H.Y., Chu, E.S., Ng, E.K., Chan, F.K., Sung, J.J., and Chan, H.L. (2009). High serum interleukin-6 level predicts future hepatocellular carcinoma development in patients with chronic hepatitis B. Int J Cancer *124*, 2766-2770.

Wu, Z.H., Shi, Y., Tibbetts, R.S., and Miyamoto, S. (2006). Molecular linkage between the kinase ATM and NF-kappaB signaling in response to genotoxic stimuli. Science *311*, 1141-1146.

Xu, Y., Ashley, T., Brainerd, E.E., Bronson, R.T., Meyn, M.S., and Baltimore, D. (1996). Targeted disruption of ATM leads to growth retardation, chromosomal fragmentation during meiosis, immune defects, and thymic lymphoma. Genes Dev *10*, 2411-2422.

Yadav, D., Ngolab, J., Lim, R.S., Krishnamurthy, S., and Bui, J.D. (2009). Cutting edge: down-regulation of MHC class I-related chain A on tumor cells by IFN-gamma-induced microRNA. J Immunol *182*, 39-43.

Yamamoto, K., Wang, Y., Jiang, W., Liu, X., Dubois, R.L., Lin, C.S., Ludwig, T., Bakkenist, C.J., and Zha, S. (2012). Kinase-dead ATM protein causes genomic instability and early embryonic lethality in mice. J Cell Biol *198*, 305-313.

Yanai, H., Ban, T., Wang, Z., Choi, M.K., Kawamura, T., Negishi, H., Nakasato, M., Lu, Y., Hangai, S., Koshiba, R.*, et al.* (2009a). HMGB proteins function as universal sentinels for nucleic-acid-mediated innate immune responses. Nature *462*, 99-103.

Yanai, H., Savitsky, D., Tamura, T., and Taniguchi, T. (2009b). Regulation of the cytosolic DNA-sensing system in innate immunity: a current view. Curr Opin Immunol *21*, 17-22.

Yang, P., An, H., Liu, X., Wen, M., Zheng, Y., Rui, Y., and Cao, X. (2010). The cytosolic nucleic acid sensor LRRFIP1 mediates the production of type I interferon via a beta-catenin-dependent pathway. Nature immunology *11*, 487-494.

Yang, S., Liu, F., Wang, Q.J., Rosenberg, S.A., and Morgan, R.A. (2011). The shedding of CD62L (L-selectin) regulates the acquisition of lytic activity in human tumor reactive T lymphocytes. PLoS One *6*, e22560.

Yang, Y.G., Lindahl, T., and Barnes, D.E. (2007). Trex1 exonuclease degrades ssDNA to prevent chronic checkpoint activation and autoimmune disease. Cell *131*, 873-886.

Yousefi, S., Gold, J.A., Andina, N., Lee, J.J., Kelly, A.M., Kozlowski, E., Schmid, I., Straumann, A., Reichenbach, J., Gleich, G.J*., et al.* (2008). Catapult-like release of mitochondrial DNA by eosinophils contributes to antibacterial defense. Nat Med *14*, 949-953.

Yousefi, S., Mihalache, C., Kozlowski, E., Schmid, I., and Simon, H.U. (2009). Viable neutrophils release mitochondrial DNA to form neutrophil extracellular traps. Cell Death Differ *16*, 1438-1444.

Yukawa, K., Kikutani, H., Inomoto, T., Uehira, M., Bin, S.H., Akagi, K., Yamamura, K., and Kishimoto, T. (1989). Strain dependency of B and T lymphoma development in immunoglobulin heavy chain enhancer (E mu)-myc transgenic mice. The Journal of experimental medicine *170*, 711-726.

Zhang, W., Zhou, Q., Xu, W., Cai, Y., Yin, Z., Gao, X., and Xiong, S. (2013). DNA-dependent activator of interferon-regulatory factors (DAI) promotes lupus nephritis by activating the calcium pathway. J Biol Chem *288*, 13534-13550.

Zhang, X., Brann, T.W., Zhou, M., Yang, J., Oguariri, R.M., Lidie, K.B., Imamichi, H., Huang, D.W., Lempicki, R.A., Baseler, M.W*., et al.* (2011a). Cutting edge: Ku70 is a novel cytosolic DNA sensor that induces type III rather than type I IFN. J Immunol *186*, 4541-4545.

Zhang, Z., Yuan, B., Bao, M., Lu, N., Kim, T., and Liu, Y.J. (2011b). The helicase DDX41 senses intracellular DNA mediated by the adaptor STING in dendritic cells. Nature immunology *12*, 959-965.

Zuckerman, L.A., Pullen, L., and Miller, J. (1998). Functional consequences of costimulation by ICAM-1 on IL-2 gene expression and T cell activation. J Immunol *160*, 3259-3268.